

This is to certify that the
dissertation entitled

PHENOTYPIC CHARACTERIZATION OF PROGRESSIVE
RETINAL ATROPHY IN THE CARDIGAN WELSH CORGI
WITH A MUTATION IN THE PDE6A GENE

presented by

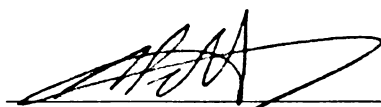
NALINEE TUNTIVANICH

has been accepted towards fulfillment
of the requirements for the

Doctoral

degree in

Comparative Medicine and
Integrative Biology



Major Professor's Signature

August, 2006

Date

MSU is an Affirmative Action/Equal Opportunity Institution

LIBRARY
Michigan State
University

PLACE IN RETURN BOX to remove this checkout from your record.
TO AVOID FINES return on or before date due.
MAY BE RECALLED with earlier due date if requested.

DATE DUE	DATE DUE	DATE DUE

**PHENOTYPIC CHARACTERIZATION OF PROGRESSIVE RETINAL
ATROPHY IN THE CARDIGAN WELSH CORGI WITH A MUTATION IN THE
PDE6A GENE**

By

Nalinee Tuntivanich

A DISSERTATION

Submitted to
Michigan State University
in partial fulfillment of the requirements
for the degree of

DOCTOR OF PHILOSOPHY

Comparative Medicine and Integrative Biology

2006

ABSTRACT

PHENOTYPIC CHARACTERIZATION OF PROGRESSIVE RETINAL ATROPHY IN THE CARDIGAN WELSH CORGI WITH A MUTATION IN THE PDE6A GENE

By

Nalinee Tuntivanich

The purpose of this study was to perform a detail characterization of the electroretinographic and morphological aspects of progressive retinal atrophy (PRA) in the Cardigan Welsh corgi (CWC) due to a mutation in the gene encoding the alpha subunit of the rod cyclic GMP phosphodiesterase (PDE6A), and to investigate expression of the canine PDE6A gene in other tissues. Homozygous *PDE6A* mutant, heterozygous *PDE6A* carrier, and homozygous *PDE6A* normal dogs were used in this study. Short flash and long flash electroretinograms (ERG) were recorded as well as pharmacological dissections of the abnormal ERG responses of the *PDE6A* mutant dogs. Morphological characterization of the mutant retina was performed by light and electron microscopy. Retinal cell counting and layer thickness measurement were performed in addition to immunohistochemical staining using specific cell markers. The *PDE6A* mutant dogs had very reduced scotopic ERG responses with elevated amplitude threshold at all ages investigated, starting from 2 weeks of age. Qualitative analysis of the leading edge of the rod-mediated a-wave showed absent or substantially reduced and delayed rod response with loss of sensitivity. This concurred with results from the Naka-Rushton analysis. Application of 2-amino-4-phosphonobutyric acid (APB) to block ON-bipolar activity failed to enhance the a-wave from the mutant dog at 6 weeks of age strongly suggesting a severe loss of photoreceptor response prior to retinal maturation. Reduction of photopic

a-wave response with elevated amplitude threshold present from 3 weeks of age onwards indicated an initial development of cone responses followed by a gradual deterioration. Flicker and long flash ERGs also showed a decrease in amplitudes indicating decreased responses from inner retinal cells. Early morphological changes were present in the rod outer segments (OSs) at 3 weeks of age. By around 4 weeks of age there was evidence of apoptotic cell death affecting the rod photoreceptor cells. Reduction of the OS layer thickness was shown at 5 weeks of age, at which age a loss of rod OSs was shown by rhodopsin immunohistochemistry. Significant loss of cone OSs was apparent by 7 weeks of age, demonstrated by red/cone opsin staining, with the remaining inner segments (IS) stunted. At this age, there was a notable decrease in the number of photoreceptor nuclei row and number of rod nuclei per unit length of the retina while the number of cones was maintained. By 60 days of age only one row of photoreceptor nuclei remained in the mutant retina. Morphological alterations were also observed in rod bipolar cells, horizontal cells and Müller cells. Expression of PDE6A amplicons by RT-PCR was not only found in normal control retina but also in iris, choroid, pituitary gland, pineal gland, normal and mutant kidney, normal and mutant small intestine and mutant retina at 5 weeks of age. The PDE6A transcript in the kidney appeared to be shorter than that from the retina and in the mutant dog an alternatively spliced transcript was found that had a skipped exon. The exon skipping had the result that the premature termination codon was excluded and the reading frame restored. Further investigation would be required to see if the predicted shortened PDE6A product is translated in kidney and to investigate its possible function.

My deepest appreciation is extended to my family for their support, patience, love and understanding shown to me throughout this endeavor.

To

my father, Mr. Vorasak Tuntivanich

my mother, Professor Pranee Tuntivanich

my sister, Miss Vareemon Tuntivanich

my husband, Mr. Kittipob Smitalamba

ACKNOWLEDGMENTS

I wish to acknowledge those who have contributed to my completion of this milestone in my professional career. I would like to express my sincere appreciation to my committee members: Dr Arthur Weber, Dr John Fyfe, Dr Matti Kiupel and Dr James Render. I am deeply grateful for their kind guidance. I sincerely appreciate the support from the Thai government, Chulalongkorn University and the faculty of Veterinary science, Chulalongkorn University, Thailand, in particular, the department of Surgery. I am thankful for the support from the administrative people in the Comparative Medicine and Integrative Biology program; Dr Vilma Yuzbasiyan-Gurkan, Victoria Hoelzer-Maddox, collaborators; Naheed Khan, Andy Fischer, technicians; Ralph Common, Thomas Wood, Scott Marsh, Nicole Grosjean, Dionne Rodgers, Christine Harman and Walter Bobrowski.

I am appreciative to Dr Cheri Johnson and Lisa Allen for taking care of the dog colony at the MSU vivarium, Michelle Curcio for molecular guidance, Juan Steibel for statistical consultance, Dr Paul Sieving for ERG consultance, people from comparative ophthalmology laboratory and staffs of the department of Small Animal Clinical Sciences, College of Veterinary Medicine, MSU for their supports. Thanks to friends, the Thai Student Association at MSU and others whose names are not mentioned but their supports are unforgettable.

I would like to acknowledge the funding sources of this project. They include Companion Animal Funds, MSU, Purebred Dog Endowment Fund, MSU, MidWest Eye Banks, Fight for Sight and National Institutes of Health.

Finally, I would like to give a special acknowledgment to Dr Simon Petersen-Jones who has served as my advisor. His encouragement, constant support and kindness are not only needed for me to finally bring this dissertation to completion but also broaden my scientific experience. I am sincerely grateful for his significant role in this phase of my life.

TABLE OF CONTENTS

LIST OF TABLES	xiii
----------------------	------

LIST OF FIGURES	xiv
-----------------------	-----

CHAPTER 1

INTRODUCTION

1.1. Ocular embryology	1
1.2. Ocular anatomy	4
1.2.1. Retinal pigment epithelium	7
1.2.2. Photoreceptor layer	8
1.2.3. Outer limiting membrane	11
1.2.4. Outer nuclear layer	12
1.2.5. Outer plexiform layer	12
1.2.6. Inner nuclear layer	14
1.2.6.a. Amacrine cells	15
1.2.6.b. Bipolar cells	16
1.2.6.c. Müller cells	17
1.2.6.d. Horizontal cells	17
1.2.6.e. Interplexiform cells	18
1.2.7. Inner plexiform layer	19
1.2.8. Ganglion cell layer	19
1.2.9. Nerve fiber layer	21
1.2.10. Inner limiting membrane	21
1.3. The Central visual pathway	22
1.4. The phototransduction pathway and visual cycle	24
1.5. Electroretinography	30
1.6. Inherited retinal dystrophies in humans	37
1.7. Inherited retinal degenerations in dogs and cats	39
1.8. Laboratory animal models for inherited retinal dystrophies	50

CHAPTER 2

DETAILED ELECTRORETINOGRAPHIC CHARACTERIZATION OF THE *PDE6A* DOG PHENOTYPE

2.1. Introduction	53
2.2. Materials and methods	
2.2.1. Animals	54
2.2.2. Electroretinographic recording	
2.2.2.a. Anesthesia	54
2.2.2.b. Recording electrode placement and animal positioning	55
2.2.2.c. Electroretinographic recording	56

2.2.3.	Electroretinographic test protocols	
2.2.3.a.	Intensity-series electroretinography	
2.2.3.a.(i)	Scotopic intensity-series electroretinography	56
2.2.3.a.(ii)	Photopic intensity-series electroretinography	57
2.2.3.b.	Flicker electroretinography	
2.2.3.b.(i).	Rod flicker ERG	58
2.2.3.b.(ii).	Cone flicker ERG	58
2.2.3.c.	Electroretinography using blue flashes	58
2.2.3.d.	Long flash electroretinography	58
2.2.4.	Data analysis	
2.2.4.a.	The mean a- and b-wave amplitude and implicit time	59
2.2.4.b.	Flicker amplitude and implicit time	60
2.2.4.c.	Analysis of by using Naka-Rushton function equation	60
2.2.4.d.	Criterion threshold of means of ERG scotopic and photopic amplitudes	61
2.2.4.e.	Rod-isolated responses	62
2.2.4.f.	Oscillatory potentials	62
2.2.4.g.	Photopic Negative Response	63
2.3.	Results	
2.3.1.	Scotopic ERG responses	
2.3.1.a.	Scotopic ERG amplitude	64
2.3.1.b.	Scotopic ERG implicit time	71
2.3.1.c.	Rod-isolated a-wave response	74
2.3.1.d.	Scotopic ERG responses to blue light flashes	76
2.3.1.e.	Naka-Rushton fitting of the first limb of the scotopic intensity-response curves	77
2.3.1.f.	Rod flicker ERG response	81
2.3.1.g.	Oscillatory potentials	83
2.3.2.	Photopic ERG responses	
2.3.2.a.	Photopic a- and b-wave amplitudes	85
2.3.2.b.	Photopic ERG implicit time	91
2.3.2.c.	Cone flicker ERG response	94
2.3.2.d.	Photopic negative response	97
2.3.2.e.	Long flash ERG response	98
2.4.	Discussion	101

CHAPTER 3

PHARMACOLOGICAL DISSECTION OF THE *PDE6A* ELECTRORETINOGRAM

3.1.	Introduction	106
3.2.	Materials and methods	
3.2.1.	Animals	107
3.2.2.	Pharmacological agents	107
3.2.3.	Intravitreal injection	108
3.2.4.	Electroretinographic recording	
3.2.4.a.	Anesthesia and recording electrode placement	108

3.2.4.b. Electrophoretic recording	109
3.2.4.c. Electrophoretic test protocols	
3.2.4.c (i). Scotopic and photopic short flash electrophoretography	109
3.2.4.c (ii). Flicker electrophoretography	110
3.2.4.c (iii). Long flash electrophoretography	110
3.2.5. Data analysis	110
3.3. Results	
3.3.1. Results after the intravitreal injection of APB	
3.3.1.a. Short flash scotopic and photopic ERG intensity-series responses from normal control dogs	111
3.3.1.b. Cone flicker responses	115
3.3.1.c. Long flash ERG responses	116
3.3.2. Results after the intravitreal injection of PDA	
3.3.2.a. ERG photopic intensity-series response	120
3.3.2.b. Cone flicker response	122
3.3.2.c. Long flash ERG response	124
3.3.3. Results after the intravitreal injection of tetrodotoxin	
3.3.3.a. Photopic ERG response	127
3.3.3.b. Cone flicker response	127
3.4. Discussion	130

CHAPTER 4

DETAILED HISTOPATHOLOGICAL CHARACTERIZATION OF THE *PDE6A* DOG PHENOTYPE

4.1. Introduction	136
4.2. Materials and methods	
4.2.1. Morphological analyses by light microscopy	
4.2.1.a. Tissue collection and processing	137
4.2.1.b. Data collection	140
4.2.1.c. Data analysis	142
4.2.2. Morphological analyses by transmission electron microscopy	
4.2.2.a. Tissue collection and processing	142
4.2.2.b. Data analysis	143
4.2.3. Immunohistochemical analyses of paraffin-embedded sections	
4.2.3.a. Tissue collection and processing	143
4.2.3.b. Data analysis	146
4.2.4. Immunohistochemical analyses of frozen sections	
4.2.4.a. Tissue collection	147
4.2.4.b. Data analysis	149
4.2.5. Terminal Deoxynucleotidyl Transferase-mediated dUTP Nick End Labeling (TUNEL) staining	
4.2.5.a. Tissue collection and processing	150
4.2.5.b. Data analysis	150
4.3. Results	

4.3.1. Morphological assessment of the retina by light and electron microscopy	
4.3.1.a. Retinal sections at 3 to 10 days of age.....	151
4.3.1.b. Retinal sections at 2 to 3 weeks of age	153
4.3.1.c. Retinal sections at 4 to 5 weeks of age	162
4.3.1.d. Retinal sections at 7 to 12 weeks of age	170
4.3.1.e. Retinal sections at 16 weeks of age	177
4.3.1.f. Retinal sections at 24 weeks of age	188
4.3.1.g. Retinal sections at age greater than 60 weeks.....	193
4.3.2. Immunohistochemical analyses of paraffin-embedded and frozen sections	
4.3.2.a. Immunohistochemistry using rhodopsin.....	197
4.3.2.b. Immunohistochemistry using cone arrestin	201
4.3.2.c. Immunohistochemistry using red/green opsin	203
4.3.2.d. Immunohistochemistry using PKC α	205
4.3.2.e. Immunohistochemistry using calbindin.....	207
4.3.2.f. Immunohistochemistry using Hu C/D	208
4.3.2.g. Immunohistochemistry using calretinin	209
4.3.2.h. Immunohistochemistry using GFAP	211
4.4. Discussion	213

CHAPTER 5

INVESTIGATION OF THE TISSUE EXPRESSION OF THE *PDE6A* GENE

5.1. Introduction	221
5.2. Materials and Methods	
5.2.1. Tissue collection	222
5.2.2. Isolation of total RNA	
5.2.2.a. Preparation of instruments and RNA handling.....	223
5.2.2.b. Isolation of total RNA using RNeasy Mini Kit	224
5.2.2.c. Visualization of total RNA for integrity using a formaldehyde gel	
5.2.2.c.(i). Preparation of materials	225
5.2.2.c.(ii). Formaldehyde (FA) gel electrophoresis	225
5.2.2.c.(iii). Analysis of total RNA by FA gel electrophoresis	225
5.2.3. Spectrophotometry of RNA	226
5.2.4. Reverse Transcription-Polymerase Chain Reaction	
5.2.4.a. Synthesis of cDNA	226
5.2.4.b. Polymerase Chain Reaction (PCR) for <i>PDE6A</i> gene expression	227
5.2.5. Sequencing of PCR products	
5.2.5.a. DNA preparation.....	229
5.2.5.b. DNA sequencing.....	229
5.2.6. Rapid Amplification of cDNA Ends (RACE) to determine full-length sequence of kidney transcript	
5.2.6.a. Dephosphorylation of RNA	230

5.2.6.b.	Removal of the mRNA cap structure.....	230
5.2.6.c.	Ligation of the RNA oligo to de-capped mRNA	231
5.2.6.d.	Reverse transcription of mRNA	231
5.2.6.e.	Amplification of cDNA ends	232
5.2.7.	Cloning of PCR products	
5.2.7.a.	Cloning reaction.....	234
5.2.7.b.	Transformation of competent cells	234
5.2.7.c.	Analysis transformed clones	235
5.2.8.	Northern hybridization	
5.2.8.a.	Preparation of FA gel for electrophoresis.....	235
5.2.8.b.	FA gel electrophoresis	
5.2.8.b.(i).	Preparation of RNA samples and RNA size marker	236
5.2.8.b.(ii).	FA gel electrophoresis	236
5.2.8.c.	Preparation for an upward capillary transfer	
5.2.8.c.(i).	Preparation of FA gel	237
5.2.8.c.(ii).	Preparation of nylon membrane, wicked papers and blotting papers	237
5.2.8.c.(iii).	Assembly of the capillary transfer system	237
5.2.8.c.(iv).	Fixation of the transferred RNA to the membrane.....	239
5.2.8.d.	Northern hybridization	
5.2.8.d.(i).	Preparation of the DNA probe	240
5.2.8.d.(ii).	Prehybridization	241
5.2.8.d.(iii).	Hybridization	241
5.2.8.d.(iv).	Washing of the membrane	242
5.2.8.e.	Exposure of the nylon membrane to phosphor-imager	242
5.3.	Results	
5.3.1.	Expression of PDE6A mRNA in canine tissues	
5.3.1.a.	Investigation of PDE6A expression by RT-PCR	242
5.3.1.b.	Investigation of kidney transcript of the normal control	249
5.3.1.c.	Investigation of PDE6A expression by northern blot	255
5.4.	Discussion	257
CHAPTER 6		
FINAL DISCUSSION & CONCLUSIONS		262
CHAPTER 7		
FUTURE STUDIES		
7.1.	Investigation of retinal PDE activity and cGMP levels	
7.1.1.	Background and Hypothesis	268
7.1.2.	Methods	
7.1.2.a.	Investigation of PDE activity of the retina	
7.1.2.a.(i)	HPLC analysis	269
7.1.2.a.(ii)	Western blot analysis	269
7.1.2.b.	Investigation of cGMP level of the retina	270

7.2. Assessment of canine cone-specific electroretinography	
7.2.1. Background and Hypothesis	270
7.2.2. Methods	271
7.2.2.a. ERG assessment of S cone function	272
7.2.2.b. ERG assessment of M cone function	272
7.3. Investigation of the distribution of canine cone photoreceptors and the pattern of cell loss	
7.3.1. Background and Hypothesis	272
7.3.2. Methods	273
APPENDIX	276
BIBLIOGRAPHY	286

LIST OF TABLES

Table 1.1.	Summary of the different types of progressive retinal atrophy (PRA) in dogs and cats	41-42
Table 4.1.	A list of the primary antibodies, their working dilution and source that are used in paraffin-embedded sections	146
Table 4.2.	A list of the primary antibodies, their working dilution and source that are used in frozen sections	149

LIST OF FIGURES

Figure 1.1.	Human ocular embryology	2
Figure 1.2.	Cross section of canine retina	7
Figure 1.3.	(A) Schematic drawing of structural elements of rod and cone and (B) A Differential Interference Contrast image of canine central retina from a flat mount preparation focused at the level of the inner segments (magnification 100X)	9
Figure 1.4.	Histological section showing canine photoreceptors at 3 (A) and 10 (B) days of age	11
Figure 1.5.	A simple diagram of the organization of the retina.....	14
Figure 1.6.	A schematic diagram demonstrating the central projection of the retina to subcortical regions of the brain as to the visual cortex	22
Figure 1.7.	A simplified diagram of the rod phototransduction cascade and visual cycle	26
Figure 1.8.	Diagram of electrical components (PI, PII and PIII) recorded in the retina as described by Granit	30
Figure 1.9.	Canine clinical ERG recordings as recommended by the ERG committee of the ECVO	32
Figure 1.10.	Components of canine scotopic full-field intensity-series ERG recorded after 1 hour of dark adaptation	35
Figure 1.11.	A canine long flash ERG recorded after 10 minutes of light adaptation	37
Figure 1.12.	Fundus photography of a normal control (A) and a Cargian Welsh corgi (B) with progressive retinal atrophy at 18 weeks of age	43
Figure 1.13.	A diagram demonstrating sequences of the PDE6A transcript and amino acid of the normal (A) and mutant (B) alleles	49

Figure 2.1.	Representative scotopic ERG recordings from a normal control (A) and the <i>PDE6A</i> mutant dog (B) at 4 weeks of age	66
Figure 2.2.	Representative scotopic ERG recordings from a normal control (A) and the <i>PDE6A</i> mutant dog (B) at 6 weeks of age	67
Figure 2.3.	Mean scotopic a-wave amplitudes with standard errors (1x +/- SEM) plotted against stimulus intensity on a log-log scale for normal control and <i>PDE6A</i> mutant puppies	68
Figure 2.4.	Mean scotopic b-wave amplitudes with standard errors (1x +/- SEM) plotted against stimulus intensity on a log-log scale from normal control and <i>PDE6A</i> mutant puppies	69
Figure 2.5.	Mean scotopic intensity threshold with standard errors (1x +/- SEM) using 5 μ V and 10 μ V criterion for a- and b-wave amplitude from normal control and <i>PDE6A</i> mutant dogs at all ages	70
Figure 2.6.	Mean scotopic a-wave implicit times with standard errors (1x +/- SEM) plotted against stimulus intensity on a log-log scale from normal control and <i>PDE6A</i> mutant dogs at 2 & 3 (A), 4 & 5 (B), 6 & 7 (C), 9 & 12 (D) and 16 & 20 (E) weeks of age	72
Figure 2.7.	Mean scotopic b-wave implicit times with standard errors (1x +/- SEM) plotted against stimulus intensity on a log-log scale from normal control and <i>PDE6A</i> mutant dogs at 2 & 3 (A), 4 & 5 (B), 6 & 7 (C), 9 & 12 (D) and 16 & 20 (E) weeks of age	73
Figure 2.8.	Normalization (for a-wave amplitude) of the rod-isolated a-wave derived from a subtraction of intensity-matched photopic and scotopic ERGs in a normal control and the <i>PDE6A</i> mutant dog at 3 weeks of age	75
Figure 2.9.	Representative recordings of rod-mediated ERG response to dim blue flashes of light from dark-adapted normal controls and <i>PDE6A</i> mutant dogs at 4 and 7 weeks of age.....	76
Figure 2.10.	Scotopic b-wave intensity-response function obtained from a normal control and the <i>PDE6A</i> mutant dog at 3 weeks of age.....	78
Figure 2.11.	A comparison of the mean and standard errors (1x + SEM) of the Naka-Rushton variables; Vmax (A), k value (B) and n value (C) of the normal controls and the <i>PDE6A</i> mutant dogs at all age groups	80

Figure 2.12. A comparison of representative rod flicker responses ($-1.6 \log$ cds/m ² , 5Hz) from a normal control (A) and the <i>PDE6A</i> mutant dog (B) at different ages	82
Figure 2.13. Representative scotopic oscillatory potential ($0.85 \log$ cds/m ²) from normal control and <i>PDE6A</i> mutant dogs at 5 weeks of age (band pass at 73 to 500 Hz)	83
Figure 2.14. Mean scotopic oscillatory potential amplitudes with standard errors ($1x + \text{SEM}$) of normal controls and the <i>PDE6A</i> mutant dogs plotted against age	84
Figure 2.15. Representative photopic ERG recordings from a normal control (A & C) and the <i>PDE6A</i> mutant dog (B & D) at 4 (A & B) and 6 (C & D) weeks of age.....	87
Figure 2.16. Mean photopic a-wave amplitudes with standard errors ($1x \pm \text{SEM}$) plotted against stimulus intensity on a log-log scale from normal control and <i>PDE6A</i> mutant dogs at 2 & 3 (A), 4 & 5 (B), 6 & 7 (C), 9 & 12 (D) and 16 & 20 (E) weeks of age	88
Figure 2.17. Mean photopic b-wave amplitudes with standard errors ($1x \pm \text{SEM}$) plotted against stimulus intensity on a log-log scale from normal control and <i>PDE6A</i> mutant dogs at 2 & 3 (A), 4 & 5 (B), 6 & 7 (C), 9 & 12 (D) and 16 & 20 (E) weeks of age	89
Figure 2.18. Mean intensity at threshold from photopic recordings with standard errors ($1x \pm \text{SEM}$) using a $5\mu\text{V}$ criterion for a- and b-wave amplitudes from normal control and <i>PDE6A</i> mutant groups at all ages tested	90
Figure 2.19. Mean photopic a-wave implicit times with standard errors ($1x \pm \text{SEM}$) plotted against stimulus intensity on a log-log scale from normal control and <i>PDE6A</i> mutant dogs at 2 & 3 (A), 4 & 5 (B), 6 & 7 (C), 9 & 12 (D) and 16 & 20 (E) weeks of age	92
Figure 2.20. Mean photopic b-wave implicit times with standard errors ($1x \pm \text{SEM}$) plotted against stimulus intensity on a log-log scale from normal control and <i>PDE6A</i> mutant dogs at 2 & 3 (A), 4 & 5 (B), 6 & 7 (C), 9 & 12 (D) and 16 & 20 (E) weeks of age	93
Figure 2.21. A comparison of representative cone flicker responses ($0.39 \log$ cds/m ² , 33 Hz) from a normal control and the <i>PDE6A</i> mutant dog at 9 weeks of age	95

Figure 2.22.	Mean and standard errors ($1x + SEM$) of cone flicker amplitudes (A) and cone flicker implicit times (B) of normal controls and <i>PDE6A</i> mutant dogs ($0.39 \log \text{ cds/m}^2$, 33 Hz) at all age groups	96
Figure 2.23.	Representative photopic ERG responses ($1.36 \log \text{ cds/m}^2$) from a normal control and the <i>PDE6A</i> mutant dog at different ages demonstrating the photopic negative response	97
Figure 2.24.	A representative long flash ERG from a normal control dog of 60 weeks of age	99
Figure 2.25.	Representative long flash ERG recordings from normal controls (A) and <i>PDE6A</i> mutant dogs (B) with age (week)	100
Figure 3.1.	Representative scotopic (A) and photopic (B) intensity-series ERGs from a normal control at 60 weeks of age performed before and at 1.5 hours following an intravitreal injection of APB	113
Figure 3.2.	Representative scotopic intensity-series ERGs from a normal control at 4 weeks of age (A), the <i>PDE6A</i> mutant dog at 4 weeks of age (B) and scotopic ERG from the <i>PDE6A</i> mutant dog at 6 weeks of age (C) performed before and at 1.5 hours following an intravitreal injection of APB	114
Figure 3.3.	Representative cone flicker response ($0.39 \log \text{ cds/m}^2$, 33Hz) of a normal control (A) and the <i>PDE6A</i> mutant dog (B) at 6 weeks of age performed before and at 2 hours following an intravitreal injection of APB.....	115
Figure 3.4.	Representative long flash ERG response from normal controls (A) and the <i>PDE6A</i> mutant dogs (B) at 4 weeks of age performed injection of APB	117
Figure 3.5.	Representative long flash ERG response from a normal control (A) and the <i>PDE6A</i> mutant dog (B) at 6 weeks of age performed before and 2 hours following an intravitreal injection of APB	118
Figure 3.6.	Subtraction of post APB long flash ERG from pre APB administration long flash ERG from a normal control (A) and the <i>PDE6A</i> mutant dog (B) at 6 weeks of age	119
Figure 3.7.	Representative photopic ERGs at -0.001 , 0.39 and $1.36 \log \text{ cds/m}^2$ from a normal control (A) and the <i>PDE6A</i> mutant dog (B) at 7 weeks of age performed before and at 2 hours following an intravitreal injection of PDA	121

Figure 3.8.	Representative cone flicker response ($0.39 \log \text{ cds/m}^2$, 33Hz) of a normal control (A) and the <i>PDE6A</i> mutant dog (B) at 7 weeks of age before and 2 hours following an intravitreal injection of PDA	123
Figure 3.9.	Representative long flash ERG responses from a normal control (A) and the <i>PDE6A</i> mutant dog (B) at 7 weeks of age performed before and at 1, 1.5, 2 and 2.5 hours following an intravitreal injection of PDA	125
Figure 3.10.	Subtraction of post PDA long flash ERG from pre PDA long flash ERG from a normal control (A) and the <i>PDE6A</i> mutant dog (B) at 7 weeks of age	126
Figure 3.11.	Representative photopic ERGs at $0.85 \log \text{ cds/m}^2$ from a normal control (A) and the <i>PDE6A</i> mutant dog (B) at 10 weeks of age performed before and at 1.5 hours following an intravitreal injection of TTX	128
Figure 3.12.	Representative cone flicker response ($0.39 \log \text{ cds/m}^2$, 33Hz) of a normal control (A) and the <i>PDE6A</i> mutant dog (B) at 10 weeks of age before and at 1.5 hour following an intravitreal injection of TTX	129
Figure 4.1.	Diagram of the right eyecup of a dog illustrating planes of section and regions of the retina where the thickness of individual retinal layers is measured, and the number of outer nuclear layer (ONL) rows and photoreceptor nuclei per unit length are counted.....	139
Figure 4.2.	Diagram of the right eyecup of a dog illustrating the regions of the retina where detailed morphological analysis is performed	140
Figure 4.3.	Diagram of a cross section of retina showing a measurement of the number of rows of the ONL and the number of rod and cone nuclei per 100-micrometer length of the retina	141
Figure 4.4.	Representative photomicrographs of retinal morphology of a normal control (A & C) and the <i>PDE6A</i> mutant dog (B & D) at 4 (A & B) and 10 (C & D) days of age	152
Figure 4.5.	Representative photomicrographs of retinal morphology of a normal control (A & C) and the <i>PDE6A</i> mutant dog (B & D) at 2 (A & B) and 3 (C & D) weeks of age	155
Figure 4.6.	Mean retinal thickness of each of the different retinal layers from superior to inferior ora ciliaris retina (vertical section; see Figure	

4.1 in materials and methods) from normal control (A), <i>PDE6A</i> carrier (B) and <i>PDE6A</i> mutant dogs (C) at 3 weeks of age .	156
Figure 4.7. Mean retinal thickness of each of the different retinal layers from nasal to temporal region (horizontal section; see Figure 4.1 in materials and methods) from normal control (A) and <i>PDE6A</i> mutant dogs (B) at 3 weeks of age	157
Figure 4.8. Photomicrographs of retinal morphology of the ONL of a normal control (A) at 23 days of age, and <i>PDE6A</i> mutants dogs (B & C) at 24 (B) and 27 (C) days of age and a photomicrograph of the anti-caspase 3 immunohistochemistry in the <i>PDE6A</i> mutant retina at 24 (D) days of age	159
Figure 4.9. Ultra structural sections of the ONL of a normal control (A) and the <i>PDE6A</i> mutant dog (B) at 23 days of age	160
Figure 4.10. Ultra structural appearance of photoreceptor nuclei of normal control (A) and <i>PDE6A</i> mutant dogs (B, C & D) at 27 days of age	161
Figure 4.11. Representative photomicrographs of retinal morphology of normal control (A & C) and the <i>PDE6A</i> mutant dogs (B & D) at 4 (A & B) and 5 (C & D) weeks of age	161
Figure 4.12. Photomicrographs of retinal morphology of the ONL of a normal control (A) at 38 days of age, a <i>PDE6A</i> mutant dog (B) at 42 days of age and caspase 3 immunohistochemistry in a <i>PDE6A</i> mutant retina at 42 days of age (C)	165
Figure 4.13. Photomicrographs of TUNEL labeling of retina from normal controls (A, C & E) and the <i>PDE6A</i> mutant dogs (B, D, F & G) at 25 day (A & B), 28 day (C & D), 5 weeks (E & F) and 10 weeks (G) of age	166
Figure 4.14. Mean retinal thickness of each of the different retinal layers from superior to inferior ora ciliaris retina (vertical section; see Figure 4.1 in materials and methods) from normal control (A), <i>PDE6A</i> carrier (B) and <i>PDE6A</i> mutant dogs (C) at 5 weeks of age	167
Figure 4.15. Mean retinal thickness of each of the different retinal layers from nasal to temporal region (horizontal section; see Figure 4.1 in materials and methods) from normal control (A) and the <i>PDE6A</i> mutant dogs (B) at 5 weeks of age	168

Figure 4.16. Ultra structural sections of the photoreceptor segments of a normal control (A) and the <i>PDE6A</i> mutant retina (B) at 5 weeks of age	169
Figure 4.17. Representative photomicrographs of retinal morphology of a normal control (A & C) and the <i>PDE6A</i> mutant dog (B & D) at 7 (A & B) and 12 (C & D) weeks of age	172
Figure 4.18. Ultra structural sections of the photoreceptor layer of the <i>PDE6A</i> mutant retina at 9 weeks of age	173
Figure 4.19. Ultra structural sections of the ONL of a normal control (A) and the <i>PDE6A</i> mutant retina (B) at 9 weeks of age	174
Figure 4.20. Mean retinal thickness of each of the different retinal layers from superior to inferior ora ciliaris retina (vertical section; see Figure 4.1 in materials and methods) from normal control (A), <i>PDE6A</i> carrier (B) and <i>PDE6A</i> mutant dogs (C) at 9 weeks of age	175
Figure 4.21. Mean retinal thickness of each of the different retinal layers from nasal to temporal region (horizontal section; see Figure 4.1 in materials and methods) from normal control (A) and <i>PDE6A</i> mutant dogs (B) at 9 weeks of age	176
Figure 4.22. Representative photomicrographs of retinal morphology of a normal control (A) and the <i>PDE6A</i> mutant dog (B) at 16 weeks of age	178
Figure 4.23. Ultra structural sections of the outer retina of a normal control (A & D) and the <i>PDE6A</i> mutant dog (B, C & E) at 16 weeks of age	179
Figure 4.24. Mean retinal thickness of each of the different retinal layers from superior to inferior ora ciliaris retina (vertical section; see Figure 4.1 in materials and methods) from normal control (A), <i>PDE6A</i> carrier (B) and <i>PDE6A</i> mutant dogs (C) at 16 weeks of age	180
Figure 4.25. Mean retinal thickness of each of the different retinal layers from nasal to temporal region (horizontal section; see Figure 4.1 in materials and methods) from normal control (A) and <i>PDE6A</i> mutant dogs (B) at 16 weeks of age	181
Figure 4.26. Scatter plot showing the number of nuclei rows in the ONL (A), number of rod (B) and number of cone (C) nuclei per unit length (100 μ m) of the retina (of region #3) plotted against age for normal control (blue), carrier (green) and mutant (orange) dogs.....	182

Figure 4.27. Mean number of nuclei rows in the ONL of retinal regions (#1 to #8) in a vertical section through the optic nerve head at 5 (A), 9 (B), 16 (C) and 60 (D) weeks of age	183
Figure 4.28. Mean number of nuclei rows in the ONL of retinal regions (#9 to #12) in a horizontal section temporal from the optic nerve head at 5 (A), 9 (B), 16 (C) and 60 (D) weeks of age	184
Figure 4.29. Mean number of rod nuclei per unit length (100 μ m) of retinal regions (#1 to #8) in a vertical section through the optic nerve head at 5 (A), 9 (B), 16 (C) and 60 (D) weeks of age	185
Figure 4.30. Mean number of rod nuclei per unit length of retinal regions (#9 to #12) in a horizontal section temporal from the optic nerve head at 5 (A), 9 (B), 16 (C) and 60 (D) weeks of age	186
Figure 4.31. Mean number of cone nuclei per unit length (100 μ m) of all retinal regions (#1 to #8) in a vertical section through the optic nerve head (A & B) and horizontal section temporal through the optic nerve head (C) at 5 (A) and 16 (B & C) weeks of age	187
Figure 4.32. Thickness of the inner segments of normal control and the <i>PDE6A</i> mutant dog for different retinal regions (see Figure 4.2 in materials and methods) at 24 weeks of age	189
Figure 4.33. Thickness of the ONL of normal control and the <i>PDE6A</i> mutant dog for different retinal regions (see Figure 4.2 in materials and methods) at 24 weeks of age	190
Figure 4.34. Number of nuclei rows in the ONL at different retinal regions (see Figure 4.2 in materials and methods) in normal control and the <i>PDE6A</i> mutant dog at 24 weeks of age	191
Figure 4.35. Number of photoreceptor nuclei per unit length (100 μ m) of retina at different retinal regions (see Figure 4.2 in materials and methods) in normal control and the <i>PDE6A</i> mutant dog at 24 weeks of age	192
Figure 4.36. Representative photomicrographs of retinal morphology of a normal control (A) and the <i>PDE6A</i> mutant dog (B, C & D) at 100 weeks of age	194
Figure 4.37. Mean retinal thickness of each of the different retinal layers from superior to inferior ora ciliaris retina (vertical section; see Figure 4.1 in materials and methods) from normal control (A) and <i>PDE6A</i> mutant dogs (B) at greater than 60 weeks of age	195

Figure 4.38. Mean retinal thickness of each of the different retinal layers from nasal to temporal region (horizontal section; see Figure 4.1 in materials and methods) from a normal control (A) and <i>PDE6A</i> mutant dogs (B) at greater than 60 weeks of age .	196
Figure 4.39. Immunohistochemical expression of anti-rhodopsin (a gift from Dr. P. Hargrave, University of Florida) in retinal sections of normal control (A, C & E) and the <i>PDE6A</i> mutant dogs (B, D & F) at 3 (A & B), 5 (C & D) and 9 (E & F) weeks of age	198
Figure 4.40. Immunohistochemical expression of anti-rhodopsin (Lab Vision) in retinal sections of normal control (A & C) and the <i>PDE6A</i> mutant dogs (B, D, E and F) at 4 (A & B), 8 (C & D), 60 (E) and 210 (F) weeks of age	200
Figure 4.41. Immunohistochemical expression of anti-cone arrestin (a gift from Dr. S. Craft, University of Southern California) in retinal sections of normal control (A & C) and the <i>PDE6A</i> mutant dogs (B & D) at 9 (A & B) and 210 (C & D) weeks of age	202
Figure 4.42. Immunohistochemical expression of anti-red/green opsin fluorescence in retinal sections of normal control (A & E) and the <i>PDE6A</i> mutant dogs (B, C, D & F) at 5 (A & E), 7 (B), 16 (C & F), and 60 (D) weeks of age	204
Figure 4.43. Immunohistochemical expression of anti-protein kinase C alpha (PKC α) in retinal sections of normal control (A, C & E) and the <i>PDE6A</i> mutant dogs (B, D & F) at 7 (A & B), 9 (C & D) and 60 (E & F) weeks of age	206
Figure 4.44. Immunohistochemical expression of anti-calbindin fluorescence in retinal sections of normal control (A & C) and the <i>PDE6A</i> mutant dogs (B & D) at 10 (A & B) and 60 (B & D) weeks of age	207
Figure 4.45. Immunohistochemical expression of anti-Hu C/D fluorescence in retinal sections of normal control (A) and the <i>PDE6A</i> mutant dogs (B & C) at 5 (A), 7 (B) and 60 (C) weeks of age	208
Figure 4.46. Immunohistochemical expression of anti-calretinin fluorescence in retinal sections of normal control (A, C & E) and the <i>PDE6A</i> mutant dogs (B, D & F) at 5 (A & B), 10 (C & D) and 60 (E & F) weeks of age	210
Figure 4.47. Immunohistochemical expression of anti-GFAP in retinal sections of normal control (A, C & E) and the <i>PDE6A</i> mutant dogs (B, D, & F) at 3 (A & B), 5 (C & D) and 60 (E & F) weeks of age	212

Figure 5.1.	Upward capillary transfer apparatus	239
Figure 5.2.	Diagram illustrating PDE6A fragments amplified from RT-PCR with various designed primer sets	244
Figure 5.3.	RT-PCR analysis of the PDE6A gene expression in various tissues	246
Figure 5.4.	RT-PCR analysis of the PDE6A gene expression in various tissues using gene specific primers (PDEA1/6835; Figure 5.1)	248
Figure 5.5.	Nucleotide sequence of the assembled kidney PDE6A full-length transcript, the shorter product missing exon 16 from the <i>PDE6A</i> mutant kidney and predicted translated amino acid sequence	250-252
Figure 5.6.	Comparison of a portion of the two fragments of mutant canine kidney PDE6A transcript and amino acid sequence in the region of the mutation responsible for PRA in the <i>PDE6A</i> mutant dog	253
Figure 5.7.	Diagram demonstrating different PDE6A domains from the retina (A) and PDE6A fragment from kidney (B)	254
Figure 5.8.	Total RNAs separated by gel electrophoresis using 1.5% formaldehyde prior to blotting on a nylon membrane	258
Figure 5.9.	Northern blot probed with full-length canine retinal PDE6A cDNA probe	256

Chapter 1

Introduction

1.1. Ocular embryology

The components of the canine eye are derived from basically 3 embryonic tissues: neuroectoderm, surface ectoderm and mesenchyme (from neural crest cells) (Moore & Persaud, 1998). The eye starts to develop early in gestation, with ocular structures starting to form at the embryonic plate (neural plate) stage. At the site of the developing eye a flattened area develops on both sides of neural groove in the forebrain region. The neural groove sinks into the mesoderm, and detaches from the overlying surface ectoderm to form the neural tube from which the primitive central nervous system develops. At gestation day 13, before the anterior end of the neural tube closes, the optic grooves (optic sulci) are formed in dogs (Figure 1.1A) (Aguirre et al., 1972). A localized area of neuroectoderm grows outwards towards the surface ectoderm to form the primary optic vesicle (Figure 1.1B) at gestation day 15 in dogs. The optic vesicle remains connected to the forebrain by the optic stalk.

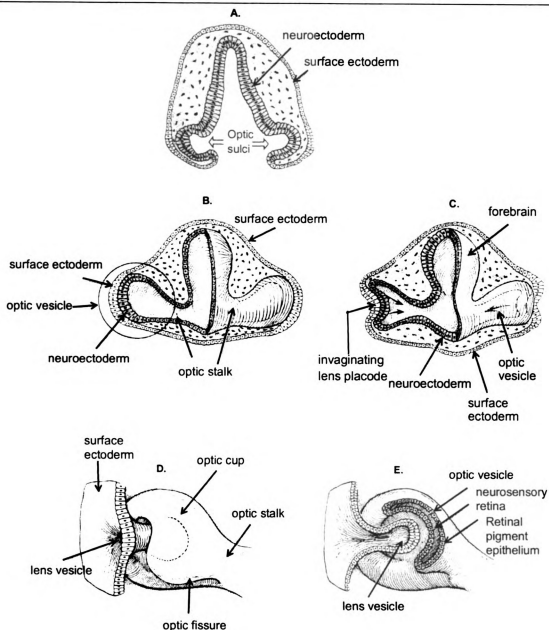


Figure 1.1. Human ocular embryology. Note that after optic sulci are formed (A), the surface ectoderm cells overlying the optic vesicles thicken to form the early lens placode (B). The lens placode invaginates to form the lens vesicle as the optic vesicle is forming the optic cup (C & D). Lens vesicle is positioned within the optic cup (E). (Moore & Persaud, 1998)

The optic vesicle induces the overlying surface ectoderm to thicken into lens placode at gestation day 17 (Figure 1.1C), on gestation day 19 as the optic vesicle invaginates and folds onto itself creating the optic cup, the lens placode also invaginates to form the lens vesicle (Figure 1.1D & 1.1E). A separation of the lens vesicle from the surface ectoderm later in development leads to the formation of the anterior chamber. An accompanying migration of mesenchyme between the surface ectoderm and the optic cup forms cornea endothelium and stroma. Surface ectoderm overlying the optic cup forms the corneal epithelium, while the neuroectoderm cells located at the anterior aspect of the optic cup become the epithelium of the iris, which is continuous with the epithelium of the ciliary body. At gestation day 25 where the optic cup meets the optic stalk there is an opening on the ventral surface, the optic fissure, which allows vasculature access to the inside of the developing globe (Flower et al., 1985).

The inner (non-pigmented) layer and the outer (pigmented) layer of the posterior aspect of the bi-layered optic cup become the neurosensory retina and retinal pigment epithelium (RPE), respectively. At the time of lens placode induction (gestation day 17), the retinal primordium consists of an outer (nuclear) zone and inner (anuclear) zone, which then form outer and inner neuroblastic layers, which are separated by the fiber layer of Chievitz at gestation day 32. Retinal primordium at this stage consists of the nerve fiber layer, inner neuroblastic layer, proliferative zone, outer neuroblastic layer and outer limiting membrane. Cellular differentiation of the retina, after the opening of the eyelids (postnatal day 10-14), results in 3 layers of neurons. The outer layer consists of photoreceptor cells (rods and cones), the first-order neurons. The middle layer consists of

the second-order neurons, mainly bipolar, horizontal, amacrine and also the cell bodies of glial cells known as Müller cells. The inner layer consists of ganglion cells (the third-order neurons) and displaced amacrine cells.

1.2. Ocular anatomy

The globe and extraocular muscles are contained within a conical cavity, called the orbit. The orbit provides protection to the eyeball and is accessed by various blood vessels and nerves involved in the function of the eye. The wall of the globe comprises of 3 layers: the fibrous tunic (sclera and cornea), the vascular tunic (choroid, ciliary body and iris), and the nervous tunic (retina).

The fibrous tunic is composed of two parts; sclera and cornea. It is responsible for maintaining the shape of the eye, protecting it from the external environment, transmitting and refracting of light rays via the cornea and providing a location for insertion of the extraocular muscles. The sclera consists of a dense network of collagen and elastic fibers and encloses the posterior three-fourths of the globe. The cornea is transparent and located in the anterior portion of the globe. Its transparency is due to a highly ordered arrangement of collagen fibrils and lack of pigment, vessels, and myelinated nerve fibers.

The vascular tunic (uveal tract) is the middle layer of the eye and is interposed between the retina and the sclera. It is composed of choroid, ciliary body and iris. The

choroid is a pigmented vascular layer that makes up the posterior portion of the uveal tract. The tapetum lucidum, a specialized reflective layer of the choroid, is present in the superior fundus of most domestic species including the dog. It is thought to increase the sensitivity of the retina to low light levels by reflecting light back through the overlying photoreceptor layer (Elliott & Futterman, 1963). The ciliary body is the middle segment of the vascular tunic positioned between the iris and choroid and is highly vascular. It is responsible for aqueous production and outflow. The zonular ligament, which originates from the ciliary body attaches to the lens capsule to suspend the lens. Ora ciliaris retina (ora ciliaris retina) is the boundary where the ciliary body ends posteriorly at the adjacent retina. The iris is the anterior most segment of the vascular tunic, connecting with the ciliary body at the periphery. It acts as a diaphragm to regulate the amount of light that enters through the pupil via two muscles; the sphincter muscle innervated by the parasympathetic nervous system, and the dilator muscle innervated by sympathetic and some parasympathetic nerves.

The retina is the innermost layer of the posterior segment of the globe. It develops from the two walls of the optic cup. The outer wall, a single layer of cells, forms the retinal pigment epithelium (RPE) whereas the invaginated inner wall of the optic cup adjacent to the vitreous chamber develops into the neurosensory retina. Macula is a small area near the center of the retina of the human eye, where it is histologically defined as having two or more layers of ganglion cells. Near its center is the fovea, a small cone-rich region, which is also present in primates, birds and reptiles. The fovea is free from rods. Instead of a fovea many domestic species have an area centralis, an area of higher cone

density (Henkind, 1966). Nutrient supply to the inner and outer layers of the retina originates from retinal and chorioidal vessels, respectively. The vascular pattern of the retina varies between species (Simoens et al., 1988). The dog has a holoangiotic retina in which there is a relatively uniform vascularization of the entire retina (Engerman et al., 1966).

Histologically 10 layers of the retina are recognized (Figure 1.2.). The 10 layers from proximal to distal are RPE, photoreceptor layer (PRL), outer limiting membrane (OLM), outer nuclear layer (ONL), outer plexiform layer (OPL), inner nuclear layer (INL), inner plexiform layer (IPL), ganglion cell layer (GCL), nerve fiber layer (NFL), and inner limiting membrane (ILM).

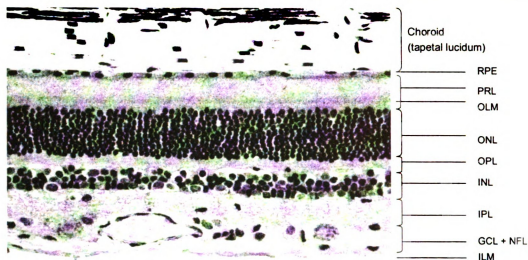


Figure 1.2. Cross section of canine retina. A cross section of canine retina shows the 10 layers recognized histologically. Key: RPE = retinal pigment epithelium, PRL = photoreceptor layer, OLM = outer limiting membrane, ONL = outer nuclear layer, OPL = outer plexiform layer, INL = inner nuclear layer, IPL = inner plexiform layer, GCL = ganglion cell layer, NFL = nerve fiber layer, and ILM = inner limiting membrane.

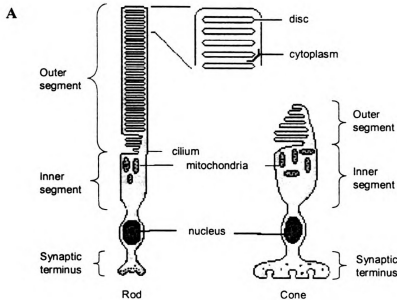
1.2.1. Retinal pigment epithelium

The RPE is a single layer of epithelial cells located between the choroidal vasculature and the neurosensory retina. Cells within the RPE are pigmented because they contain melanosomes except for those overlying the tapetal lucidum. The apical surface of the RPE has cytoplasmic apical processes which engulf the outermost portion of photoreceptor outer segments. They act to support the photoreceptors as well as phagocytize photoreceptor outer-segment discs. Disc shedding from the outer segments and phagocytosis by the RPE is controlled by several factors, such as duration of the light/dark cycle (Besharse et al., 1977) and melatonin levels (Besharse & Dunis, 1983).

The RPE is involved in the visual cycle whereby 11-*cis* retinal is generated and supplied to the photoreceptors. In addition, the RPE serves as part of the blood-retinal barrier which limits the diffusion of large molecular-weight molecules from choroidal vessels into the retina (Steuer et al., 2004).

1.2.2. Photoreceptor layer

There are two main types of photoreceptors (rod and cone), both of which consist of four functional segments: the outer segment, the inner segment, the cell body/soma and the receptor terminus (Figure 1.3.). The photoreceptor layer consists of the outer and inner segments of photoreceptors, while their nuclei and termini are positioned in the ONL and OPL, respectively. Rods are responsible for night time vision and cones are for day time vision, as well as higher visual acuity and color vision.



B.

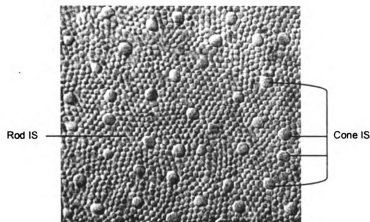


Figure 1.3. A. A schematic drawing of structural elements of rod and cone. Note that the structure of rods and cones is similar, except for size and shape. Additionally, cone outer segment discs are continuous with the cell membrane, whereas rod outer segment discs are separated from the cell membrane. B. A Differential Interference Contrast image of canine central retina from a flat mount preparation focused at the level of the inner segments (magnification 100X). Cone inner segment diameter is approximately 6 times that of rod inner segments (as shown in B).

The outer segments of rods are long and uniform in width while those of cones are cone-shaped. The outer segments consist of a stack of disc shaped membrane. In rods, the discs are separated from the plasma membrane whereas in cones, discs are continuous with the membrane (Steinberg et al., 1980). Rod and cone outer segments are connected to the inner segment by a cilium. The protein kinesin is closely associated with connecting cilia of photoreceptors. It is located at the axoneme that extends to the outer segment tip of cones (Eckmiller & Toman, 1998) whereas it is surrounding the basal body of the cilium, outer segment axoneme and part of inner segment in rods (Beech et al., 1996; Eckmiller & Toman, 1998). Not only is this protein involved in the translocation of materials between outer and inner segments (Muresan et al., 1997), but it is also involved in the formation of new photoreceptor disc membranes (Williams et al., 1992). During postnatal development in the mouse, membranous discs are formed by the random fusion of small vesicles with the apical swelling of the connecting cilium into a partial stack in order. A partial stack of discs is progressively rearranged during development to form a regular arrangement of outer segments in the mature retina (Obata & Usukura, 1992). The inner segments of rods and cones are responsible for metabolic function, protein synthesis and homeostasis (Baldridge et al., 1998). They contain cell organelles; centrioles, mitochondria, free ribosomes, smooth and rough endoplasmic reticulum, microtubules and small vesicles. Cone inner segments contain more number of mitochondria than rods, compared per unit volume of outer segment (Hoang et al., 2002).

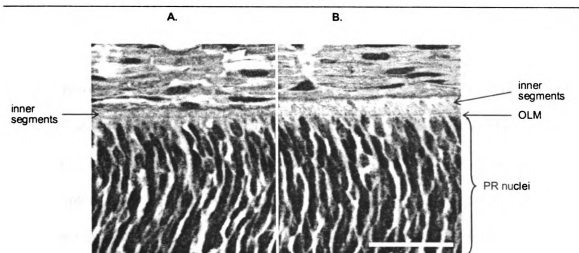


Figure 1.4. Histological section showing canine photoreceptors at 3 (A) and 10 (B) days of age. Note the inner segments have developed by 3 days of age. By 10 days of age, they have elongated. The outer limiting membrane is present. At this age, photoreceptor nuclei are oval in shape. Bar = 25 μ m.

1.2.3. Outer limiting membrane

The inner segments of photoreceptors are separated from the soma by the OLM (Figure 1.2 & 1.4). This thin membrane is composed of zonular adherens, which firmly attach the inner segments of photoreceptors to Müller cells and Müller cells to each other to provide structural support. Gap junctions within the OLM are composed of aggregates of particles of variable size and shape (Whiteley & Young, 1986). The pore radius of the zonulae adherens of the OLM is between 30 and 36 \AA , and thus helps to prevent the penetration of protein-rich fluid from the PRL to the inner retina when the outer blood retinal barrier is compromised from disease or injury (Buntmilam et al., 1985).

1.2.4. Outer nuclear layer

Photoreceptor cell bodies (soma) are located in the outer nuclear layer. Mature rod nuclei are round in shape, small and more heterochromatic than nuclei of cones. Cone nuclei are large, euchromatic and located close to the OLM. The density of photoreceptors is not uniform across the retina (Curcio, 1986). The density of cones in the dog is reported to be greater in the central retina compared to the periphery (Koch & Rubin, 1972). In humans, cone density declines rapidly towards the periphery from a peak at the fovea while rod density is the highest at a distance of about 3-5mm from the fovea, then its density decreases toward the periphery (Jonas et al., 1992).

1.2.5. Outer plexiform layer

Photoreceptor synaptic termini lie at the outer aspect of the OPL. Two morphologic categories of synaptic termini are recognized. The rod terminus is called a spherule and is small and round. The cone terminus is called a pedicle and is large and flat. Rod spherules have one or two invaginations whereas cone pedicles have numerous invaginations. Photoreceptor termini are filled with synaptic vesicles. Synaptic ribbons (synaptic lamella) are dense laminar structures present within the photoreceptor termini at the site of synaptic contact. Proteins that have a function in synaptic vesicle docking and fusion as well as endocytosis are present in ribbon synapses. This is an indication of synaptic membrane traffic in ribbon synapses (Ullrich & Sudhof, 1994). Glutamate, a

neurotransmitter, is released at ribbon synapses by the calcium-dependent exocytosis of synaptic vesicles (Morgans, 2000).

The typical appearance of invaginated synaptic processes in the photoreceptor termini are called triads and consists of a pair of horizontal cell processes flanking a bipolar cell dendrite (Sikora et al., 2005). Occasionally, synaptic units consist of two horizontal cells and two bipolar cells. This arrangement is called a tetrad (Migdale et al., 2003). Rods and cones are primarily interconnected by horizontal cells, the neurotransmitter glutamate, is released from photoreceptor termini to stimulate wide-field and narrow-field horizontal cells (Smith, 1995). Cone synaptic termini make contact with both a superficial, non-invaginated synapse to flat bipolar cells (Hopkins & Boycott, 1995) and an invaginating synapse within the triad to invaginating bipolar cells (Boycott & Hopkins, 1991).

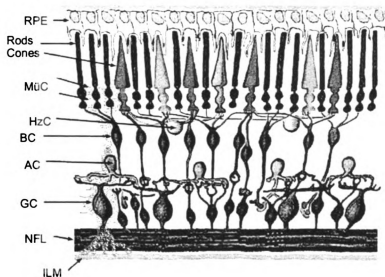


Figure 1.5. A simple diagram of the organization of the retina. Key: RPE = retinal pigment epithelium, MüC = Müller cell, HzC = horizontal cell, BC = bipolar cell, AC = amacrine cell, GC = ganglion cell, NFL = nerve fiber layer, and ILM = inner limiting membrane. (Source: www.webvision.med.utah.edu)

1.2.6. Inner nuclear layer

The inner nuclear layer is composed of the cell bodies of amacrine cells (AC), bipolar cells (BC), Müller cells (MüC), horizontal cells (HzC) and interplexiform cells. The average percentages of AC, BC, MüC and HzC differ among species. For example, in the mouse retina there are 41% of AC, 40% of BC, 16% of MüC and 3% of HzC (Jeon et al., 1998).

1.2.6.a. Amacrine cells

Amacrine cell bodies are located in the inner region of the INL. Narrow-field, bistratified amacrine cells (AII amacrine cells) are the most numerous amacrine cells in mammals and are known as rod-mediated depolarizing cells. Their axons terminate at the sublamina b of the IPL close to the GCL. Not only do the AII amacrine cell transmits the signal from rod bipolar cells via gap junction to ganglion cells, the AII amacrine cells also couple to themselves to improve signal/noise ratio in their network (Vardi & Smith, 1996). The A17 amacrine cells have diffuse axonal processes terminating at the sublamina b of the IPL. Reciprocal synapses of the A17 amacrine cells to rod bipolar cells suggest their role in the rod pathway (Hartveit, 1999). In addition to AII and A17 amacrine cells, other types of amacrine cells such as A2 and A8 amacrine cells are involved in cone pathways. The amacrine cells express ionotropic (NMDA, AMPA and kainate) and metabotropic (mGluR1, mGluR2, mGluR4 and mGluR7) glutamate receptors to uptake glutamate from the synaptic cleft (Duarte et al., 1998). Activation of these glutamate receptors stimulates the release of gamma aminobutyric acid (GABA) (Gleason et al., 1994) and acetylcholine (Linn et al., 1991) from amacrine cells. Calretinin is present in the AII amacrine cells (Gabriel & Witkovsky, 1998) and can be used as a marker for these cells.

1.2.6.b. Bipolar cells

Bipolar cells are the second-order neuron in the retina connecting the photoreceptors to the ganglion cells. Their dendrites synapse with photoreceptors and horizontal cells in the OPL, and axons synapse with amacrine and ganglion cells in the IPL. Each rod bipolar cell in the monkey connects to about 20 rods at 2-4 mm eccentricity and 60 rods at 6-7 mm eccentricity (Grunert & Martin, 1991). The connections have a sign-inverting synapse (ON-bipolar cells). Rod bipolar cell termini in the mammalian retina contact to ganglion cells via amacrine cells. There is no direct synapse between rod bipolar cells and ganglion cells. In some instances, rod bipolar cells contact the narrow-field, bistratified (AII) amacrine cells, which in turn make gap junctions with cone bipolar cells in the sublamina b of the IPL (Strettoi et al., 1994). Alternative rod pathways in rodents have been shown where rods bypass the rod bipolar cells and directly contact cone OFF-bipolar cells (Soucy et al., 1998; Hack et al., 1999).

All cone bipolar cells synapse with amacrine and ganglion cells. Two classes of cone bipolar cells based on responsiveness to light stimulation are recognized. They are depolarizing (ON or invaginating bipolar cells) and hyperpolarizing (OFF or flat bipolar cells). The synapses between cones and ON-bipolar cells and cones and OFF-bipolar cells are sign-inverting and a sign-preserving, respectively. Cone bipolar cells substantially outnumber rod bipolar cells all across retina in rabbits (Strettoi & Masland, 1995).

1.2.6.c. Müller cells

During development of the retina the retinal microglial cells originate from hemopoietic cells. These cells invade the developing retina via blood vessels. They play an important role in host defense against invading microorganisms, in immunoregulation, and tissue repair (Chen et al., 2002). Müller cells are the principal glial cells of the retina. Their nuclei are angular in shape with dense chromatin and are located toward the outer region of the INL. Müller cell processes extend radially from the OLM to the ILM. The classic type of Müller cell in mammals has diffuse and abundant descending processes. Numerous voltage-gated channels and neurotransmitter receptors are expressed in Müller cells and these modulate neuronal activity by regulating the extracellular concentration of neuroactive substances, including potassium (K^+), glutamate, GABA and hydrogen (H^+) (Newman & Reichenbach, 1996). In the OLM, Müller cell processes tightly ensheath photoreceptor termini (Derouiche, 1996). Müller cell processes at the end feet have the ability to phagocytose foreign substances and enwrap the axons of the nerve fiber layer to enhance electrical transmission along the ganglion cell axons. Morphological and cellular changes develop in Müller cell in response to retinal damage reflect their role in neuroprotection (Derouiche, 1996; Garcia & Vecino, 2003). Horizontal cells

1.2.6.d. Horizontal cells

Horizontal cell nuclei are located at the outer region of the INL with their processes extending horizontally through the OPL to couple with photoreceptors.

Horizontal cell dendrites are arranged on either side of the photoreceptor ribbon synapses along with bipolar cell dendrites at the center of the triad. This organization helps to include responses from the surrounding region of retina. Two types of horizontal cell are recognized in domestic species. Type A horizontal cells have no axons and synapse with all types of cones. Type B horizontal cells have axons and synapse with both rods and cones. The type A horizontal cell is strongly reactive to anti-calbindin-D antibody compared to type B horizontal cell (Lyser et al., 1994; Gabriel & Witkovsky, 1998). Calbindin can be used as a marker for type A horizontal cells.

1.2.6.e. Interplexiform cells

In the INL, interplexiform cells are positioned among amacrine cells and have processes that ramify in the OPL and IPL. They provide a feedback mechanism between the inner and outer retina. Most interplexiform cells are dopaminergic and well developed in Teleost fish, rodents, rabbit and primates (Nguyenlegros, 1991). In other species, these cells release either GABA or other neuroactive substances, such as glycine, somatostatin or serotonin. In the goldfish the synthesizing enzyme for epinephrine was identified in the interplexiform cells, and this transmitter influences horizontal cells (Baldridge & Ball, 1993; Savy et al., 1995). Dopaminergic interplexiform cells, along with amacrine cells are involved in the generation of the oscillatory potentials of the electroretinogram (ERG) (Citron et al., 1985).

1.2.7. Inner plexiform layer

The IPL is a multilaminated region containing different types of synapses between bipolar, amacrine, interplexiform and ganglion cell processes. A synapse between presynaptic cells (bipolar cells) and two postsynaptic cells; either a ganglion cell or amacrine cell process or two amacrine cells is known as a dyad. In the cat, OFF-bipolars and ON-bipolar cell axon termini are positioned in sublamina a (outer region) and sublamina b (inner region), respectively. They correspondingly synapse with ganglion cell subtype a and b. Rod bipolar axons synapse with A17 and AII amacrine cells in sublamina b (Kolb, 1979; Derouiche, 1996; Garcia & Vecino, 2003). In monkey and human retina, the IPL is divided into five layers. Amacrine processes are distributed in three bands corresponding to different levels of the peptides, dopamine, and GABA, whereas bipolar cell processes are distributed in four broadly overlapping bands (Koontz & Hendrickson, 1987). Some horizontal cells in the bovine retina have additional thick processes descending to the IPL, where they are postsynaptic at the dyads (Chun & Wassle, 1993).

1.2.8. Ganglion cell layer

This layer contains cell bodies of most of the ganglion cells, displaced amacrine cells and some astroglial cells as well as blood vessels. Morphologically, ganglion cells can be divided into three types; alpha, beta and gamma. The alpha ganglion cells have the largest cell bodies, uni-stratified dendrites and axons occupying two strata in the outer half of the

IPL (Wassle et al., 1981b). The beta ganglion cells have more branching dendrites than the alpha cells. The gamma ganglion cells have the smallest cell bodies, widely extended thin and winding dendrites, and are concentrated in the visual streak (Saito, 1983). In the cat retina, 55% of all ganglion cells are beta, 41% are gamma, and 4% are alpha cells (Wassle et al., 1981a).

Ganglion cells receive inputs from neighboring photoreceptors in a circumscribed area of the retina (their receptive field) and transmit these inputs as a train of action potentials. Two classes of ganglion cells, based on differential illumination of their receptive fields, are ON-center and OFF-center ganglion cells. The ON-center ganglion cells are depolarized when light is directed to the center of their receptive field, whereas OFF-center ganglion cells are hyperpolarized (Purves et al., 2004).

Displaced amacrine cells are present in the GCL in many species, including the dog (Marroni et al., 1995). These cells form synapses with other cell processes in the IPL (Wong & Hughes, 1987) and can be labeled for either GABA or glycine (Koontz et al., 1993). The proportion of displaced amacrine cells to ganglion cells varies among species. This ratio decreases during growth of the fish's eye (Mack et al., 2004). Five to 20% and more than 40% of the neurons in the GCL are displaced amacrine cells in the cat (Koontz et al., 1993) and hamster retina (Linden & Esberard, 1987), respectively.

1.2.9. Nerve fiber layer

Axons of ganglion cells, inner fragments of Müller cell processes and retinal blood vessels are present in the NFL. Ganglion cells have axons that converge to form the optic nerve, which projects to the lateral geniculate nucleus (LGN) of the thalamus. In the NFL, the axons are unmyelinated but as they converge on the optic nerve head, they gain a myelin sheath. The myelination of the fibers at the optic nerve head gives the canine optic nerve head its characteristic slightly raised appearance. Astroglial cells have a simultaneous contact with ganglion cell axons and blood vessels (Runggerbrandle et al., 1993). The majority of astroglial processes are aligned in parallel with the ganglion cell axons in the central region of the retina and are radially arranged in the periphery (Karschin et al., 1986).

1.2.10. Inner limiting membrane

The ILM is the innermost layer of the retina. Astrocytes and Müller cells contribute to the formation of this membrane. In the rabbit the ILM is a thin basement membrane throughout all areas of the retina, whereas the ILM of the cynomolgus monkey is a thick basement membrane in the peripapillary region and a thin basement membrane in the region of the fovea (Matsumoto et al., 1984). Like humans, the ILM in cynomolgus monkeys thickens with age (Matsumoto et al., 1984).

1.3. The central visual pathway

Visual information from the retina is conducted from all ganglion cells axons to the optic nerve where ganglion cell axons are bundled and myelinated. At the optic chiasm, the axons from the nasal portion of each retina cross to the contralateral side of the brain whereas axons from the temporal portion of the retina remain on the ipsilateral side of the brain. The degree of axon decussation varies between species. In the dog 78% of axons cross over to the contralateral side of the brain (Lee et al., 1999). From the optic chiasm, axons from the left portion of each retina project in the left optic tract and vice versa for axons from the right half. All axons project to three major subcortical regions; the lateral geniculate nucleus (LGN), the pretectum and the superior colliculus (Figure 1.6).

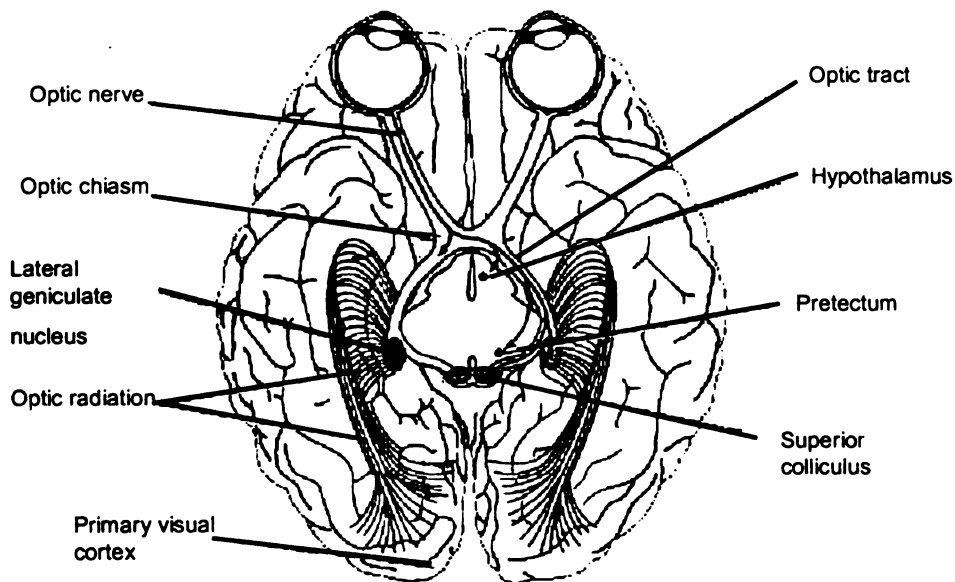


Figure 1.6. A schematic diagram demonstrating the central projection of the retina to subcortical regions of the brain as to the visual cortex. (Source: www.brain.phgy.queensu.ca/pare)

The superior colliculus lies on the roof of the midbrain. Signals are sent to the pulvinar nucleus of the thalamus and are involved in saccadic eye movements (Soetedjo et al., 2002). The pretectal area is located rostral to the superior colliculus in the midbrain. Cells in the pretectal area project to neurons in the Edinger-Westphal nucleus, which in turn provides parasympathetic innervation to the pupillary sphincter muscle that constricts the pupil (Hultborn et al., 1978). The majority of ganglion cell axons synapse in the LGN, a multilayered structure in the thalamus. The dog LGN consists of six layers A, A1, C, C1, C2, and C3. Layers A, C, and C2 receive contralateral inputs, and layers A1 and C1 receive ipsilateral inputs (Lee et al., 1999). Inputs from the right portion of the retina of each eye project to different layers of the right LGN to create a complete illustration of the left visual field and vice versa.

Axons from the LGN form the optic radiation that transmits the visual signal to the primary visual cortex (also called visual area 1, Brodmann's area 17 or striate cortex) lying on the medial aspect of the occipital lobe. Two classes of neurons; simple and complex cell, were described in the primary visual cortex (Dean & Tolhurst, 1983) based on discreteness of inhibitory and excitatory regions in the receptive field, spatial structure within each region and degree of relative modulation of the response. These cortical neurons in each cerebral hemisphere receive input exclusively from the contralateral hemi-field through different layers of the thalamus in an orientation-selective manner. Therefore, each area in the primary visual cortex is devoted to a specific part of the visual field (Vanduffel et al., 2002). Mapping of the visual field on the brain (retinotopic

mapping) through the retino-thalamo-striated pathway reflects the physiologic processing of the signal that has occurred in the retina (Roe et al., 1990).

1.4. The phototransduction pathway and visual cycle

Photoreceptors contain photopigments, light-sensitive elements, essential for phototransduction. Phototransduction is the process by which light energy (photons) are absorbed by photopigments in the outer segment of photoreceptors and converted to an electrical message. Rods function well in a dim light environment because they are exquisitely sensitive to light at low intensities. In addition, rods are highly convergent (Berntson et al., 2004); 20 to 60 rod photoreceptors converge upon each rod bipolar cell, thus adding to the retinal sensitivity. Due to these characteristics, rods are therefore responsible for the detection of shape and motion under a dim environment (Gegenfurtner et al., 2000). Cones on the other hand function well under bright light illumination. The presence of more than one cone type with different spectral sensitivity is responsible for color vision (Rabin, 1996). Moreover cones provide high visual acuity. As with most diurnal mammalian species, approximately 95% of photoreceptors in dogs are rods (Koch and Rubin, 1972) whereas only 5% are cones.

Photopigments consist of two components; a transmembrane protein (opsin) and 11-*cis*-retinal (a vitamin A₁-derived chromophore). In the rod the combination of opsin and 11-*cis*-retinal is known as rhodopsin. The rod and cone photopigments differ between species having peak sensitivity to different wavelengths of light. In most species, rods

only have one type of photopigment. The peak rod sensitivity in the dog is 508 nm (Jacobs et al., 1993) whereas in humans it is 497 nm (Bowmaker & Dartnall, 1980). One or more cone photopigments are present in most species. Dogs have two types of cone photopigments giving them dichromatic vision. One cone photopigment has peak sensitivity to light of 555 nm (green) and the other to 430 nm (blue) (Neitz et al., 1989). Mice also have two types of cone photopigment, one with peak sensitivity to 350 nm (UV-cone pigment) and the other one at 510 nm (midwave-cone pigment) (Lyubarsky et al., 1999). Humans have three types of cones providing trichromatic vision. The short-wave cones (blue cones) have peak sensitivity at 420.3 ± 4.7 nm, the middle-wave cones (green cones) 533.8 ± 3.7 nm and the long-wave cones (red cones) 562.8 ± 4.7 nm (Bowmaker & Dartnall, 1980).

Rods and cones exhibit similar phototransduction pathways although the proteins involved differ. The rod phototransduction pathway shown in figure 1.7 has been studied in detail while cone phototransduction has not been investigated in such detail.

The opsin protein has seven transmembrane domains and these surround the chromophore (11-*cis*-retinal). Absorption of light energy by the photopigment (rhodopsin) results in a conformational change converting inactive rhodopsin (Rho) into an activated form (Rho*) and photoisomerization of the chromophore from 11-*cis*-retinal into all-*trans*-retinal. The regeneration of the photopigment starts in the outer segment of photoreceptors by a reduction of the all-*trans*-retinal into all-*trans*-retinol (Fain et al., 2001), which is then transported to RPE via interstitial retinoid-binding protein (IRBP). Several intermediate steps occur in the RPE to convert all-*trans*-retinol into 11-*cis*-retinal, which is then transported via IRBP back to the outer segment of photoreceptors where it combines with opsin to form rhodopsin. This process is known as the visual cycle.

Activated rhodopsin formed by light bleaching stimulates transducin, which is the second protein complex in the phototransduction cascade, by forming rhodopsin-transducin binding complex. Transducin is a member of the G-protein family. It is a trimeric protein (Zhang et al., 2004) composed of three subunits; T α , T β , and T γ and is tightly bound to guanosine diphosphate (GDP). Transducin remains in an inactive state when the γ subunit is present. Following light stimulation, a conversion of GDP in the binding complex to guanosine triphosphate (GTP) occurs by the catalytic activity of activated rhodopsin, which in turn dissociates T β and T γ subunits. Activated transducin (T α -GTP) stimulates the cyclic GMP phosphodiesterase holoenzyme (cGMP-PDE).

CGMP-PDE is a heterotetrameric complex, consisting of two large catalytic subunits; alpha (PDE α ; 88 kDa) and beta (PDE β ; 84 kDa), and two identical inhibitory gamma subunits (PDE γ ; 11 kDa) (Stryer, 1991). Activated transducin molecules activate PDE by removing the two PDE γ subunits, leaving the PDE $\alpha\beta$ complex. Although each of the alpha (PDE $\alpha\alpha$) and beta (PDE $\beta\beta$) subunit complex of PDE have a low level of cGMP-hydrolytic activity, the presence of PDE in heteromeric (PDE $\alpha\beta$) form is required for full enzymatic activity (Piriev et al., 1993).

Activated PDE hydrolyzes cGMP to GMP. A reduction of cGMP concentration result in a closure of the cGMP-gated ion channels in the plasma membrane of the rod outer segment. Rod cGMP-gated channel protein is a heterotetrameric complex consisting of two molecules of each of the alpha and beta subunits. A glutamate residue in the pore region of the α -subunit of cGMP-gated ion channel is responsible for external cation blockage (Molday, 1998). Closure of the channels reduces the inward flow of cations. The Ca^{2+} level in the outer segment also decreases because of extrusion via the Na/Ca-K exchanger (Haase et al., 1990) primarily located on the rod outer segment plasma membrane. Under these conditions, rods become hyperpolarized (the dark current is abolished), and the release of neurotransmitter (glutamate) at the synaptic terminus of the rod is inhibited. In the dark where cGMP-PDE activity is low, about 5% of cGMP-gated channels are open allowing an influx of cations keeping the rod depolarized. This ion flow is responsible for the "dark current" and there is a constant release of the neurotransmitter glutamate from the rod synaptic terminal.

Several reaction pathways are responsible for inactivation of the phototransduction cascade. Phosphorylation of activated rhodopsin by rhodopsin kinase (RK) reduces the enzymatic activity of activated rhodopsin and generates an affinity of rhodopsin to bind to arrestin (Arr) (Alloway & Dolph, 1999). Arrestin binding to rhodopsin prevents future transducin activation. Hydrolysis of $T\alpha$ -GTP into $T\alpha$ -GDP results in deactivation of PDE (Vuong & Chabre, 1991) by releasing $PDE\gamma$ molecules to rebind to the $PDE\alpha\beta$ complex. In the mean time, $T\alpha$ -GDP is deactivated by rebinding to $T\beta$ and $T\gamma$ subunits. A decrease of intracellular Ca^{2+} due to closure of cGMP-gated channels mediates recoverin (RC), a Ca^{2+} -binding protein, to relieve inhibition of guanylate cyclase (GC) (Venkataraman et al., 2003). Activated guanylate cyclase synthesizes cGMP, and is activated by guanylate cyclase activating protein (GCAP) (Palczewski et al., 1994). Because activated GC re-synthesizes cGMP, an elevation of cGMP concentration results in a re-opening of some of the cGMP-gated ion channels, which consecutively increases the inward cation flow responsible for the dark current, leading to rod depolarization.

The reduction of intracellular Ca^{2+} levels following illumination also facilitates the termination of the phototransduction cascade. It helps to speed PDE deactivation (Kawamura & Murakami, 1991), and to increase cGMP levels by reducing the affinity of cGMP-gated channel for cGMP (Hsu & Molday, 1993).

1.5. Electroretinography

Stimulation of the retina by light alters electrical currents in the retina. Summation of these electrical activities throughout the entire retina can be recorded at the corneal surface as an electroretinogram (ERG). The components of the ERG reflecting responses from different retinal cell types have been studied for many years. The basis underlying ERG components were described by Ragnar Granit (Granit, 1933). Three components of the ERG; PI (process I), PII (process II), and PIII (process III) were described according to the order of disappearance of each electrical waveform recorded in the cat under deepening anesthesia. PI is a slow corneal positive potential responsible for the c-wave; PII is a faster corneal positive potential responsible for the b-wave; PIII is a fast negative potential responsible for a-wave (Figure 1.8).

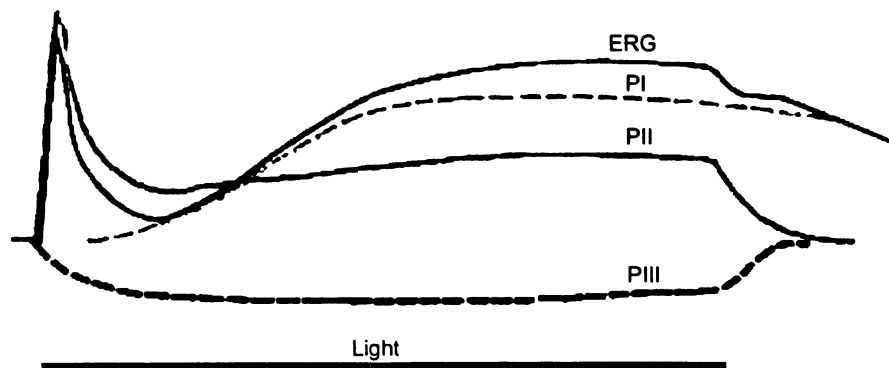


Figure 1.8. A diagram representing the electrical components (PI, PII and PIII) recorded in the retina as described by Granit. These components make up the electroretinogram. Bar indicates the duration of light stimulus.

Electroretinography is a very specific tool used to assess retinal function. Clinically ERG is often used to diagnose retinal diseases, particularly inherited retinal degenerative diseases (Acland, 1988), distinguish certain retinal disease from disease of the central nervous system, and to screen candidates for cataract surgery (Cruz & chi-Usami, 1989). A full-field ERG is recommended in order to record the summed activity of the entire retina, by homogeneously illuminating the retina (Birch & Anderson, 1992). This is typically achieved by the use of a ganzfeld bowl which is a hollow sphere with an opening for the subject's eye. The interior surface of the bowl is diffusely coated with a diffuse and reflective spectrally non-selective material.

Many factors, including biological factors (age, breed, and sex), recording techniques, type of light stimulation, anesthesia (Yanase & Ogawa, 1997) or technical problems, can affect the ERG recording (Komaromy et al., 2002). To ensure that the ERG is performed with uniformity, a global standard for clinical ERG is recommended for humans (Marmor et al., 2004d) by the International Society for Clinical Electrophysiology of Vision (ISCEV). A similar global standards is recommended for dogs (Narfstrom et al., 2002) by a committee of the European College of Veterinary Ophthalmologists (ECVO). A representative canine clinical ERG following these guidelines is shown in Figure 1.9.

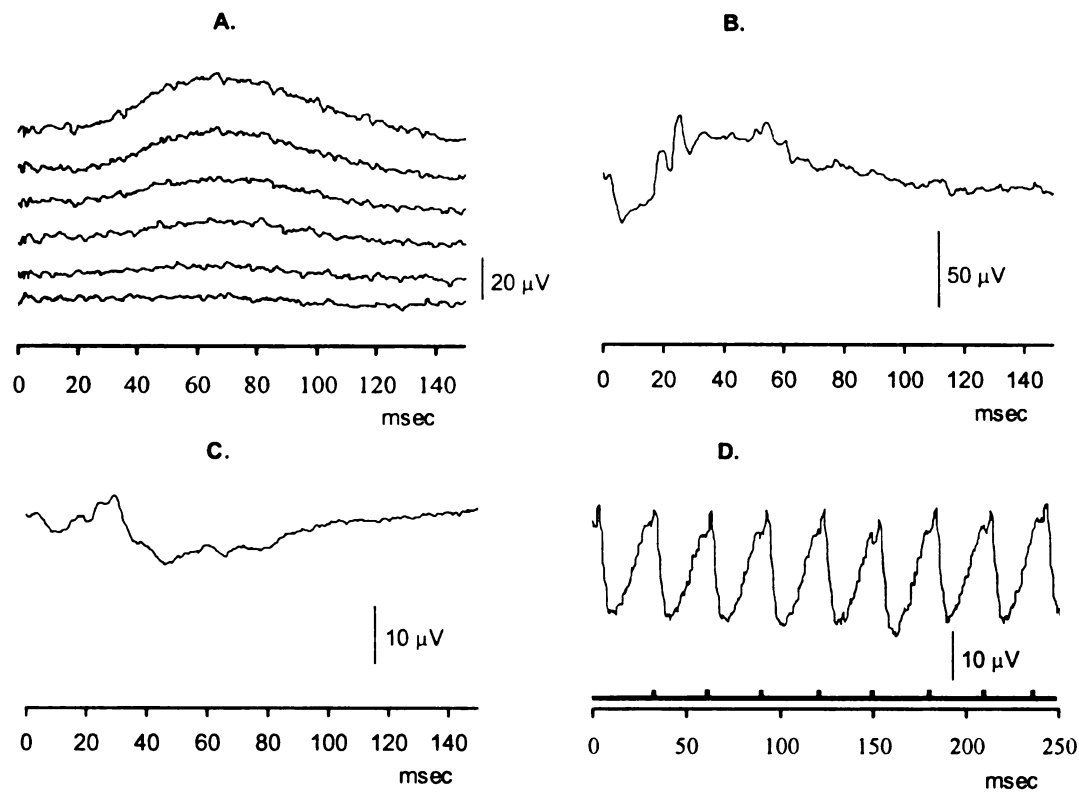


Figure 1.9. Canine clinical ERG recordings as recommended by the ERG committee of the ECVO; (A) single flash rod response recorded during dark adaptation (from bottom to top; 1, 4, 8, 12, 16 and 20 minutes of dark adaptation), (B) dark-adapted combined rod and cone response resulting from a stimulus of 1.9 log cds/m², (C) light-adapted cone only response resulting from a stimulus of 1.9 log cds/m² on a background of 1.47 log cd/m² and (D) cone flicker response of 0.39 log cds/m² at 33Hz. Light onset for A, B and C is at 0 msec. Spiking bar indicates light onset of cone flicker stimulus.

Research using pharmacological agents to block retinal pathways and the use of intra-retinal recording of ERG has been used to provide a better understanding of the origin of the components that make up the ERG. Detailed studies have revealed the following: A slow negative component seen at low light intensity prior to the b-wave threshold is the scotopic threshold response (STR) (Figure 1.10A). The STR in dogs, as well as other species, is transiently elicited by very dim light stimuli under dark-adapted

conditions (Yanase et al., 1996). Intraretinal recordings showed that the STR mainly originates from the proximal retina (Frishman & Steinberg, 1989). Further evidence for a proximal origin of the STR was provided by studies using sodium aspartate, a drug that blocks post-synaptic activity, unmasking photoreceptor responses. Application of this drug markedly reduced the STR amplitude, while the a-wave amplitude was undiminished (Wakabayashi et al., 1988).

An early signal after light stimulation which is generated by photopigment molecules during bleaching mechanism is called the early receptor potential (ERP). The ERP comprises of positive (R_1) and negative (R_2) deflections that appear very quickly after the onset of light. A blockage of cation influx due to closure of the cGMP-gated channel induces hyperpolarization of photoreceptors, shown as a negative-going potential (a major component of the a-wave) (Figure 1.10B). At appropriate light intensities the a-wave results from both rods and cones. It is present at bright lighter stimulus and grows in amplitude with increasing intensities. The canine a-wave is recordable by 10 days of age with higher intensities light stimulus (Kirk & Boyer, 1973b), and the amplitude increases with age. Because the a-wave is intruded upon by the rising phase of the b-wave (with the b-wave being derived from the ON-pathway), application of 2-amino-4-phosphonobutyrate (APB), a neurotransmitter agonist that selectively blocks the light response of ON-bipolar cells, to isolate the PIII (photoreceptor response) by eliminating the PII response (Knapp & Schiller, 1984a). Administration of APB showed that postsynaptic retinal activity postsynaptic to the photoreceptors contributes to the a-wave

(Bush & Sieving, 1994; Jamison et al., 2001) possibly by a feedback through horizontal cells.

The canine b-wave is first recordable at approximately 15 days of age (Kirk & Boyer, 1973a), which was similar to the age recorded in albino rabbit (Gorfinkel et al., 1988). The b-wave origin has long been investigated. A combination of electrical signals recorded from ON-bipolar (depolarized) cells and Müller cells result in a positive-going potential or the b-wave of the ERG (Stockton & Slaughter, 1989) (Figure 1.10A & 1.10B). Dissecting the origin of the b-wave using pharmacological agent revealed that b-wave is primarily the result of the depolarization of the ON-bipolar cells and partly from the Müller cells due to light-induced increase in extracellular potassium concentration in the inner retina (Dick & Miller, 1985c; Stockton & Slaughter, 1989) as well as from the depolarized third-order neurons (Wurzig et al., 2001). Moreover, the OFF-bipolar (hyperpolarized) cells and horizontal cells have been shown to play a role in shaping the photopic b-wave (Sieving et al., 1994).

Wavelets superimposed on the ascending and the top of the b-wave are called oscillatory potentials (OPs) (Fig 1.10B). These are present in responses recorded from both dark- and light-adapted retina (Wachtmeister, 1998). The major origin of OPs is the amacrine cells. These cells generate a tangential inhibitory feedback circuit within the retina (Heynen et al., 1985). OPs are markedly reduced by administration of the inhibitory neurotransmitter glycine. Interplexiform cells are believed to play a role in developing the OPs (VAEGAN & Millar, 1994).

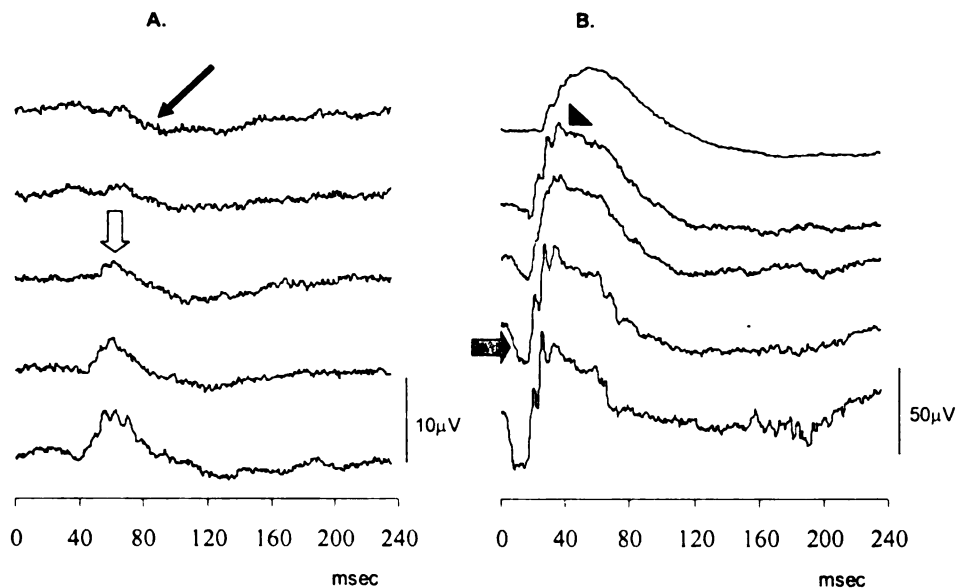


Figure 1.10. Components of canine scotopic full-field intensity-series ERG recorded after 1 hour of dark adaptation. Intensities are -3.39, -3.18, -2.98 -2.79 and -2.6 log cds/m² (1.10A) and -2.0, -0.79, -0.39, -0.001 and 0.39 log cds/m² (1.10B). Key: thin arrow = STR, open arrow = b-wave, arrowhead = OPs, solid arrow = a-wave.

The c-wave is a slow corneal-positive waveform that can be recorded using the direct current (d.c.) recording technique. It is not seen when the more commonly utilized alternating current (a.c.) recording technique is used. The c-wave originates from the RPE (Hanitzsch & Lichtenberger, 1997) and Müller cells (Zeumer et al., 1994) as a result of an increase of K⁺ concentration around the cells after light stimulation. Changes in c-waves are mostly the result of pathological changes in the RPE or occlusion of the central retinal artery in humans.

The Photopic Negative Response (PhNR) is a negative-going wave that follows the b-wave (Figure 1.11) in the light-adapted eye. PhNR is reduced in patients with glaucoma (Colotto et al., 2000) and optic neuropathy (Rangaswamy et al., 2004b). Blockage of the voltage-gated sodium current by tetrodotoxin eliminates the PhNR in rat (Bui & Fortune, 2004b) and monkey (Viswanathan et al., 1999).

Rod and cone pathways, active when the retina is stimulated by light, are the on-pathway through a sign-inverting synapse between photoreceptors and ON-bipolar cells. In addition to synapsing with ON-bipolar cells, cones also contact OFF-bipolar cells through a sign-preserving synapse in the cone off-pathway. This pathway is active when retinal illumination stops. The resulting response recorded at light offset is an off-response (d-wave). In the ERG resulting from a brief flash of light, on- and off- responses are superimposed. Using a long duration light illumination separates off response from the responses that occur at light onset. There are 2 forms of recognized d-wave. The d-wave in human and monkey is a phasic wave of positive polarity (Brown, 1979). The d-wave is suggested to originate from the off-bipolar cells (Dick et al., 1979) through a potassium-mediated mechanism. The canine d-wave has a small positive component followed by a predominant negative-going wave (Figure 1.11). Cats and amphibians also have a negative off-response (Dick & Miller, 1985b). Granit (1935) suggested that the positive d-wave can be recorded from the I-type (inhibitory) retina where the negative d-wave is recorded from the E-type (excitatory) retina. The difference between the I- and E-type retinas might depend on the difference in the number of cones between species.

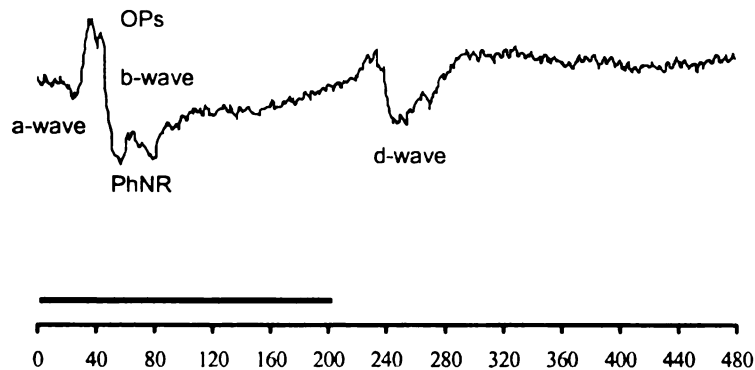


Figure 1.11. A canine long flash ERG recorded after 10 minutes of light adaptation; a-wave, b-wave, OPs, PhNR, and d-wave are indicated. Bar indicates the flash duration (200 msec).

1.6. Inherited retinal dystrophies in humans

Inherited retinal dystrophies or degenerations are one of the leading causes of hereditary blindness in humans and animals. They may be categorized by phenotypic features (fundus features, age of onset, rate of progression, etc), and mode of inheritance or where the caused mutation is known by the function of the mutant gene.

Retinitis pigmentosa (RP) is one group of inherited retinal dystrophies in humans. Patients with RP typically have progressive loss of visual field resulting in tunnel vision, night blindness and degenerative changes of the retina. In addition to vision loss, symptoms associated with RP include headache, light flashes (Heckenlively et al., 1988) and photophobia. Secondary cataract formation, in particular the posterior subcapsular

form, is common, usually manifesting at the later stage of the disease (Dilley et al., 1976; Merin, 1982). Ocular abnormalities progress over the years, and result in a severe reduction or a complete loss of vision. Autosomal dominant (auRP), autosomal recessive (arRP) and X-linked (XLRP) forms of RP are recognized. Patients with X-linked RP have the worst visual acuity among RP of the three major modes of inheritance (Grover et al., 1999).

The overall incidence of RP in the United States was approximately 1:3,700 (Boughman et al., 1980). At the time of writing, 34 genes and an additional 26 gene loci have been identified as cause for RP (www.sph.uth.tmc.edu/Retnet/home.htm). Mutations have been identified in genes involving in biochemical pathways, such as the phototransduction cascade or visual cycle, in gene involved in retinal structure and in gene involved in retinal development and maintenance. Twenty six loci (14 identified genes) are known to cause adRP. The commonest known mutations for adRP are in the rhodopsin (Musarella, 1990; Sung et al., 1991; Scott et al., 1993; Arning et al., 1996) and peripherin/RDS genes (Goldberg & Molday, 2000). For arRP, 16 caused genes and additional 11 gene loci have been identified such as the genes encoding Retinal pigment epithelium-specific 65 kD protein (RPE65) (Morimura et al., 1998), beta subunit of rod cGMP-PDE (PDE6B) (Danciger et al., 1995), alpha subunit of rod cGMP-PDE (PDE6A) (Danciger et al., 1995; Dryja et al., 1999), and retinaldehyde-binding protein 1 (RLBP1) (Burstedt et al., 2000). Retinitis Pigmentosa GTPase regulator (RPGR) is known to be responsible for some forms of the X-linked RP (Humphries et al., 1990; Musarella, 1990) that have been mapped and cloned. Simultaneous mutation in the two independent genes,

peripherin-2 and Rom-1, have been reported as a cause of digenic inheritance in RP patients (Loewen et al., 2001).

The characteristic features of ophthalmoscopic changes due to RP are spindle-shaped pigmented deposits around retinal vasculature that result from pigmentary disturbance in the RPE layer, a thinning of the RPE in the mid- and far-peripheral retinal region, a waxy pallor of the optic disc head and attenuation of retinal arterioles. The severity of these features increases with age. Histologically, patients with RP develop degenerative changes in photoreceptors and RPE cells. Patients have a significant reduction in rod function and sensitivity recorded from a full-field electroretinogram (Shady et al., 1995) while a reduction of cone-isolated responses was found in peripheral regions of the retina (Holopigian et al., 2001).

1.7. Inherited retinal degenerations in dogs and cats

Progressive retinal atrophy (PRA) describes a group of inherited retinal degenerations in dogs and cats and is the equivalent of retinitis pigmentosa. PRA was first reported in the English setter in the early 1900's. It is now recognized in many breeds of dog (see Table 1.1.) as well as two forms in the Abyssinian cat (Narfstrom, 1983; Curtis et al., 1987) and one form in Persian cats (Rah et al., 2005). PRA can be divided by age at disease onset into developmental (early-onset) and degenerative (late-onset) forms. In the early-onset form there is arresting photoreceptor development prior to maturation, while those with the late-onset form have normal photoreceptor

development followed by subsequent degeneration. Most forms of PRA in dogs are inherited in an autosomal recessive manner. However, a dominant inherited form of PRA has been described in the English mastiff and Bull Mastiff breeds (Kijas et al., 2002; Kijas et al., 2003). Additionally, two X-linked forms of PRA have been described in dogs. One in the Siberian husky (Acland et al., 1994; Zeiss et al., 1999) and the other in crossbred dogs (Zhang et al., 2002). Of the two forms of PRA in the Abyssinian cat, one is dominant (Curtis et al., 1987) and the other is recessive (Narfstrom, 1983).

BREED	DISEASE	GENE	ONSET OF FUNDUS ABNORMALITY	REFERENCES
EARLY ONSET				
Irish setter	rcd1	PDE6B	16 wks	(Lewis, 1977)
Collie	rcd2	?	16 wks	(Wolf et al., 1978)
Cardigan welsh corgi	rcd3	PDE6A	16 wks	(Petersen-Jones et al., 1999)
Norwegian elkhound	rd	?	5 mths	(Aguirre & Rubin, 1971)
Norwegian elkhound	erd	?	6 mths	(Acland and Aguirre, 1987)
Belgian shepherd	UN	?	11 wks	X
Miniature schnauzer	pd	PDC	1.5-5 yrs	(Zhang et al., 1999)
Sloughi	UN	PDE6B	> 4-5 yrs	(Dekomien et al., 2000)
Persian cat	pra	?	6 wks	(Rah et al., 2005)
Abyssinian cat	rdy	?	8-12 wks	(Curtis et al., 1987)
LATE ONSET				
Poodle; Miniature, Toy & Standard	prcd	*	3-5 yrs	(Koskinen et al., 1985)
American cocker spaniel	prcd	*	3-5 yrs	(MacMillan & Lipton, 1978)
Portugese water dog	prcd	*	3-6 yrs	X
Labrador retriever	prcd	*	4-8 yrs	(Kommonen & Karhunen, 1990)
English cocker spaniel	prcd	*	4-6 yrs	X
Dachshund; miniature longhaired	pra	?	5-7 mths	(Curtis & Barnett, 1993)

Table 1.1. Summary of the different types of progressive retinal atrophy (PRA) in dogs and cats. Key: PDE6A = alpha subunit of phosphodiesterase, PDE6B = beta subunit of phosphodiesterase, erd = early retinal degeneration, NR = no report, PDC = phosducin, pd = photoreceptor dysplasia, pra = progressive retina atrophy, prcd = progressive rod cone degeneration, rdy = retinal dystrophy, rcd = rod-cone dysplasia, rd = rod dysplasia, UN = un-classified, X-pra = X-linked progressive retina atrophy.

BREED	DISEASE	GENE	ONSET OF FUNDUS ABNORMALITY	REFERENCES
LATE ONSET				
Tibetan terrier	pra	?	1-1.5 yrs	(Barnett & Curtis, 1978)
Akita	pra	?	1.5-2 yrs	(Toole & Roberts, 1984)
Samoyed	pra	?	2-4 yrs	(Dice, 1980)
Irish wolfhound	pra	?	NR	(Gould et al., 1997)
English setter	pra	?	> 7yrs	(Bjerkas, 1990)
Tibetan spaniel	pra	?	3-4 yrs	(Bjerkas & Narfstrom, 1994)
Papillon	pra	?	> 3 yrs	(Narfstrom & Wrigstad, 1999)
Mastiff	pra	Rod opsin	?	(Kijas et al., 2003)
Abyssinian cat	pra	?	1.5-2 yrs	(Narfstrom, 1983)
Siberian husky	X-pra	RPGR	1.5-2 yrs	(Acland et al., 1994)
Mixed breed	X-pra	RPGR	?	(Zhang et al, 2002)

Table 1.1 (continued)

Star (*) indicates the gene for prcd locus reportedly been identified although this information has not been published of the time of writing. Question mark (?) indicated the gene responsible for PRA in the particular breed has not been indicated. X indicated no direct scientific reference for that particular breed.

Note that PRA is also reported in other dog breeds; American Eskimo dog, Australian cattle dog, Australian shepherd, Basenji, Chesapeake bay retriever, Doberman pinscher, Entlebucher mountain dog, German shorthaired pointer, Newfoundland, Nova Scotia duck tolling retriever, Border collie and Shetland sheepdog (www.optigen.com).

Similar to RP, PRA is a bilateral condition with both eyes affected to a similar extent. The earliest clinical sign in PRA-affected dogs is often impaired vision in dim light. As the retina undergoes degeneration, the pupillary light reflex is affected, and becomes more sluggish with progression of the disease. Nystagmus is reported in Abyssinian cat with dominant PRA (Curtis et al., 1987). Ophthalmoscopically, most PRA forms show a progressive development of tapetal hyperreflectivity and attenuation of retinal blood vessels as the retina undergoes degeneration (Figure 1.12). Depigmentation mixed with patchy areas of increased pigmentation develops in the nontapetal fundus with advanced disease. Atrophy of the optic nerve head also develops. Secondary cataracts are common in PRA-affected dogs, particularly those with late-onset disease (Priester, 1974). Electroretinography is a useful tool to detect functional changes in the retina of the PRA-affected animals prior to development of ophthalmoscopic changes.

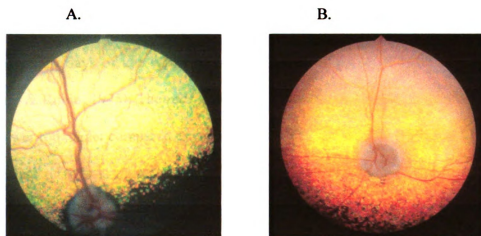


Figure 1.12. Fundus photography of a normal control dog (A) and a Corgian Welsh corgi with progressive retinal atrophy at 18 weeks of age (B). Note that mutant fundus (B) has tapetal hyperreflectivity, attenuation of retinal blood vessels and optic nerve head atrophy.

Several genes associated with PRA had been identified (Lin et al., 2002), however more genetic investigation is still required. Two mutations in the gene encoding the beta subunit of PDE (PDE6B) protein are reported as a cause of PRA in two breeds of dog; Irish setter (Suber et al., 1993) and Sloughi (Dekomien et al., 2000). Mutations in this gene are also reported in humans with arRP (Danciger et al., 1995). PRA in the Irish setter is known as rod-cone dysplasia type 1 (*rcd1*) and is due to a nonsense mutation at codon 807 of the PDE6B (Suber et al., 1993). The PDE6B gene in the *rcd1* dog has a transition of guanine to adenine at nucleotide 2420 that is predicted to cause a premature termination of the PDE6B protein by 49 amino acid residues. The truncated PDE6B protein, if translated, would be lacking the membrane binding site and part of the catalytic domain. Mutant dogs have a deficiency in PDE catalytic activity and subsequently develop on accumulation of cGMP (Suber et al., 1993). A significant reduction in the level of PDE6B mRNA is present in the developing *rcd1* retina prior to retinal degeneration (Farber et al., 1992). Rod flicker ERG responses could not be detected at 24 days of age whereas cone flicker responses were present but abnormal (Aguirre & Rubin, 1975). The *rcd1* Irish setter has disorganization of rod outer segments with fewer rod nuclei compared to cone nuclei by 6 weeks of age. These changes reflect a severe loss of rods at an early age, with simultaneous a slower degeneration of cones. Loss of day time vision was present by as early as one year of age.

PRA in the Sloughi was found to be due to an 8-bp insertion in exon 21 of PDE6B (Dekomien et al., 2000). It seems likely that the form of PRA in the Sloughi will also be rod-cone dysplasia, although there are no histological or ERG studies to

characterize the disease. Mice with PDE6B defects have a variability in phenotype that correlates to the predicted effect of the mutation (Hart et al., 2005).

A dominantly inherited form of PRA has been described in the Mastiff and Bull Mastiff breeds (Kijas et al., 2003) (Kijas et al., 2002). Dominant PRA in the Mastiffs is caused by a mutation in the rod opsin gene, a common cause of RP. The affected dogs have an abnormal ERG by 12-18 months of age. The ophthalmoscopic signs of this form of PRA are not typical. The more severely affected parts of the retina are those that are predicted to receive more light exposure. Therefore, the central retina is more severely affected, with hyperreflectivity being seen around and lateral to the optic nerve head. Hyperreflectivity of the peripheral retina does not develop until later in the disease.

At the time of writing the genes that cause PRA in cats have not been reported. However, Rhodopsin, ROM1, PDE6G (Gould & Sargan, 2002) and phosducin (Gorin et al., 1995) were excluded as candidate genes for retinal dystrophy in the *rdy* Abyssinian cats. The *rdy* Abyssinian cats with an autosomal dominant trait (Curtis et al., 1987) develop ocular abnormalities at a young age. Severe degeneration of outer segments of photoreceptors occurs in *rdy* kittens by 22 days of age with impairment of development of inner segments. Persian cats with PRA develop vascular attenuation as early as 5 weeks of age, followed by marked tapetal hyperreflectivity at 16 weeks of age. At this time, retinal vascularization is barely visible and only one or two rows of photoreceptor nuclei remain. Abnormality of RPE such as cytoplasmic vacuolation and cell swelling also occurs in cats with the PRA in this breed (Rah et al., 2005).

In the Miniature schnauzer affected with photoreceptor dysplasia (pd), a missense mutation was detected in codon 82 of phosducin (Zhang et al., 1998). It was predicted that the mutation would create a non-conservative substitution (Arginine to Glycine) in the translated protein, with the altered amino acid being located close to the amino acid that directly interacts with the $\beta\alpha$ -subunits of transducin. This mutation is deleterious to retinal function and causes by a decrease in ERG response and a retardation of photoreceptor development by 24 days of age (Parshall et al., 1991). However, some dogs with the mutation are heterozygous for the mutant allele, and some are homozygous for the wild-type allele. Thus, the disease alleles at more than one PRA causing locus may be segregating in the Miniature schnauzer breed.

Currently two forms of X-linked PRA in dogs are recognized and they are due to separate mutations within a similar region of the RP GTPase regulator (RPGR) gene. Despite the mutations being in the same region of the same gene, the phenotypes differ. The disease, X-linked PRA type 1 (*XLPR1*) that occurs in the Siberian husky and Samoyed breeds, is less severe than disease the X-linked PRA type 2 (*XLPR2*) that was identified in a line of crossbred dogs (Zhang et al., 2002). The mutations in the two canine diseases involve the gene called open reading frame 15. The mutations are in the same region of the human gene that has been described as being a mutation “hot-spot” for several different X-linked retinitis pigmentosa (Vervoort et al., 2000). Dogs with *XLPR1* have ERG abnormalities are present from 6 months of age and there is a rod-led retinal degeneration leading to an “end-stage” retina by 4 years of age. *XLPR2*-affected dogs have abnormal photoreceptor development with ERG abnormalities from 6 weeks

of age. A progressive retinal degeneration follows, resulting in an “end-stage” retina by approximately 2 years of age.

A late-onset PRA or progressive rod-cone degeneration (*prcd*) has been reported in several breeds of dogs (see table 1.1) and a phenotypically similar disease is seen in the Abyssinian cat with a recessive mode of inheritance. Opsin (Ray et al., 1999), rhodopsin, rds/peripherin (Ray et al., 1996), phosducin (Lin et al., 1998), and PDE6B (Acland et al., 1998) were excluded as breeds responsible for *prcd*. The *prcd* locus was mapped to canine chromosome 9. The mutation is reported to have been identified but not published at the time of writing and is in previously undescribed gene (G. Acland personal communication to S. Petersen-Jones, 2005). Histopathological and ERG studies have shown that *prcd* dogs have a normal development and functional maturation of the retina followed by rod-led photoreceptor degeneration.

PRA in Cardigan Welsh corgis was first reported in the veterinary literature in 1972 (Keep, 1972). It is an early-onset form of PRA that leads to night blindness detectable from as early as 7 weeks of age. Loss of daytime vision occurs more slowly and the age of which the dogs are totally blinded varies between individuals.

PRA in Cardigan Welsh corgis is autosomal recessive and due to a one-base pair deletion of an adenine at codon 616, nucleotide 1939-1940 (numbering according to Kylma and others (Kylma et al., 1997) in the alpha subunit of rod cGMP-PDE (PDE6A). This results in a frame shift with a run of 28 codons encoding for altered amino acids and

followed by a premature termination codon (Figure 1.13B). This is predicted to result in truncation of the protein by 218 amino acids, if the mRNA is translated (Petersen-Jones et al., 1999). The translated protein would be missing part of the catalytic domain (Baehr et al., 1991) and the C-terminal cysteine responsible for membrane binding (Ong et al., 1989). It is therefore most likely a functional null mutation.

```

      Exon 14      Exon 15
901  CAGAGGCACC AACAATCTCT ACCAGATGAA GTCCCGAAGC CCACTGGCCA
      R   G   T   N   N   L   Y   Q   M   K   S   Q   N   P   L   A

951  AGCTCCATGG GTCCTCCATC TTGGAAAGAC ACCACTTGGG GTTCGGCAAA
      K   L   H   G   S   S   I   L   E   R   H   H   L   E   F   G   K
                                Exon 16
1001 ACGTTGCTGC GAGATGAGAG CCTGAATATC TTTCAAAACC TCAATCGCAG
      T   L   L   R   D   E   S   L   N   I   F   Q   N   L   N   R   R

1051 GCAGCAGGAG CACGCCATCC ACATGATGGA CATAGCAATC ATTGCCACAG
      Q   H   E   H   A   I   H   M   M   D   I   A   I   I   A   T
                                Exon 17
1101 ACCTCGCCCT GTATTTCAAG AAGAGGACAA TGTTCAGAAA GATCGTGGAT
      D   L   A   L   Y   R   K   K   R   T   M   F   Q   K   I   V   D

```

901 CAGAGGCACC AACAATCTCT ACCAGATGAA GTCCCGAGACC CACTGGCCAA
 R G T N N L Y Q M K S Q T H W P
 951 GCTCCATGGG TCCTCCATCT TGGAAAGACA CCACTTGGAG TTCGGCAAAA
 S S M G P P S W K D T T W S S A K
 1001 CGTTGCTGCG AGATGAGAGC CTGAATATCT TTCAAACCT CAATCGCAGG
 R C C E M R A .
 1051 CAGCACGAGC ACGCCATCCA CATGATGGAC ATAGCAATCA TTGCCACAGA
 1101 CCTCGCCCTG TATTTCAGA AGAGGACAAT GTTCCAAAAG ATCGTGGATC

49

A DNA-based test using a mismatch PCR-restriction enzyme digestion was developed (Petersen-Jones & Entz, 2002) to ascertain the genotype of dogs for the presence of the codon 616 adenine 1-bp deletion in the PDE6A gene responsible for PRA in Cardigan Welsh corgi.

1.8. Laboratory animal models for inherited retinal dystrophies

Studies of mouse and rat models of retinal dystrophies has not only provided candidate genes for the investigation of ocular conditions in humans, but has also offered the opportunity to investigate the effect of gene dysfunction in more detail. Animals with retinal dystrophies that were homologous to human retinal dystrophies have also become useful in the development of drug or gene therapy for these retinal conditions. For example, expression of functional bovine PDE6B delivered via a recombinant adeno-associated virus (rAAV) vector in *rdl* mice which have a nonsense mutation in the gene encoding the PDE6B protein (Pittler & Baehr, 1991) have increased the number of photoreceptors and caused a two-fold increase of light sensitivity in the mice (Jomary et al., 1997).

The *RCS* (The Royal College of Surgeons) rat has a retinal dystrophy that is a classic model of recessively inherited retinal degeneration. In these rats, the RPE fails to phagocytose shed outer segments, leading to photoreceptor cell death (Katai et al., 1999a). The defect is due to the mutation in the gene encoding the receptor tyrosine kinase (*Mertk*) (D'Cruz et al., 2000) that is expressed in phagocytic monocytes. This

protein is co-localized with outer segment material during phagocytosis by the RPE cells. Several attempts have been made to rescue photoreceptors in this model. Delivery of rat Mertk to cultured RCS RPE cells by means of a recombinant adenovirus results in infected RCS RPE cells ingested exogenous outer segments to the same extent as wild-type RPE cells (Feng et al., 2002). Subretinal transplantation of brain-derived precursor cells promote photoreceptor survival in the RCS rat at very young age (Wojciechowski et al., 2002).

In addition to studies of spontaneous gene mutations causing retinal dystrophies in mice, the laboratory mouse offers the opportunity for genetic manipulation. Transgenic mice or gene knockout mice may be created to mimick genetically caused human diseases or to over express a target gene. These mice may be used to study the role of a specific gene product on retinal function *in vivo*. For example, the Pro23His rhodopsin mutant mouse with a missense mutation (P23H) in the rod opsin gene was used as an animal to study rod degeneration in adRP patients (Olsson et al., 1992). The *rd*s mouse carrying a mutation in the peripherin gene, which encodes a protein that is located at the periphery of the outer segment disc membrane of photoreceptors, was not only used to study the mechanism of retinal degeneration, but also for gene therapy trials (Ali et al., 2000).

In addition to creating animals carrying gene mutations in gene encoding phototransduction proteins, several mouse models have been produced to investigate the role of proteins in the visual cycle. For example: *rpe65* knockout mice that lack RPE65

protein, which is essential for formation of 11-cis retinal (Redmond et al., 1998). This model can be used to study the mutations in the human RPE65 gene that causes to Leber congenital amaurosis (Allikmets, 2004), a disease that causes of childhood blindness characterized by a severe retinal dystrophy at a young age.

Although the mouse is the most commonly used model species for the study of retinal degeneration, the small eyes of the mouse means they are not ideal for modeling certain procedures that would need to be performed on human eyes for drug or gene therapy. The larger eyes of dogs and cats are more suitable for such manipulations. The dog model for arRP due to the PDE6B mutation has provided an opportunity to study the cellular mechanisms of the disease as described above. Briard dogs, an animal model of Leber congenital amaurosis in humans due to RPE65 mutation, have added to understanding the impact of the genetic defects on retinal cell death, and as a model for the use of gene therapy (Narfstrom et al., 2003).

Chapter 2

Detailed electroretinographic characterization of the *PDE6A* dog phenotype

2.1. Introduction

The electroretinogram (ERG) has been used as a measurement of retinal function in the study of many retinal diseases. Various procedures, based on light intensity, duration and color of light stimulus, or light or dark adaptation condition, can be used to identify and characterize the contributions to the ERG components from different neurons in the retinal pathways. Alterations of the shape of the ERG waveform are often used to qualitatively indicate reduced contributions of some pathways to the ERG waveforms. However, quantitative measurement of the amplitude and the time course (implicit time) of each ERG components can provide us with a measure of retinal function and how it is altered by the disease process.

The ERG is a summation of the electrical responses recorded from the entire retina, meaning that quantitative measurement of isolated ERG components can be used to assess the function of specific retinal cells. For instance: variables of maximum rod response and rod sensitivity obtained by fitting the leading edge of the isolated rod a-wave in response to intensity flashes (Hood & Birch, 1996) have been used to assess rod photoreceptor function in patients with retinitis pigmentosa (RP) (Hood & Birch, 1994). Additionally, fitting the scotopic b-wave amplitude to a non-linear regression model

allowing assessment of maximal rod response and rod sensitivity has also been used to investigate rod function in RP patients (Birch & Fish, 1987).

The purpose of this study was to use the ERG to characterize retinal dysfunction in the *PDE6A* mutant dog.

2.2. Materials and methods

2.2.1. Animals

Homozygous *PDE6A* mutant, heterozygous *PDE6A* carrier, and homozygous *PDE6A* normal dogs were used in this experiment. Genotyping for the *PDE6A* mutation was performed as previously described (Petersen-Jones & Entz, 2002). All dogs were maintained at the vivarium of the College of Veterinary Medicine, Michigan State University under 12 hours light/dark cycles.

2.2.2. Electroretinographic recording

2.2.2.a Anesthesia

Animals were anesthetized under a dim red light. Two anesthesia protocols were used based on the age of the animals: less than 9 weeks of age; induction and maintenance with halothane delivered in oxygen, at 9 weeks of age and higher; premedication with acepromazine maleate (0.1-0.3 mg/kg) intramuscularly, followed by

induction of anesthesia with intravenous thiopental sodium (Pentothal®; 6-12 mg/kg). Anesthesia was maintained with halothane delivered in oxygen. A pulse-oximeter (Vet/Ox 4400, Heska Corporation, Fort Collins, CO) was used to record pulse rate and oxygen saturation for the duration of the procedure. Body temperature was maintained using a heat pad. Pulse rate, oxygen saturation and body temperature were recorded every 5 minutes during the ERG recording.

2.2.2.b. Recording electrode placement and animal positioning

Dogs were positioned in sternal recumbency. The left eye was used for ERG recording; the right eye was taped close. The left pupil was maximally dilated by applying 1% tropicamide (Mydracyl®, Alcon Laboratories, Honolulu, HI) and 10% phenylephrine hydrochloride (AK-Dilate®, Akorn Inc, Buffalo Grove, IL). The globe was positioned in primary gaze with stay sutures of 4-0 silk (Ethicon, Inc, Piscataway, NJ) placed in the conjunctiva adjacent to the limbus. A drop of 2.5% hydroxypropyl methylcellulose solution (Goniosol®, Iolab Pharmaceutical Inc, Claremont, CA) was applied to keep the cornea moist. Burian-Allen bipolar contact lenses (Hansen Ophthalmic Development Laboratory, Coralville, IA) were used. These have a loop silver electrode that contacts the cornea and are referenced to a spectrum that contacts the palpebral conjunctiva and is coated in a silver conductive paint. The ground electrode consisted of needle electrode and was placed subcutaneously at the back of cervical region.

2.2.2.c. Electroretinographic recording

Full-field short flash ERGs were recorded using the UTAS-E 3000 electrophysiology unit (LKC Technologies Inc; Gaithersburg, MD). The band pass was set at 1 to 500 Hz; gain setting varied from 2×10^3 to 4×10^4 . The time base was set to record 20 msec pre-stimulus. Inter-stimulus intervals were set and ERG responses averaged based on flash intensities. Flash stimuli were delivered to the tested eye via a spherical bowl (Spafford et al., 1993) painted with reflective white paint. ERG responses were amplified and stored for further analysis.

2.2.3. Electroretinographic test protocols

2.2.3.a. Intensity-series electroretinography

Intensity-series ERGs were recorded from four homozygous *PDE6A* mutant, five heterozygous *PDE6A* carriers, and four homozygous *PDE6A* normal dogs at 2, 3, 4, 5, 6, 7, 9, 12, 16, 20 and 52 weeks of age.

2.2.3.a.(i) Scotopic intensity-series electroretinography

After dogs were dark-adapted for 60 minutes, scotopic ERG responses from a series of 16 white flash stimuli (-3.18, -2.98, -2.79, -2.6, -2.0, -1.6, -1.19, -0.79, -0.39,

-0.001, 0.39, 0.85, 1.36, 1.9, 2.38, and 2.82 log cds/m²) were recorded. Inter-stimulus intervals were increased from one second at low intensities to 360 seconds at the highest intensity to avoid light adapting the rods. Preliminary studies showed that these inter-stimulus intervals were adequate to present rod adaptation (data not shown).

2.2.3.a.(ii) Photopic intensity-series electroretinography

Dogs were light-adapted to a rod saturating white background white light of 30 cd/m² for 10 minutes after the dark-adapted ERG had been recorded. Photopic ERG responses were recorded from a series of 10 white flashes (-0.39, -0.22, -0.001, 0.16, 0.39, 0.85, 1.36, 1.9, 2.38, and 2.82 log cds/m²), superimposed on the same background white light. Inter-stimulus intervals were one second from -0.39 to 1.36 log cds/m² and 5, 10, and 15 seconds for 1.9, 2.38, and 2.82 log cds/m², respectively.

2.2.3.b. Flicker electroretinography

Flicker ERGs were recorded from four homozygous mutant, five heterozygous carriers, and four homozygous normal dogs at 2, 3, 4, 5, 6, 7, 9, 12 and 16 weeks of age. Recording electrode placement and animal positioning were described in 2.2.2.b. The band pass was set at 1 to 500 Hz; gain setting varied from 4×10^3 to 4×10^4 .

2.2.3.b.(i). Rod flicker ERG

While the dog was dark-adapted, rod flicker ERG responses were recorded in response to white flashes of light $-1.6 \log \text{ cds/m}^2$ in intensity at 5Hz, and 15 tracings averaged.

2.2.3.b.(ii). Cone flicker ERG

Cone flicker ERG was recorded while the dog was still dark-adapted using white flash stimulus at $0.39 \log \text{ cds/m}^2$ intensity at 33 Hz, and 15 tracings averaged.

2.2.3.c. Electroretinography using blue flashes

Rod-mediated ERGs were recorded from dark-adapted retina using blue flashes (wavelength 400-560 nm) obtained with a #47A Wratten filter (Kodak, Rochester, NY). See 2.2.2.c. for ERG setting.

2.2.3.d. Long flash electroretinography

Full-field long flash ERGs were recorded using a customized Ganzfeld stimulator unit connected to the UTAS-E 3000 electrophysiology unit (LKC Technologies Inc; Gaithersburg, MD). The flash duration was set at 150 msec. The light source was a 12-V 50-W tungsten-halogen lamp giving a maximum white light stimulus of 180 cds/m^2 .

Constant background illumination inside the Ganzfeld bowl was generated from a 12-V light bulb. A diffuser in front of the bulb was adjusted to give a homogeneous background white light of 42cd/m^2 (Sieving, 1993). Responses were amplified with a bandwidth of 0.3 to 500 Hz, and 30 responses averaged. All ERG waveforms were averaged, stored and displayed by LKC software for further analysis.

2.2.4. Data analysis

2.2.4.a. The a- and b-wave amplitude and implicit time

The a- and b-wave amplitude (microvolt; μV) and implicit time (millisecond; msec) were measured for each averaged response. The a-wave amplitude was measured from the onset of light stimulus to the trough of the first negative wave; b-wave amplitude from the trough of the first negative wave to the peak of the first positive wave. A-wave implicit time was time measured from the onset of the light stimulus to the time when the maximal a-wave trough occurred and b-wave implicit time from the onset of the light stimulus to the time when the peak b-wave was present. Means (\pm SEM) of scotopic and photopic ERG amplitudes and implicit time were calculated and plotted as a function of light stimulus.

2.2.4.b. Flicker amplitude and implicit time

Flicker amplitude (μV) and implicit time (msec) were measured for the entire recording period (250msec) and averaged. Amplitude was measured from trough to peak of each wave; implicit time was duration of time measured from time at the trough to time at the peak of each wave.

2.2.4.c. Naka-Rushton function

The first limb of the scotopic b-wave amplitude as a function of log stimulus was fitted by a non-linear regression with the 3-parameter Hill equation as follow:

$$V(I) = (V_{\max} * I^n) / (I^n + k^n) \quad (1)$$

In this equation, V , retinal responsiveness, is the b-wave amplitude (μV) to a stimulus of luminance I , V_{\max} is the maximum response amplitude, I is the stimulus luminance, k is the semi-saturation constant or luminance required to elicit a response equal to one-half the amplitude of V_{\max} , which is considered to represent retinal sensitivity, and n is proportional to the slope of the graph of equation 1 at the point where the stimulus luminance is taken to be k , and is considered an indicator of retinal homogeneity. The b-wave response curve was fit to equation 1 using SigmaPlot, version 5.0 (Systat Software, Inc, Richmond, CA), and independent variables (V_{\max} , k and n) were derived.

From 2.2.4.a. to 2.2.4.c. the experiments have a repeated measures structure. Data was statistically analyzed using Proc Mixed, SAS version 9.1 (SAS Institute Inc., Cary, NC). Analysis of residuals were obtained and the experiment variables (amplitude, implicit time, Vmax, k value and n value) were transformed to a logarithmic scale to obtain approximately normally distributed residuals, and the value of the confidence interval (CI) was calculated. A set of models with the same fixed effects, but different covariance structures was compared using the Bayesian Information Criterion (BIC). The model with the smaller value (best fit) was selected. A different covariance structure for the repeated measures was allowed for each variable. Comparisons among fixed effects (age, genotype and their interaction) were performed based on the selected model. Interaction between age and genotype was tested at each flash intensity used. For any situations where statistical significance was found, difference among genotypes was tested at each given age. Data were considered significant at a level of significance less than 0.05 ($P < 0.05$).

2.2.4.d. Criterion threshold of means ERG amplitudes

Criterion threshold of means of ERG scotopic and photopic amplitudes were assigned based on data from normal control animals; 10 μ V was selected for b-wave scotopic amplitude, 5 μ V for a- and b-wave photopic and a-wave scotopic amplitudes. A calculation of flash intensity-at-criterion threshold was performed by linear interpolation.

On every occasion that the highest value of ERG amplitude was below the given threshold, the data was labeled as censored. Censored values were then replaced by the maximum light intensity ($2.82 \log \text{ cds/m}^2$). A non-parametric ANOVA was computed using the Npar1way procedure of SAS (SAS version 9.1, SAS Institute Inc., Cary, NC). An exact Kruskal-Wallis test was used to analyze the difference among genotypes at each age. For ages where a significant difference among genotypes was found, a parametric Tukey-Kramer test was applied to detect differences between each genotype. Data were considered significant at a level of significance of less than 0.05 ($P < 0.05$).

2.2.4.e. Rod-isolated responses

Rod-isolated responses were derived by subtraction of intensity-matched photopic (cone only) ERG responses from scotopic (rod plus cone) ERG responses (Hood & Birch, 1990). The a-wave of the rod-isolated responses at $1.36 \log \text{ cds/m}^2$ were normalized for amplitude and the leading edge of the a-wave compared between *PDE6A* mutant and normal control dogs from 2 to 6 weeks of age.

2.2.4.f. Oscillatory potentials

Oscillatory potentials are high-frequency ERG components located on ascending limb and peak of b-wave. Scotopic OPs were isolated from scotopic ERGs recorded from $-0.001, 0.39, 0.85 \log \text{ cds/m}^2$ flash stimuli by electronically applying a band pass filter at frequencies of 73 to 500 Hz. OP amplitude was measured from the peak of a positive

wave to the preceding negative trough. Amplitudes of five OPs were summed in each dog, averaged within the genotype, and then compared between two homozygous *PDE6A* mutant and two homozygous *PDE6A* normal dogs at 3, 5, 7, 9, and 12 weeks of age.

2.2.4.g. Photopic Negative Response

Photopic Negative Response is a negative waveform that occurs after the photopic b-wave. PhNR at -0.001, 0.16, 0.39, 0.85, 1.36 log cds/m² was compared between homozygous *PDE6A* mutant and homozygous *PDE6A* normal dogs at 5, 7, 12 and 50 weeks of age.

2.3. Results

There were no significant differences ($P>0.05$) between the ERGs recorded from *PDE6A* carriers and the normal controls for any of the parameters examined in this study.

2.3.1. Scotopic ERG responses

The scotopic ERG waveforms were analyzed in the following ways:

- a- and b-wave amplitudes and implicit times
- amplitude of a- and b-wave at selected criterion threshold (5 μ V and 10 μ V for a- and b-wave amplitude, respectively)

- the slope of the leading edge of the derived rod-isolated a-wave
- the response in dark-adapted dogs to blue flashes of light
- modeling of the first limb of the b-wave intensity-response curve by Naka-Rushton fit to derive maximal rod response and photoreceptor sensitivity
- rod flicker responses
- oscillatory potentials

2.3.1.a. Scotopic ERG amplitude (Figures 2.1, 2.2, 2.3, 2.4 & 2.5)

Scotopic a- and b-waves could be recorded in normal controls and the *PDE6A* mutant dogs after the opening of the eyelids (approximately 2 weeks of age). With age, the mean a- and b-wave amplitudes of normal controls progressively increased and reached a peak at about 6 weeks of age (Figures 2.2A, 2.3 & 2.4) while the mean scotopic intensity threshold of a- and b-wave amplitudes continuously declined from 2 to 6 weeks of age, after which they slightly increased and then plateaued until 20 weeks of age (Figure 2.5).

The mean scotopic a- and b-wave amplitudes from the mutant dogs (Figures 2.3 & 2.4) reached their peaks at approximately 3 weeks of age, at which time they were significantly smaller ($P<0.05$) compared to those of normal controls. Loss of a-wave response and OPs continued with age in the mutant dog (Figures 2.1B & 2.2B). The mean scotopic intensity threshold of the a-wave was significantly higher ($P<0.05$) by 1.5 to 2.0

log units at all ages investigated compared to that of the normal controls (Figure 2.5). After 5 weeks of age, it did not reach the $5\mu\text{V}$ -criterion threshold.

Although the mean b-wave amplitude decreased from 3 weeks of age in the mutant dogs, a temporary increase was observed at 6 weeks of age followed by a constant decline (Figure 2.4). The ratio of b-wave amplitude to a-wave amplitude (b/a ratio) was relatively constant in normal controls, whereas it increased in mutant dogs with increasing age and stayed at abnormally high levels throughout the period ERGs could be recorded. With age, development of the b-wave intensity threshold of the mutant dogs paralleled that of normal controls until 5-6 weeks of age, after which there was a sharp increase in threshold from 7 to 9 weeks of age. The mean b-wave threshold values were significantly higher ($P < 0.05$) by about 2.5 log units than those of the normal controls at all ages investigated (Figure 2.5). It is of interest that the scotopic and photopic waveforms of mutant dogs were similar suggesting a response primarily from cones.

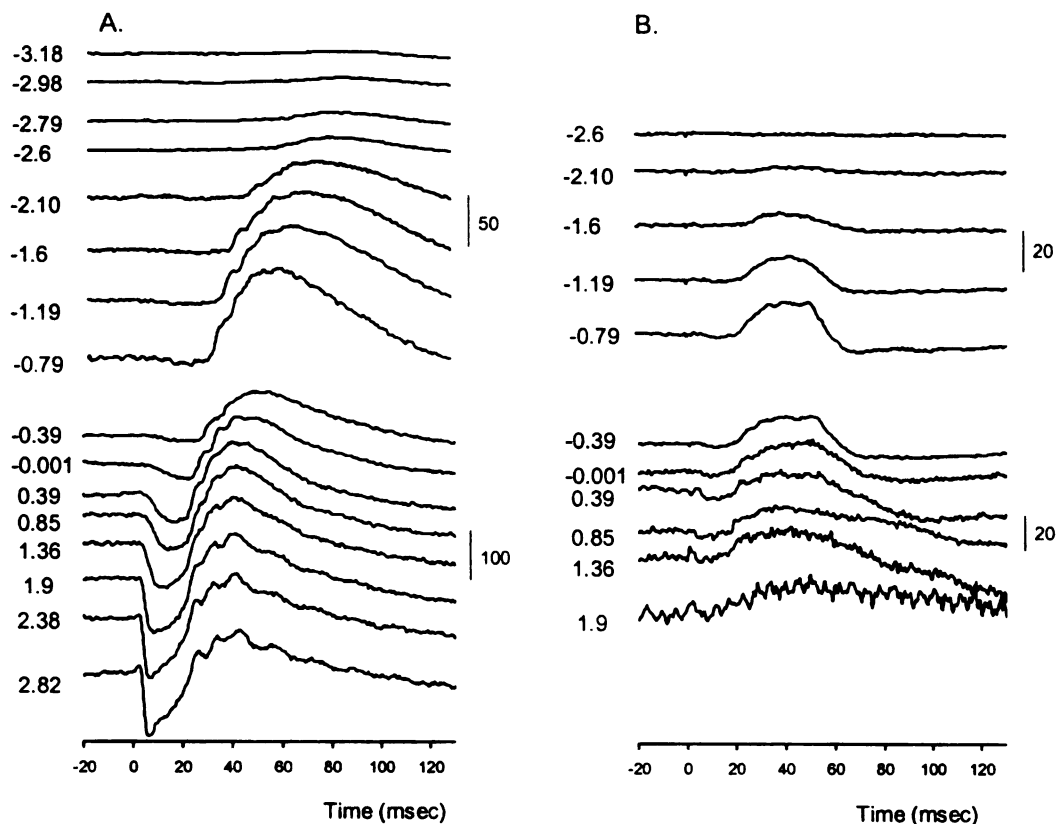


Figure 2.1. Representative scotopic ERG recordings from a normal control (A) and the *PDE6A* mutant dog (B) at 4 weeks of age. Light intensities (cds/m^2) are indicated in the figure. The onset of flash is at 0 msec. A) In the normal control, scotopic ERG amplitude increases with flash intensity whereas ERG implicit time shortens. The b-wave threshold is at $-2.79 \log \text{cds/m}^2$. The a-wave threshold is at approximately $-0.39 \log \text{cds/m}^2$. Both a- and b-wave amplitude increases with increasing intensity. Four small oscillatory potential wavelets are present on the b-wave, in particular at high light intensities. B) The b-wave threshold of the *PDE6A* mutant dog is elevated ($-2.10 \log \text{cds/m}^2$) compared to that of the normal control. The a-wave is much reduced at this age and the b-wave response is small and peaks at an intensity of $0.001 \log \text{cds/m}^2$ then decreases with further increases in light intensity. This is suggestive of a predominantly cone response. B-wave implicit time normally gets shorter with higher light intensities, whereas in the mutant dog it tends to stay the same at first then increases. ERGs of this mutant dog can not be recorded at very high light intensities (2.38 and $2.82 \log \text{cds/m}^2$). Size bars indicate amplitude in microvolt.

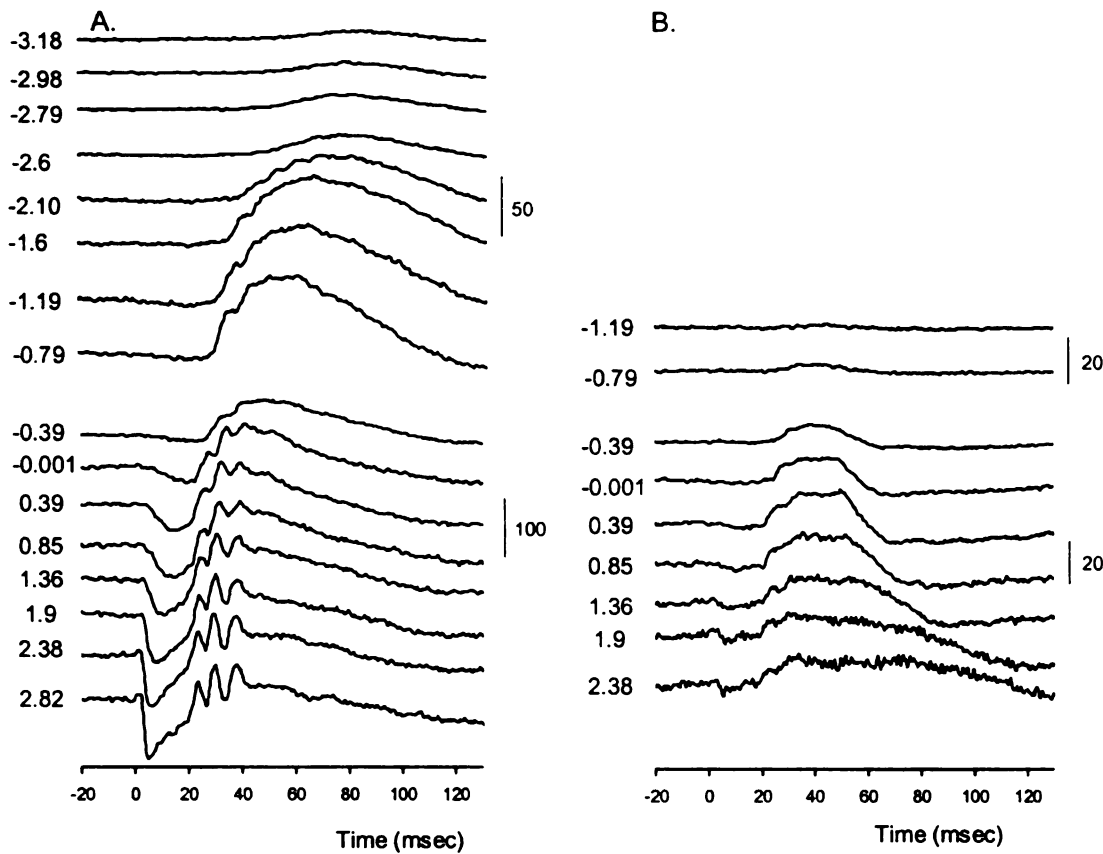


Figure 2.2. Representative scotopic ERG recordings from a normal control (A) and the *PDE6A* mutant dog (B) at 6 weeks of age. Light intensities (cds/m^2) are indicated on the figure. The onset of flash is at 0 msec. A) Compared to responses at 4 weeks of age (Figure 2.1) the b-wave threshold of the normal control is decreased ($-3.18 \log \text{cds/m}^2$) while a- and b-wave amplitudes are increased. Oscillatory potentials are more prominent. B) Compared to the normal control, intensity threshold of the *PDE6A* mutant dog is markedly higher ($-0.79 \log \text{cds/m}^2$). A small a-wave is present only at very bright flash intensities while the b-wave amplitude is markedly reduced and decreases with increasing flash intensity after 0.85 cds/m^2 . The b-wave implicit time in the normal control decreases with increasing stimulus intensity whereas in the mutant dog the implicit time increases with the brighter intensities. Size bars indicate amplitude in microvolt.

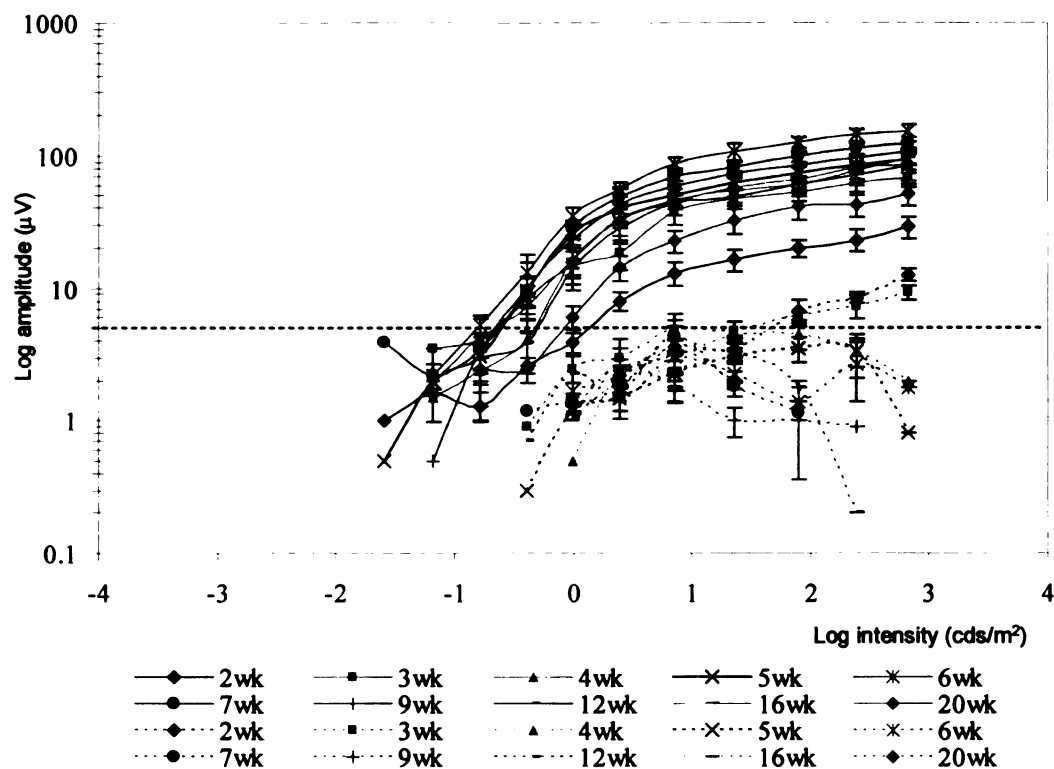


Figure 2.3. Mean scotopic a-wave amplitudes with standard errors ($1x \pm$ SEM) plotted against stimulus intensity on a log-log scale for normal control and *PDE6A* mutant puppies. The selected a-wave scotopic criterion threshold is 5 μ V (dashed black line). Solid lines and dot lines represent values from normal controls and the mutant dogs, respectively. Various colors represent the mean scotopic a-wave amplitude at different ages. ($n = 4$ for each group of dogs) Note a significant difference ($P < 0.05$) of the mean a-wave amplitude is found between the normal controls and the *PDE6A* mutant dogs at all age groups investigated. The *PDE6A* mutant photoreceptors do not respond to light at low intensities, and after 3 weeks of age their mean amplitudes decrease at very bright intensities. Increased scotopic a-wave criterion threshold in the *PDE6A* mutant reflects a marked reduction of photoreceptor sensitivity. Key: μ V = microvolt, wk = week.

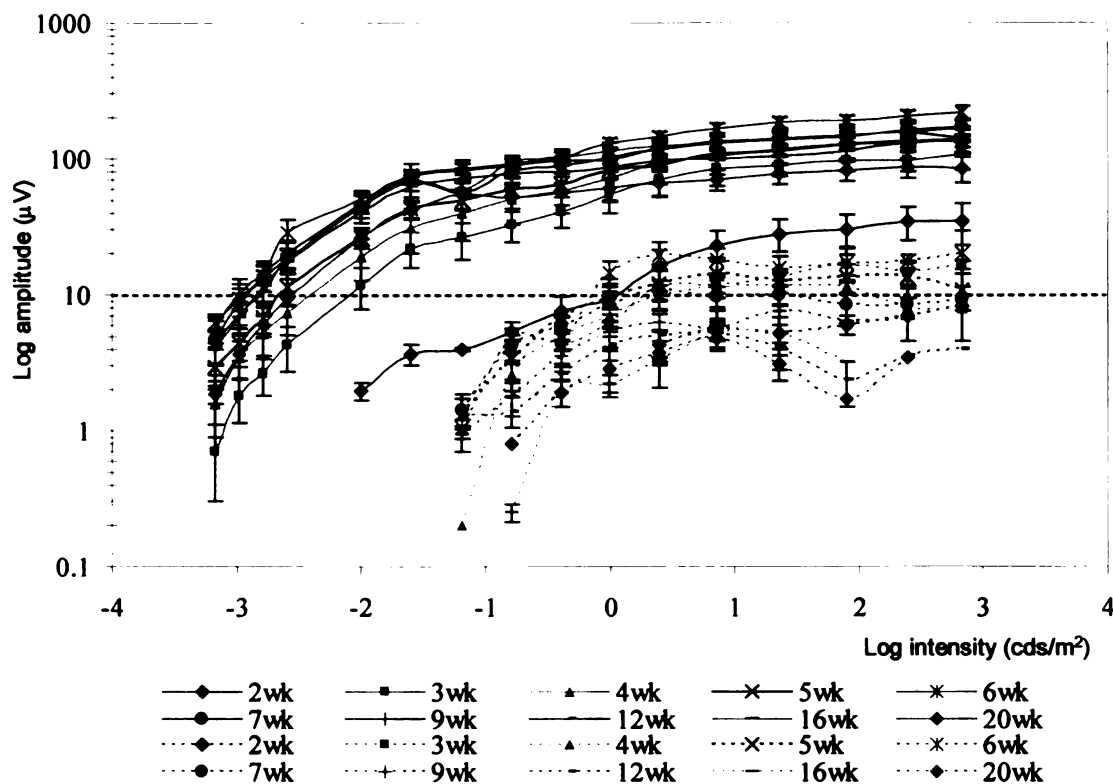


Figure 2.4. Mean scotopic b-wave amplitudes with standard errors ($1x \pm SEM$) plotted against stimulus intensity on a log-log scale from normal control and *PDE6A* mutant puppies. The selected b-wave scotopic criterion threshold is $10 \mu V$ (dashed black line). Solid lines and dot lines represent values from normal controls and the mutant dogs, respectively. Various colors represent the mean scotopic b-wave amplitude at different ages. ($n = 4$ for each group of dogs). Note a significant difference ($P < 0.05$) of the mean b-wave amplitude is found between the normal controls and the *PDE6A* mutant dogs at all age groups investigated. The mean scotopic b-wave amplitudes in both normal and *PDE6A* mutant dogs develop to peak level at 6 weeks of age. In the normal control after this age there is a slight decrease to adult levels. In the *PDE6A* mutant dogs, there is a progressive decrease in amplitudes with age. At 6 weeks of age the $10 \mu V$ -amplitude criterion threshold is approximately 2.5 log units higher in the mutant dogs than in the controls, after that the b-wave amplitudes in the mutant dogs decline to below the threshold criterion level. Key: μV = microvolt, wk = week.

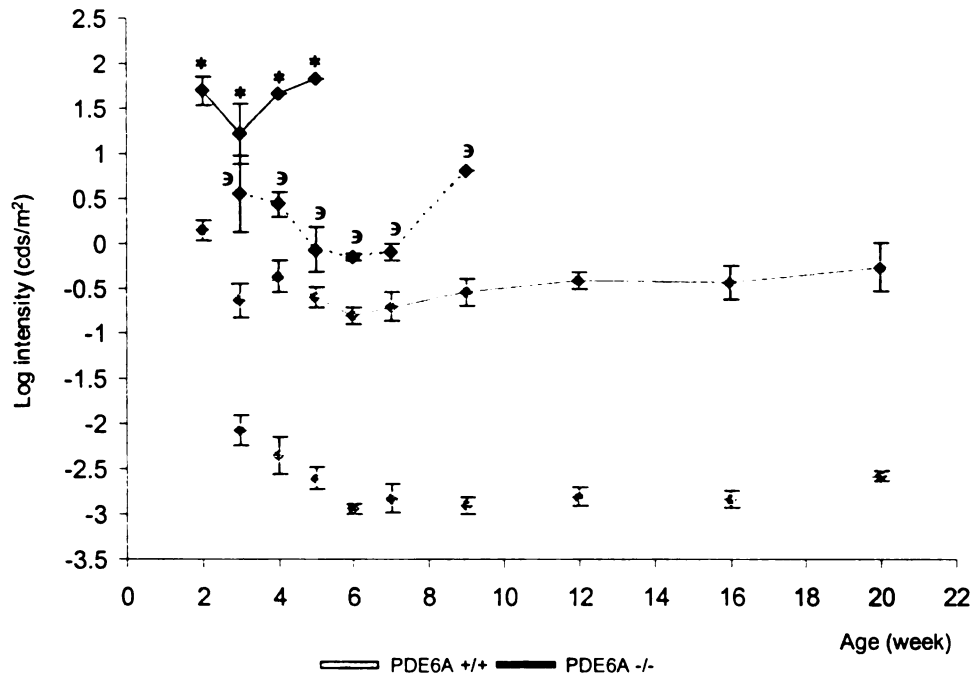


Figure 2.5. Mean scotopic intensity threshold with standard errors ($1x \pm \text{SEM}$) using $5\mu\text{V}$ and $10\mu\text{V}$ criterion for a- and b-wave amplitude from normal control and *PDE6A* mutant dogs at all ages. ($n = 4$ for each group of dog) Solid lines represent a-wave intensity threshold, and dot lines represent b-wave intensity threshold. Note that significantly higher ($P < 0.05$) mean a- and b-wave intensity thresholds are observed in the *PDE6A* mutant group at all ages examined. Key: * and ‡ indicate statistical differences of the a- and b-wave intensity threshold, respectively, at $P < 0.05$.

2.3.1.b. Scotopic ERG implicit time (Figures 2.1, 2.2, 2.6 & 2.7)

The mean a- and b-wave implicit times of normal control dogs decrease with increasing light intensities. Development of the implicit times is related to age. In normal controls, a- and b-wave implicit times shortened over the period of retinal maturation to 6 or 7 weeks of age and then stayed similar for the rest of the study period. A delay of both implicit times was observed in the ERGs recorded from mutant dogs (examples are shown in Figure 2.1B & 2.2B). A significant delay ($P<0.05$) of the mean a-wave implicit time was found at 2, 3, 7, 16 and 20 weeks of age at $0.39 \log \text{ cds/m}^2$ at lower intensities, whereas it was significantly delayed at 7 weeks of age compared to normal control at higher intensities (Figure 2.6). For the mean b-wave implicit time, it was significantly delayed ($P<0.05$) in the mutant dogs at 4, 5, 7, 9, 12, 16 and 20 weeks of age at low light intensities, as well as at intensities higher than $0.85 \log \text{ cds/m}^2$ (Figure 2.7).

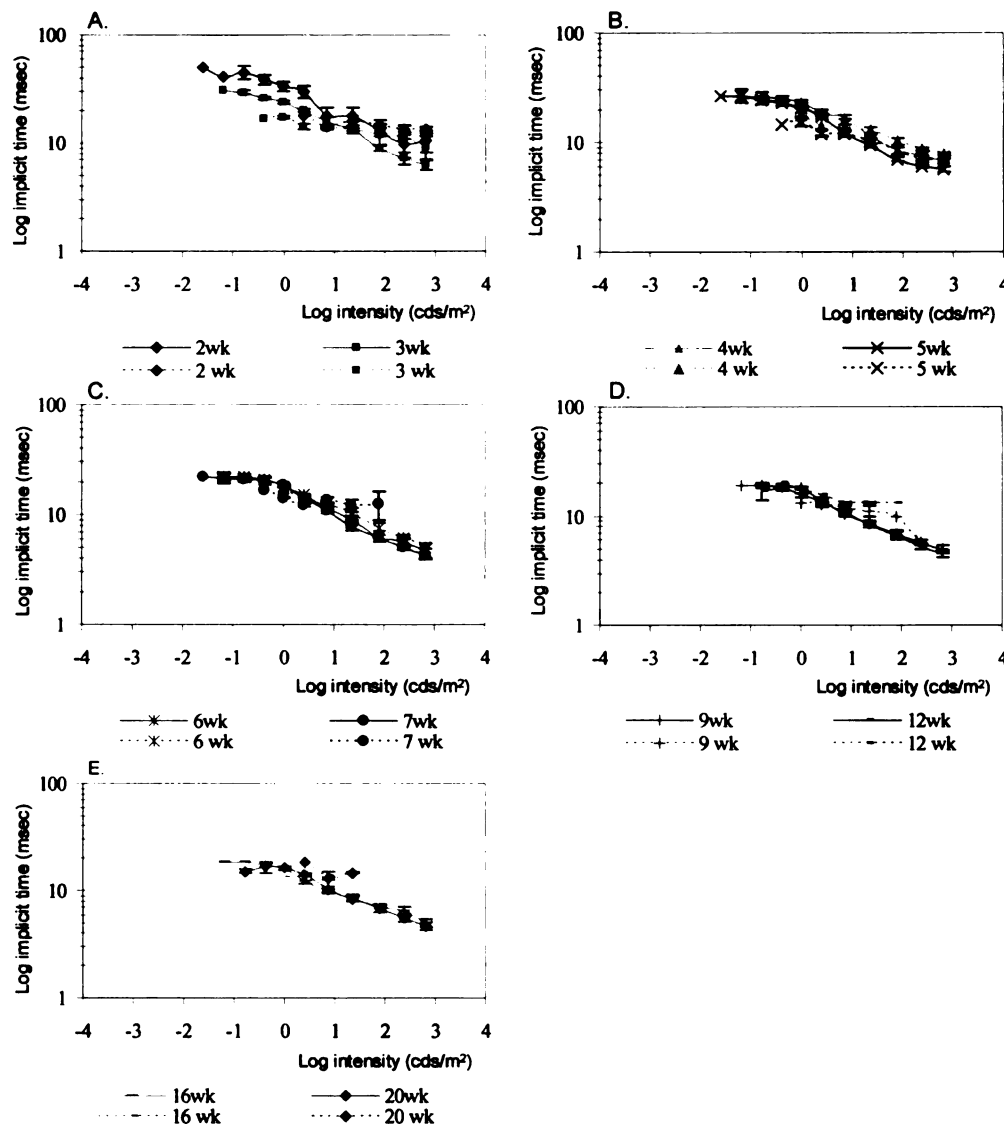


Figure 2.6. Mean scotopic a-wave implicit times with standard errors ($1x \pm \text{SEM}$) plotted against stimulus intensity on a log-log scale from normal control and *PDE6A* mutant dogs at 2 & 3 (A), 4 & 5 (B), 6 & 7 (C), 9 & 12 (D) and 16 & 20 (E) weeks of age. Solid lines and dot lines represent values from normal controls and the mutant dogs, respectively. Various colors represent the mean scotopic a-wave implicit time at different ages. ($n = 4$ for each group of dogs). Note a significant delay ($P < 0.05$) of the mean scotopic a-wave implicit time of the *PDE6A* mutant group is found at light intensity between 1 to 2 log cds/m^2 in most of age groups. Key: msec = millisecond, wk = week.

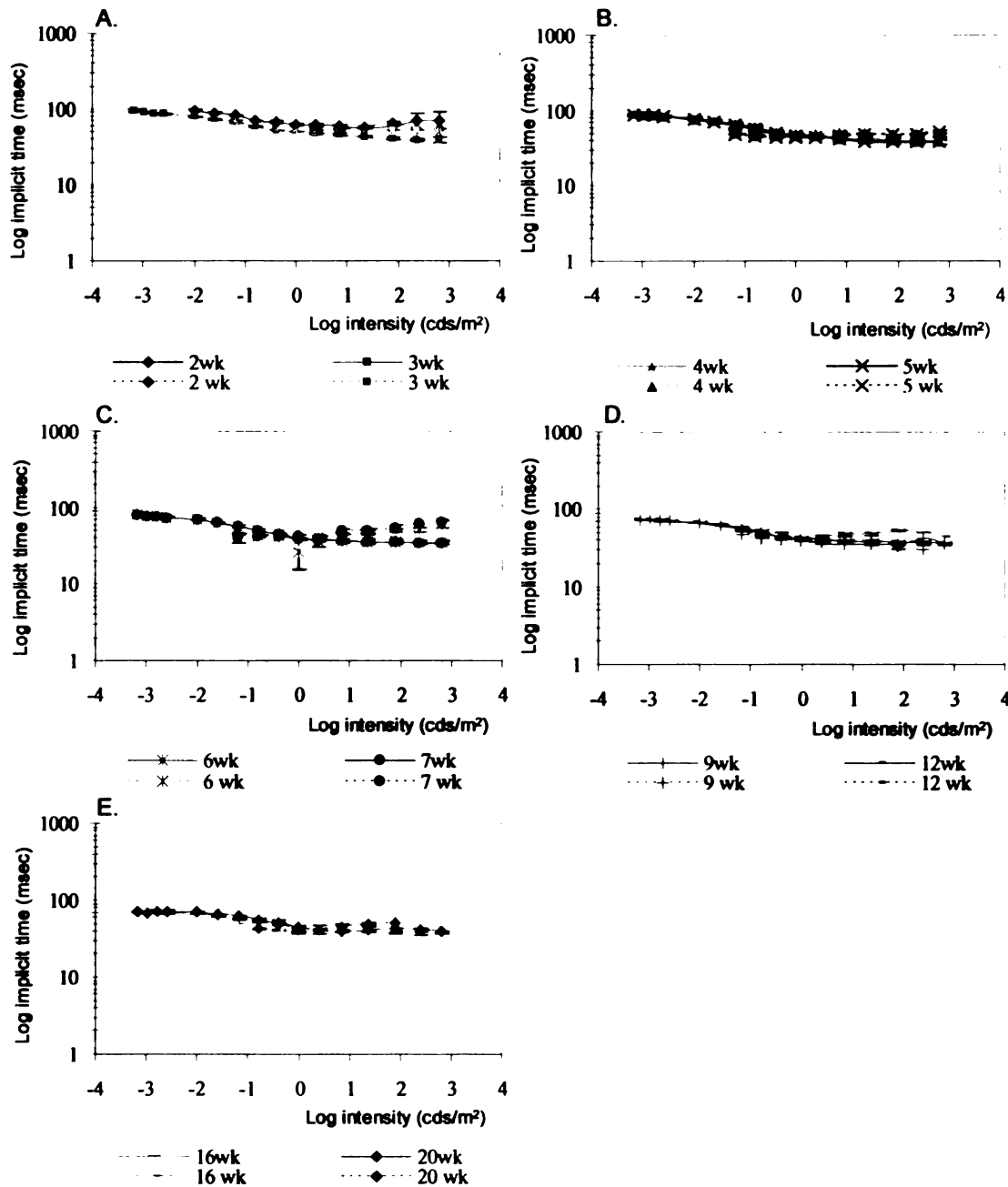


Figure 2.7. Mean scotopic b-wave implicit times with standard errors ($1x \pm \text{SEM}$) plotted against stimulus intensity on a log-log scale from normal control and *PDE6A* mutant dogs at 2 & 3 (A), 4 & 5 (B), 6 & 7 (C), 9 & 12 (D) and 16 & 20 (E) weeks of age. Solid lines and dot lines represent values from normal controls and the mutant dogs, respectively. Various colors represent the mean scotopic b-wave implicit time at different ages. ($n = 4$ for each group of dogs). Note that from statistical data, the mean scotopic b-wave implicit times between the two groups are comparable at 2 to 3 weeks of age (A). A significantly delayed implicit time ($P < 0.05$) is observed at ages greater than 4 weeks, and at intensities higher than 1 log cds/m² in particular. Key: msec = millisecond, wk = week.

2.3.1.c. Rod-isolated a-wave response

In an attempt to detect the presence of a rod-mediated a-wave in the *PDE6A* mutant dog, a subtraction of cone-mediated responses from mixed rod-cone responses was performed. To allow a comparison of a-wave slope, subtracted waveforms were normalized for a-wave amplitude (Figure 2.8). The subtraction showed that the rod-mediated a-wave responses of the *PDE6A* mutant dogs were either non-recordable or delayed. At 3 weeks of age a very low amplitude negative waveform of delayed implicit time (for an a-wave) was present after the subtraction and preceded a positive waveform (b-wave) also of increased implicit time compared to the normal control. With such low amplitude responses it is difficult to be certain that this actually represents a true rod-driven a-wave. Furthermore the subtraction of light-adapted cone responses from dark-adapted cone responses may have affected the appearance of the final waveform because it is known that dark-adapted cone response differ from those of light-adapted cones.

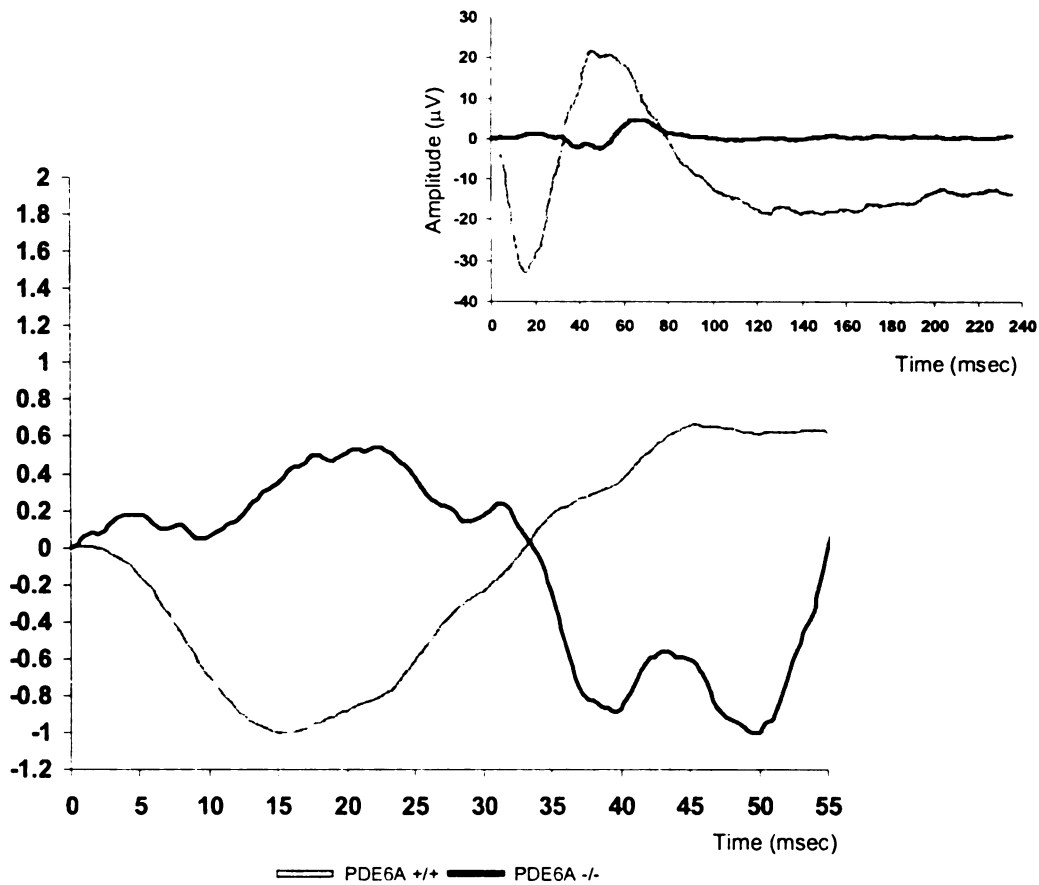


Figure 2.8. Normalization (for a-wave amplitude) of the rod-isolated a-wave derived from a subtraction of intensity-matched photopic and scotopic ERGs in a normal control and the *PDE6A* mutant dog at 3 weeks of age. The onset of flash is at 0 msec. Inset illustrates actual scotopic ERG responses from the same normal control and the *PDE6A* mutant dog from which the normalized waves are derived. Note that rod-isolated ERG responses in the *PDE6A* mutant dog are much reduced compared to the normal control (inset). The time to peak of the normalized "a-wave" of the *PDE6A* mutant dog is considerably delayed at 50 milliseconds, compared to 15 milliseconds in a normal control. Key: μV = microvolt, msec = millisecond.

2.3.1.d. Scotopic ERG responses to blue light flashes

Dim blue flashes were used to preferentially stimulate rod photoreceptors of dark-adapted dogs. In normal controls the scotopic ERG response to blue flashes developed at 2 weeks of age (data not shown). The response grew in amplitude with age, to peak at 6 and 7 weeks of age for a- and b-wave amplitude, respectively. The blue flash ERG of *PDE6A* mutant dogs in contrast was of very low amplitude. An a-wave could not be recorded at any age. A b-wave of very low amplitude could only be detected at 7 weeks of age (Figure 2.9).

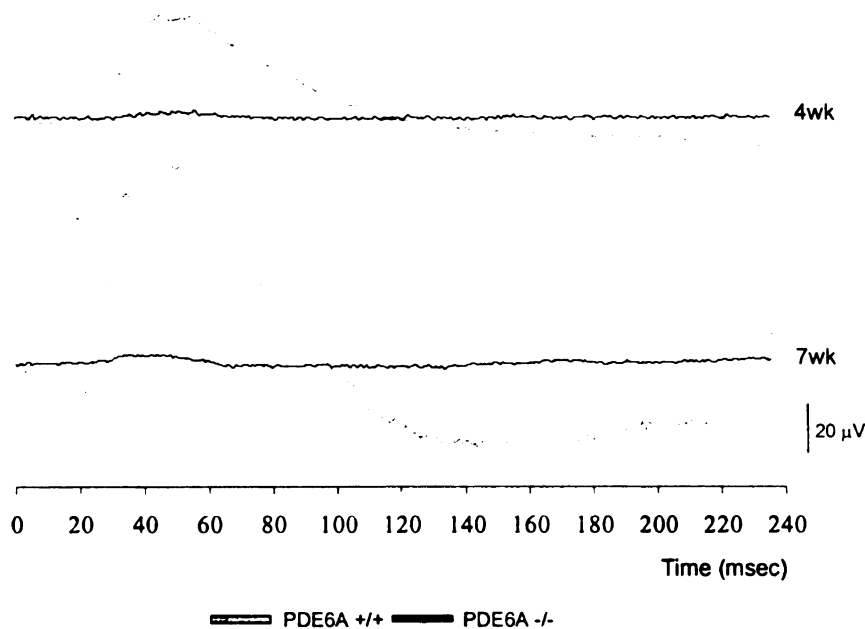


Figure 2.9. Representative recordings of rod-mediated ERG response to dim blue flashes of light from dark-adapted normal controls and *PDE6A* mutant dogs at 4 and 7 weeks of age. The onset of flash is at 0 msec. Note the amplitude of the waveform from the normal control dog increases with age. ERG responses are barely detectable in the *PDE6A* mutant dog suggesting very reduced or absent rod responses. Key: μV = microvolt, msec = millisecond, wk = week.

2.3.1.e. Naka-Rushton fitting of the first limb of the scotopic intensity-response curves

A plot of b-wave amplitude against stimulus intensity typically results in a two-limbed curve. The first limb is considered to primarily represent rod responses and the second limb consists of a saturated rod response plus cone response. To analyze rod responses the first limb of the response curve is fitted using the Naka-Rushton formula.

The Naka-Rushton equation (non-linear regression) successfully fitted the first limb (portion) of the normal canine scotopic b-wave intensity-response curve (Figure 2.10). The correlation coefficient (Burstedt et al., 2000), which is a measure of the covariation in the magnitude of two variables, was used to describe how well the predicted value from the model (predicted by Naka-Rushton equation) fits with the actual data (scotopic b-wave amplitude from the first limb). R^2 is a number between 0 and 1.0. As the strength of the relationship between the predicted values and actual values increases, the R^2 value is close to 1.0. The majority of the first-limb scotopic b-wave of the normal control dogs had R^2 value at 0.97 to 0.99 except for 0.93 at 2 weeks of age. The *PDE6A* mutant dogs also had R^2 value at 0.93 at 2 weeks of age. Even though the value increased to 0.97 at 4 to 5 weeks of age, it decreased afterward to approximately 0.88 at older ages indicating a poorer fit between the predicted value and the actual data.

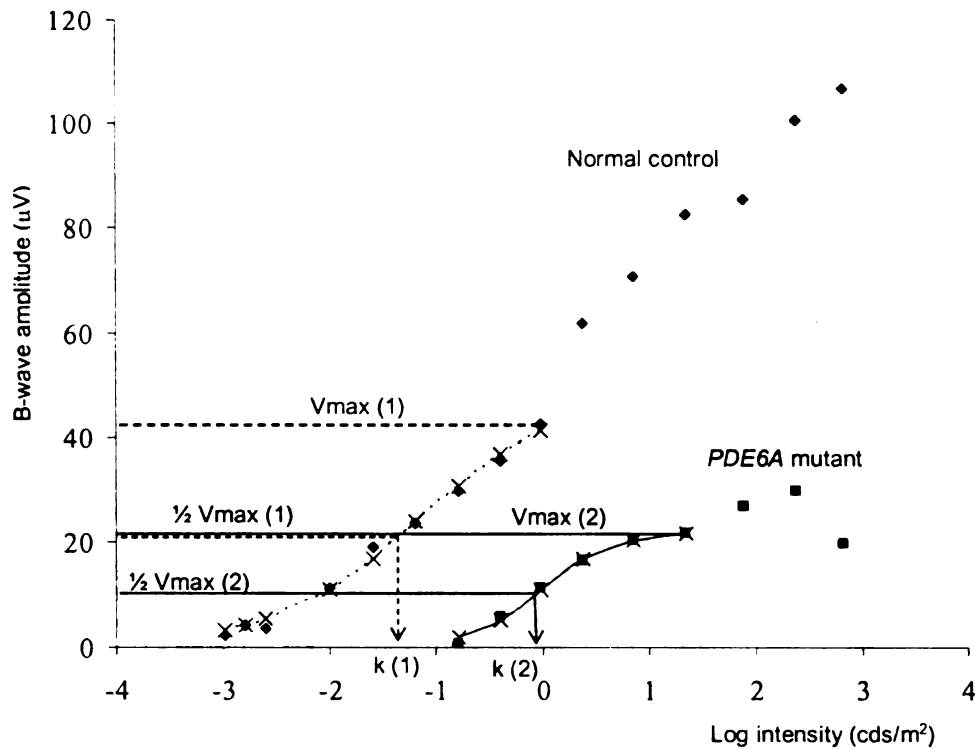


Figure 2.10. Scotopic b-wave intensity-response function obtained from a normal control (diamond symbol) and the *PDE6A* mutant dog (square symbol) at 3 weeks of age. The superimposed curve represents the predicted rod b-wave amplitude from normal control (dot curve) and the *PDE6A* mutant dog (continuous curve) that are fitted from the Naka-Rushton model. Note that the *PDE6A* mutant dog has a low V_{max} and high k value compared to normal controls, which indicates low rod response and low rod sensitivity. Key: 1 = normal control, 2 = the mutant dog, V_{max} = maximal rod response, k = log intensity at half maximal rod response.

A progressive increase of the mean V_{max} was observed from 2 to 6 weeks of age in both normal control and the *PDE6A* mutant groups although it was considerably slower for the *PDE6A* mutant group (Figure 2.11A). The mean V_{max} reached the peak at 6 weeks of age at $102.93 \pm 9.09 \mu V$ and $19.7 \pm 7.42 \mu V$ for normal controls and the *PDE6A* mutant dogs, respectively. Following 6 weeks of age, it was maintained in the normal controls but progressively declined in the mutant dogs. A significant difference

($P < 0.05$) of the mean V_{max} for the *PDE6A* mutant groups was found at all ages investigated except at 2 weeks of age.

The k variable corresponds to the luminance required to elicit a b-wave amplitude equal to one-half the amplitude of V_{max} , and it is considered to represent rod sensitivity. In the normal control, the mean k value rapidly decreased from 2 (3.87 \pm 2.11) to 4 (0.06 \pm 0.03) weeks of age whereas it slowly declined in the *PDE6A* mutant dogs (1.36 \pm 0.25 to 0.85 \pm 0.39). After that, the mean k value continued to decrease in both groups of dogs however, that of the *PDE6A* mutant dog was significantly elevated ($P < 0.05$) compared to normal controls (Figure 2.11B). The n variable represents retinal homogeneity and is thought to be superior when it is close to 1.0 in normal retina. The mean n value was significantly larger in the *PDE6A* mutant dogs at all ages except for at 4 weeks of age (Figure 2.11C).

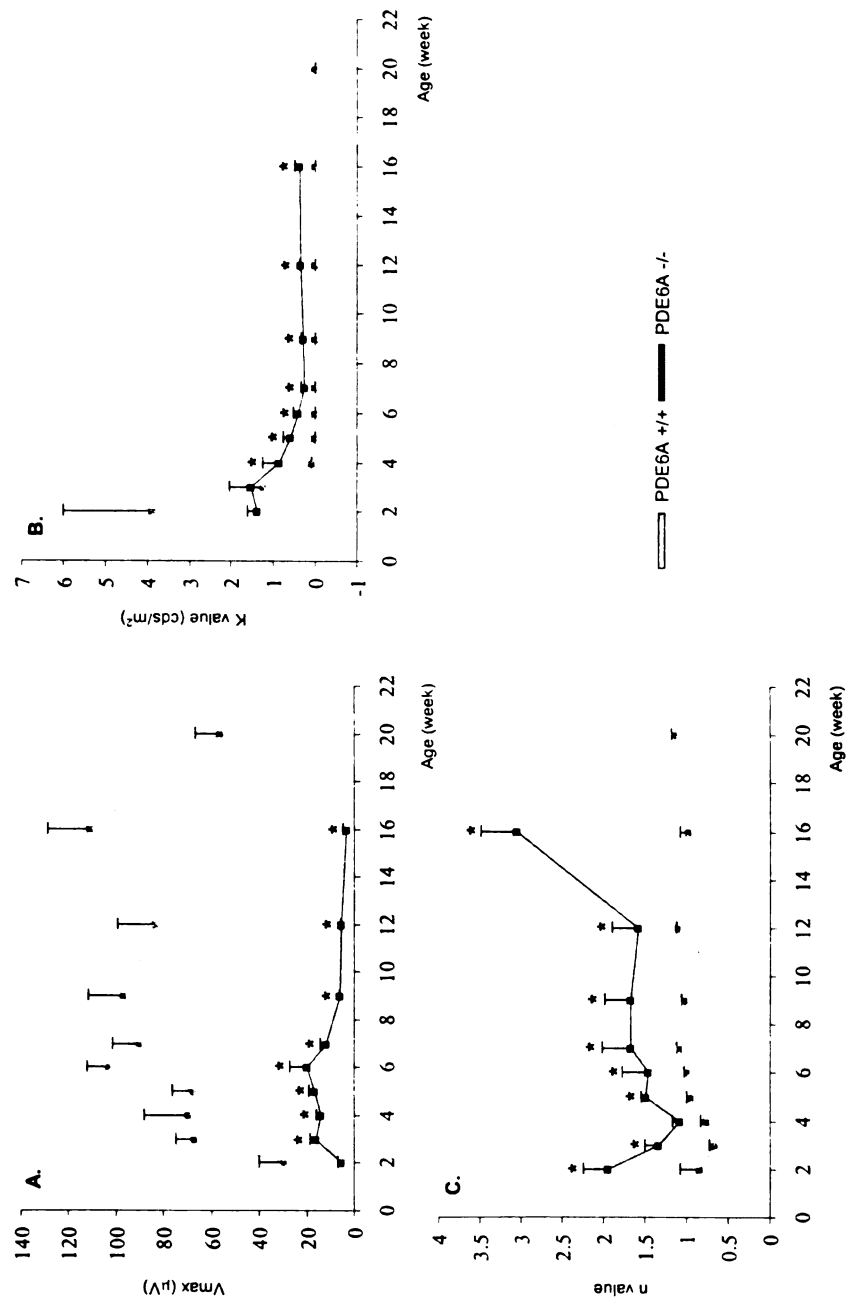


Figure 2.11. A comparison of the mean and standard errors (1x + SEM) of the Naka-Rushton variables; Vmax (A), k value (B) and n value (C) of the normal controls and the *PDE6A* mutant dogs at all age groups. (n = 4 for each group of dog) Note that all mean Naka-Rushton variables are significantly different ($P < 0.05$) in the *PDE6A* mutant group at most ages tested. Key: * indicates statistical difference of the mean variables at $P < 0.05$, $\mu V = \text{microvolt}$.

2.3.1.f. Rod flicker ERG response

Rod flicker response in normal dogs was detectable at 3 weeks of age, and had an adult-like appearance by 4 weeks of age. Its peak amplitude and implicit time was found at 6 weeks of age in the normal controls. In comparison, a rod flicker response could not be recorded in the *PDE6A* mutant dogs (Figure 2.12).

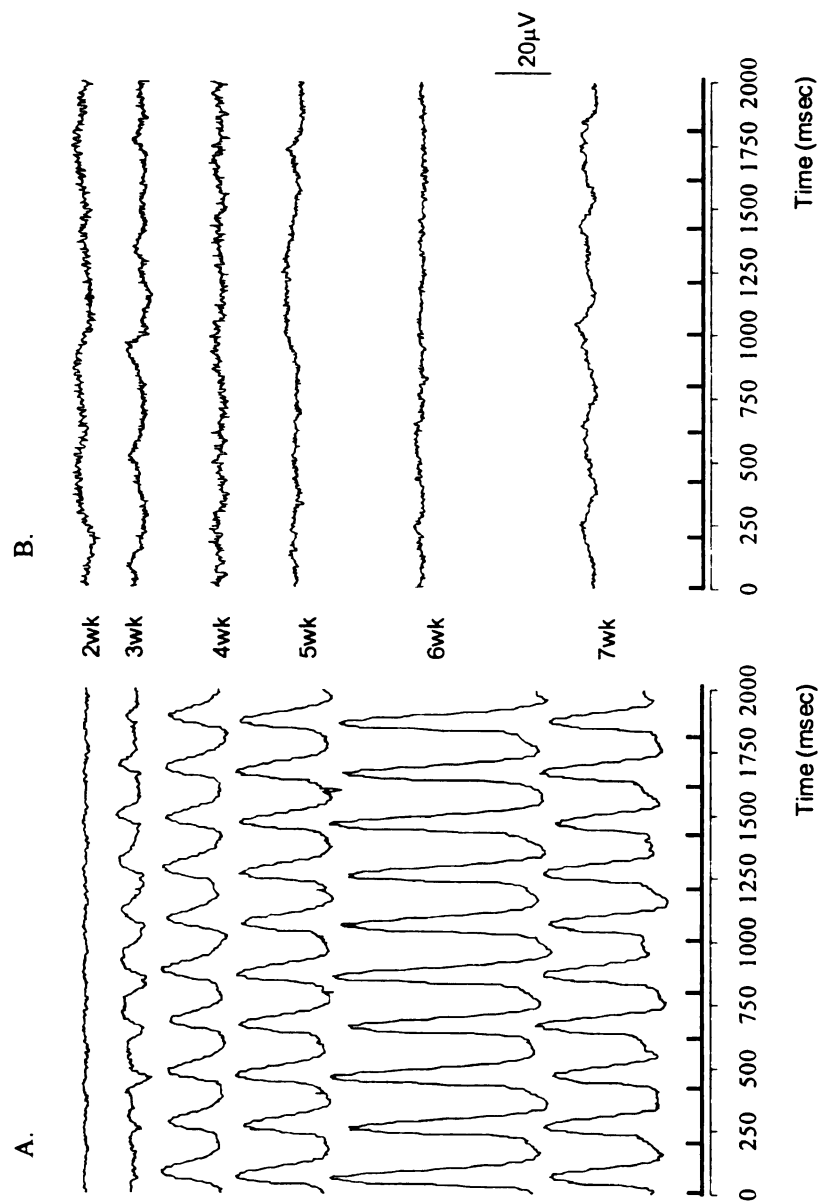


Figure 2.12. A comparison of representative rod flicker responses ($-1.6 \log \text{ cds/m}^2$, 5Hz) from a normal control (A) and the *PDE6A* mutant dog (B) at different ages. Spiking bar indicates onset of flicker flashes. Note the lack of flicker response from a *PDE6A* mutant dog. Key: μV = microvolt, msec = millisecond, wk = week.

2.3.1.g. Oscillatory potentials

Four major OPs are present in the ERG of normal dogs with the greatest peak at the OP3 (Figure 2.13). In normal controls, OPs obtained from 0.85 log cds/m² flash stimulus were first observed at 3 weeks of age with a mean summed value of 22.95 +/- 6.65 μ V, and then peaked at 9 weeks of age (131.4 +/- 16.8 μ V). Very small values of summed OPs were measured in the *PDE6A* mutant dogs at all ages investigated compared to normal controls. There was no significant change in OPs recorded from mutant dogs from 3 to 12 weeks of age (Figure 2.14).

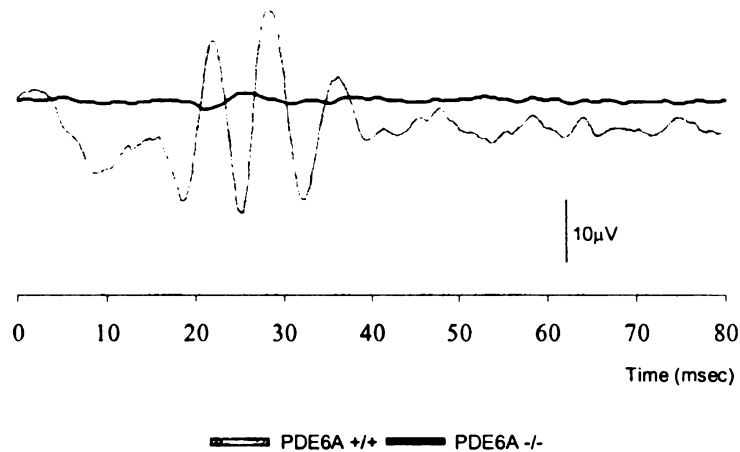


Figure 2.13. Representative scotopic oscillatory potential (0.85 log cds/m²) from normal control and *PDE6A* mutant dogs at 5 weeks of age (band pass at 73 to 500 Hz). The light onset is at 0 msec. Note that the scotopic ERG response of the mutant dog does not contain a typical canine OP feature such as that seen in the normal control. Key: μ V = microvolt, msec = millisecond.

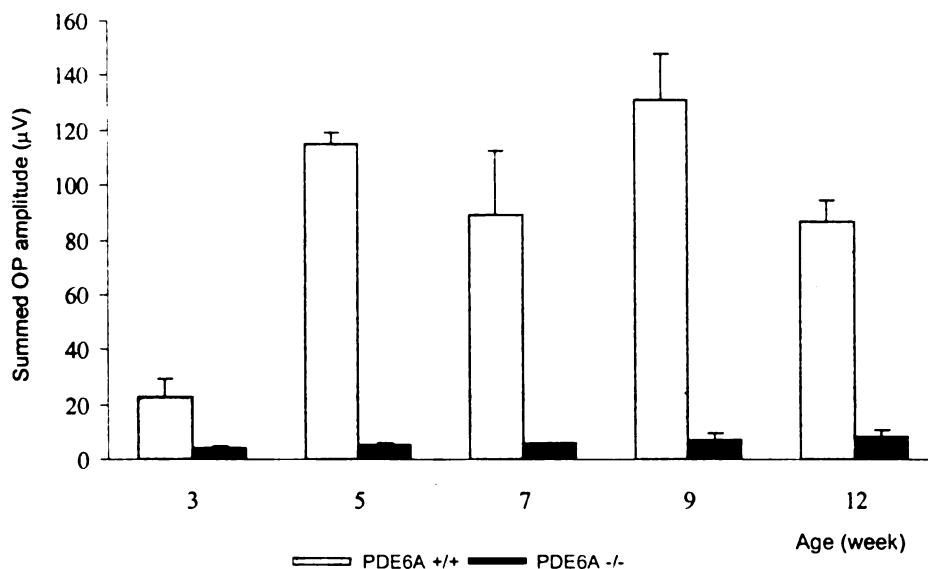


Figure 2.14. Mean scotopic oscillatory potential amplitudes with standard errors ($1x + SEM$) of normal controls and the *PDE6A* mutant dogs plotted against age. ($n = 2$ for each group of dogs). Note that the *PDE6A* mutant dogs have diminutive OP amplitudes at all ages investigated. Key: μV = microvolt.

2.3.2. Photopic ERG responses

The photopic ERG waveforms were analyzed in the following ways:

- a- and b-wave amplitudes and implicit times
- amplitude of a- and b-wave at selected criterion threshold ($5 \mu V$)
- cone flicker responses
- photopic negative responses
- long flash ERG responses

2.3.2.a. Photopic ERG amplitudes (Figures 2.15, 2.16, 2.17 & 2.18)

The mean photopic ERG amplitudes of normal controls increased with increasing flash intensity up to an intensity of about 1.9 log cds/m². The amplitudes, particularly of the b-wave tended to decrease slightly at the brightest of intensity. In the *PDE6A* mutant dogs the means of both a- and b-wave peaked at 3 weeks of age, after which the mean a-wave amplitudes progressively decreased and were significantly smaller ($P<0.05$) compared to those of normal controls. Following a comparable photopic a-wave intensity threshold at 2 weeks of age between the *PDE6A* mutant group and normal controls, the mean intensity threshold of the *PDE6A* mutant dogs was significantly higher ($P<0.05$) than the normal controls (Figure 2.18).

Although after 3 weeks of age, the mean a-wave photopic amplitudes of the mutant dogs decreased with age, those of the b-wave were relatively well maintained (Figure 2.17). By 6 weeks of age (Figures 2.15D & 2.16C), the mean a-wave amplitude of the *PDE6A* mutants did not reach the threshold criterion, while the threshold of the normal controls remained constant (Figure 2.18). A significant difference ($P<0.05$) between the mean photopic a-wave amplitude of the two groups of dogs was found from 6 weeks of age onward at the higher light intensities investigated (Figure 2.16C to E). The mean b-wave amplitudes were comparable until 7 weeks of age then decreased afterward particularly at the higher intensities (Figure 2.17). The b-wave intensity threshold response was also comparable between the two groups throughout the

investigation (Figure 2.18). The mutant dogs had a significantly smaller b-wave amplitude ($P<0.05$) for the brightest stimulus intensities at 9, 12 and 16 weeks of age.

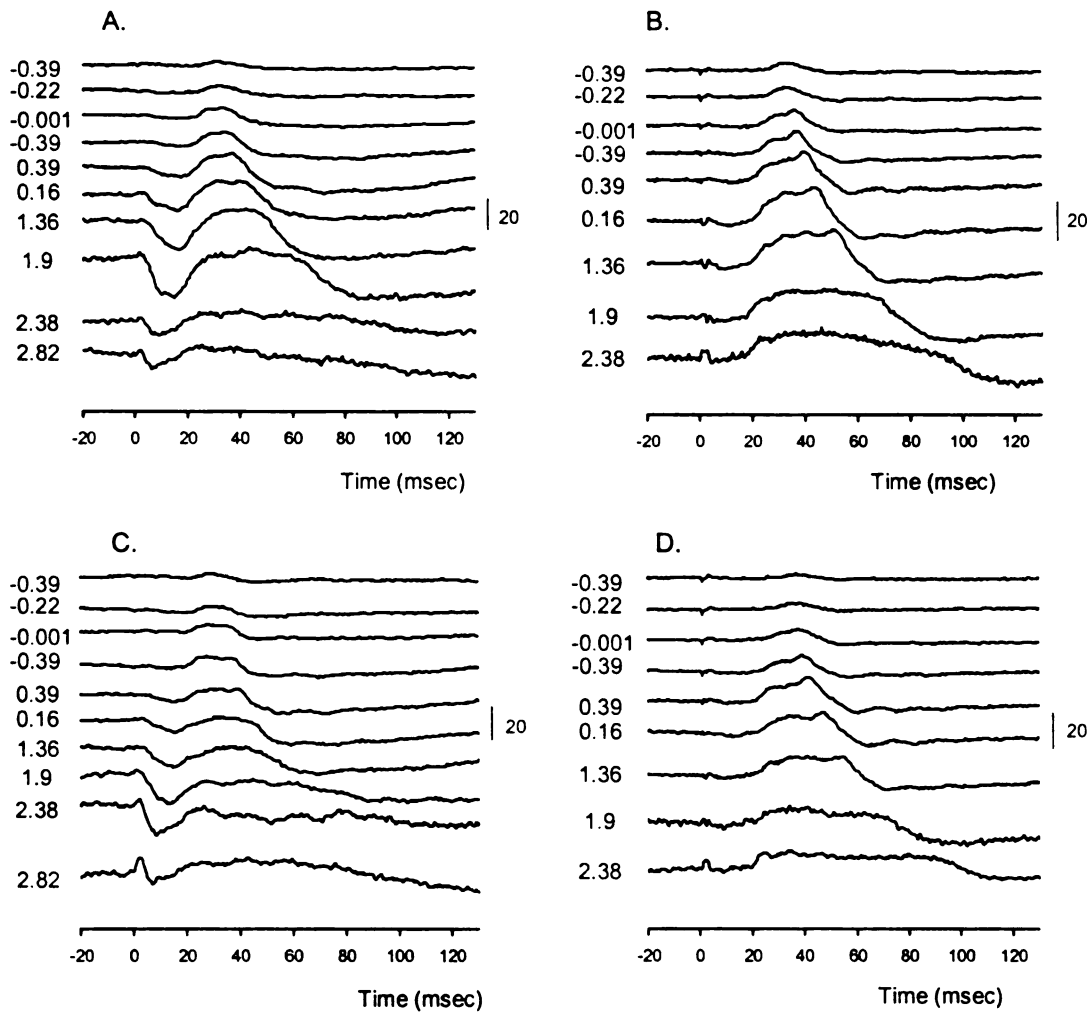


Figure 2.15. Representative photopic ERG recordings from a normal control (A & C) and the *PDE6A* mutant dog (B & D) at 4 (A & B) and 6 (C & D) weeks of age. Light intensities are indicated in the figure. The onset of flash is at 0 msec. A & B) In the normal control at 4 weeks of age, photopic ERG responses consist of a- and b-wave. A reduction in b-wave amplitude occurs at very bright flashes such as 2.38 and 2.82 log cds/m². This phenomenon is known as the photopic hill. In the *PDE6A* mutant dog in contrast, the a-wave is considerably smaller while b-wave is similar in amplitude to normal control. C & D) At 6 weeks of age, a small a-wave is only recordable in the *PDE6A* mutant dog at 0.16 and 1.36 log cds/m². The b-wave is still present at all light intensities, but is reduced in amplitude in comparison to that of the normal control. Size bars indicate amplitude in microvolt.

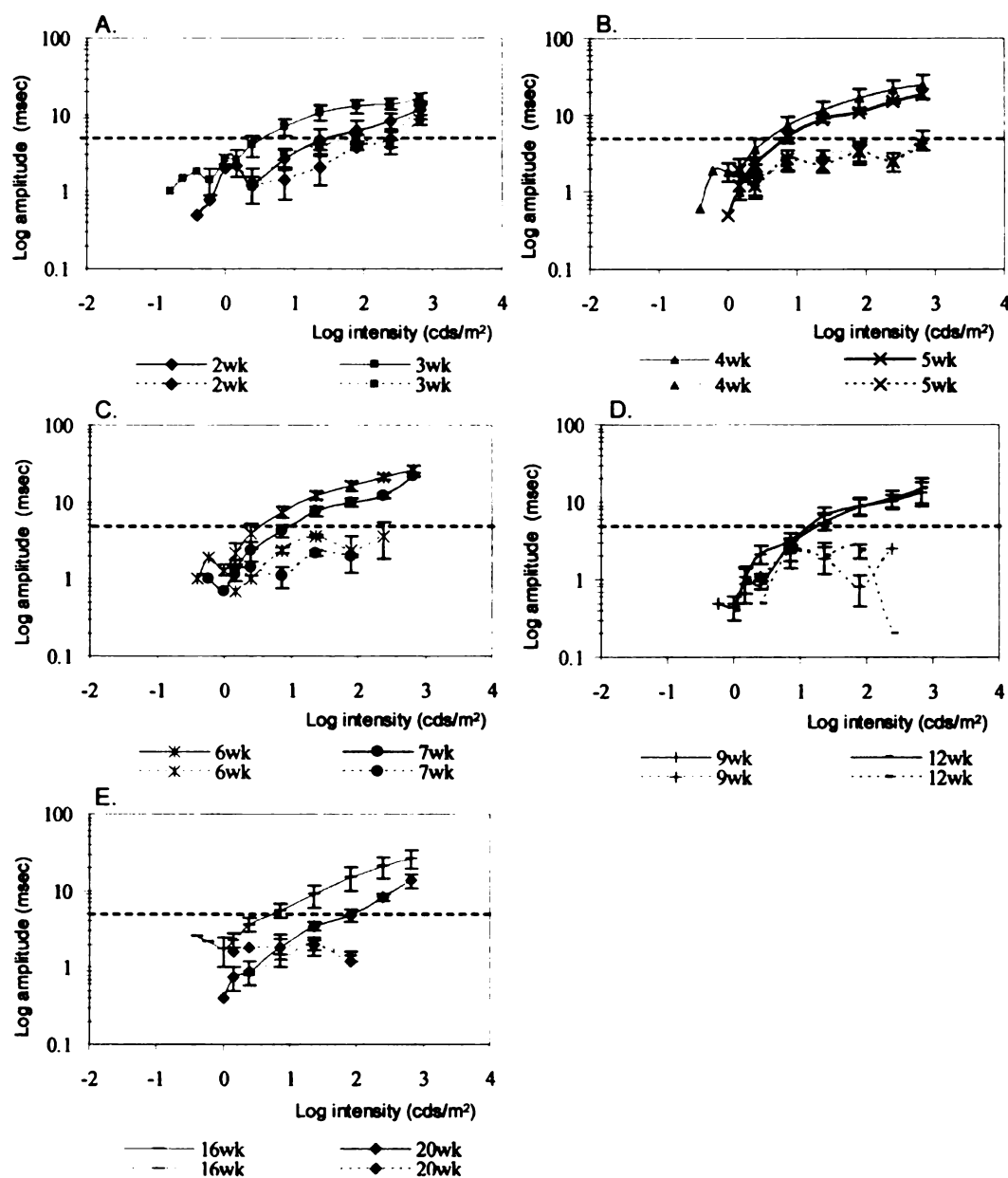


Figure 2.16. Mean photopic a-wave amplitudes with standard errors ($1x \pm$ SEM) plotted against stimulus intensity on a log-log scale from normal control and *PDE6A* mutant dogs at 2 & 3 (A), 4 & 5 (B), 6 & 7 (C), 9 & 12 (D) and 16 & 20 (E) weeks of age. The selected a-wave photopic criterion threshold is 5 μ V (dashed black line). Solid lines and dot lines represent values from normal controls and the mutant dogs, respectively. Various colors represent the mean photopic a-wave amplitudes at different ages. ($n = 4$ for each group of dogs) Note that at flash intensities higher than 0.5 log cds/m², a significant difference ($P < 0.05$) in the mean photopic a-wave amplitudes between the two groups of dog is observed at all ages for nearly all intensities. After 5 weeks of age the a-wave amplitudes of the *PDE6A* mutant dogs do not reach the selected criterion threshold.

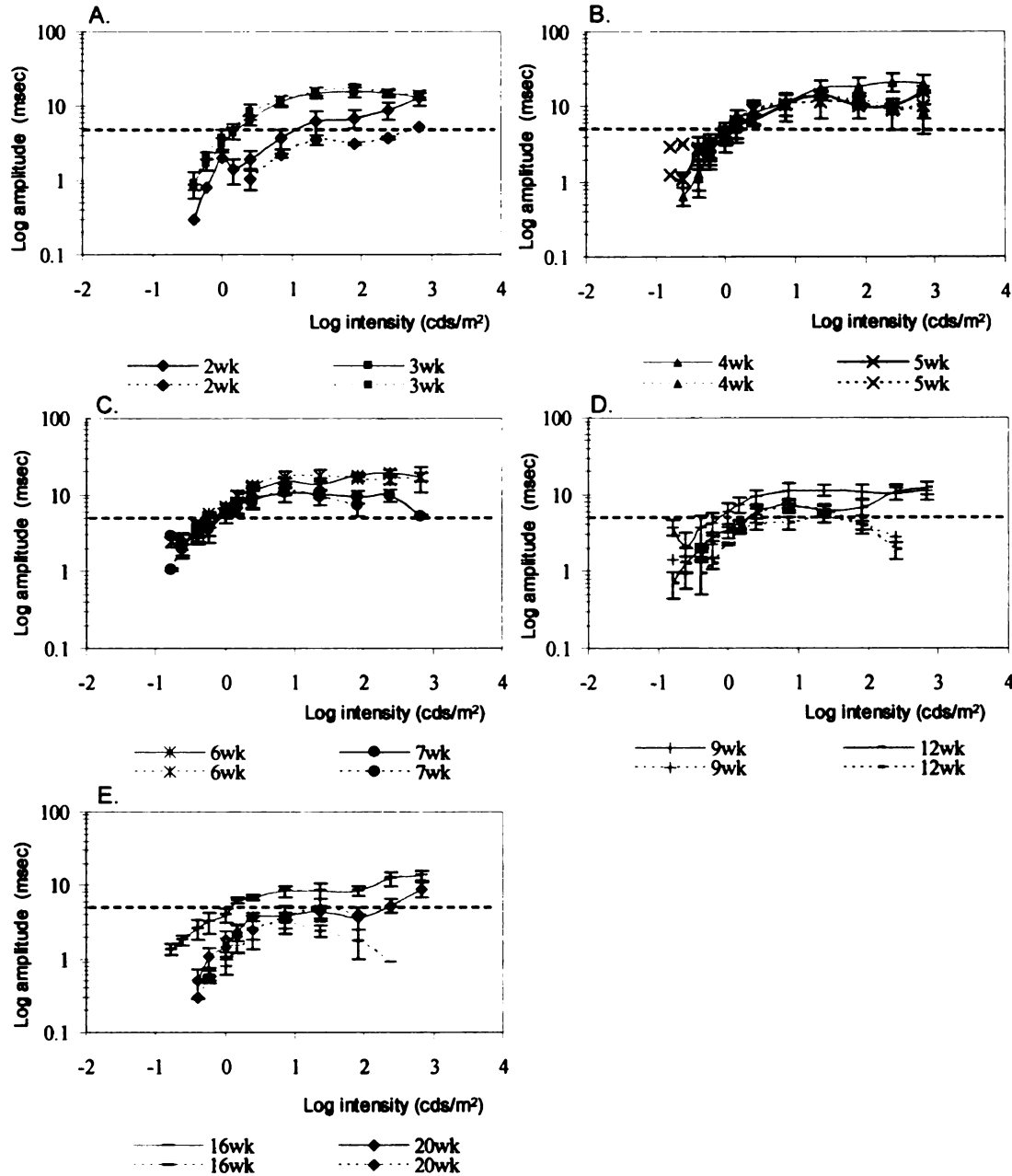


Figure 2.17. Mean photopic b-wave amplitudes with standard errors ($1x \pm \text{SEM}$) plotted against stimulus intensity on a log-log scale from normal control and *PDE6A* mutant dogs at 2 & 3 (A), 4 & 5 (B), 6 & 7 (C), 9 & 12 (D) and 16 & 20 (E) weeks of age. The selected b-wave photopic criterion threshold is $5 \mu\text{V}$ (dashed black line). Solid lines and dot lines represent values from normal controls and the mutant dogs, respectively. Various colors represent the mean photopic b-wave amplitudes at different ages. ($n = 4$ for each group of dogs) The mean photopic b-wave amplitudes are similar between control and *PDE6A* mutant dogs except for the brighter intensities from 9 weeks of age onwards when the amplitudes are significantly smaller ($P < 0.05$) in mutant dogs.

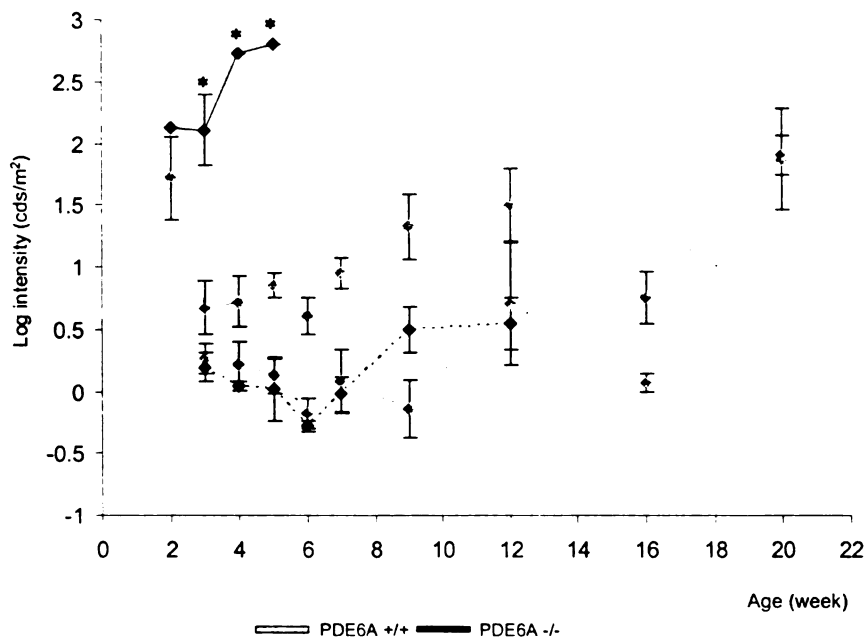


Figure 2.18. Mean intensity at threshold from photopic recordings with standard errors ($1x \pm \text{SEM}$) using a $5\mu\text{V}$ criterion for a- and b-wave amplitudes from normal control and *PDE6A* mutant groups at all ages tested. ($n = 4$ for each group of dog) Solid lines represent a-wave intensity threshold, and dot lines represent b-wave intensity threshold. Note that there is a significant difference ($P < 0.05$) in mean a-wave intensity threshold in the *PDE6A* mutant group at 3 weeks of age and older whereas there is no significance difference ($P > 0.05$) in b-wave intensity threshold between the two groups. Key: * indicates statistical difference of the a-wave intensity threshold at $P < 0.05$.

2.3.2.b. Photopic ERG implicit time (Figures 2.19 & 2.20)

The mean photopic a- and b-wave implicit times tended to decrease with increasing light intensity in normal dogs. There was a more marked reduction in a-wave implicit time than b-wave implicit time. The a- and b-wave implicit times of the mutant dogs were similar to controls. For the older age groups tested, the a-wave of the mutant dogs was not always recordable in response to brighter flashes and in some instances when it was still recordable had a longer implicit time at the brighter intensities.

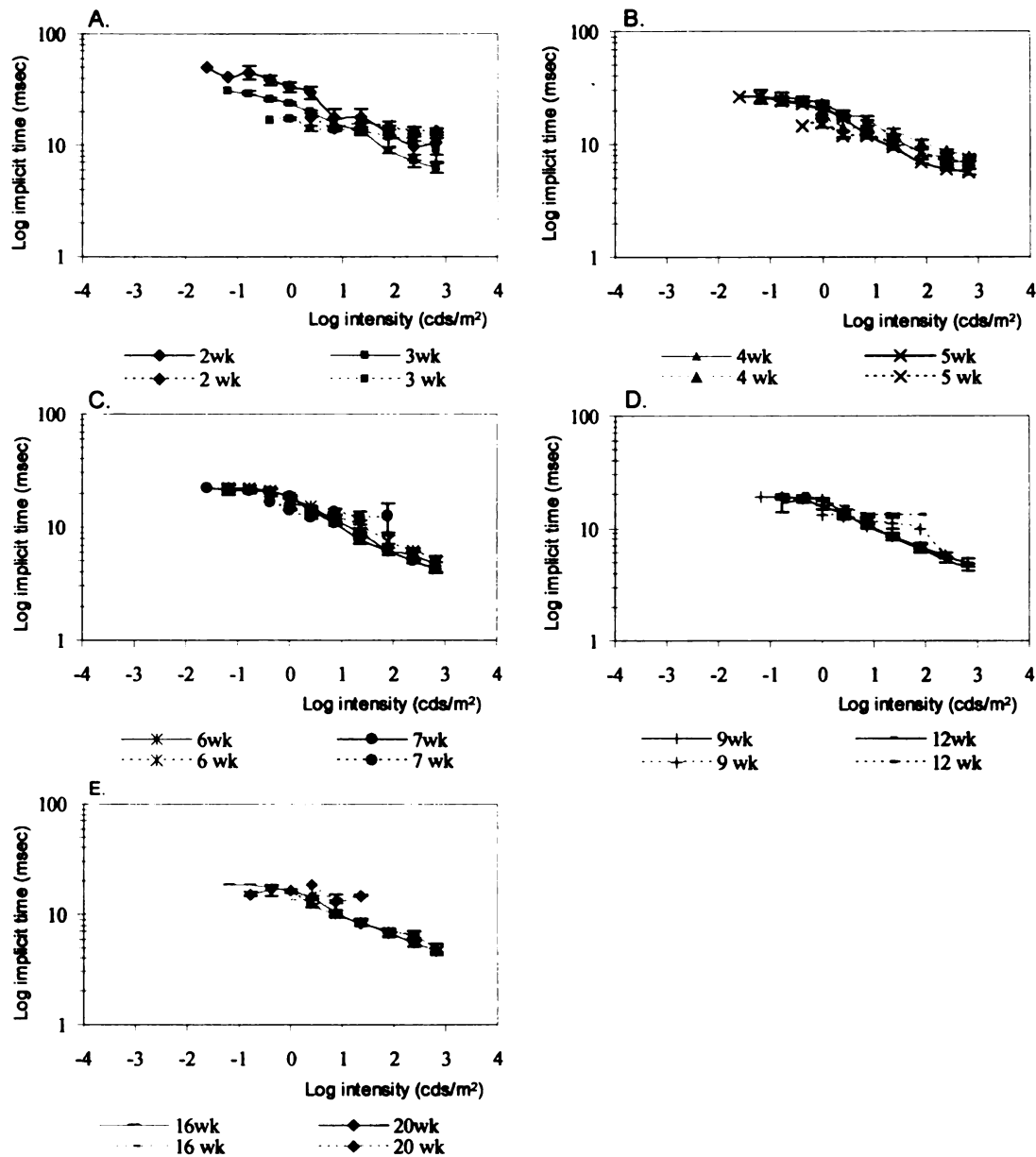


Figure 2.19. Mean photopic a-wave implicit times with standard errors ($1x \pm$ SEM) plotted against stimulus intensity on a log-log scale from normal control and *PDE6A* mutant dogs at 2 & 3 (A), 4 & 5 (B), 6 & 7 (C), 9 & 12 (D) and 16 & 20 (E) weeks of age. Solid lines and dot lines represent values from normal controls and the mutant dogs, respectively. Various colors represent the mean photopic a-wave implicit times at different ages. ($n = 4$ for each group of dogs) Note a similar pattern of a decrease in the mean photopic a-wave implicit time with increasing light intensity in both groups of dogs. From 9 to 20 weeks of age the a-wave implicit time of the mutant dogs is significantly increased compared to controls ($P < 0.05$) and not recordable at some of the brightest intensities.

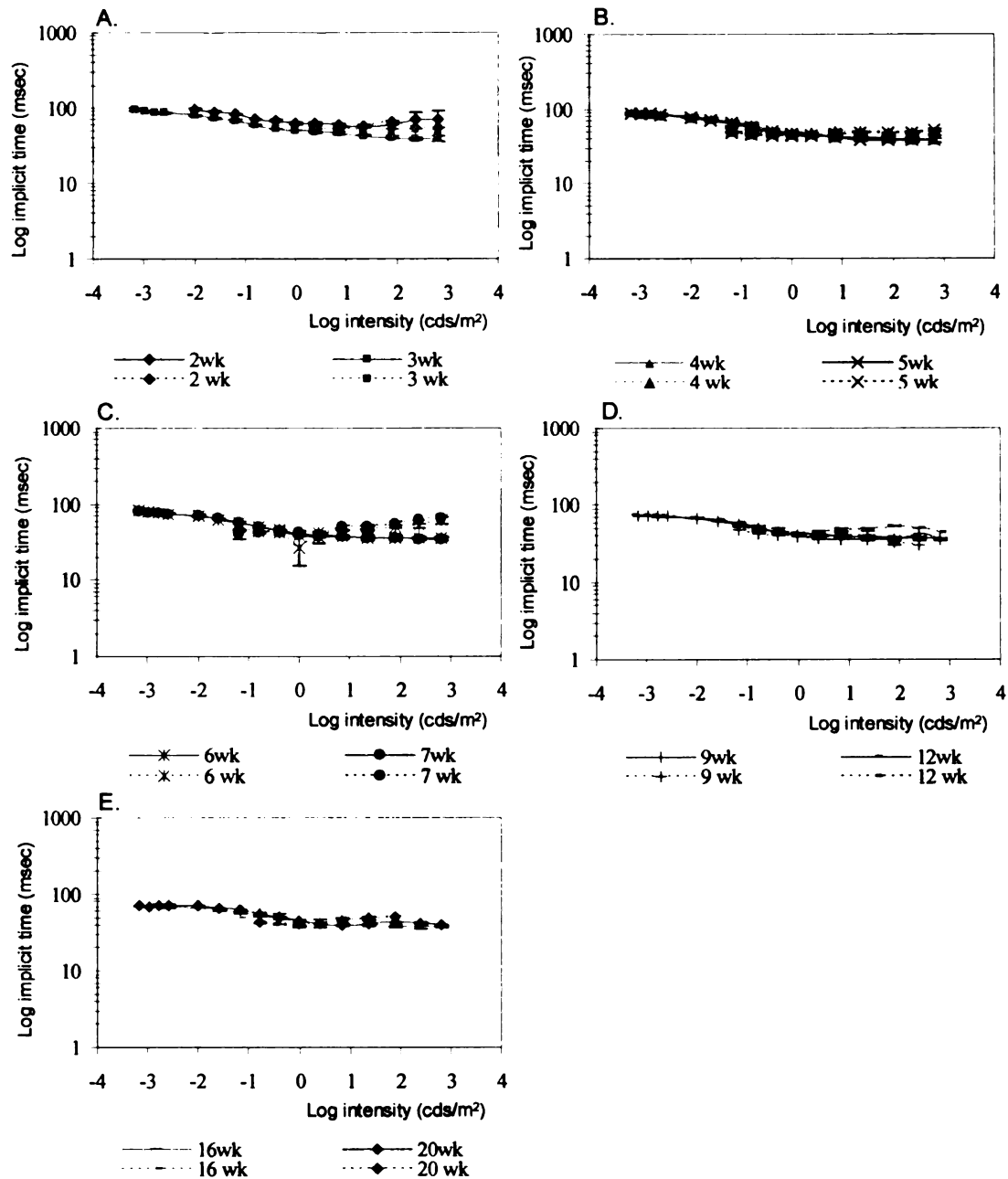


Figure 2.20. Mean photopic b-wave implicit times with standard errors ($1x \pm$ SEM) plotted against stimulus intensity on a log-log scale from normal control and *PDE6A* mutant dogs at 2 & 3 (A), 4 & 5 (B), 6 & 7 (C), 9 & 12 (D) and 16 & 20 (E) weeks of age. Solid lines and dot lines represent values from normal controls and the mutant dogs, respectively. Various colors represent the mean photopic b-wave implicit times at different ages. ($n = 4$ for each group of dogs) Note that the mean b-wave implicit time tends to become significantly delayed ($P < 0.05$) from 5 weeks of age at higher light intensity and in older puppies also at lower intensities.

2.3.2.c. Cone flicker ERG response (Figures 2.21 & 2.22)

The cone flicker response could be detected from 3 weeks of age and at that age was similar between normal controls and mutant dogs. In normal controls the amplitude increased with retinal maturation to peak at 6 weeks of age. This was followed by a gradual decrease with age. In the *PDE6A* mutant dogs the cone flicker amplitude followed a similar pattern to the normal controls, however it was significantly smaller ($P<0.05$) from 5 weeks of age onward (Figure 2.22A) although at 20 weeks of age the difference was not significant. By 52 weeks of age the cone flicker response could not be detected in the *PDE6A* mutant dogs (data not shown). A similar pattern of the mean cone flicker implicit time development was also observed; it slightly increased with age prior to 5 weeks of age in normal controls and mutant dogs and then progressively decreased until 16 weeks of age. Except at 3 weeks of age, the mean cone flicker implicit time was smaller in the *PDE6A* mutant dogs compared to the normal controls, but these differences were not significant (Figure 2.22B).

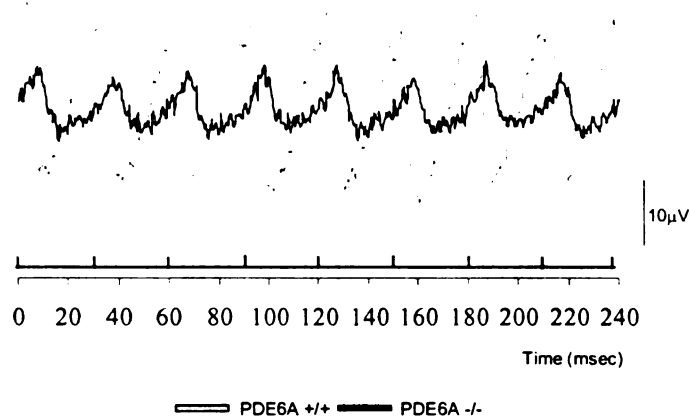


Figure 2.21. A comparison of representative cone flicker responses ($0.39 \log \text{ cds/m}^2$, 33 Hz) from a normal control and the *PDE6A* mutant dog at 9 weeks of age. Spiking bar indicates onset of flicker flashes within the recording time (250 msec). A bi-phasic appearance of cone flicker response is seen in the normal control. Note that the *PDE6A* mutant dog has reduced flicker amplitude and slight delayed flicker implicit time compared to the control. Key: μV = microvolt, msec = millisecond.

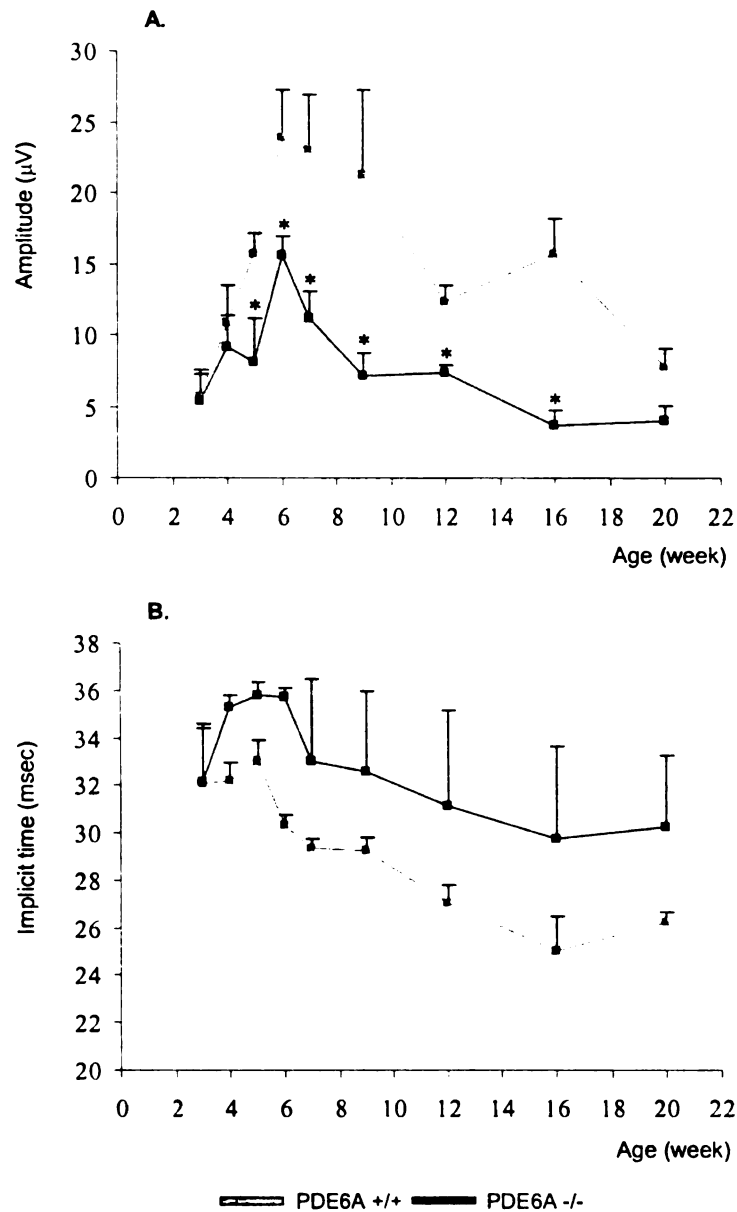


Figure 2.22. Mean and standard errors ($1x + \text{SEM}$) of cone flicker amplitudes (A) and cone flicker implicit times (B) of normal controls and *PDE6A* mutant dogs ($0.39 \log \text{ cds/m}^2$, 33 Hz) at all age groups. ($n = 4$ for each group of dog) Note there is a significantly smaller ($P < 0.05$) photopic flicker amplitude in the *PDE6A* mutant group in comparison to normal controls for 5 to 16 weeks of age. Note that the differences in implicit times are not statistically significant. Key: μV = microvolt, msec = millisecond.

2.3.2.d. Photopic negative response (Figure 2.23)

A PhNR was present at 2 weeks of age in normal controls and increased with age. In the normal controls it matured at 5 to 6 weeks of age ($\sim 15 \mu\text{V}$) (Figure 2.23) and was maintained until the last time point examined (52 weeks of age) (data not shown). The PhNR in the *PDE6A* mutant dogs was smaller than in controls. It also increased with age from 2 weeks and matured at 5 to 7 weeks of age. It then progressively decreased. By 52 weeks of age, it was non-recordable (data not shown).

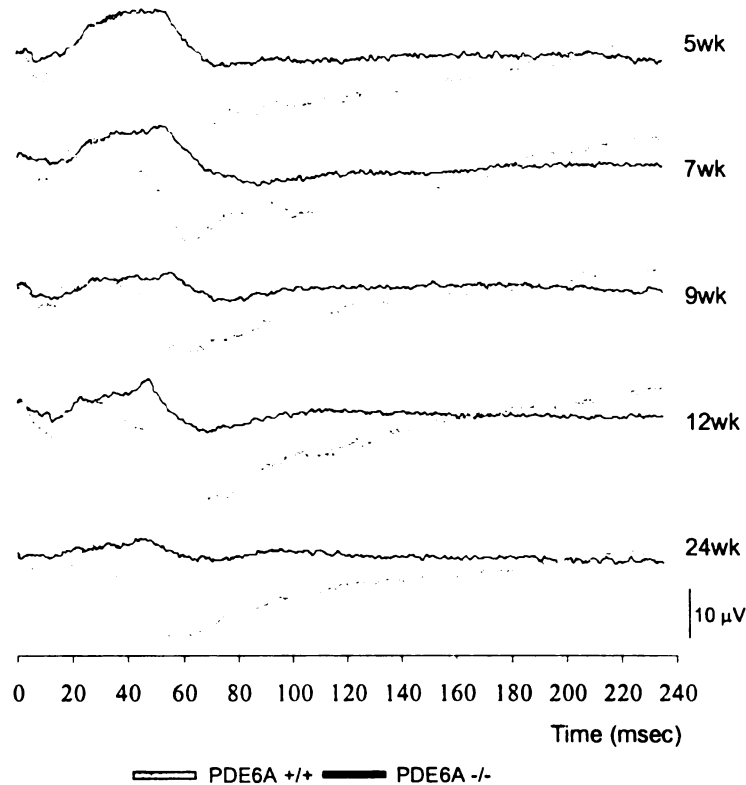


Figure 2.23. Representative photopic ERG responses ($1.36 \log \text{cds/m}^2$) from a normal control and the *PDE6A* mutant dog at different ages demonstrating the photopic negative response. The light onset is at 0 msec. Note that the PhNR, a response measured from the baseline to the negative trough after the peak of the b-wave is smaller in the *PDE6A* mutant dog when compared to that of the normal control. Key: μV = microvolt, msec = millisecond, wk = week.

2.3.2.e. Long flash ERG response (Figure 2.24 & 2.25)

The long flash ERG response in dogs following 10 minutes of white light adaptation consists at light onset of an a-wave, followed by a b-wave and a post negativity of the b-wave (PhNR). While the light remained on, there was usually a slow increase towards the baseline. Approximately 20 to 25 milliseconds after the light offset, a small positive wave appeared, which was then followed by a larger negative wave (d-wave) (Figure 2.24). In normal controls, long flash ERG responses increased with age over the period of retinal maturation, whereas they diminished in the *PDE6A* mutant dogs (Figure 2.25A & 2.25B). The b/d amplitude ratio of the normal control increased from 4 to 7 weeks of age and was then fairly constant. The d-wave recorded from mutant dogs at 5 to 6 weeks of age appeared to have one of two forms. In 3 of 7 mutant dogs tested the amplitude was decreased while in 4 of the 7 there was very much increased d-wave amplitude (Figure 2.25B shows one example of each response seen). By 28 weeks of age in the mutant dog, the d-wave had vanished while b-wave was still present but very small (data not shown). By 52 weeks of age, long flash ERG responses were not recordable in the *PDE6A* mutant dogs (data not shown). With the exception of the puppies with large d-wave amplitudes at 5 to 6 weeks of age, the b/d amplitude ratio in mutant dogs was high compared to that of normal controls at all ages tested.

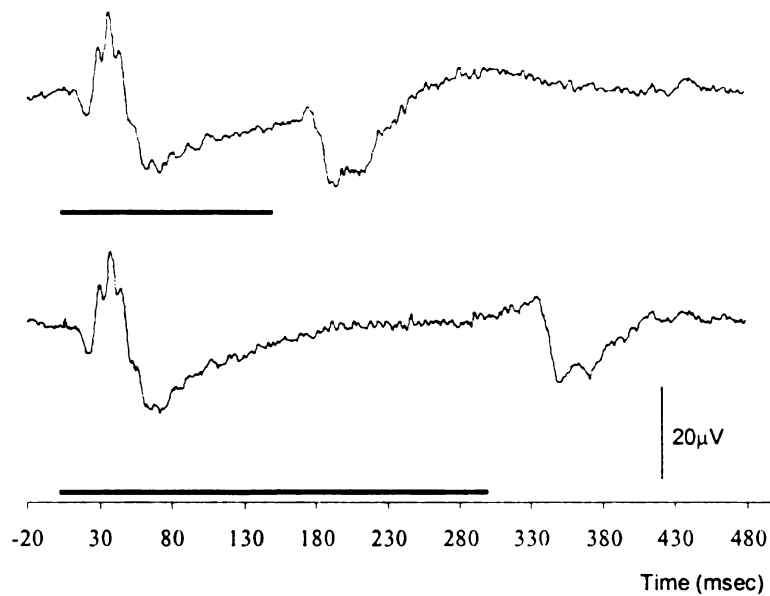


Figure 2.24. A representative long flash ERG from a normal control dog of 60 weeks of age. ERG-Jet lens is used as a corneal recording electrode. Bar indicates flash duration, which is 150 msec (top tracing) and 300 msec (bottom tracing). At light onset, a-wave (the first negative potential) is seen preceding the b-wave (the first positive potential). Following the post b-wave negativity there is a slight increase towards the baseline. The off-response is shown at light offset, and it comprises of a small positive potential immediately followed by a larger negative response. Key: μV = microvolt, msec = millisecond.

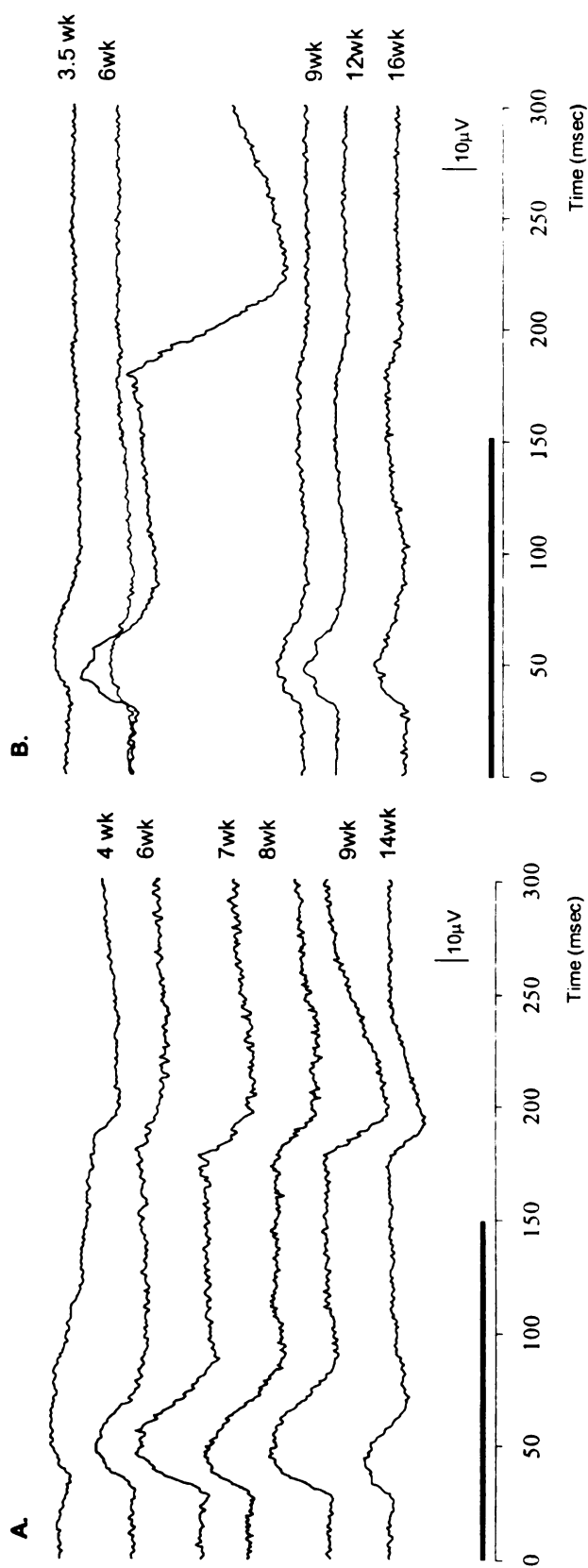


Figure 2.25. Representative long flash ERG recordings from normal controls (A) and *PDE6A* mutant dogs (B) with age (week). Note that the ERGs are recorded using Burian-Allen bipolar recording electrode. Bar indicates flash duration (150 msec). The normal control shows developing a-, b- and d-wave responses with age whereas the responses are smaller in the *PDE6A* mutant dog. Note that two waveforms are shown for the *PDE6A* mutant dog at 6 weeks of age. In some dogs a very large negative off-response is transiently recordable. In other dogs, despite weekly recordings, this feature is not seen. Key: μ V = microvolt, msec = millisecond, wk = week.

2.4. Discussion

The ERG study showed that the *PDE6A* mutant dogs have a severe lack of rod response from an early postnatal age. There was a marked increase in scotopic threshold, reduced scotopic amplitudes, undetectable a-wave responses to blue flashes and an absence of rod flicker responses. Similar abnormal changes in the ERGs were recorded from *rcd1* dogs at very young age (Buyukmihci et al., 1980), the *rcd2* dogs (Wolf et al., 1978) and the *erd* dogs (Acland & Aguirre, 1987), all of which have an early-onset retinal degeneration. Cone responses of the *PDE6A* mutant dogs are initially normal but show a progressive decline with age.

Several ways were used in this study to investigate whether any rod function developed in mutant puppies. An attempt was made to assess rod function by analysis of the leading edge of the rod-mediated a-wave at high flash intensity (a-wave modeling) as derived from a subtraction of intensity-matched cone-only response from rod plus cone response (Lamb & Pugh, Jr., 1992a). A-wave modeling was not possible in the mutant dog because scotopic ERG amplitudes were very small and hardly met the minimum amplitude criterion of 9 μ V suggested for the analysis of the a-wave leading edge in humans. Fitting very low rod-mediated response to an equation of the a-wave leading edge may considerably lose the fitting quality, which could lead to data misinterpretation (Lamb & Pugh, Jr., 1992b; Tzekov et al., 2001). Therefore a-wave modeling using the data from mutant dogs was not performed. One of the alternative methods that we used in this study to assess rod function was to qualitatively evaluate the subtracted rod a-wave

response using a normalization (Hood & Birch, 1996) to standardize and compare the slope of the a-wave leading edge between the normal and mutant dogs. Using this technique a delayed negative amplitude response was derived from the rod-only mutant dog ERG, which was very rapidly lost in the first few weeks of age, suggesting a lack of rod function. It is not clear whether this waveform was truly the result of residual rod phototransduction in the young mutant puppy.

Application of the Naka-Rushton equation to fit the first limb of the scotopic b-wave intensity-response curve is suggested as a method to assess rod function. The first limb of the scotopic b-wave plotted against flash intensity from the *PDE6A* mutant dogs yielded poor fitting to the model, markedly reduced V_{max} values, increased k and n values. It seems likely that the response in the mutant dog was primarily from cones and it was the initial portion of the cone b-wave intensity-response curve that was fitted to the equation.

All of our investigations have shown severely reduced or absence rod responses in the *PDE6A* mutant puppies from an early age. It should be noted that the scotopic ERG waveforms recorded from the mutant dog at 6 weeks of age were very similar to those of the photopic waveforms suggesting that the residual responses may be due primarily or completely to cone-only function. Although cone responses were initially similar between mutant dogs and controls, a significant decrease in the mean photopic a-wave amplitude from the *PDE6A* mutant dogs was observed after a few weeks of age. This ERG finding is similar to that reported in the *rcd1* dogs in the postnatal period

(Buyukmihci et al., 1980), which showed that cone responses were also lost and that this was subsequently to rod degeneration. Significantly diminished cone sensitivity is shown as a shift to the right of the photopic a-wave intensity-response plot as well as significantly increased mean photopic a-wave threshold in contrast to the mean a-wave threshold of normal controls.

Photopic hill is a phenomenon that as the flash intensity increases, the photopic b-wave reaches peak amplitude and then decreases as the flash intensity increases. This results from the reduction of the ON-bipolar response and a delay in the OFF-bipolar response at high light intensities (Ueno et al., 2004). Compared to normal controls, the photopic hill from the *PDE6A* mutant dogs was shifted to the left as seen on the intensity-response plot suggesting that cone response was reduced. Besides a change of the photopic hill, a reduction of the mean photopic b-wave amplitude occurred in the mutant dogs at 9 weeks of age onward indicative of a progressive loss of cone function. Interestingly the photopic a-wave of mutant dogs started to decrease in amplitude in response to the brighter flashes and in some instances the ERG became unrecordable. The photopic a-wave has major contributions from the inner retina and there may have been some alteration of inner retinal responses in the mutant dog retina in response to brighter light stimulation.

Long flash ERG was performed to investigate any differential effect in ON- and OFF-pathways. It was shown that canine off-response consists of a transient small positive-going potential preceding a larger negative-going potential, which was then

followed by a slow off-component toward the baseline. Features of canine long flash waveform had previously been described (Shirao et al., 1997). A negative d-wave is also seen in amphibians (Dick & Miller, 1985a) and some mammals such as cats (Frishman & Steinberg, 1990), rabbits (Dick et al., 1985) and rats (Lei, 2003). Conversely, a positive d-wave is present in humans, primates and chickens. An ERG with a negative d-wave was described as the E-type (excitatory) retina and that with a positive d-wave the I-type (inhibitory) retina by Granit (1935). Granit (1935) suggested that the difference between these two types of retina might depend on the number of cones. Evers and Gouras (1986) suggested that it may depend on the type of cones, with S-cone responses in monkeys having an E-type response and M- and L-type cones an I-type d-wave. Granit's theory is supported by evidence in humans with cone-rod dystrophy, once the photopic ERG amplitudes were reduced by 90%, the d-wave became negative.

We showed that the d-wave of normal controls increased in amplitude to about 9 weeks of age, whereas in the mutant dogs, the d-wave was small at all ages investigated except for a subpopulation of mutant dogs at 5 to 6 weeks of age. Size of the d-wave is proportional to the b-wave in both normal controls and mutant dogs although the b/d amplitude ratio in mutant dogs was higher. The abnormally large d-wave transiently recordable from some mutant dogs at 5 to 6 weeks of age may represent some differential effect of the disease on the ON- and OFF- pathways and requires investigation to elucidate it further. A dissection of the components of the on- and off-responses to identify their neuron of origin forms part of chapter 3. In addition to changes of d-wave, OPs and PhNR are also influenced by photoreceptor loss.

The results of our ERG studies in the *PDE6A* mutant dogs showed that rod function is reduced or absent from an early stage in retinal maturation, and is followed by a slow deterioration in cone function. Reduced signal transmission from photoreceptors to the second- and the third-order neurons reflects reduced responses from rod and cone pathways in the mutant dogs. A long flash study using different light wavelength to differentially stimulate the two types of cones could be used to detect any differential effect of the disease on the two cone types of the dog.

Chapter 3

Pharmacological dissection of the *PDE6A* electroretinogram

3.1. Introduction

As described in Chapter 1, intravitreal drugs that block intraretinal pathways have been used to investigate the origin of components of the electroretinogram (ERG). Conventional ERG investigations (Chapter 2) showed the *PDE6A* mutant dogs have very reduced ERG waveforms. To further investigate this, we used drugs to dissect the canine ERG. It was necessary to establish the effect of the drugs on the ERG of normal dog before they were applied to the ERG of the *PDE6A* mutant dog.

The glutamate analog 2-amino-4-phosphonobutyric acid (APB) selectively blocks the influence of photoreceptors on ON-bipolar cells. Thus APB blocks rod and cone transmission to ON-bipolar cells, leaving the cone connected to OFF-bipolar cells intact. Application of APB in primates eliminates the scotopic and photopic OPs indicating that the drug has an effect on the third-order neurons as well (Jamison et al., 2001).

The glutamate antagonist *Cis*-2,3-piperidine-dicarboxylic acid (PDA) blocks transmission through OFF-bipolar cells, horizontal cells and amacrine cells without diminishing the light response of ON-bipolar cells (Sieving et al., 1994).

Tetrodotoxin (TTX), a voltage-gated sodium channel blocker, prevents action potentials in ganglion cells, some types of amacrine cells (Bloomfield, 1996) and interplexiform cells (Bui & Fortune, 2004b). TTX has been used to block the PhNR and mimic the effect on the ERG of glaucoma or optic neuropathy in a primate model (Rangaswamy et al., 2004a).

3.2. Materials and methods

3.2.1. Animals

Homozygous *PDE6A* mutant dogs and normal controls at 4, 7, 16, and 60 weeks of age were used in this experiment.

3.2.2. Pharmacological agents

3.2.2.a. 2-amino-4-phosphonobutyric acid (APB) (Sigma Aldrich; St. Louis, MO)

3.2.2.b. *Cis*-2,3-piperidine-dicarboxylic acid (PDA) (Sigma Aldrich; St. Louis, MO)

3.2.2.c. Tetrodotoxin (TTX) (Sigma Aldrich; St. Louis, MO)

3.2.3. Intravitreal injection

The maximum volume injected for all agents was 60 μ l in puppies and 150 μ l in 16 and 60 week-old dogs. To calculate the amount of agent that had to be injected to achieve the desired final vitreal concentration, the volume of the vitreous body of euthanized dogs had been previously measured by aspirating it into a syringe. The target vitreal concentrations of APB, PDA and TTX were selected based on the results of studies in other species and were 3mM, 7mM and 6 μ M, respectively.

APB was dissolved in 0.9% sterile saline, heated at 60°C for 3 hours and filtered through a sterile 0.22 μ m filter (Millex-GS, Millipore Corp, Bedford, MA). PDA and TTX were dissolved in 0.9% sterile saline and filtered through a sterile 0.22 μ m filter (Millex-GS, Millipore Corp, Bedford, MA). Agents were injected into the vitreous through the pars plana approximately 4-7 mm posterior to the dorsal corneal limbus using a Hamilton syringe fitted with a 30-gauge needle. The needle was directed towards the region of the optic nerve head to avoid contacting the lens.

3.2.4. Electroretinographic recording

3.2.4.a. Anesthesia and recording electrode placement

These were as described previously (see Chapter 2; section 2.2.2.a and 2.2.2.b.)

3.2.4.b. Electroretinographic recording

A baseline ERG was recorded immediately before the intravitreal injection and at several different times after the injection to detect when the maximum response had developed. A Burian–Allen bipolar contact lens was used as the recording electrode. A needle electrode placed subcutaneously at the back of cervical region was used as a ground electrode. The UTAS-E 3000 electrophysiology unit (LKC Technologies Inc; Gaithersburg, MD) was used to record scotopic and photopic short flash ERG and flicker responses. The band pass was set at 1 to 500 Hz; gain setting varied from 2×10^3 to 4×10^4 . The time base was set to record 20 msec pre-stimulus. Inter-stimulus intervals were set and ERG responses averaged based on flash intensities as described in chapter 2.

Full-field long flash ERGs were recorded using a customized Ganzfeld stimulator unit connected to the UTAS-E 3000 electrophysiology unit and the duration of flash was set at 150 msec. Responses were amplified with a bandpass of 0.3 to 500 Hz, and up to 30 responses averaged. All ERG waveforms were averaged, and then stored for further analysis using LKC software.

3.2.4.c. Electroretinographic test protocols

3.2.4.c (i). Scotopic and photopic short flash electroretinography

For scotopic ERGs dogs were dark-adapted for 60 minutes. A series of white flash stimuli ranging in intensity from -2.6 to 1.9 log cds/m² were used. For photopic response, the dogs were light-adapted for 10 minutes to a background white light of 30 cd/m². Then a series of white light stimuli ranging in intensity from -0.001 to 1.36 log cds/m² were superimposed on the same background light. (See Chapter 2 for more details)

3.2.4.c (ii). Flicker electroretinography

Rod and cone flicker ERGs were recorded using a white light of -1.6 log cds/m² at 5 Hz and 0.39 log cds/m² at 33 Hz, respectively, on the dark-adapted eye.

3.2.4.c (iii). Long flash electroretinography

Dogs were light-adapted for 10 minutes to a background light of 42 cd/m², followed by a white flash stimulus of 2.25 log cds/m² of 150 msec duration superimposed on the same background light. (See chapter 2 for more details)

3.2.5. Data analysis

ERG was qualitatively compared between age-matched homozygous *PDE6A* mutant dogs and normal controls before and after the intravitreal injections.

3.3. Results

3.3.1. Results after the intravitreal injection of APB (Figures 3.1 to 3.6)

3.3.1.a. Short flash scotopic and photopic ERG intensity-series responses from normal control dogs

In studies using a normal dog as a control, intensity-series ERGs performed before and after the intravitreal injection of APB revealed that the peak effect of the APB had developed at between 1.5 and 2 hours post injection. The action of the drug to block ON-bipolar cells almost completely eliminates the b-wave. At dim lights, the scotopic b-waves were suppressed. At brighter intensities, the scotopic a-waves were slightly increased in amplitude most likely by removal of the imposition of the b-wave on the a-wave (Figure 3.1A). Following the a-wave there was a positive-going potential that returned towards the baseline. The OPs were suppressed by the action of APB.

The effect of the APB on the photopic intensity-series ERGs was similar to the effect of the APB on the scotopic intensity-series ERGs. A-wave amplitudes were slightly increased; and the b-waves and OPs were suppressed (Figure 3.1B).

In the normal control and the mutant puppies at 4 weeks of age (Figure 3.2A & 3.2B), APB suppressed the b-wave leaving the a-wave. By 6 weeks of age, in the mutant puppy the a-wave was not recordable and the b-wave was reduced in amplitude.

However, the effect of APB was still evident and eliminated the residual b-wave (Figure 3.2C).

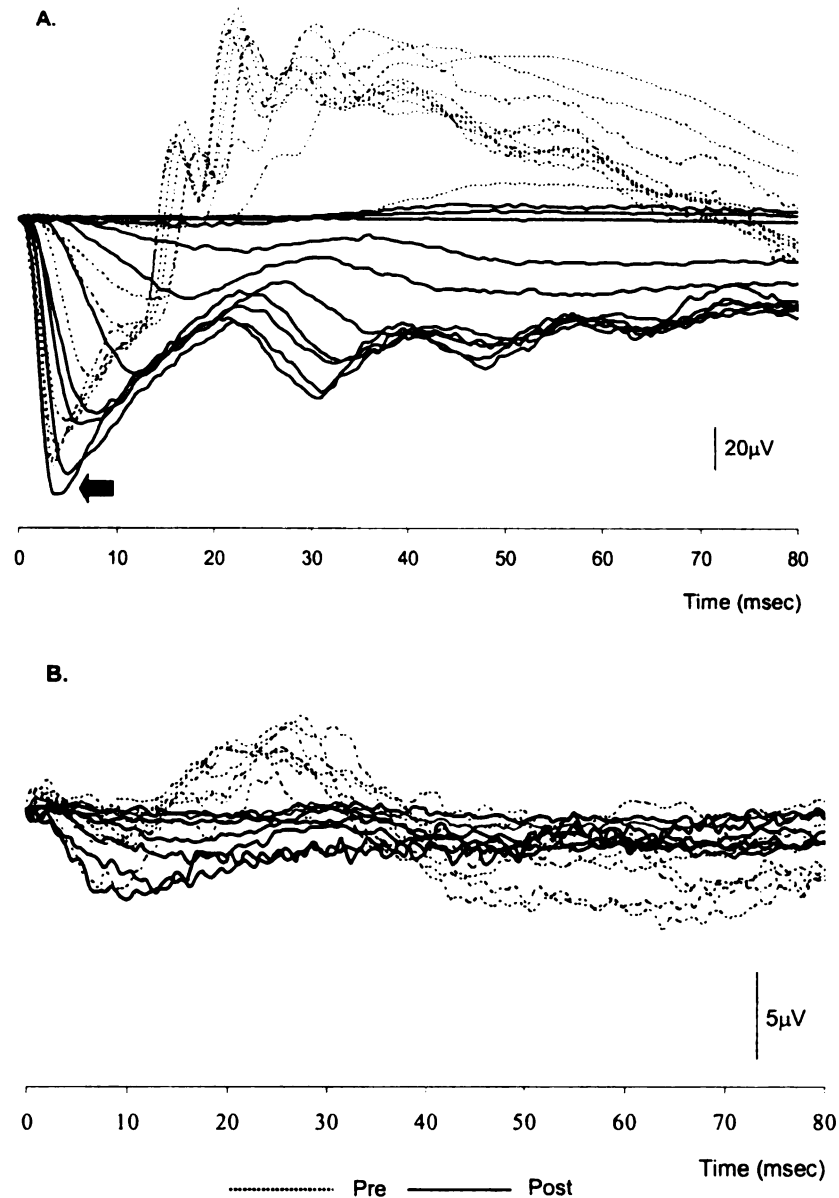


Figure 3.1. Representative scotopic (A) and photopic (B) intensity-series ERGs from a normal control at 60 weeks of age performed before and at 1.5 hours following an intravitreal injection of APB. Light intensities are -1.19, -0.79, -0.39, -0.001, 0.39, 0.85, 1.36, 1.9, 2.38, and 2.82 log cds/m² (note that the highest two intensities are not used in mutant dog; see Figure 2). Light onset is at 0 msec. Note that the effect of APB is similar between scotopic and photopic ERG. A-wave amplitude is slightly increased at the brightest intensity (solid arrow) while the b-wave is suppressed.

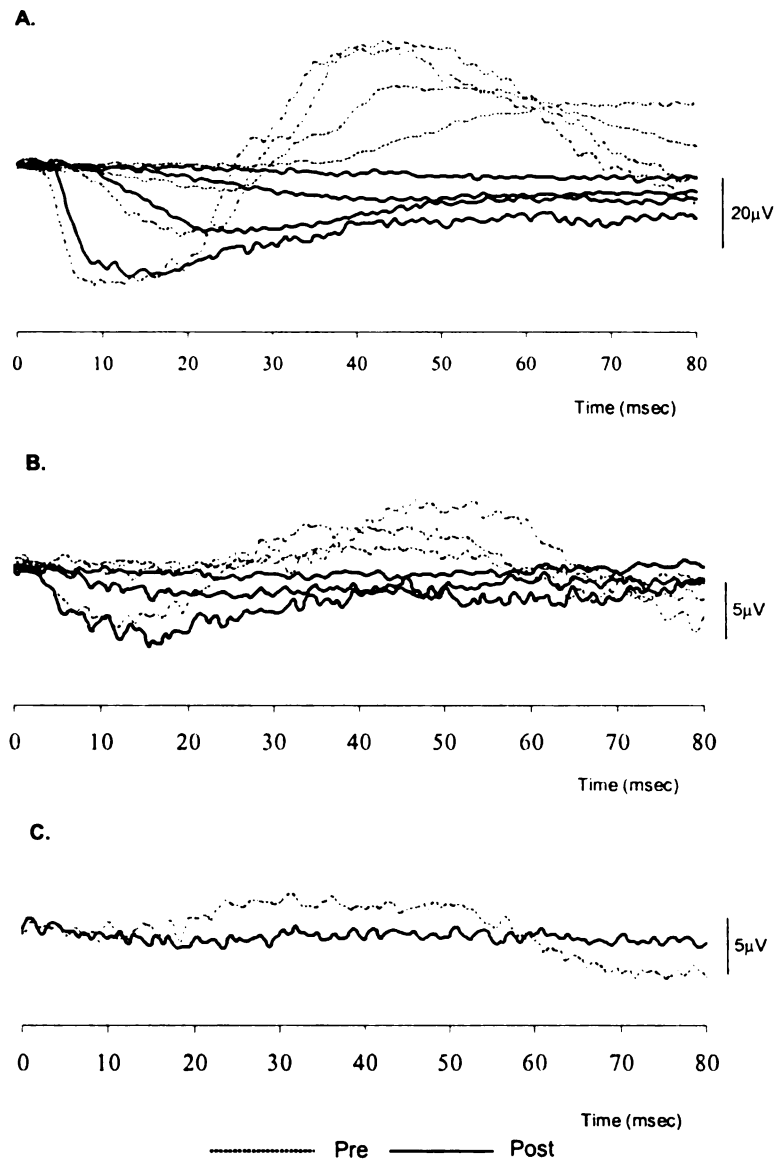


Figure 3.2. Representative scotopic intensity-series ERGs from a normal control at 4 weeks of age (A), the *PDE6A* mutant dog at 4 weeks of age (B) and scotopic ERG from the *PDE6A* mutant dog at 6 weeks of age (C) performed before and at 1.5 hours following an intravitreal injection of APB. Light intensities used for A & B are -0.001, -0.39, 0.39 and 1.9 log cds/m², and for C is 1.9 log cds/m². Light onset is at 0 msec. As in normal adult dogs, APB suppresses the b-wave of both control and mutant puppies. Key: μV = microvolt, msec = millisecond.

3.3.1.b. Cone flicker responses

APB markedly reduced the amplitude of the cone flicker response from the normal control dog and also resulted in a delay in response, although the peak to peak time was unaffected (Figure 3.3A). Cone flicker response post APB was not recordable in the mutant dog (Figure 3.3B).

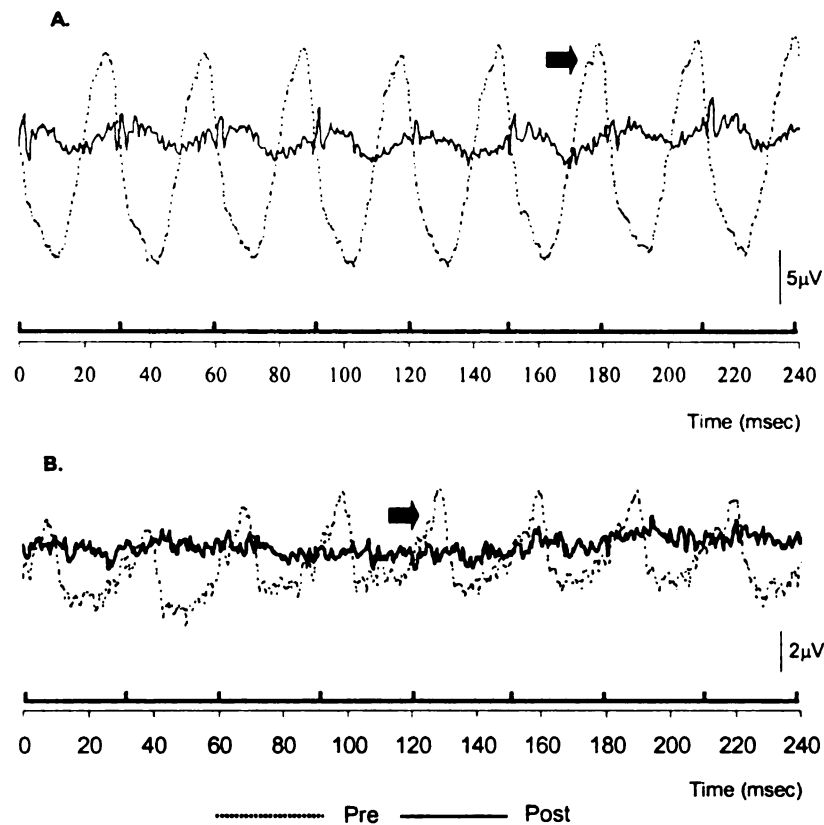


Figure 3.3. Representative cone flicker response ($0.39 \log \text{cds/m}^2$, 33Hz) of a normal control (A) and the *PDE6A* mutant dog (B) at 6 weeks of age performed before and at 2 hours following an intravitreal injection of APB. Light onset is at 0 msec. Spike bar indicates onset of flicker flashes within the recording time (240 msec). Note that a biphasic peak of cone flicker response is present (solid arrows). Following the administration of APB, the flicker response is reduced in the control dog and effectively eliminated in the mutant dog. The biphasic peak disappears in both groups of dogs. Key: μV = microvolt, msec = millisecond.

3.3.1.c. Long flash ERG responses

Long flash ERG responses recorded in a normal control at 4 and 6 weeks of age at 2 hour post injection of APB showed suppression of b-wave and an enlarged and extended a-wave (Figure 3.4A & 3.5A). At light offset there was a small positive d-wave followed by a slow recovery to the baseline. A similar response was recorded from the *PDE6A* mutant dog at 4 weeks of age (Figure 3.4B). However in the *PDE6A* mutant dog at 6 weeks of age, the a-wave was not recordable pre-APB injection and elimination of the b-wave by APB did not reveal a PIII component. A small negative d-wave was still recordable prior to APB injection and this was converted to a positive waveform by the action of APB (Figure 3.5B). Subtraction of the long flash ERG waveform pre/post APB injection (Figure 3.6) demonstrated that APB mainly suppresses b- and d-wave.

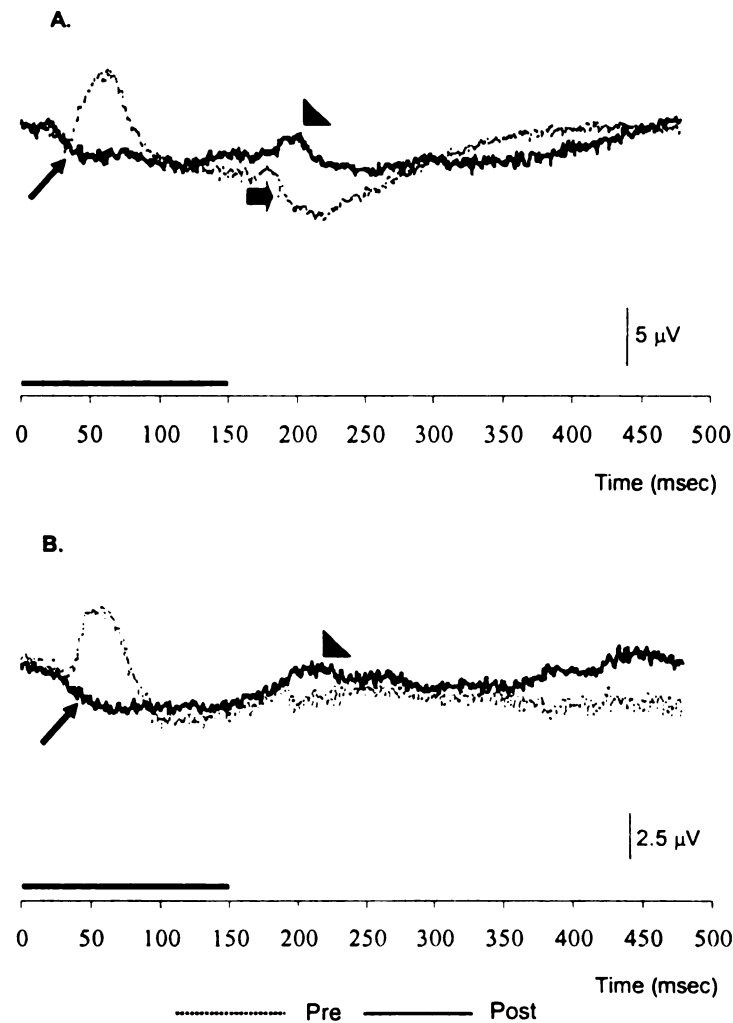


Figure 3.4. Representative long flash ERG response from normal controls (A) and the *PDE6A* mutant dogs (B) at 4 weeks of age performed before and at 2 hours following an intravitreal injection of APB. Bar indicates flash duration (150 msec). Note that APB has a similar effect to retinas of a normal control and the *PDE6A* mutant dog. A-wave is isolated while the b-wave is suppressed (black arrow). Pre drug administration, the off-response consists of a small positive potential followed by a large negative waveform (the d-wave; solid arrow). In both control and mutant dogs, the off-response is converted to a positive waveform (arrowheads). Key: μV = microvolt, msec = millisecond.

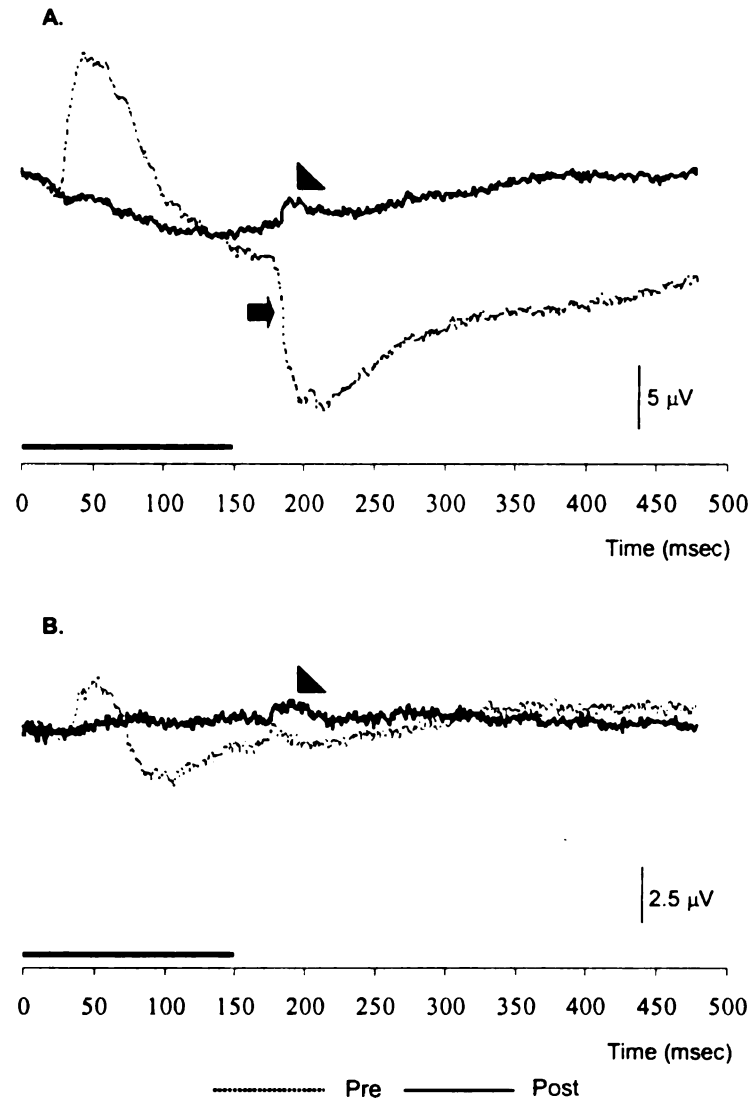


Figure 3.5. Representative long flash ERG response from a normal control (A) and the *PDE6A* mutant dog (B) at 6 weeks of age performed before and 2 hours following an intravitreal injection of APB. Bar indicates flash duration (150 msec). A) Amplitude of a-wave of the normal control is slightly increased by APB and the b-wave is eliminated. The D-wave is altered from a negative response before APB (solid arrow) to a small positive wave (arrowhead) after APB administration. B) In the *PDE6A* mutant dog, APB eliminates the b-wave. After APB, the d-wave is converted to a positive wave (arrowhead) as in the normal control. Key: μ V = microvolt, msec = millisecond.

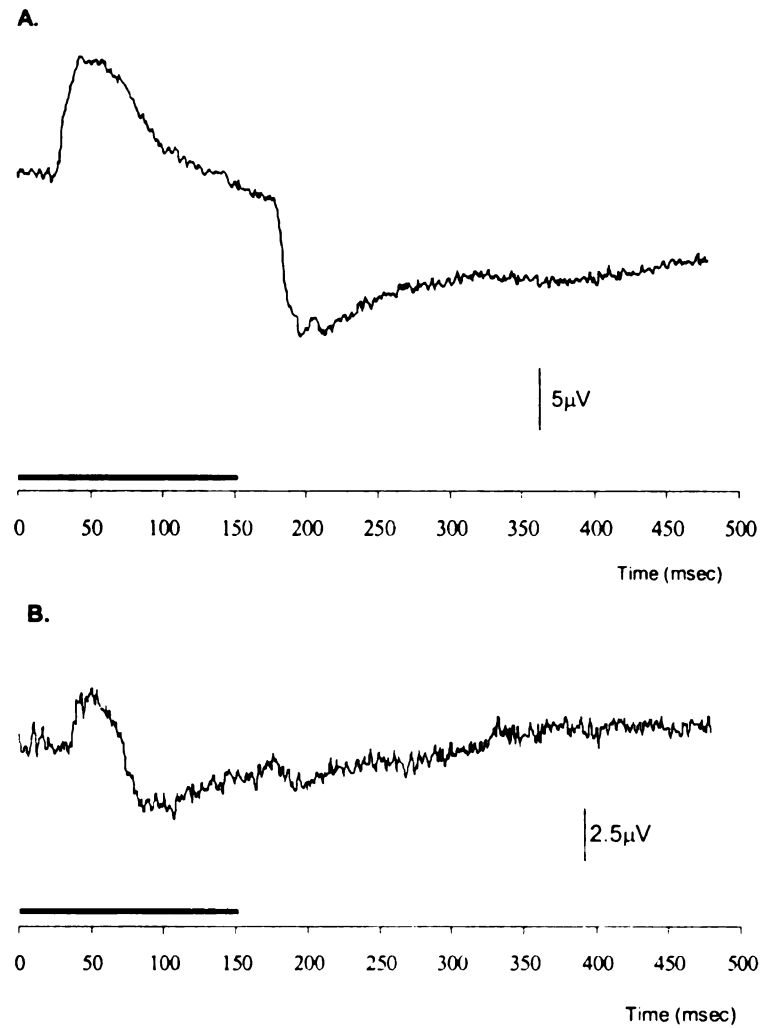


Figure 3.6. Subtraction of post APB long flash ERG from pre APB administration long flash ERG from a normal control (A) and the *PDE6A* mutant dog (B) at 6 weeks of age. Bar indicates flash duration (150 msec). The subtraction reveals the portion of the long flash ERG that is suppressed by APB. As APB predominantly suppresses ON-bipolar cells, this waveform represents the ON-bipolar response. Note that APB has the same effect to both control and mutant dogs by suppressing the positive on-response (b-wave) and the negative off-response (d-wave). Key: μV = microvolt, msec = millisecond.

3.3.2. Results after the intravitreal injection of PDA (Figures 3.7 to 3.10)

3.3.2.a. ERG photopic intensity-series response

After 2 hour post injection of PDA, a small reduced a-wave was only observed at 1.36 log cds/m² in a normal control as well as the *PDE6A* mutant dog (Figure 3.7). The b-wave was partially suppressed at all intensities. B-wave implicit time was increased, particularly in the *PDE6A* mutant dog and there was a reduction in the photopic negative response (PhNR). OPs were reduced by the action of PDA and this was more obvious in the control dogs where OPs were more prominent prior to PDA injection (Figure 3.7).

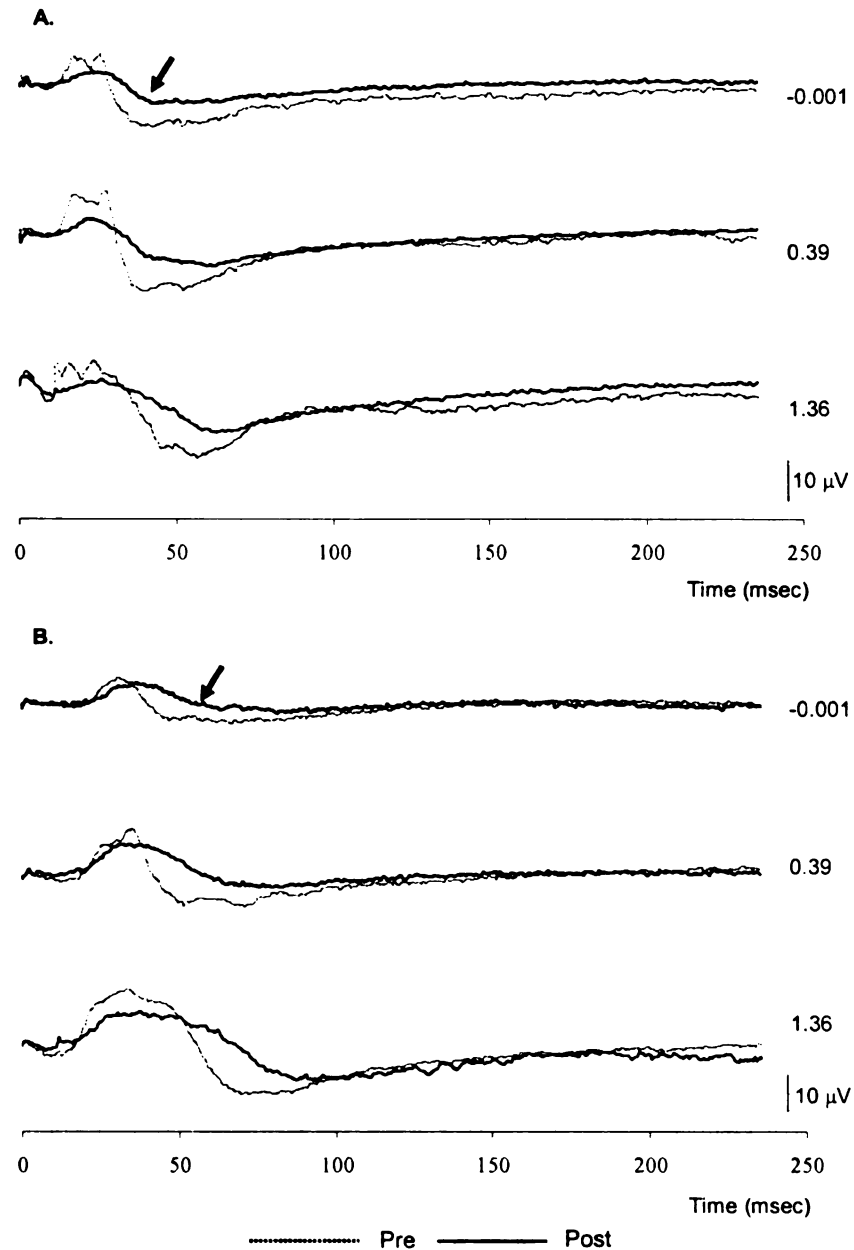


Figure 3.7. Representative photopic ERGs at -0.001, 0.39 and 1.36 log cds/m² from a normal control (A) and the *PDE6A* mutant dog (B) at 7 weeks of age performed before and at 2 hours following an intravitreal injection of PDA. Light onset is at 0 msec. Note that in both groups of dogs, PDA has very little effect on the a-wave while it reduces b-wave amplitude and increases b-wave implicit time. B-wave post negativity is reduced (black arrow) and returns to a baseline at the same time shown at before the injection of PDA. OPs are also diminished. Key: µV = microvolt, msec = millisecond.

3.3.2.b. Cone flicker response

PDA had a similar effect on the cone flicker response recorded from the normal control and *PDE6A* mutant dogs at 7 weeks of age (Figure 3.8). The amplitude was reduced and the response delayed by 5 milliseconds although the peak to peak interval was unaffected. The biphasic peak of the flicker response was partially removed.

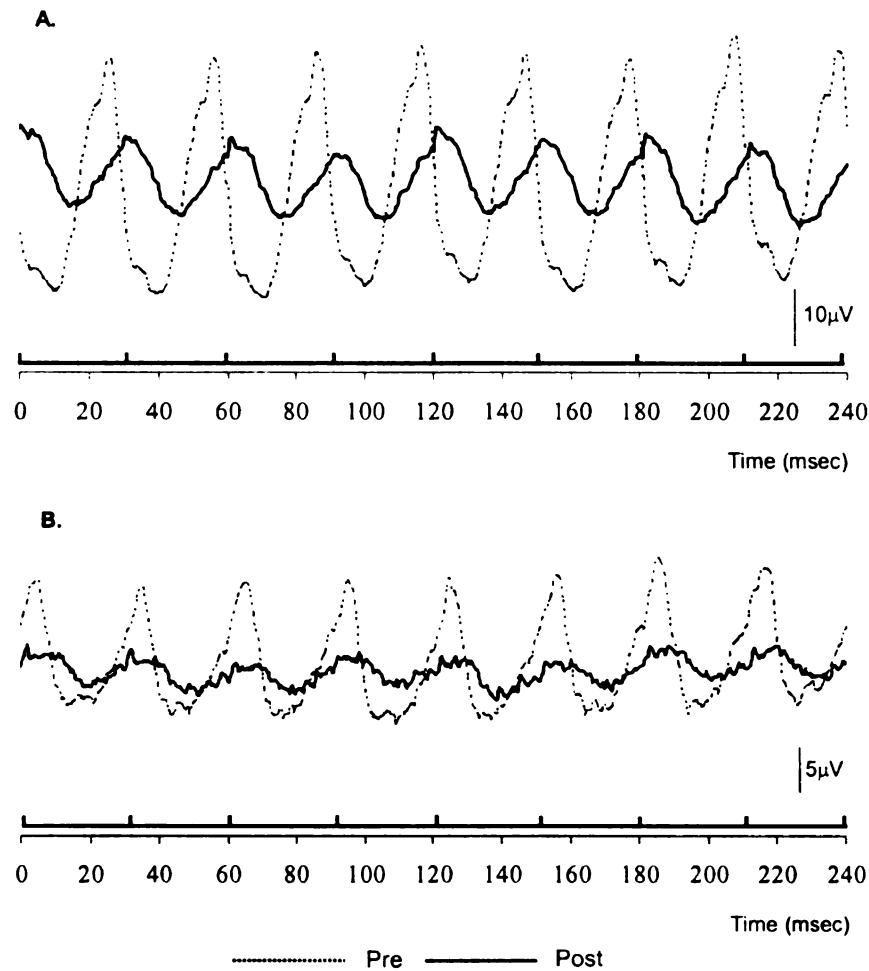


Figure 3.8. Representative cone flicker response ($0.39 \log \text{ cds/m}^2$, 33Hz) of a normal control (A) and the *PDE6A* mutant dog (B) at 7 weeks of age before and 2 hours following an intravitreal injection of PDA. Light onset is at 0 msec. Spike bar indicates onset of flicker flashes within a recording time (240 msec). Note that following an application of PDA cone flicker response is reduced and delayed. The delay induced by PDA is more pronounced in the normal control than in the mutant dog. In the mutant dog, the pre-PDA flicker response is delayed compared to that of the normal control. Key: μV = microvolt, msec = millisecond.

3.3.2.c. Long flash ERG response

The maximal effect of PDA on the long flash ERG had developed by 2 to 2.5 hours post injection (Figure 3.9). PDA had a similar effect on the long flash ERG of both the *PDE6A* mutant dog at 7 weeks of age and an age-matched normal control. The small a-wave present prior to injection was completely suppressed. Compared to the response at pre injection, the b-wave had an increased implicit time and a more rounded shape with a lack of the post b-wave negativity. Instead, there was an elevation of the b-wave descending limb, which lasted for the entire duration of light exposure. At the light offset, the small initial positive component of the d-wave was not detected and the negative component was increased in amplitude. Subtraction of the long flash ERG waveform pre/post PDA injection (Figure 3.10) demonstrated that PDA enhances d- and a-wave, suppresses the post b-wave negativity and the PhNR. This subtracted waveform shows the responses from the OFF-bipolar cells and horizontal cells that are PDA responsive.

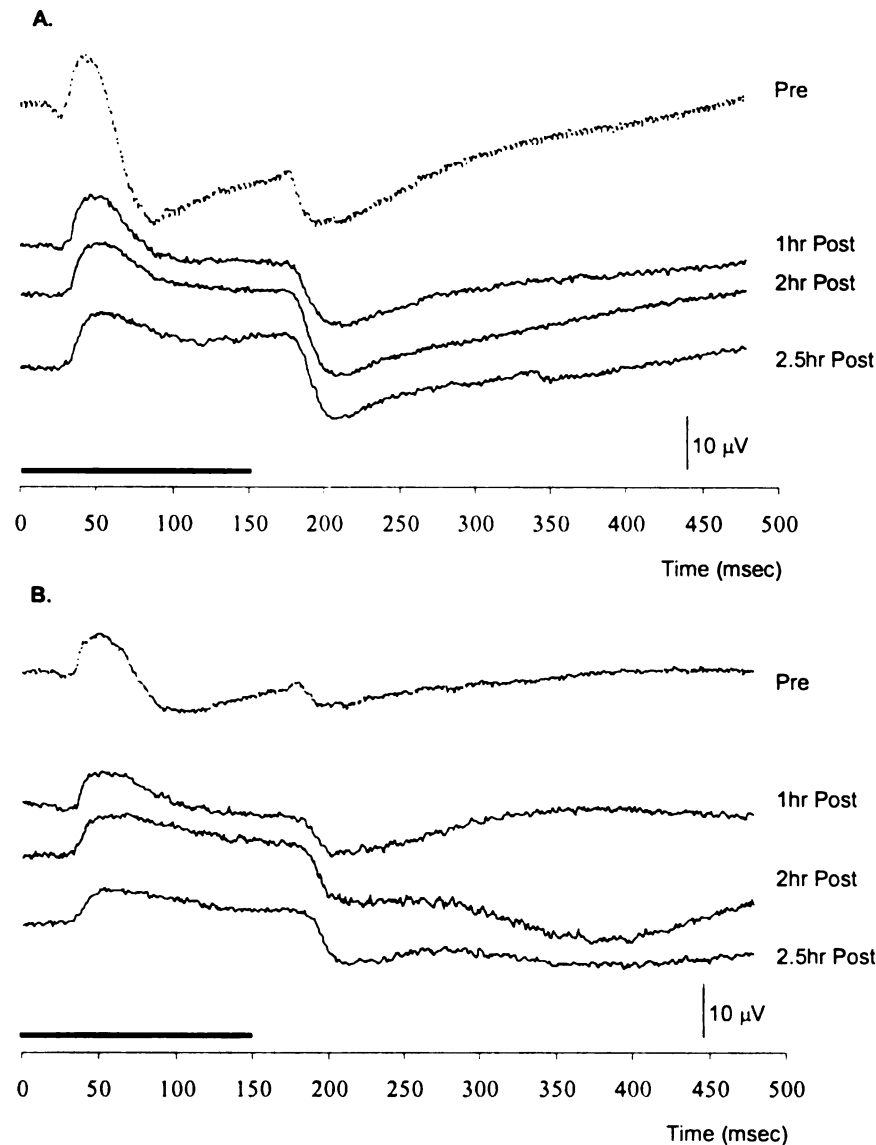


Figure 3.9. Representative long flash ERG responses from a normal control (A) and the *PDE6A* mutant dog (B) at 7 weeks of age performed before and at 1, 1.5, 2 and 2.5 hours following an intravitreal injection of PDA. Bar indicates flash duration (150 msec). A) A-wave amplitude of the normal control is eliminated by PDA. B-wave maintains its amplitude but has a delayed implicit time and the degree of the post b-wave negativity is decreased. The negative d-wave response is increased. B) In the *PDE6A* mutant dog, the small a-wave is suppressed after the injection of PDA the b-wave response delayed and its post negativity eliminated. The negative component of the d-wave is also enlarged by PDA. Note that the small positive potential at light offset is blocked by the action of PDA. Key: μ V = microvolt, msec = millisecond.

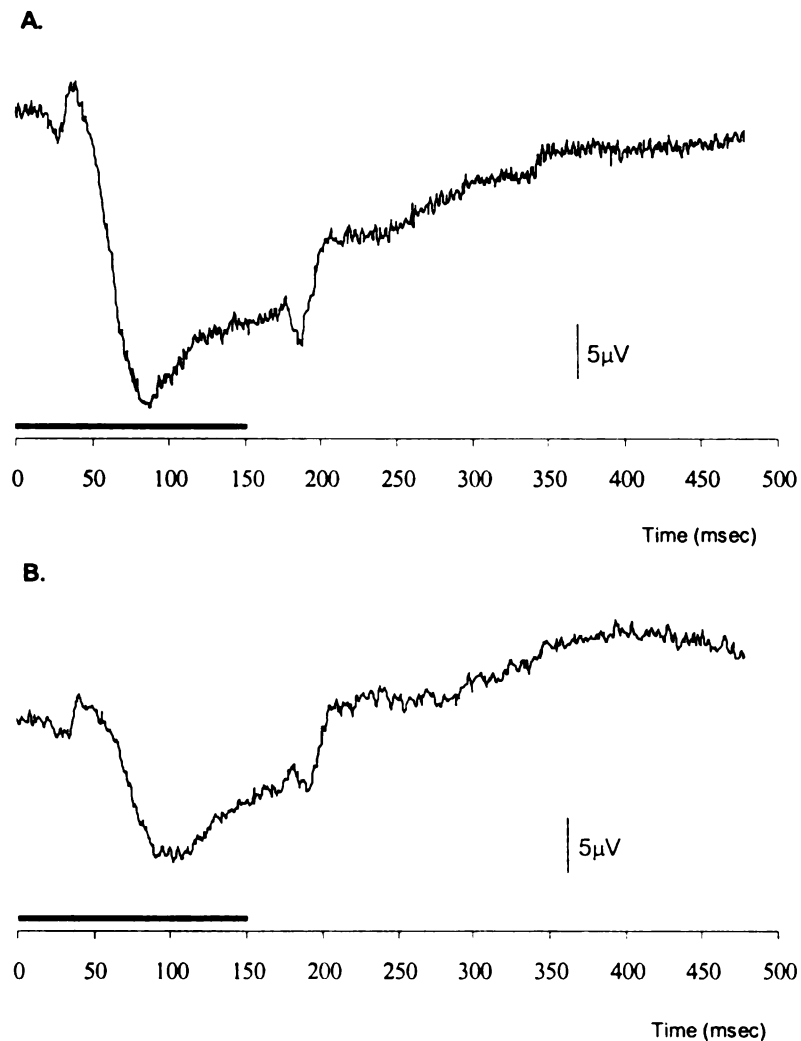


Figure 3.10. Subtraction of post PDA long flash ERG from pre PDA long flash ERG from a normal control (A) and the *PDE6A* mutant dog (B) at 7 weeks of age. Bar indicates flash duration (150 msec). This represents the components of the long flash ERG response that result from OFF-bipolar and horizontal cells. Note that PDA has the same effect to both control and mutant dogs by suppressing the a-wave, the post b-wave negativity, the PhNR and the small positive d-wave at light offset, whereas the b-wave amplitude is fairly maintained and the negative d-wave response is slightly increased. Key: μ V = microvolt, msec = millisecond.

3.3.3. Results after the intravitreal injection of tetrodotoxin (Figures 3.11 & 3.12)

3.3.3.a. Photopic ERG response

In the normal control (Figure 3.11A), TTX slightly increased the b-wave amplitude and partly suppressed OPs. A slight delay in the b-wave descending limb was noticed with an elimination of the post b-wave negativity. The PhNR was suppressed by approximately 70% compared to the pre injection response. The a-wave was not affected by TTX. In the *PDE6A* mutant dog (Figure 3.11B) TTX reduced the b-wave amplitude but had a similar effect on the PhNR as shown in the normal control.

3.3.3.b. Cone flicker response

The cone flicker amplitude was approximately 25-30% reduced after 1.5 hour post injection of TTX, in both normal control and *PDE6A* mutant dogs. The biphasic peak of the normal control flicker response was still present even though the amplitude was smaller (Figure 3.12A). The peak of the positive flicker waveform in the *PDE6A* mutant dog was relatively broader, which obscured the biphasic peak present pre injection (Figure 3.12B). The phase of the flicker responses were not altered by TTX in the normal control or the *PDE6A* mutant dog.

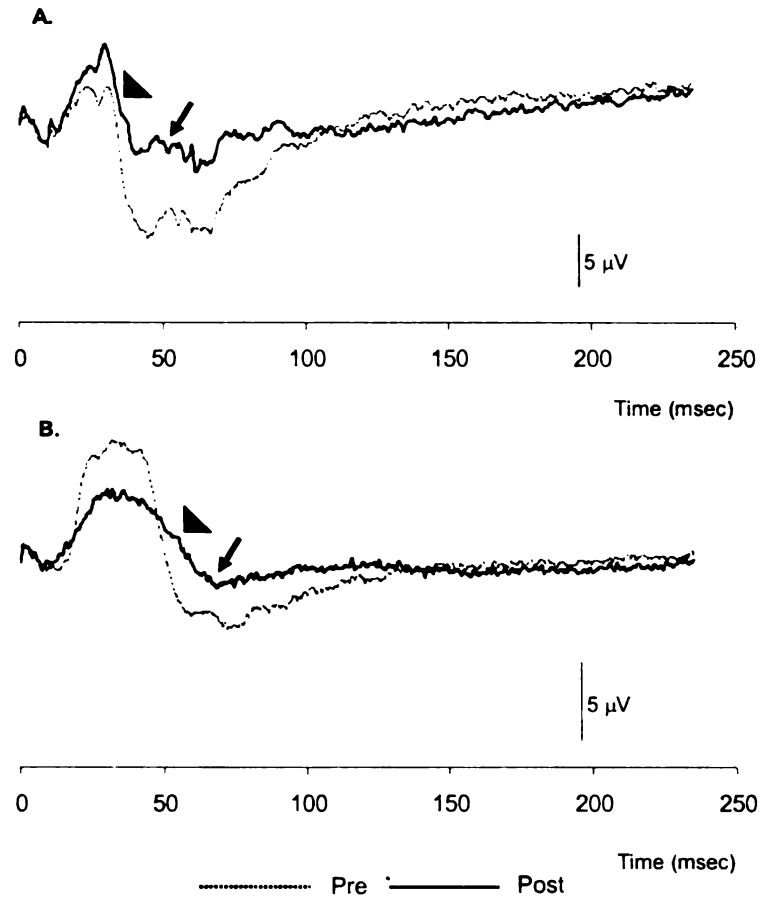


Figure 3.11. Representative photopic ERGs at $0.85 \log \text{cds/m}^2$ from a normal control (A) and the *PDE6A* mutant dog (B) at 10 weeks of age performed before and at 1.5 hours following an intravitreal injection of TTX. Light onset is at 0 msec. Note that TTX increases the b-wave amplitude of the normal control whereas it suppresses the b-wave amplitude of the *PDE6A* mutant dog as well as eliminates the OPs. B-wave of a normal control and the *PDE6A* mutant dog slowly recovers (arrowheads), which then follows by elevated post negativity (black arrows). Key: μV = microvolt, msec = millisecond.

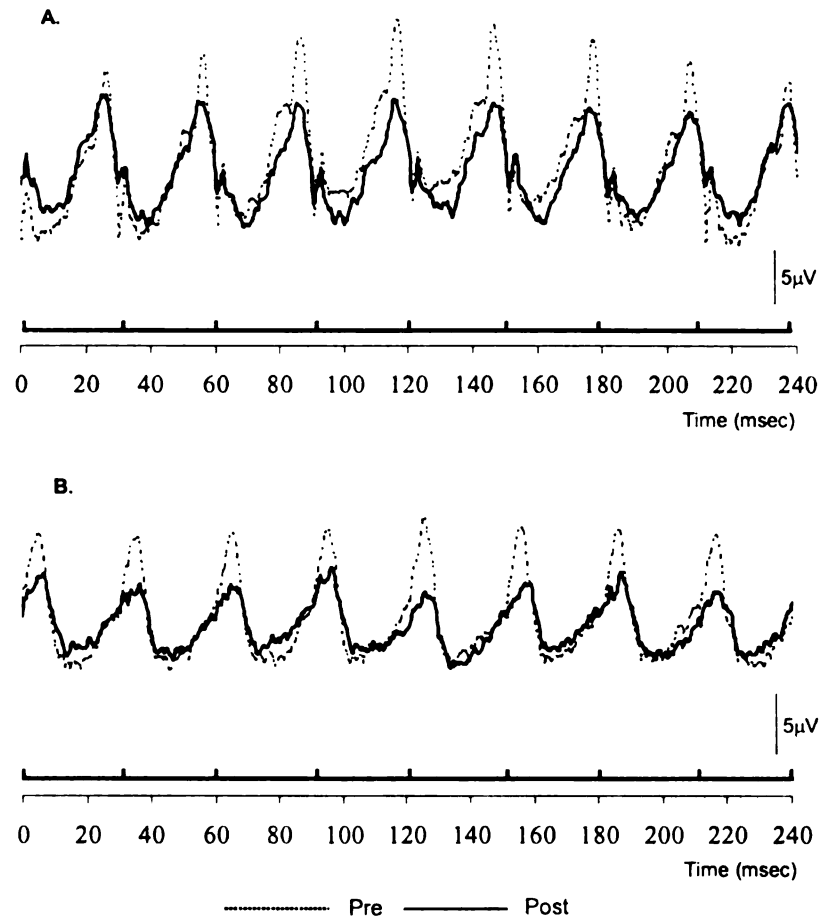


Figure 3.12. Representative cone flicker response ($0.39 \log \text{cds/m}^2$, 33Hz) of a normal control (A) and the *PDE6A* mutant dog (B) at 10 weeks of age before and at 1.5 hour following an intravitreal injection of TTX. Light onset is at 0 msec. Spike bar indicates onset of flicker flashes within a recording time (240 msec). Note that the cone flicker delay is observed from the mutant dog compared to a normal control. A reduction of the flicker response is noticed in both groups of dogs. Key: μV = microvolt, msec = millisecond.

3.4. Discussion

The effect on the short and long flash ERG of the intravitreal injection of APB, PDA and TTX to block specific retinal neuron pathways in normal and mutant dogs was investigated. The use of these drugs allowed the contributions of difference neurons to the formation of the normal ERG waveform of the dog to be investigated. Blockage of photoreceptor input to ON-bipolar cells by APB virtually eliminated the normal scotopic and photopic b-waves. Thus in the dog, similar to other species, the ON-bipolar cell makes a major contribution to the shape of the b-wave. The action of PDA is to block the OFF-bipolar cells and horizontal cells leaving the ON-bipolar response unaffected. Blocking the OFF-bipolar and horizontal cell pathway with PDA results in a modification of the shape of the photopic b-wave tending to reduce its amplitude and broaden its shape. In the short flash recordings PDA did not eliminate the a-wave, whereas in the long flash ERGs the a-wave was eliminated, while the effect on the b-wave was similar to that seen in the short flash ERG. These results are in contrast to those in the primate photopic ERG (Sieving et al., 1994) where PDA and kynurenic acid were used to block the OFF-bipolar and horizontal cell responses. This resulted in a reduction in a-wave amplitude and an enhancement of the b-wave. Subtraction of post drug injection responses from predrug injection responses showed that the contribution of OFF-bipolar and horizontal cell pathways to the primate photopic ERG is a sustained negative response that lasts the duration of light exposure (Sieving et al., 1994). We performed a similar subtraction and found that the canine OFF-bipolar and horizontal cell responses had an initial brief small negative and then small positive response followed by a much

larger sustained negative response that was maintained while the light was on and then a small negative response at lights off followed by a larger positive waveform. This predominantly negative component is similar to that of the primate but appears to be a slower response in the dog so that its peak negativity coincides with the normal descending phase of the b-wave and thus it has the effect of broadening the b-wave and extending it, eliminating the post b-wave negativity, rather than increasing the peak of the b-wave as it does in primates. Similar subtraction to demonstrate the ON-bipolar cell response (the portion of the waveform blocked by APB) showed the major contribution the ON-bipolar cell pathways make to the scotopic and photopic b-wave and also the negative component of the canine d-wave.

APB had a similar effect on cone flicker (33Hz) as previously described in primates (Sieving et al., 1994) (Hare & Ton, 2000). The amplitude of response was very reduced and the response slightly delayed although it remained in phase with the stimulus. A similar, but less severe, reduction in cone flicker amplitudes resulted from administration of PDA. These results show the major contribution to the flicker response made by the ON- and OFF- pathways in the inner retina. The alteration to canine cone flicker responses by administration of PDA was similar to that described in primates by the work of Hare and Ton (2002), but differed from the result obtained in primates in an earlier study by Bush and Sieving (Bush & Sieving, 1996) who found that PDA had little effect on the primate cone flicker response. These contradictory results were discussed by Hare and Ton (2002) who suggested that they may have been due to differences in the

type of stimulus used, Hare and Ton (2002) used a brief flash from a xenon flash unit (as we used in this study) whereas Bush and Sieving used a square wave stimulus.

The use of these drugs allowed investigation of the source of the OFF-response of the long flash ERG in the dog. Intravitreal injection of APB changed the d-wave polarity from predominantly negative to a small positive potential. A similar result has been described in rabbits (Knapp & Schiller, 1984b). A study in macaque monkey using different colored light stimuli to investigate the responses from different cones concluded that the S-cones have a negative off-response whereas the d-wave recorded when medium and long wave cones were stimulated was positive (Evers & Gouras, 1986). Furthermore the administration of APB eliminated the negative d-wave of S-cones but enhanced the positive going d-wave of the M- and L-cones. The effect of intravitreal PDA in the dog was to increase the negativity of the off-response. In primates PDA tends to reduce the d-wave response (push it towards negativity) (Bush & Sieving, 1994). The difference in off-responses in dogs compared to primates can simply be explained by the difference in the amplitudes and timings of responses originating from the APB responsive on-pathway and the PDA responsive off-pathway. The response from ON-bipolar cells was a positive deflection at light onset that was maintained, but slowly drifted down, while the lights remained on and then, in both primates and dogs, when the light stimulus stopped the waveform had a negative deflection. The response from the OFF-bipolar cell pathway is negative at light onset and remains negative with a slow positive drift while the light is on and then has a positive deflection at light offset. The ON-bipolar cell response accounts for the major component of the off response in the dog resulting in an overall

negative deflection whereas the OFF-bipolar response probably accounts for the small positive deflection that typically precedes the negative d-wave and then a the initial positive return towards the baseline following the negative deflection of the d-wave. In primates the OFF-bipolar response positive deflection at light offset appears to be faster and is greater in amplitude than the ON-bipolar negative response resulting in an overall positive d-wave.

Intravitreal injection of TTX enhanced the b-wave amplitude of the normal control dog and reduced the post b-wave negativity (photopic negative response). This result is the same as obtained from rabbits under bright light stimulation (Dong & Hare, 2000) and in primates independent on light stimulation (Hare & Ton, 2000).

Considering the major differences in ERG amplitudes between normal dogs and mutant dogs the administration of APB and PDA to mutant dogs had very similar effects on short flash, long flash and flicker ERG responses to those in the control dogs. This suggests that early in the disease process there are no profound abnormalities in the ON and OFF pathways in the mutant retina. Considering the lack of rod driven responses in mutant puppies the effect of APB on the short flash in the dark adapted mutant dog is most likely to represent the drug's blockage of cone ON-bipolar cells rather than rod ON-bipolar cells as the latter are unlikely to be contributing much to the overall ERG tracing because of the lack of rod function.

The relatively smaller d-wave of the mutant dog compared to b-wave appears to result from changes in the ON-bipolar pathway. Subtraction of the post APB long flash ERG from the pre APB injection ERG showed that the negative deflection at light off from the ON-bipolar pathway was proportionally smaller in amplitude than the positive deflection at light on. The OFF-bipolar pathway response revealed by intravitreal PDA from the mutant dog seemed to have waveforms of reduced but similar proportions to the normal control. This finding may indicate an early abnormality in the cone ON-bipolar pathway as a result of the disease process in the retina of the mutant dog.

There was a difference in the mutant dog response to TTX compared to the control. In the mutant, TTX acted to decrease the b-wave amplitude, whereas in the control it increased it. The effect on post b-wave negativity was similar between mutant and control, although the mutant dog had a smaller PhNR prior to drug administration than the control. The effect on the mutant dog b-wave is similar to that described for the rabbit under low light stimulation (Dong & Hare, 2000). TTX was found to eliminate the action potential-dependent inhibition to the glycinergic and GABAergic amacrine cells in rabbit retina (Dong & Hare, 2000) while its effect on rat photopic ERG was attributable to voltage-gated sodium current mainly in amacrine and interplexiform cells (Bui & Fortune, 2004a). According to different results following TTX administration in various species, the effect of TTX may reflect some combination of blocking activity in amacrine cells, ganglion cells and interplexiform cells (Hare & Ton, 2000). Failure of TTX to increase the photopic b-wave in the *PDE6A* mutant dog and an absence of photopic OPs suggest a loss of action potentials originating in the third-order neurons. A smaller

reduction of PhNR in the *PDE6A* mutant dog compared to the normal control after the intravitreal injection of TTX supports the conclusion that the third-order neurons are affected in the *PDE6A* mutant dog at young age probably due to altered input from the outer retina.

Chapter 4

Detailed histopathological characterization of the *PDE6A* dog phenotype

4.1. Introduction

The *PDE6A* mutant dogs are night blind at the earliest age they can be tested (approximately 6 to 8 weeks of age). Scotopic ERG responses are dramatically decreased suggesting a lack of rod activity. Results of electroretinographic studies (Chapter 2 & 3) indicate that rod photoreceptors in the *PDE6A* mutant dogs fail to develop normal function in the early postnatal period. An arrest in rod differentiation followed by a rapid decrease in number of rod photoreceptors occurs in animals with PDE6B mutation (Buyukmihci et al., 1980; Jimenez et al., 1996). Furthermore, there were major pathological changes of second-order neurons in the *rdl* mouse following rod degeneration (Strettoi et al., 2002).

The aims of this part of the study were to document the morphological changes in photoreceptors in the *PDE6A* mutant dogs over time, investigate the effect of degeneration on the cellular organization of the inner retina, and to document modifications in the retina after photoreceptor cell loss.

4.2. Materials and methods

Animals: see 2.2.1. (Chapter 2)

4.2.1. Morphological analyses by light microscopy

4.2.1.a. Tissue collection and processing

Dogs at 2, 3, 4, 5, 7, 9, 12, 16, and 60 weeks of age were euthanized by administration of an overdose of pentobarbital sodium (Fatal-Plus; Vortech pharmaceuticals, Dearborn, MI) intravenously. After euthanasia, enucleations were performed. All globes were trimmed of extraocular muscles. Four slits 3mm from and parallel to the limbus were made on the right globe using a #11 scalpel blade to facilitate intraocular penetration of the fixative, and then the globe was submerged in a mixture of 3% glutaraldehyde, 2% paraformaldehyde, and 0.1M Sodium-cacodylate buffer (pH 7.2) for two hours at 4°C. The anterior half of the globe, lens and vitreous were then removed. The posterior half of the globe (eyecup) was transferred to the same fixative and left overnight at 4°C.

The globe was dehydrated in a graded series of ethanol solutions and infiltrated with Immuno-Bed solution, prepared according to the manufacturer's instructions

(Electron Microscopy Sciences, Ft. Washington, PA). After the eyecup had polymerized overnight at -20°C , a vertical cut was made from the superior ora ciliaris retina through the optic nerve head to the inferior ora ciliaris retina (Fig 4.1). The nasal half of the hemisectioned eyecup was mounted to an EBH-2 block holder (Electron Microscopy Sciences, Ft. Washington, PA). The remaining temporal half of the eyecup was hemisectioned in the horizontal plane from the optic nerve head to the temporal ora ciliaris retina, and mounted to an EBH-2 block holder (Electron Microscopy Sciences, Ft. Washington, PA). Sections, each approximately $3\text{ }\mu\text{m}$ thick, were cut at three-micrometer thickness using a glass knife and stained with hematoxylin and eosin (H&E) for light microscopic analysis.

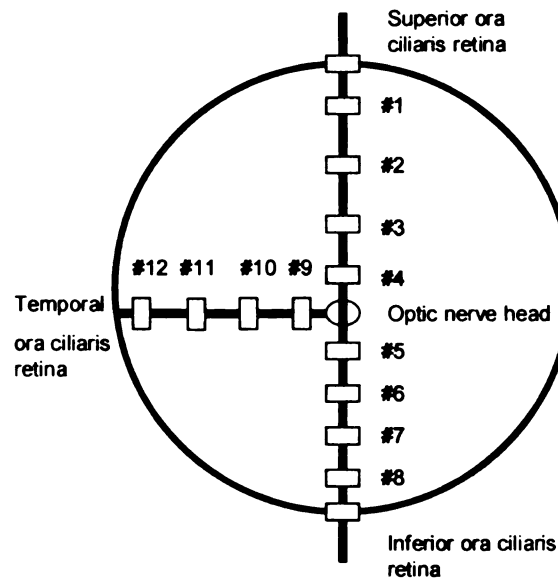


Figure 4.1. Diagram of the right eyecup of a dog illustrating planes of section and regions of the retina where the thickness of individual retinal layers is measured, and the number of outer nuclear layer (ONL) rows and photoreceptor nuclei per unit length are counted. Key: location 1, 8, and 12 are 500-micrometers from the ora ciliaris retina, location 4, 5, and 9 are 500-micrometers from the edge of the optic nerve head.

To allow investigation of additional retinal regions, globes from homozygous *PDE6A* mutant and homozygous *PDE6A* normal dogs at ages from 5 to 7 months were plastic-embedded and sectioned as shown in figure 4.2. Three-micrometer sections were stained with H&E for measurement of retinal thickness and counting of photoreceptor nuclei in the outer nuclear layer.

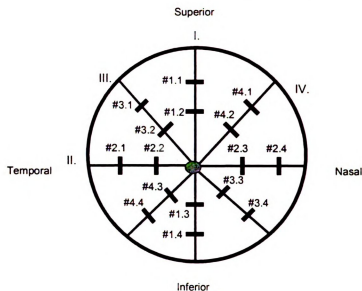


Figure 4.2. Diagram of the right eyecup of a dog illustrating the regions of the retina where detailed morphological analysis is performed.

4.2.1.b. Data collection

Images were captured using a Nikon microphot-FXA microscope (Nikon Inc, Garden City, NY). The length of each retinal section was measured using NeuroExplorer software (MicroBrightField Inc, Williston, VT), acquired with NeuroLucida software; version 3 (MicroBrightField Inc, Williston, VT), and then divided by three to allow the same relative retinal region to be examined independent of the size of the globe.

The thickness of the following retinal layers were measured at 3 different areas within one microscopic field: retinal pigment epithelium (RPE), photoreceptor outer segment (OS), photoreceptor inner segment (IS), outer nuclear layer (ONL), outer plexiform layer (OPL), inner nuclear layer (INL), inner plexiform layer (IPL), ganglion

cell layer and nerve fiber layer (GCL & NFL). Measurements were taken at all regions across the retina (Figure 4.1 & 4.2) under 40-time magnification using the Neurolucida software; version 3 (MicroBrightField Inc, Williston, VT).

The number of rows of photoreceptor nuclei in the ONL and the number of rod and cone nuclei identified by morphological features of their nuclei (see introduction; Chapter 1) were counted over 100-micrometer length of the retina at the regions above using the Neurolucida software; version 3 (MicroBrightField Inc, Williston, VT) (Figure 4.3).

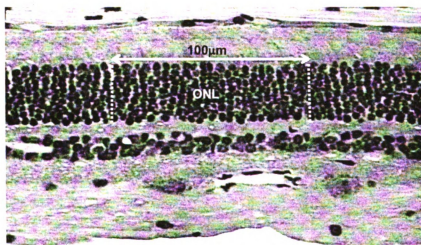


Figure 4.3. Diagram of a cross section of retina showing a measurement of the number of rows of the ONL and the number of rod and cone nuclei per 100-micrometer length of the retina. Key: ONL = outer nuclear layer.

4.2.1.c. Data analysis

The thickness of the eight retinal layers measured and number of cells counted (4.2.1.b.) were mapped across the length of all sections. All measurements derived from the *PDE6A* mutant dogs were compared with the identical areas from age-matched normal controls, and analyzed using ANOVA. Independent analyses for each region and retinal layer were performed. The fixed effects included in the model were age and disease genotype. For measurement of retinal thickness, a random effect of dog was included to account for repeated measures (triplicates) within dog and age. For measuring the number of cells, no random effects were considered and consequently a linear model of fixed effects was used. No covariance among ages was modeled as the measures at different ages corresponded to independent dogs. No variable transformation was done because the residual analyses revealed fulfillment of model assumptions (normality, heteroskedasticity) (data not shown). Data were deemed significant when $P < 0.05$. All analyses were performed using SAS Proc Mixed software; SAS version 9.1 (SAS Institute Inc, Cary, NC).

4.2.2. Morphological analyses by transmission electron microscopy

4.2.2.a. Tissue collection and processing

Dogs at 2, 3, 4, 5, 7, 9 and 16 weeks of age were euthanized by administration of an overdose of pentobarbital sodium (Fatal-Plus; Vortech pharmaceuticals, Dearborn, MI) intravenously. After euthanasia, enucleations were performed. All globes were processed, fixed (as described in 4.2.1.a.), and then sectioned in a vertical plane through the optic nerve head. The nasal half of the eye was post-fixed in osmium tetroxide, and embedded in resin consisting of Poly/Bed, Araldite, DDSA, and DMP-30 accelerator. Semi-thin sections (0.7 to 1 micrometer thickness) were cut with a glass knife and stained with toluidine blue. Ultra-thin sections (0.06-0.08 micrometer thickness) were cut with a diamond knife and stained with uranyl acetate and lead acetate. Sections from the central tapetal regions (region #3; Figure 4.1.) were examined with a Philips 301 transmission electron microscope.

4.2.2.b. Data analysis

Sections from region #3 (Figure 4.1.) from the *PDE6A* mutant and age-matched normal control eyes were compared. The ultra structural morphologic appearance of photoreceptor outer segments as well as the photoreceptor cell bodies, inner segments, and synaptic termini were assessed.

4.2.3. Immunohistochemical analyses of paraffin-embedded sections

4.2.3.a. Tissue collection and processing

Dogs at 2, 3, 4, 5, 7, 9, 12, 16, 60 and 210 weeks of age were euthanized by administration of an overdose of pentobarbital sodium (Fatal-Plus; Vortech pharmaceuticals, Dearborn, MI) intravenously. After euthanasia, enucleations were performed. Four slits were made in the left globe (free of extraocular tissues) at 3 mm posterior to the limbus to facilitate intraocular penetration of the fixative, and then the globe was initially fixed in a mixture of 4% paraformaldehyde in 0.1M phosphate buffered saline (PBS; 0.05M sodium phosphate, 195mM NaCl; pH 7.4.) for two hours at 4°C. The anterior segment of the globe, lens, and vitreous body were removed. The posterior eyecup was further fixed in the same fixative for another 20 hours at 4°C. After that, the eyecup was gently rinsed with 0.1M PBS buffer plus 3% sucrose and cut in a vertical plane through the optic nerve head. The medial half of the eyecup was dehydrated in ethanol from 65% to 100% concentration, rinsed twice in xylene, and then embedded in paraffin. Paraffin-embedded sections (5µm thickness) were cut, mounted on positively-charged glass slides, and dried at 65°C for 20 minutes. A sample section was stained with H&E to assess the quality of the section prior to immunohistochemical processing.

Paraffin-embedded retinal sections were cut at a five-micrometer thickness, air-dried overnight, de-paraffinized in xylene (twice) followed by a gradual rehydration in 100% and 95% ethanol, and finally in distilled water. The sections were incubated in a preheat antigen retrieval buffer (Citrate buffer; DakoCytomation, Carpinteria, CA) for 20 minutes at 97°C. After the section had been cooled to 50°C, it was incubated in 50 mM

TRIS-buffered saline (TBS; pH 7.6) for 5 minutes, followed by 10 minutes incubation with a protein-blocking agent (DakoCytomation, Carpinteria, CA) prior to application of the primary antibodies (see Table 4.1. for a list of antibodies used). Goat anti-rabbit and goat anti-mouse secondary antibody from the Labelled Streptavidin-Biotin 2 System, Horseradish Peroxidase (LSAB2 System-HRP; DakoCytomation, Carpinteria, CA) was used to reveal primary antibody-positive immunoreactivity. Immunoreaction was visualized with 3,3'-diaminobenzidine substrate (Liquid DAB substrate chromogen system; DakoCytomation, Carpinteria, CA), and the sections were counterstained with hematoxylin (Gill III formulaTM; Surgipath Medical Industries Inc, Richmond, IL) for 10 minutes. The sections were then washed in distilled water, rinsed in tap water for 5 minutes, blued with 0.04% lithium carbonate, washed again in distilled water, rehydrated in 100% and 95% ethanol then in xylene before being coverslipped. Positive control was included for each set of staining.

PRIMARY ANTIBODY	CONCENTRATION OF PRIMARY ANTIBODY	SOURCE OF PRIMARY ANTIBODY
MOUSE ANTI-RHODOPSIN	1:50	A GIFT: DR PAUL HARGRAVE; U OF FLORIDA
MOUSE ANTI-RHODOPSIN	1:2	LAB VISION; FREMONT, CA
RABBIT ANTI-GFAP	1:1600	DAKOCYTOMATION; CARPINTERIA, CA
MOUSE ANTI-PKC ALPHA	1:50	BD BIOSCIENCE; ROCKVILLE, MD
RABBIT ANTI-CONE ARRESTIN	1:2000	A GIFT: DR CHERYL CRAFT; U OF SOUTHERN CALIFORNIA
RABBIT ANTI-CASPASE 3	1:100	RESEARCH DIAGNOSTICS; FLANDERS, NJ

Table 4.1. A list of the primary antibodies, their working dilution and source that are used on paraffin-embedded sections. Key: GFAP = Glial Fibrillary Acidic Protein, PKC = Protein Kinase C.

For caspase-3 immunohistochemistry, paraffin-embedded retinas sections (5-micrometer thickness) were de-paraffinized (EZ Prep™; Ventana Medical System Inc, Tucson, AZ), washed with SSC solution™ (Ventana Medical System Inc, Tucson, AZ), incubated with reaction buffer™ (Ventana Medical System Inc, Tucson, AZ) at 37°C for 2 minutes. Anti-caspase-3 antibody (1:100) (Casp3actabr; Research Diagnostics Inc, Flanders, NJ) was applied and the slide incubated at 37°C for 10 minutes, biotinylated anti-mouse and anti-rabbit secondary antibody conjugated with alkaline phosphatase-streptavidin (Enhanced alkaline phosphatase red detection kit; Ventana Medical System Inc, Tucson, AZ) was applied to locate and visualize the bound primary antibody. After that, the section was incubated at 37°C for 32 minutes, counterstained with Hematoxylin, followed with a bluing reagent to change the hue of the hematoxylin to a blue color (Ventana Medical System Inc, Tucson, AZ). To remove the liquid cover slip reagent the section was washed with a detergent and rinsed with warm tap water. Finally the section was rinsed with 100% ethanol, followed by a 1:1 mixture of 50% ethanol and 50% xylene, then 100% xylene, and then coverslipped. Positive control was included for each set of staining.

4.2.3.b. Data analysis

Retinal sections of the *PDE6A* mutant and normal control dogs were examined for differences in the distribution and morphologic appearance of the immunoreactive cells. Images were captured using an Olympus microscope model BX51 or model BX40 (Olympus America Inc, Melville, NY), equipped respectively with the In Sight QE digital camera model 4.2 (Mikron Instruments Inc, San Marcos, CA) or Olympus digital camera model E10 (Olympus America Inc, Melville, NY). Images were optimized by using SPOTTM software v. 4.5 (Westgate Software Inc, Draper, UT).

4.2.4. Immunohistochemical analyses of frozen sections

4.2.4.a. Tissue collection

Dogs at 5, 7, 9, 12, 16, and 60 weeks of age were euthanized by administration of an overdose of pentobarbital sodium (Fatal-Plus; Vortech pharmaceuticals, Dearborn, MI) intravenously. After euthanasia, enucleations were performed. The globe was dissected as described in 4.2.3.a, and fixed in a mixture of 4% paraformaldehyde plus 3% sucrose in 0.1M phosphate buffer (pH 7.4) for 15 minutes at 4°C. The anterior segment of the globe, the lens, and vitreous body were then removed. The posterior eyecup returned to the same fixative for another 20 minutes, and then washed three times in PBS. The eyecup was placed in PBS plus 30% sucrose for at least 24 hours, immersed in embedding medium (OCT-compound; Tissue-Tek; Miles Inc, Elkhart, IN), and mounted onto sectioning blocks. Sections (14 µm thickness) were cut in a vertical plane through

the optic nerve head and thaw-mounted onto Super-Frost™ slides (Fisher Scientific Ltd, Leicestershire, UK). The sections were air-dried and stored at -20°C until use.

Sections were thawed at room temperature, ringed with rubber cement, washed three times in PBS, covered with primary antibody solution (see Table 4.2. for a list of antibodies used) (200 µl of antiserum diluted in PBS plus 5% normal goat serum, 0.2% Triton X-100, and 0.01% NaN₃), and incubated for 24 hours at 20°C in a humidified chamber. The slides were washed in PBS, covered with secondary antibody solution, and incubated for 1 hour at 20°C in a humidified chamber. Secondary antibodies included goat-anti-rabbit-Alexa488, goat-anti-mouse Alexa488/568 and goat-anti-mouse-IgM Alexa568 (Molecular Probes Inc., Eugene, OR) were diluted to 1:1000 in PBS plus 0.2% Triton X-100. The detection method of streptavidin-immunoperoxidase (DakoCytomation, Carpinteria, CA) was applied to reveal primary antibody-positive immunoreactivity. Finally, the slides were washed three times in PBS, the rubber cement was removed from the slides, and a coverglass was applied in 4:1 (v/v) glycerol to water.

PRIMARY ANTIBODY	CONCENTRATION OF PRIMARY ANTIBODY	SOURCE OF PRIMARY ANTIBODY	SECONDARY ANTIBODY
RABBIT ANTI-RED/GREEN OPSIN	1:600	CHEMICON; PITTSBURGE, PA	GOAT-ANTI-RABBIT-ALEXA488
MOUSE ANTI-HU-C/D	1:200	MONOCLONAL ANTIBODY FACILITY; U OF OREGON	GOAT-ANTI-MOUSE-IGM ALEXA568
MOUSE ANTI-CALBINDIN	1:800	SIGMA ALDRICH; ST. LOUIS, MO	GOAT-ANTI-MOUSE-IGM ALEXA568

RABBIT ANTI-CALRETININ	1:1000	SWANT; BELLINZONA, SWITZERLAND	GOAT-ANTI-RABBIT-ALEXA488
------------------------	--------	--------------------------------------	---------------------------

Table 4.2. A list of the primary antibodies, their working dilution and source that are used in frozen sections. Key: Alexa-488 = green and Alexa-568 = red.

The immunohistochemical staining utilizing frozen retina was performed in Dr Andy Fischer's laboratory (Department of Neuroscience, The Ohio State University, Columbus, Ohio).

4.2.4.b. Data analysis

Photomicrographs were taken by using a Leica DM5000B microscope equipped with epifluorescence and a 12 megapixel Leica DC500 digital camera (Meyer Instruments, Houston, TX). Images were optimized for color, brightness and contrast, and double-labeled images overlaid by using PhotoshopTM 6.0. Retinal sections of the *PDE6A* mutant dogs were examined for differences in the distribution and morphology of the immunoreactive cells and compared to the normal control eyes.

4.2.5. Terminal Deoxynucleotidyl Transferase-mediated dUTP Nick End Labeling (TUNEL) staining

Direct TUNEL labeling assay was performed using *In Situ* cell death detection kit, rhodamine (Roche Diagnostics Corporation, Indianapolis, IN) to detect DNA strand breaks in apoptotic cells by using an optimized terminal transferase (TdT) to label free 3'OH ends in genomic DNA with rhodamine-dUTP.

4.2.5.a. Tissue collection and processing

Terminal enucleation was performed on dogs at 3, 4, 5 and 9 weeks of age. See 4.2.4.a. for a detail of tissue processing. Slides were thawed and fixed for 1 hour at room temperature, washed and then permeabilized on ice for 2 minutes. Samples were finally incubated with TUNEL reaction mixture (TdT and fluorescein-dUTP solution) at 37°C for 1 hour.

4.2.5.b Data analysis

Incorporated rhodamine/fluorescein was visualized by fluorescence microscopy.

4.3. Results

No significant histological differences were observed between the homozygous *PDE6A* normal and heterozygous carrier dogs.

4.3.1. Morphological assessment of the retina by light and electron microscopy

4.3.1.a. Retinal sections at 3 to 10 days of age

At 3 to 10 days of age, the morphological features of the retina of mutant dogs were similar to those of control dogs. The development of retinal layers starts with the inner layers of the retina and then moves progressively outward. The central region of the retina matures prior to the peripheral region. At 3 days of age (Figure 4.4A), the neurosensory retina consisted of two layers; inner and outer neuroblastic layer. The RPE layer was also present at this age. Primitive horizontal cells appeared within the outer neuroblastic layer at 4 days of age (Figure 4.4B) and the OLM was apparent. Separation of the outer neuroblastic layer into the INL, OPL and ONL had occurred by 7 days of age (Figure 4.4C). The inner segments of photoreceptors had begun to develop in the central retinal region, and by 10 days of age (Figure 4.4C) their length was ranged from 3 to 4.5 μm by 10 days of age (Figure 4.4D).

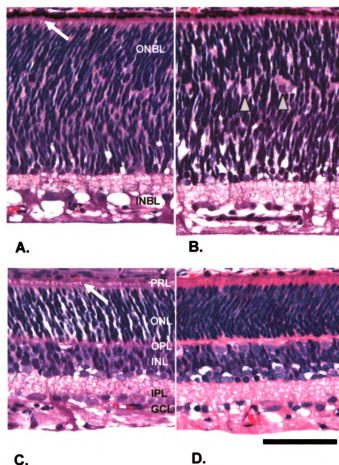


Figure 4.4. Representative photomicrographs of retinal morphology of a normal control (A & C) and the *PDE6A* mutant dog (B & D) at 4 (A & B) and 10 (C & D) days of age. Bar = 50 μ m. A & B) the RPE, IPL, GCL and NFL are formed by 4 days after birth. Retinal nuclei in the outer neuroblastic layer are elongating and photoreceptor inner segments are beginning to develop (white arrows). Primitive horizontal cells are present at this age (arrowheads; B). C & D) Retina at 10 days of age consists of three layers of nuclei; the ONL, the INL and the GCL. Photoreceptor inner segments have increased in length (white arrow). No difference is observed between the retina of the normal control and the *PDE6A* mutant dog at this age. Key: ONBL = outer neuroblastic layer, INBL = inner neuroblastic layer, PRL = photoreceptor layer, ONL = outer nuclear layer, OPL = outer plexiform layer, INL = inner nuclear layer, IPL = inner plexiform layer, GCL = ganglion cell layer, NFL = nerve fiber layer.

4.3.1.b. Retinal sections at 2 to 3 weeks of age

All retinal layers had developed by the second week of life and the photoreceptor inner segments had increased in length (Figure 4.5A & 4.5B). The photoreceptor outer segments had started to develop at this age except for in the far periphery of the retina. Chromatin-dense photoreceptor nuclei were elongated in shape in the normal control retina (Figure 4.5A). A few nuclei with less dense chromatin located at the inner region of the ONL were present in the *PDE6A* mutant retina (Figure 4.5B). They were spherical in shape with vacuolation of the cytoplasm. These changes in the nuclei indicated an early stage of degenerative alteration of cells.

At 3 weeks of age, photoreceptor inner and outer segments had elongated in the normal control retina (Figure 4.5C). Cone nuclei (large cell bodies with pale chromatin) could be seen located adjacent and internal to the OLM whereas rod nuclei (small, oval cell bodies with very dense chromatin) occupied the rest of the ONL. In the *PDE6A* mutant retina the photoreceptor outer segments appeared disorganized at this age and surrounded by empty spaces, suggesting a loss of some of photoreceptor outer segments (Figure 4.5D). The mean thickness of the photoreceptor inner segment layer was however comparable with normal control (vertical section; $10.38 \pm 0.78 \mu\text{m}$ and horizontal section; $8.89 \pm 0.38 \mu\text{m}$) and the *PDE6A* mutant (vertical section; $12.54 \pm 0.54 \mu\text{m}$ and horizontal section; $10.55 \pm 0.71 \mu\text{m}$) (Figure 4.6 & 4.7). Nearly all retinal layers have the greatest thickness at superior region close to the optic disc (region #4) and the least thickness at the far inferior region (region #8). There were no significant differences

in the thickness of each retinal layer ($P<0.05$) in vertical and horizontal sections between normal control and the *PDE6A* mutant dog retina at these ages.

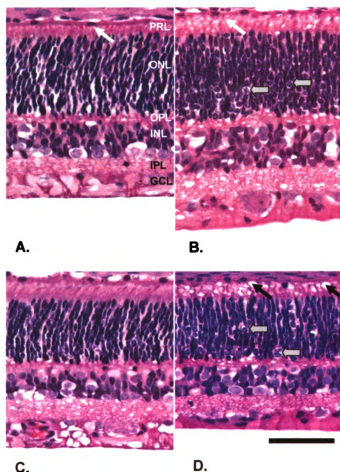


Figure 4.5. Representative photomicrographs of retinal morphology of a normal control (A & C) and the *PDE6A* mutant dog (B & D) at 2 (A & B) and 3 (C & D) weeks of age. Bar = 50 μ m. A & B) Photoreceptor outer segments of both groups have begun to develop at 2 weeks of age (white arrows) while the inner segments have grown in length. Photoreceptor segments of the *PDE6A* mutant are of comparable length to those of normal control. Changes of chromatin pattern present in several photoreceptor nuclei (solid arrows) that are indicative of cell death (apoptosis) in the retinal section of the *PDE6A* mutant dog. C & D) Photoreceptor cell bodies of the normal retina at 3 weeks of age are arranged in an organized manner, and the photoreceptor inner segment and outer segment are longer compared to those at 2 weeks of age. Spaces in the PRL of the *PDE6A* mutant retina (black arrows) indicate degenerative outer segments. Apoptotic nuclei indicated by the presence of spherical-shaped photoreceptor nucleus are present (solid arrows) with weak surrounding euchromatin staining and fragmented heterochromatin. Key: PRL = photoreceptor layer, ONL = outer nuclear layer, OPL = outer plexiform layer, INL = inner nuclear layer, IPL = inner plexiform layer, GCL = ganglion cell layer.

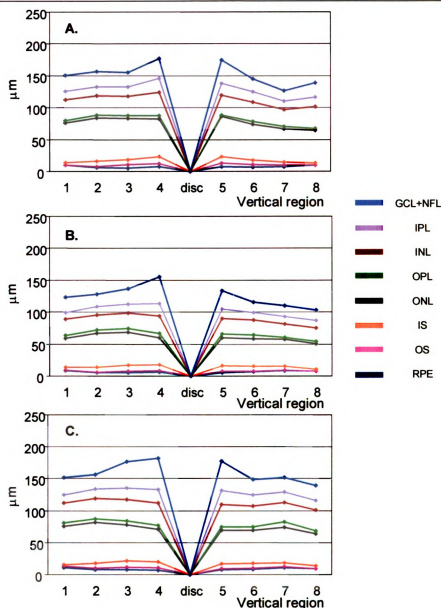


Figure 4.6. Mean retinal thickness of each of the different retinal layers from superior to inferior ora ciliaris retina (vertical section; see Figure 4.1 in materials and methods) from normal control (A), *PDE6A* carrier (B) and *PDE6A* mutant dogs (C) at 3 weeks of age (n=3). Note that photoreceptor outer segments of all genotypes have developed in particular the central region. All retinal layers are thinner at the superior and inferior regions close to the ora ciliaris retina (#1 & #8). The central retinal thickness tends to be greater than the periphery. There are no obvious differences in thickness of the various retinal layers at this age. Key: RPE = retinal pigment epithelium, OS = outer segment, IS = inner segment, ONL = outer nuclear layer, OPL = outer plexiform layer, INL = inner nuclear layer, IPL = inner plexiform layer, GCL = ganglion cell layer, NFL = nerve fiber layer.

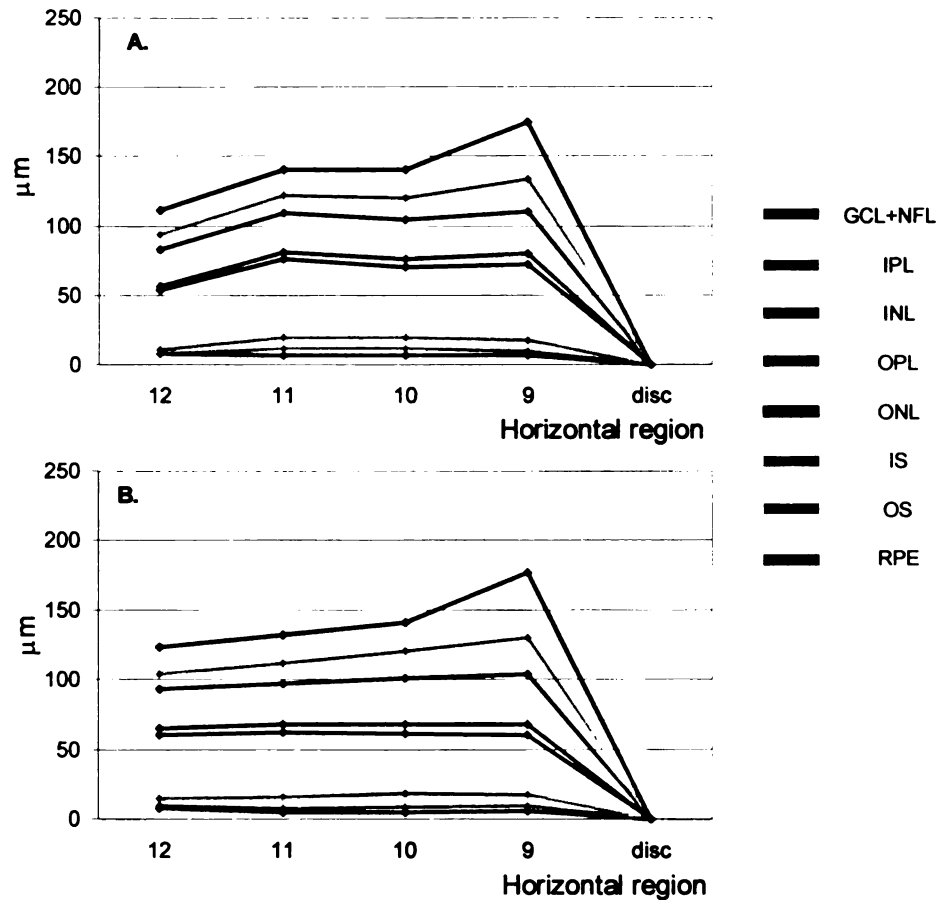


Figure 4.7. Mean retinal thickness of each of the different retinal layers from nasal to temporal region (horizontal section; see Figure 4.1 in materials and methods) from normal control (A) and *PDE6A* mutant dogs (B) at 3 weeks of age (n=3). Note that the thickness of all retinal layers is least at the far temporal region (#12) and greatest at the region close to the optic disc (#9). Photoreceptor segments are developing. No difference in retinal thickness is apparent between normal control (A) and *PDE6A* mutant dogs at this age (B). Key: RPE = retinal pigment epithelium, OS = outer segment, IS = inner segment, ONL = outer nuclear layer, OPL = outer plexiform layer, INL = inner nuclear layer, IPL = inner plexiform layer, GCL = ganglion cell layer, NFL = nerve fiber layer.

The shape of rod nuclei, the appearance of the chromatin and of the rod cell cytoplasm of mutant dogs at approximately 3 weeks of age appeared to differ from the controls. While photoreceptor nuclei of the normal control compared to the previous week had further elongated (Figure 4.8A, 4.9A & 4.10A), some of those of the *PDE6A* mutant dog had undergone degeneration. Morphological changes representing several stages of apoptosis (programmed cell death) were seen in the *PDE6A* mutant retina during this period of time (Figure 4.8B, 4.8C & 4.8D). In the early stages of apoptosis, nuclei were spherical and swollen with densely fragmented heterochromatin and a pale euchromatin (Figure 4.9B). Fragmented heterochromatin then became clustered adjacent to the nuclear membrane and afterward the cell appeared pyknotic with significant smaller nuclei at the later stages of cell death (Figure 4.10C). Dead cells in the process of being removed appeared without distinct detail of organelles (Figure 4.10D). A dramatic increase in the number of apoptotic cells occurred from 24 to 27 days of age in the mutant retina although significant number of TUNEL-positive cells was present in the mutant retina at 28 days of age (figure 4.13D).

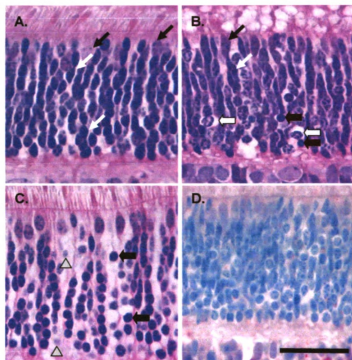


Figure 4.8. Photomicrographs of retinal morphology of the ONL of a normal control (A) at 23 days of age, and *PDE6A* mutants dogs (B & C) at 24 (B) and 27 (C) days of age and a photomicrograph of the anti-caspase 3 immunohistochemistry in the *PDE6A* mutant retina at 24 (D) days of age. Bar = 25 μ m. A) In normal control retina, photoreceptor nuclei are elongated in shape. Cone cell bodies (black arrows) with lighter chromatin are located at the outer border of the ONL whereas rod cell bodies with darker chromatin are located throughout the ONL (white arrows). B & C) The *PDE6A* mutant retinas at 24 and 27 days of age illustrate a number of apoptotic photoreceptor nuclei; spherical, swollen cells with fragmented chromatin and vacuolation (opened arrows), smaller spherical cells with very dense heterochromatin (solid arrows) and dying cells with fading euchromatic appearance (arrowheads). D) No caspase 3-immunopositive cells are detected in the immunohistochemical section of the *PDE6A* mutant retina at 24 days, which is comparable to normal control retinal section (data not shown).

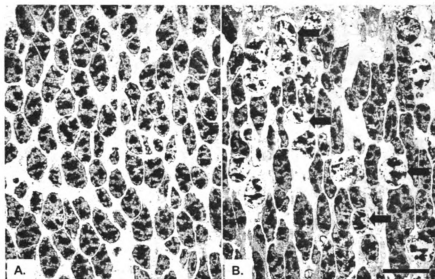


Figure 4.9. Ultra structural sections of the ONL of a normal control (A) and the *PDE6A* mutant dog (B) at 23 days of age. Bar = 10 μ m. Note that photoreceptor nuclei of the normal control dog are oval in shape with a cluster of chromatin (A). In contrast, apoptotic nuclei (arrows) are scattered in the ONL of the *PDE6A* mutant retina (B). The nuclei appear more spherical in shape with a decrease in staining of euchromatin and irregular nuclear membrane compared to those of normal nuclei surrounded.

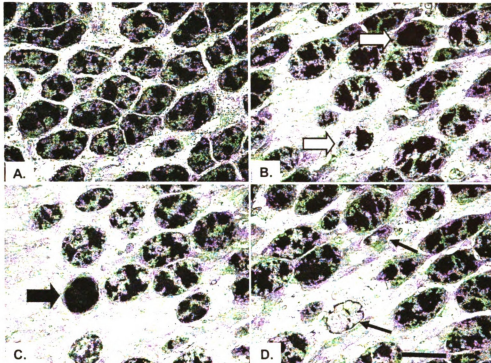


Figure 4.10. Ultra structural appearance of photoreceptor nuclei of normal control (A) and *PDE6A* mutant dogs (B, C & D) at 27 days of age. Bar = 5 μ m. Note that in B, C & D there are several photoreceptor nuclei that appear to be going through stages of apoptosis. Photoreceptor cell bodies have become round with an accumulation of electron-dense chromatin adjacent to nuclear membrane (opened arrows) (B), a well-demarcated electron-dense chromatin occupies almost an entire nuclear cytoplasm (solid arrow) (C) and small nuclei with no distinct nuclear membrane (black arrows) (D).

4.3.1.c. Retinal sections at 4 to 5 weeks of age

Between 4 to 5 weeks of age the photoreceptor outer and inner segments of normal controls continued to lengthen (Figure 4.11A & 4.11C). At this age the number of ONL row and number of rod nuclei per unit length of the retina had reached their peaks (Figure 4.27A, 4.28A, 4.29A & 4.30A). Photoreceptor nuclei had become rounder in shape and the ONL appeared well organized. Loss of outer segments in the *PDE6A* mutant retina was apparent at 4 weeks of age (Figure 4.11B), along with an apparent slight reduction of the thickness of the IS layer and the ONL. The thickness of the OS layer across the retina ranged from 0.75 +/- 0.35 to 5.42 +/- 1.18 μm in the *PDE6A* mutant dog compared to from 3.45 +/- 0.67 to 11.25 +/- 2.13 μm in the normal controls. However, this difference was not significant. There were no significant differences in the thickness of other retinal layers between mutant and normal puppies.

At 5 weeks of age photoreceptor cell layer of the *PDE6A* mutant retina was reduced in thickness (Figure 4.11D). The outer segments of the *PDE6A* mutant dog were much disoriented and stunted (Figure 4.16B). The thickness of the OS layer was significantly reduced ($P < 0.05$) compared to normal control from region #2 to #6 along the vertical plane of retinal section (Figure 4.14C), and region #9 and 11# along the horizontal plane of retinal section (Figure 4.15B). Inner segments of mutant dogs at this age appeared shortened, broadened and more prominent (Figure 4.16B). A significant difference ($P < 0.05$) in the thickness of the inner segments was found for region #5 (Figure 4.14C) as well as that of the ONL. There was a significant decrease in the number

of ONL rows ($P<0.05$) at region #3 to #7 on the vertical plane of retinal section (Figure 4.27A). The number of rod nuclei per unit length of the mutant retina was also reduced at regions #2, #3 and from #5 to #7 on the vertical plane of retinal section (Figure 4.29A), and at region #9 on the horizontal plane of section (Figure 4.30A). Pyknotic photoreceptor nuclei were evident in the ONL of the *PDE6A* mutant retina at this age (Figure 4.12B) although TUNEL staining revealed only 1-2 TUNEL-positive cells per field (Figure 4.13F). Caspase 3-immunoreactive cells could not be detected in the ONL (Figure 4.12C) at this age.

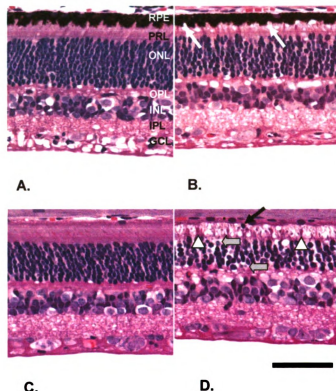


Figure 4.11. Representative photomicrographs of retinal morphology of normal control (A & C) and the *PDE6A* mutant dogs (B & D) at 4 (A & B) and 5 (C & D) weeks of age. Bar = 50 μ m. A & B) Photoreceptor outer segments continue to elongate in normal control retina while they continue to degenerate in the *PDE6A* mutant retina (white arrows) at 4 weeks of age. Thickness of the PRL and the ONL of the *PDE6A* mutant retina slightly reduces in comparison to normal control retina. C & D) At 5 weeks of age, photoreceptor segments of a normal control are well structured but fragmented and disorganized in the *PDE6A* mutant retina. Cell present in the PRL (black arrow) could possibly be a phagocytic cell or a displaced photoreceptor nucleus. Loss of inner segments appears at this age; cone inner segments (arrowheads) are broader than those of normal control retina. Apoptotic cells are observed (solid arrows) and the number of photoreceptor nuclei per unit length of the retina appears to be decreased. Key: RPE = retinal pigment epithelium, PRL = photoreceptor layer, ONL = outer nuclear layer, OPL = outer plexiform layer, INL = inner nuclear layer, IPL = inner plexiform layer, GCL = ganglion cell layer.

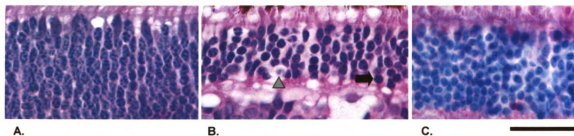


Figure 4.12. Photomicrographs of retinal morphology of the ONL of a normal control (A) at 38 days of age, a *PDE6A* mutant dog (B) at 42 days of age and caspase 3 immunohistochemistry in a *PDE6A* mutant retina at 42 days of age (C). Bar = 25 μ m. A) In the normal control retina, photoreceptor nuclei are well arranged and tightly packed. B) Apoptotic bodies (solid arrow) and dead cells (arrowhead) are present in the thinned ONL at this age. C) Anti-caspase 3 immunoreactivity is not detected in the *PDE6A* mutant retina at this age.

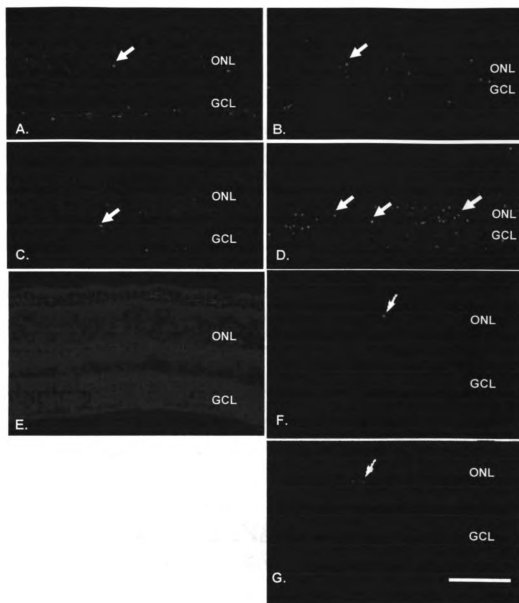


Figure 4.13. Photomicrographs of TUNEL labeling of retina from normal controls (A, C & E) and the *PDE6A* mutant dogs (B, D, F & G) at 25 day (A & B), 28 day (C & D), 5 weeks (E & F) and 10 weeks (G) of age. Bar = 50 μ m. 1 to 2 TUNEL-positive cells can be seen in all retinal sections from normal and mutant dogs (white arrows). A large number of TUNEL-positive cells are apparent in retina of mutant dogs at 28 days of age (D).

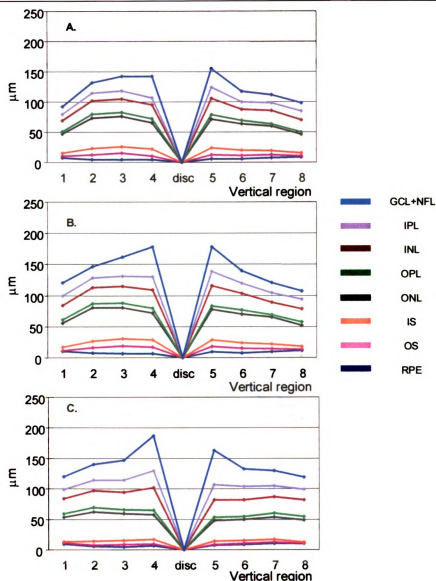


Figure 4.14. Mean retinal thickness of each of the different retinal layers from superior to inferior ora ciliaris retina (vertical section; see Figure 4.1 in materials and methods) from normal control (A), *PDE6A* carrier (B) and *PDE6A* mutant dogs (C) at 5 weeks of age ($n=3$). Note the *PDE6A* mutant dogs have a reduction in length of outer segments (C) particularly in the central retina, compared to that of normal control (A) and carrier (B). Thickness of the inner segment layer of the *PDE6A* mutant dog is also slightly reduced. Other retinal layer thicknesses are maintained among disease genotypes and in fact mean overall retinal thickness is greater in the mutant dogs compared to controls. Key: RPE = retinal pigment epithelium, OS = outer segment, IS = inner segment, ONL = outer nuclear layer, OPL = outer plexiform layer, INL = inner nuclear layer, IPL = inner plexiform layer, GCL = ganglion cell layer, NFL = nerve fiber layer.

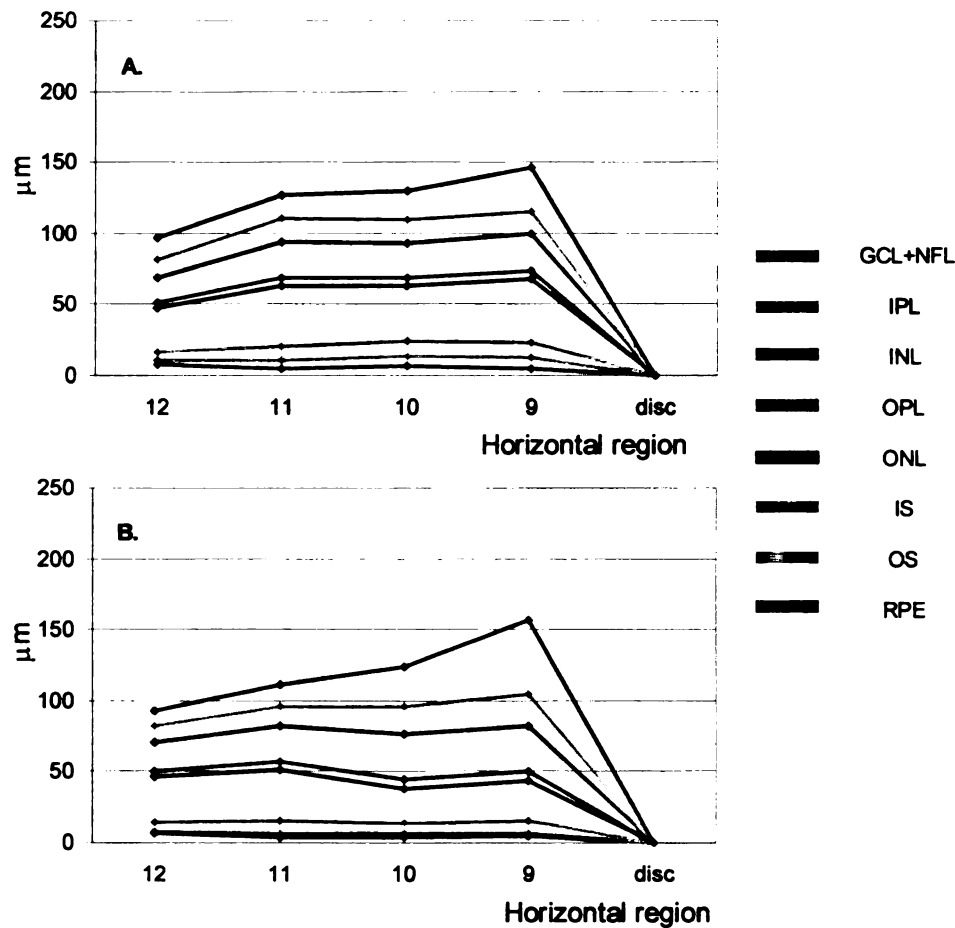


Figure 4.15. Mean retinal thickness of each of the different retinal layers from nasal to temporal region (horizontal section; see Figure 4.1 in materials and methods) from normal control (A) and the *PDE6A* mutant dogs (B) at 5 weeks of age (n=3). Note the outer segments length of in the *PDE6A* mutant dogs are decreased compared to normal control (B), while the inner segments appear slightly shorter but not significant compared to normal control (A). Key: RPE = retinal pigment epithelium, OS = outer segment, IS = inner segment, ONL = outer nuclear layer, OPL = outer plexiform layer, INL = inner nuclear layer, IPL = inner plexiform layer, GCL = ganglion cell layer, NFL = nerve fiber layer.

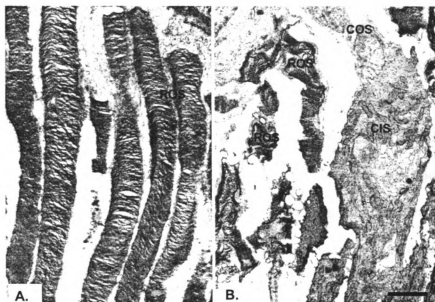


Figure 4.16. Ultra structural sections of the photoreceptor segments of a normal control (A) and the *PDE6A* mutant retina (B) at 5 weeks of age. Bar = 1 μ m. Note stacks of rod outer segment discs are well organized in the normal control (A) whereas they are short and disorganized in the *PDE6A* mutant retina (B). Cone outer and inner segments are also swollen and disoriented in the retina of mutant dogs. Key: ROS = rod outer segment, COS = cone outer segment, CIS = cone inner segment.

4.3.1.d. Retinal sections at 7 to 12 weeks of age

The normal control retina had an adult-like appearance by 7 weeks of age (Figure 4.17A); the photoreceptor inner and outer segments and cell bodies were well organized. The *PDE6A* mutant retina on the other hand had a severe loss of photoreceptor outer segments (Figure 4.17B). The thickness of the OS layer was significantly reduced ($P<0.01$) for all horizontal and vertical plane of retinal regions compared to the controls, except for the superior far periphery. Loss of inner segments was observed with the remaining inner segments having a club-shaped appearance (Figure 4.17B). A significant difference ($P<0.05$) in the thickness of the IS layer was found between the *PDE6A* mutant and normal control group at region #2 to #8 on the vertical plane section and region #9 on the horizontal plane section. In the mutant dogs, the thickness of the ONL was significantly reduced ($P<0.05$) at regions close to the optic disc (central retina) and over most of the inferior regions, as well as at all regions of the horizontal plane. Although a slight reduction of the number of ONL row and rod nuclei per unit length of the retina was found in all retinal regions of the normal control at 7 weeks of age, a significant reduction of those numbers ($P<0.05$) in the *PDE6A* mutant retina were seen in most retinal regions but those at the periphery compared to a normal control group (data not shown). No significant difference ($P<0.05$) of other retinal layers and the number of cone nuclei per unit length of the retina were observed at 7 weeks of age.

By 9 weeks of age, the mean thickness of the photoreceptor OS layer of the *PDE6A* mutant retina was significantly decreased ($P<0.01$) for all vertical and horizontal

plane of retinal regions compared to the normal control group. The mutant dog had short remaining inner segments, which still contained mitochondria (Figure 4.18). The mean thickness of the IS layer was significantly decreased ($P<0.05$) for all vertical and horizontal plane of retinal regions except for the regions at the superior, inferior and temporal periphery (Figure 4.20 & 4.21). No significant difference in the mean thickness of the ONL was found at this age, although there was a notable loss of photoreceptor nuclei with spaces appearance between the remaining nuclei (Figure 4.19B). The overall thickness of the ONL ranged from 29.42 \pm 1.67 to 43.08 \pm 2.2 μ m for the normal control compared to from 27.87 \pm 0.87 to 43.41 \pm 1.82 μ m for the *PDE6A* mutant retina along the vertical retinal section. However, the number of ONL row and rod nuclei per unit length of the retina was significantly reduced ($P<0.05$) compared to normal control at regions #3 to #7 and #9 to #10 (Figure 4.27B & 4.28B), and #2 to #8 and #9 to #11 (Figure 4.29B & 4.30B), respectively. Only 1 or 2 TUNEL-positive cells in the ONL were detected at 9 weeks of age (Figure 4.13G).

The mean thickness of the ONL at 12 weeks of age was slightly decreased in normal control dogs compared to the previous ages (data not shown). Apart from superior and inferior regions close to the optic disc, no significant difference was found at other retinal regions between two groups of dogs. The number of ONL row and rod nuclei per unit length of the mutant retina was similar to those at 9 weeks of age.

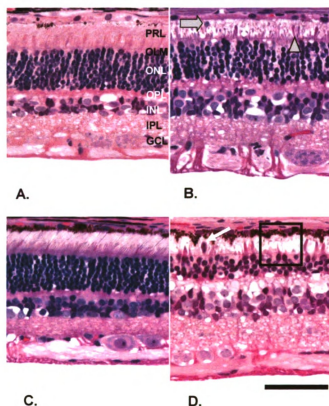


Figure 4.17. Representative photomicrographs of retinal morphology of a normal control (A & C) and the *PDE6A* mutant dog (B & D) at 7 (A & B) and 12 (C & D) weeks of age. Bar = 50 μ m. A & B) Retina of the normal control has an adult-like morphology at 7 weeks of age. Photoreceptor nuclei are spherical and very well organized. In the mutant dogs rod and cone outer and inner segments are reduced in size and number. Cone inner segments are broader and more prominent (arrowhead). There are spaces between inner and outer segments and to a lesser extent between photoreceptor nuclei. Phagocytic cells or displaced photoreceptor nuclei are occasionally seen (solid arrow) in the PRL. C & D) Photoreceptor outer segments of the *PDE6A* mutant retina are severely disrupted with focal area of loss of photoreceptor inner segments at 12 weeks of age (boxed area). Remaining cone inner segments have a club-shaped appearance; phagocytic cells are occasionally seen in the subretinal space (white arrow). In the retina of a mutant dog, the ONL is much reduced in thickness. Key: PRL = photoreceptor layer, OLM = outer limiting membrane, ONL = outer nuclear layer, OPL = outer plexiform layer, INL = inner nuclear layer, IPL = inner plexiform layer, GCL = ganglion cell layer.

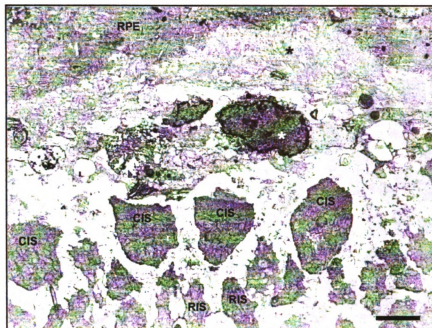


Figure 4.18. Ultra structural sections of the photoreceptor layer of the *PDE6A* mutant retina at 9 weeks of age. Bar = 1 μ m. Note a narrow PRL present with short rod and cone inner segments, remnant of degenerative segments, microvilli of the RPE (dark asterisk) and macrophage (white asterisk). Although cone inner segments are very short at this age, mitochondria are the predominant feature. Key: RPE = retinal pigment epithelium, RIS = rod inner segment, CIS = cone inner segment.

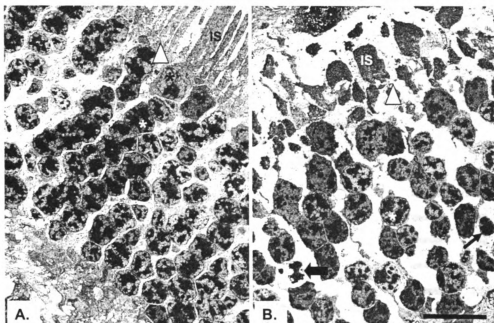


Figure 4.19. Ultra structural sections of the ONL of a normal control (A) and the *PDE6A* mutant retina (B) at 9 weeks of age. Bar = 10 μ m. A) Rod nucleus (white asterisk) of a normal control is small and contains dispersed electron-dense chromatin. Cone nucleus (black asterisk) is larger and contains less electron-dense chromatin in comparison to the rod nucleus. B) Short photoreceptor inner segments are positioned adjacent to the OLM (arrowhead), which is not as distinct as the OLM of the normal retina. The appearance of space in the ONL indicates loss of photoreceptor nuclei. Approximately six rows of photoreceptor nuclei are observed in the *PDE6A* mutant retina whereas there are 8 to 9 rows in the age-matched normal control. Apoptotic cells can be seen: note the cell with an aggregate of heterochromatin in the swollen weakly-stained euchromatin (solid arrow) and cell with a well demarcated electron dense chromatin occupying most of the nucleus (black arrow). Key: IS = inner segment.

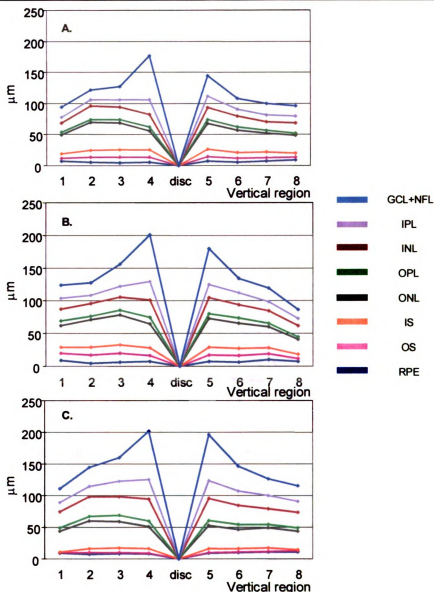


Figure 4.20. Mean retinal thickness of each of the different retinal layers from superior to inferior ora ciliaris retina (vertical section; see Figure 4.1 in materials and methods) from normal control (A), *PDE6A* carrier (B) and *PDE6A* mutant dogs (C) at 9 weeks of age ($n=3$). Note in the retina of a normal control and carrier (A & B), thickness of each retinal layer at different regions is relatively equivalent, and it increases toward the optic disc. A similar pattern also applies to retinal layer thicknesses of the *PDE6A* mutant dog (C) with the exception of the outer and inner segment layers that are significantly decreased. These layers seem thinner at regions close to ora ciliaris retina compared to other regions. Key: RPE = retinal pigment epithelium, OS = outer segment, IS = inner segment, ONL = outer nuclear layer, OPL = outer plexiform layer, INL = inner nuclear layer, IPL = inner plexiform layer, GCL = ganglion cell layer, NFL = nerve fiber layer.

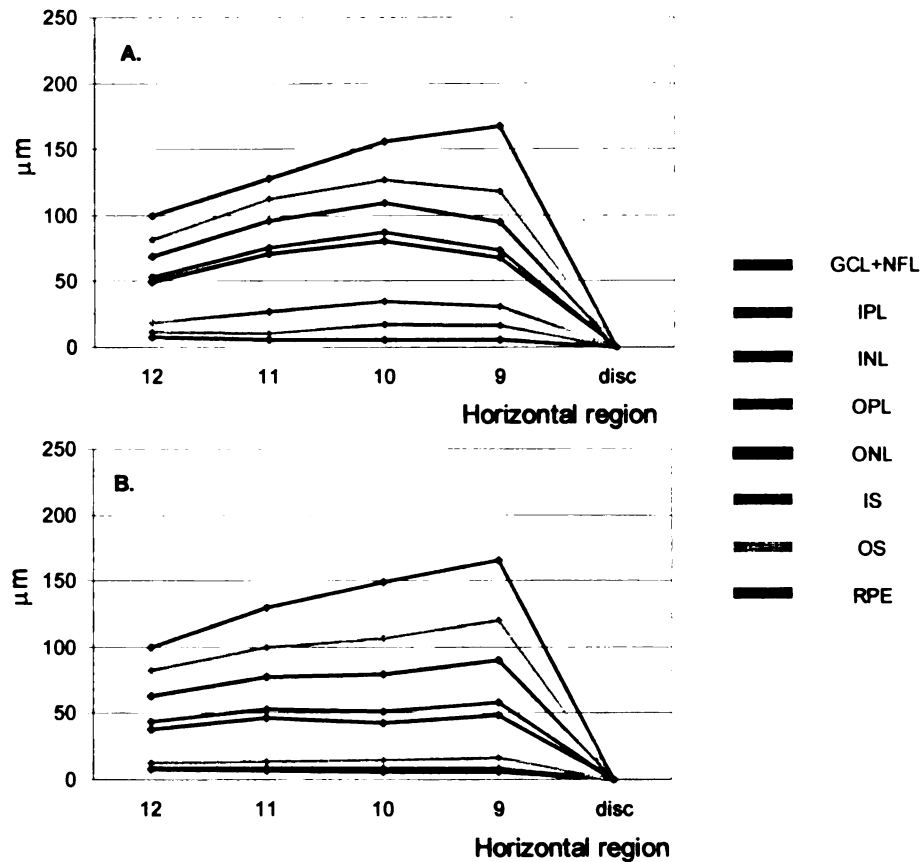


Figure 4.21. Mean retinal thickness of each of the different retinal layers from nasal to temporal region (horizontal section; see Figure 4.1 in materials and methods) from normal control (A) and *PDE6A* mutant dogs (B) at 9 weeks of age (n=3). Note that the outer and inner segment layers of the *PDE6A* mutant retinas (B) are very much narrower than in the normal control retinas (A). The entire ONL has reduced in thickness particularly at region #10 (B) in the *PDE6A* mutant dog. However, the overall retinal thickness is not reduced. Key: RPE = retinal pigment epithelium, OS = outer segment, IS = inner segment, ONL = outer nuclear layer, OPL = outer plexiform layer, INL = inner nuclear layer, IPL = inner plexiform layer, GCL = ganglion cell layer, NFL = nerve fiber layer.

4.3.1.e. Retinal sections at 16 weeks of age

By 16 weeks of age the overall thickness of the retina of the *PDE6A* mutant retina was reduced by approximately 50% compared to the controls. The photoreceptor layer was severely thinned. Outer segments were present in some areas but very reduced in size and the remaining inner segments were short and broad (Figure 4.22B & 4.23B). The mean thicknesses of the outer segment ($P<0.01$), inner segment ($P<0.01$), and the outer nuclear ($P<0.05$) layers were significantly reduced compared to normal control retinas at all retinal regions along the vertical plane except for the superior far periphery (Figure 4.24C) and all regions along the horizontal plane (Figure 4.25B). At this age the central retina had approximately 3 rows of photoreceptor nuclei remnant in the mutant ONL, compared to 10 to 11 rows in the normal control. Except for the inferior far periphery and temporal regions, the number of nuclei rows was significantly lower in the *PDE6A* mutant retina (Figure 4.27B & 4.28B). Pyknotic nuclei were also evident at this age (Figure 4.23C). The number of rod nuclei per unit length of the retina of the mutant dogs was significantly reduced at more retinal regions than at 9 to 12 weeks of age (Figure 4.29B & 4.30B). The number of cone nuclei per unit length of the retina was found to be significantly decreased at region #5 and #6 (Figure 4.31B). In addition, the OPL of the *PDE6A* mutant retina appeared to have lost its normal architecture in the mutant dog. The photoreceptor termini appeared disrupted and less synaptic ribbons were present (Figure 4.23E).

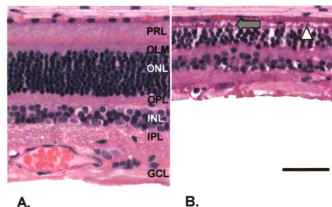


Figure 4.22. Representative photomicrographs of retinal morphology of a normal control (A) and the *PDE6A* mutant dog (B) at 16 weeks of age. Bar = 50 μ m. Note that the PRL of the *PDE6A* mutant retina is very narrow with the presence of remaining stunted cone inner segments (solid arrow). There are approximately 3 rows of photoreceptor nuclei in the ONL of the *PDE6A* mutant retina compared to 10 rows in the retina of the normal control (A). The OLM is still intact (arrowhead). Key: PRL = photoreceptor layer, OLM = outer limiting membrane, ONL = outer nuclear layer, OPL = outer plexiform layer, INL = inner nuclear layer, IPL = inner plexiform layer, GCL = ganglion cell layer.

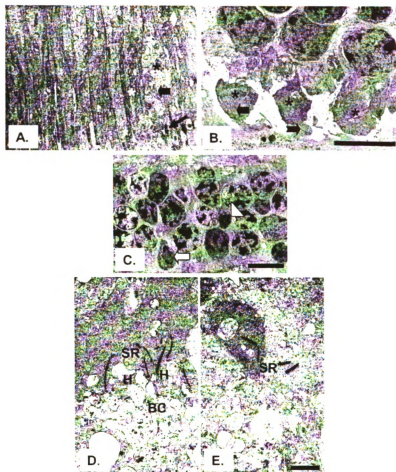


Figure 4.23. Ultra structural sections of the outer retina of a normal control (A & D) and the *PDE6A* mutant dog (B, C & E) at 16 weeks of age. Bar = 5 μ m (A, B & C) & 1 μ m (D & E). A & B) Region of the photoreceptor inner segments in: the normal dog (A) photoreceptor inner segments have an ellipsoidal shape; those of cones (black asterisks) are larger than those of rods (white asterisk). The basal region of inner segment is in contact with the OLM (black arrows) Mitochondria (solid arrows) are the major organelles in the inner segments. In the mutant dog (B) predominantly cone inner segments remains. These are stunted and club-shaped and mitochondria are still present. The inner segment remnants are still in contact with the OLM. Notched arrow indicates a remaining but shortened and distorted cone outer segment. C) The *PDE6A* mutant ONL has only 3 rows of nuclei. Apoptotic cells are present. There is a cell with cluster electron-dense chromatin adjacent to the nuclear membrane (arrowhead) and an apoptotic body with an irregular nuclear membrane (opened arrow). D & E) The OPL: The section from normal dog (D) shows characteristic synaptic termini consisting of synaptic ribbon with arciform density projecting into the invagination, lateral processes from horizontal cells and central process from bipolar cell. In the mutant dog the structure of the OPL is disrupted compared to the control. There is a decrease in the number and length of synaptic ribbons. Key: BC = bipolar cell, H = horizontal cell, SR = synaptic ribbon.

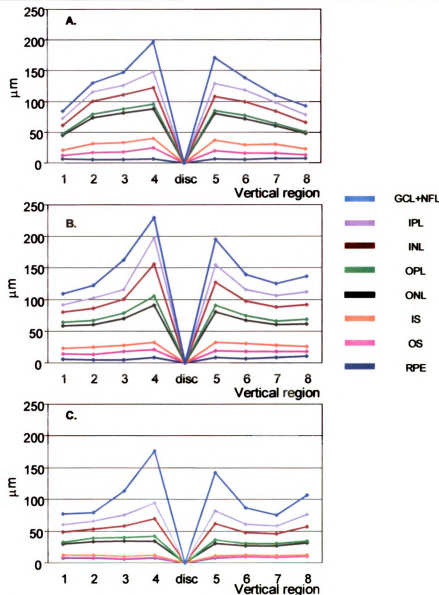


Figure 4.24. Mean retinal thickness of each of the different retinal layers from superior to inferior ora ciliaris retina (vertical section; see Figure 4.1 in materials and methods) from normal control (A), *PDE6A* carrier (B) and *PDE6A* mutant dogs (C) at 16 weeks of age ($n=3$). Note there is a marked reduction of the thickness of the outer segment, inner segment and ONL in all regions of the mutant retina (C). The outer retinal layer of the mutant dog is significantly thinner. Note that the central retinal regions are thicker than that the periphery. Key: RPE = retinal pigment epithelium, OS = outer segment, IS = inner segment, ONL = outer nuclear layer, OPL = outer plexiform layer, INL = inner nuclear layer, IPL = inner plexiform layer, GCL = ganglion cell layer, NFL = nerve fiber layer.

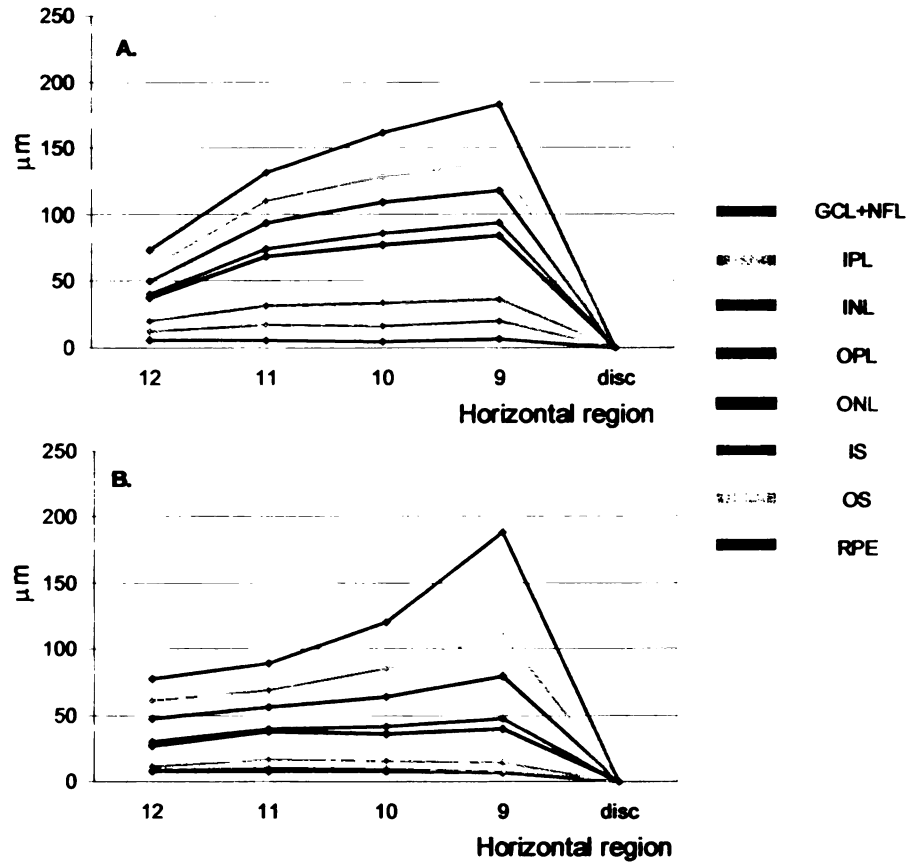


Figure 4.25. Mean retinal thickness of each of the different retinal layers from nasal to temporal region (horizontal section; see Figure 4.1 in materials and methods) from normal control (A) and *PDE6A* mutant dogs (B) at 16 weeks of age. Note the significant reduction of the ONL and OPL thickness in the *PDE6A* mutant retina (B) in comparison to a normal control (A). Thickness of the inner retinal layers rapidly declines from the center toward peripheral retina. Key: RPE = retinal pigment epithelium, OS = outer segment, IS = inner segment, ONL = outer nuclear layer, OPL = outer plexiform layer, INL = inner nuclear layer, IPL = inner plexiform layer, GCL = ganglion cell layer, NFL = nerve fiber layer.

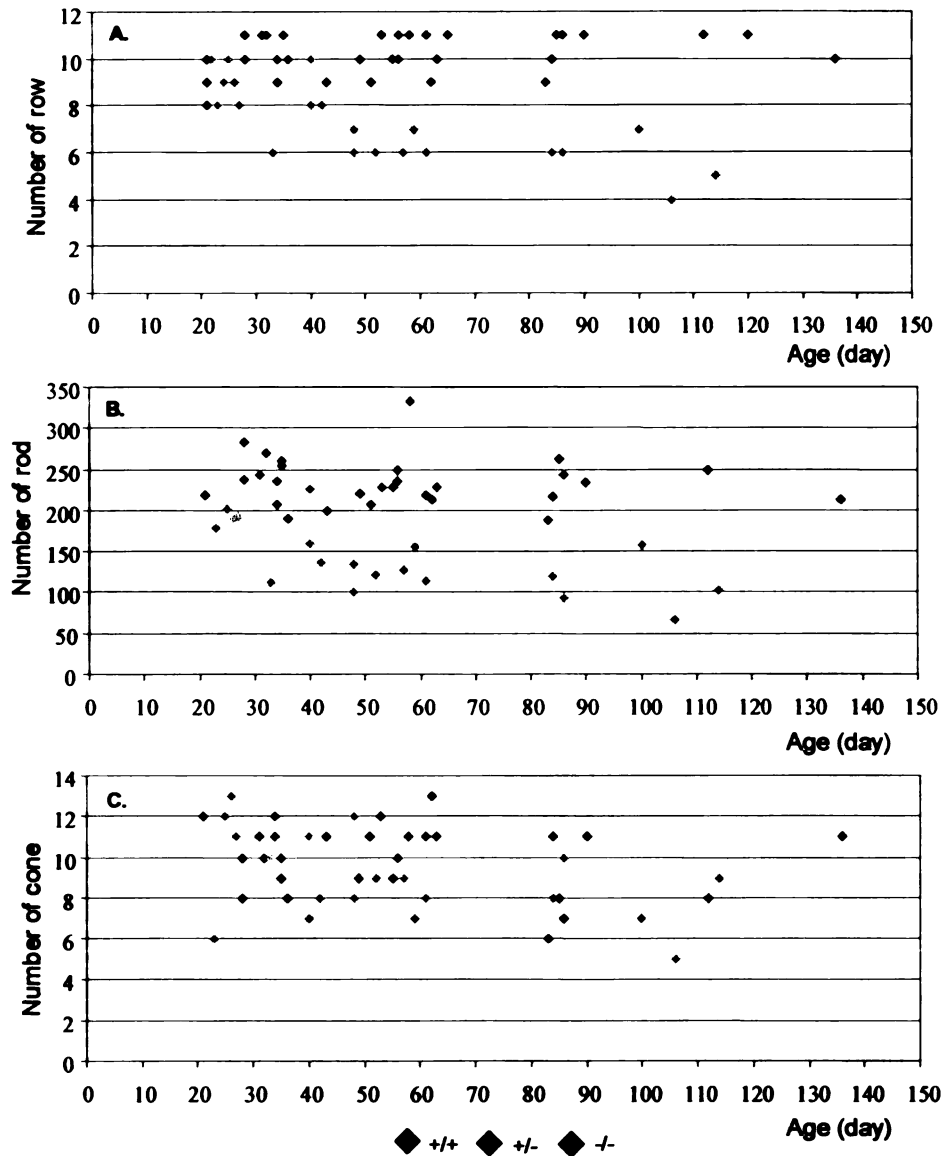


Figure 4.26. Scatter plot showing the number of nuclei rows in the ONL (A), number of rod (B) and number of cone (C) nuclei per unit length (100 μm) of the retina (of region #3) plotted against age for normal control (blue), carrier (green) and mutant (orange) dogs. Note that following an early slight increase in number of ONL row and number of rod nuclei during the first 28 days of life these numbers in normal controls and carriers seem stable throughout the investigation. Number of cone nuclei is maintained and then slightly decreases after about 80 days of age. In contrast, there is no increase in number of nuclei rows in the ONL and rod nuclei in mutant dog. The number of nuclei rows and rod nuclei rapidly decrease at about 49 days of age, and these numbers stay stable, and then slowly decrease at about 100 days of age. In the mean time, number of cone nuclei of the *PDE6A* mutant retinas slightly decreases with age but still comparable to that of normal controls and carriers.

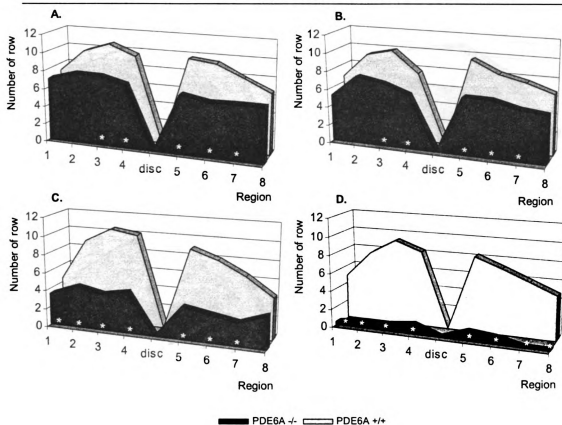


Figure 4.27. Mean number of nuclei rows in the ONL of retinal regions (#1 to #8) in a vertical section through the optic nerve head at 5 (A), 9 (B), 16 (C) and 60 (D) weeks of age (n=3). Note at 5 and 9 weeks of age that the mean number of the ONL row in the *PDE6A* mutant dogs is significantly smaller ($P < 0.05$) at region #3, #4, #5, #6 and #7 (A & B). By 16 weeks of age the number of nuclei rows in the ONL of the more peripheral region #1 and #2 were significantly reduced ($P < 0.05$) compared to controls (C). By 60 weeks of age, there is a significant reduction in the mean number of nuclei rows in the ONL in the *PDE6A* mutant dogs for all retinal regions (D). Asterisk (*) indicates significance $P < 0.05$.

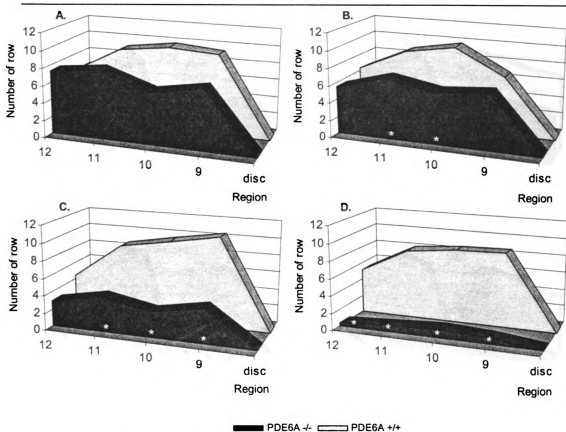


Figure 4.28. Mean number of nuclei rows in the ONL of retinal regions (#9 to #12) in a horizontal section temporal from the optic nerve head at 5 (A), 9 (B), 16 (C) and 60 (D) weeks of age (n=3). Note that there is no significant difference in the mean number of the ONL nuclei rows between normal control and the *PDE6A* mutant dogs at 5 weeks of age. By 9 weeks of age (B) region #10 and #11 are significantly thinner than controls and at 16 weeks of age (C) regions #9, #10, #11 and by 60 weeks of age (D) all regions are significantly thinner ($P < 0.05$). Asterisk (*) indicates significance $P < 0.05$.

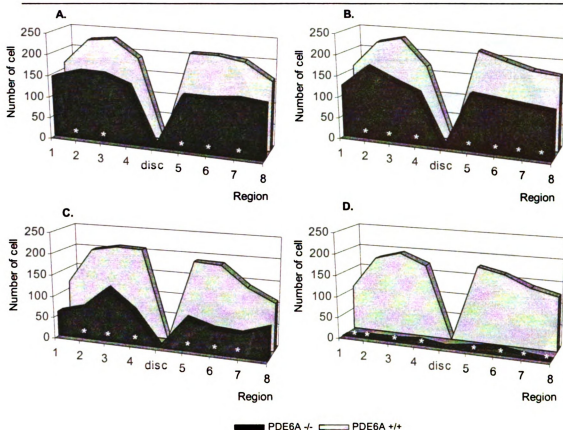


Figure 4.29. Mean number of rod nuclei per unit length (100 μ m) of retinal regions (#1 to #8) in a vertical section through the optic nerve head at 5 (A), 9 (B), 16 (C) and 60 (D) weeks of age (n=3). At 5 weeks of age (A) the mean number of rod nuclei is significantly reduced ($P < 0.05$) in regions #2, #3, #5, #6 and #7. By 9 weeks of age the number of nuclei at regions #4 and #8 is significantly reduced. At 16 weeks of age region #8 is not significantly different. By 60 weeks of age the mean number of rod nuclei is significantly reduced ($P < 0.05$) for all retinal regions (D) compared to the normal control. Asterisk (*) indicates significance $P < 0.05$.

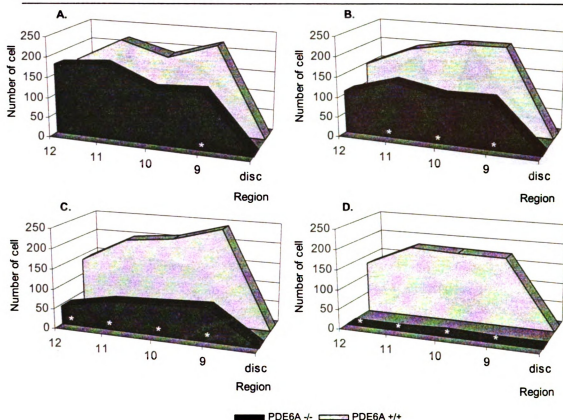


Figure 4.30. Mean number of rod nuclei per unit length of retinal regions (#9 to #12) in a horizontal section temporal from the optic nerve head at 5 (A), 9 (B), 16 (C) and 60 (D) weeks of age ($n=3$). There is a significance decrease ($P < 0.05$) in the mean number of rod nuclei in the *PDE6A* mutant dogs at region #9 at 5 weeks of age (A). By 9 weeks of age regions #10 and #11 also have a significant reduction ($P < 0.05$) in rod nuclei number (B). The mean number of rod nuclei is significantly decreased ($P < 0.05$) in all retinal regions at 16 (C) and 60 (D) weeks of age. Asterisk (*) indicates significance $P < 0.05$.

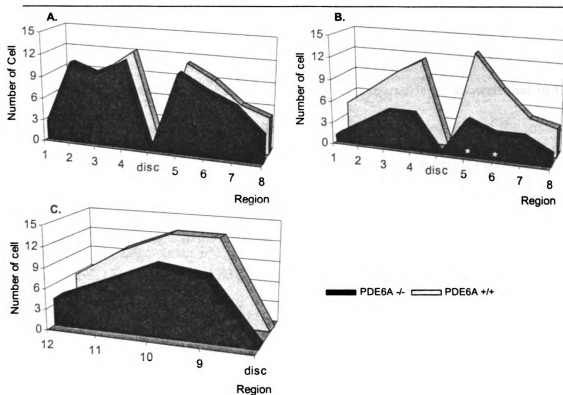


Figure 4.31. Mean number of cone nuclei per unit length (100 μ m) of all retinal regions (#1 to #8) in a vertical section through the optic nerve head (A & B) and horizontal section temporal through the optic nerve head (C) at 5 (A) and 16 (B & C) weeks of age ($n=3$). Note that although the mean number of cone nuclei is decreased for all retinal regions in the mutant dogs at 16 weeks of age (B), this difference is only significant ($P < 0.05$) for region #5 and #6. No difference between the two groups is found at 16 weeks of age for the horizontal section (C). Asterisk (*) indicates significance $P < 0.05$.

4.3.1.f. Retinal sections at 24 weeks of age

Detailed measurements of the thickness of each retinal layer showed that in the *PDE6A* mutant retina at 24 weeks of age the inferior temporal region had the greatest retinal thickness compared to other retinal regions whereas the superior central (#1.1 & #1.2) and temporal (#3.1 & #3.2) regions were thinnest. Outer segments could not be seen in the *PDE6A* mutant retina sections at any retinal regions. The thickness of the IS layer and ONL (Figure 4.32 & 4.33) was best preserved at the inferior temporal (#4.3 & #4.4) inferior nasal (#3.3 & #3.4) and central nasal (#2.3 & #2.4). The INL of the *PDE6A* mutant dog was narrow compared to that of the normal control in the superior retina (data not shown). No difference of the thickness of GCL and NFL was observed between the two groups of dogs. The number of row of nuclei in the ONL (Figure 4.34) and number of photoreceptor nuclei per unit length of the retina (Figure 4.35) were dramatically reduced at all 16 regions investigated.

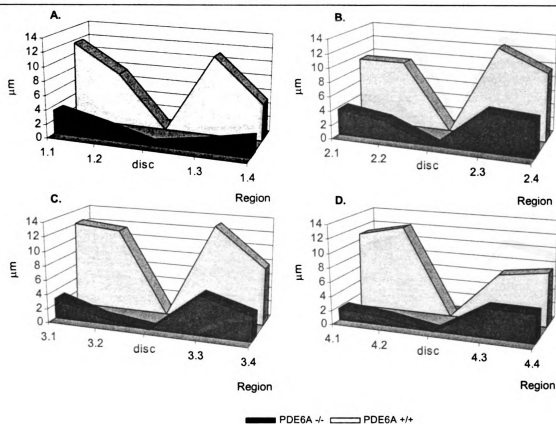


Figure 4.32. Thickness of the inner segments of normal control and the *PDE6A* mutant dog for different retinal regions (see Figure 4.2 in materials and methods) at 24 weeks of age. Note that the length of the *PDE6A* mutant inner segment is remarkably shorter than that in the normal control at all retinal regions investigated. Inner segments are somewhat preserved in the nasal areas; #2.3 & #2.4 (B), #3.3 & #3.4 (C) and the inferior temporal areas; #4.3 & #4.4 (D).

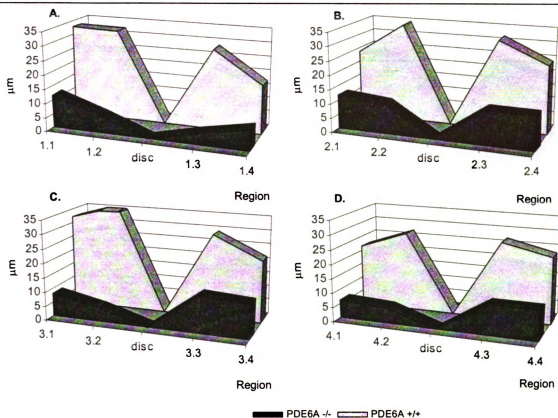


Figure 4.33. Thickness of the ONL of normal control and the *PDE6A* mutant dog for different retinal regions (see Figure 4.2 in materials and methods) at 24 weeks of age. Note that in the mutant dog there is a severe reduction of the ONL thickness affecting the superior retina and inferior central retina of region #1.3 and #1.4. Other regions of the inferior retinal area (B, C & D) are better preserved.

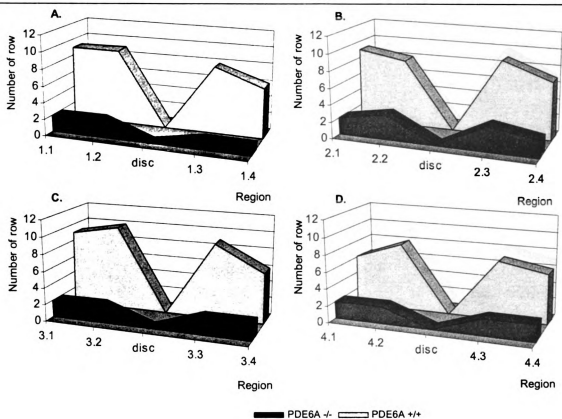


Figure 4.34. Number of nuclei rows in the ONL at different retinal regions (see Figure 4.2 in materials and methods) in normal control and the *PDE6A* mutant dog at 24 weeks of age. Note an approximate 75% reduction of the number of ONL row is found in the *PDE6A* mutant dog at all retinal regions in comparison with a normal control.

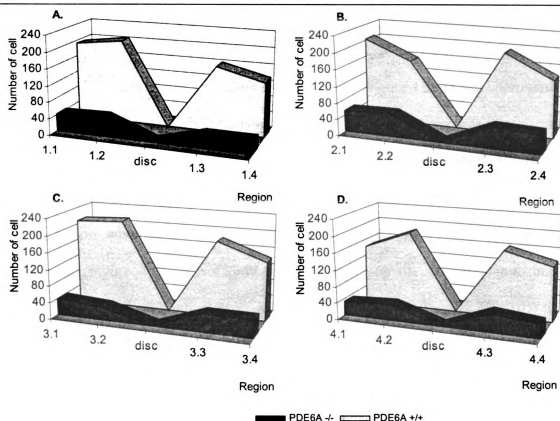


Figure 4.35. Number of photoreceptor nuclei per unit length (100 μm) of retina at different retinal regions (see Figure 4.2 in materials and methods) in normal control and the *PDE6A* mutant dog at 24 weeks of age. Note that there is a marked reduction in the number of photoreceptor nuclei at all retinal regions in the *PDE6A* mutant dog. The superior retinal area is most severely affected with an approximately 80% reduction in the number of cells.

4.3.1 g. Retinal sections at age greater than 60 weeks

By 130 weeks of age, the *PDE6A* mutant retina (Figure 4.36B) was approximately 40% of the thickness of the normal control. The photoreceptor layer was very narrowed and in some regions some stunted inner segments remained (Figure 4.36D). A cluster of a single layer of photoreceptor nuclei, presumably cones, was noticed in some retinal areas. In the region where photoreceptor nuclei were absent, cells in the INL appeared disoriented (Figure 4.36C). Not only were the INL and the IPL very thin, but the distinction between each retinal layer was lost. A significant difference ($P<0.05$) in the thickness of the IPL was found at regions #7 and #8. A significant reduction ($P<0.01$) in the thickness of OS, IS, the ONL and the OPL layers at all regions (Figure 4.37 & 4.38), as well as a significant decrease of the number of ONL row (Figure 4.27D & 4.28D) and rod nuclei per unit length of the retina (Figure 4.29D & 4.30D). Although a direct comparison of the thickness of the INL and the GCL+NFL suggested they were thinner, in mutant dogs the alteration in the overall mean thickness was not significant.

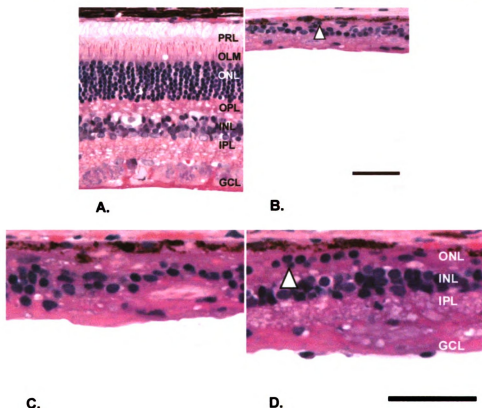


Figure 4.36. Representative photomicrographs of retinal morphology of a normal control (A) and the *PDE6A* mutant dog (B, C & D) at 100 weeks of age. Bar = 50 μ m. A) The normal control retina shows the typical canine retinal structure. B, C & D) Even though retinal thickness varies from region to region in the *PDE6A* mutant retina, the entire retinal thickness is very much reduced compared to that of the normal control. Only occasional isolated photoreceptor nuclei (arrowhead) are present (B & D). In regions of most severe retinal thinning it is difficult to differentiate the dividing retinal layers. Key: PRL = photoreceptor layer, OLM = outer limiting membrane, ONL = outer nuclear layer, OPL = outer plexiform layer, INL = inner nuclear layer, IPL = inner plexiform layer, GCL = ganglion cell layer.

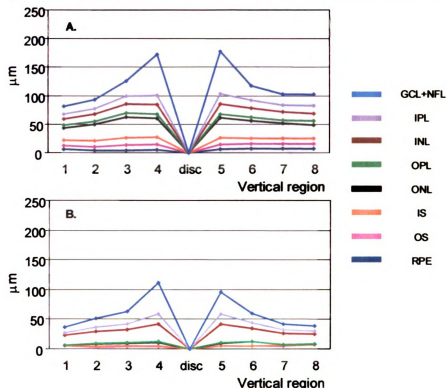


Figure 4.37. Mean retinal thickness of each of the different retinal layers from superior to inferior ora ciliaris retina (vertical section; see Figure 4.1 in materials and methods) from normal control (A) and *PDE6A* mutant dogs (B) at greater than 60 weeks of age (n=4). Note thickness of the RPE layer (obscured by the line representing the thickness of the inner and outer segments) in the *PDE6A* mutant retina is maintained (B). Photoreceptor layer of the mutant retina in contrast disappears or appears exceedingly thin. The ONL and the OPL are significantly decreased in thickness. The greatest thickness of the *PDE6A* mutant retinal layer remaining is however evident at the central retina and is due to relative preservation of thickness in the NFL and GCL. Key: RPE = retinal pigment epithelium, OS = outer segment, IS = inner segment, ONL = outer nuclear layer, OPL = outer plexiform layer, INL = inner nuclear layer, IPL = inner plexiform layer, GCL = ganglion cell layer, NFL = nerve fiber layer.

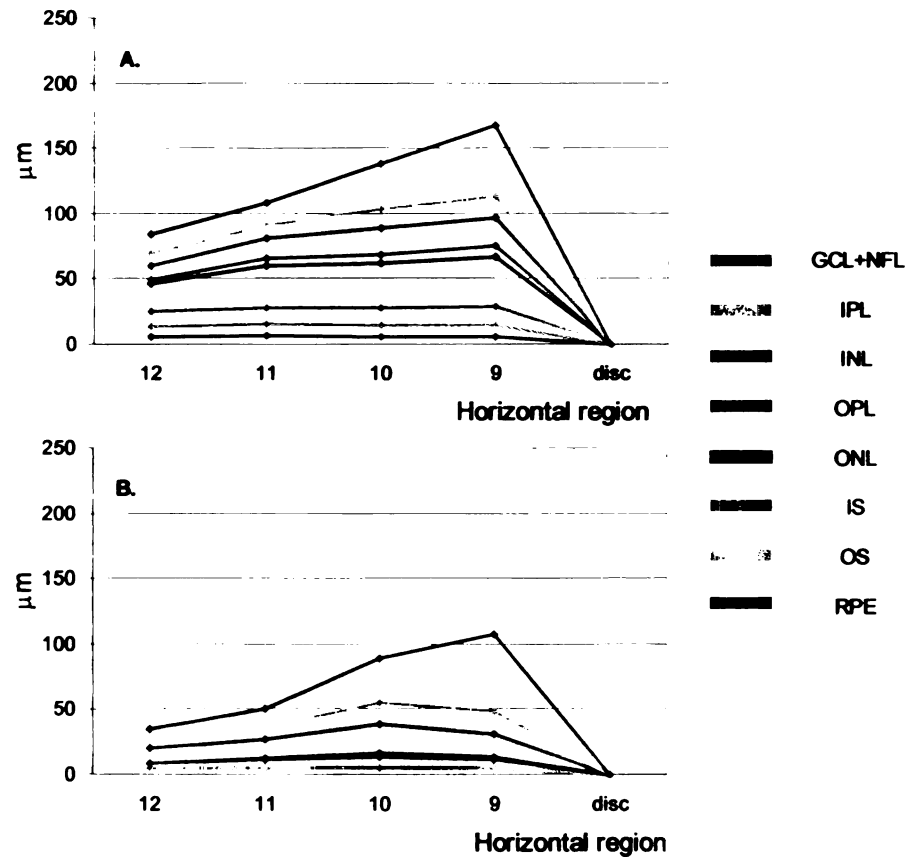


Figure 4.38. Mean retinal thickness of each of the different retinal layers from nasal to temporal region (horizontal section; see Figure 4.1 in materials and methods) from a normal control (A) and *PDE6A* mutant dogs (B) at greater than 60 weeks of age (n=4). Note that the ONL and the OPL in the retina of *PDE6A* mutant dog are severely decreased in thickness. Key: RPE = retinal pigment epithelium, OS = outer segment, IS = inner segment, ONL = outer nuclear layer, OPL = outer plexiform layer, INL = inner nuclear layer, IPL = inner plexiform layer, GCL = ganglion cell layer, NFL = nerve fiber layer.

4.3.2. Immunohistochemical analyses of paraffin-embedded and frozen sections

4.3.2.a. Immunohistochemistry using rhodopsin

Two types of antibody against rhodopsin were used in this study. Staining using antibody against bovine rhodopsin was specific to rod photoreceptors and strongly stained the outer segments and very weakly stained the inner segments of the canine retina. The use of this antibody in normal control retina demonstrated that rod outer segments elongated with age (Figure 4.39A, C & E). In contrast, growth of rhodopsin-labeled rod outer segments of the *PDE6A* mutant dog halted at about 4 weeks of age, and was followed by an apparent decrease in the number and length of immunoreactive outer segment by 5 weeks of age (Figure 4.39D). Moreover, the remaining rod outer segments in mutant dog at 5 weeks of age were disoriented compared to an age-matched normal control (Figure 4.39C). Loss of rod outer segments was very pronounced by 9 weeks of age in the *PDE6A* mutant retina, at which time only very short rhodopsin-labeled segments remained (Figure 4.39F).

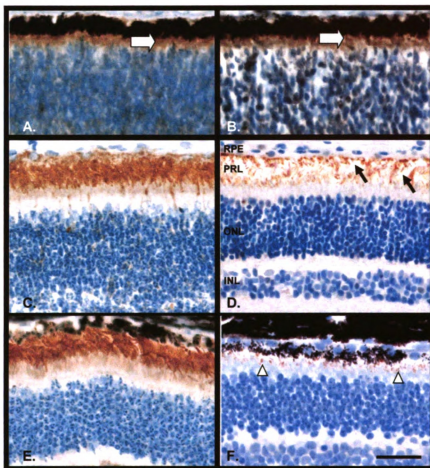


Figure 4.39. Immunohistochemical expression of anti-rhodopsin (a gift from Dr. P. Hargrave, University of Florida) in retinal sections of normal control (A, C & E) and the *PDE6A* mutant dogs (B, D & F) at 3 (A & B), 5 (C & D) and 9 (E & F) weeks of age. Bar = 25 μ m. In the control retinas rhodopsin immunoreactivity is predominantly in the rod outer segments (A, C, & E). Rhodopsin immunoreactive rod outer segments (opened arrows) are already present at 3 weeks of age in control and mutant retina (A & B). They have elongated by 5 weeks of age (C & D) even though the rhodopsin-labeled rod outer segments of the *PDE6A* mutant retina shows disorganized discs and less immunoreactive material (D). Spaces (black arrows) are present in the PRL indicating a loss of rod outer segments. By 9 weeks of age in the mutant retina only very short remaining rhodopsin immunoreactive are present (arrowheads) (F). Key: RPE = retinal pigment epithelium, PRL = photoreceptor layer, ONL = outer nuclear layer, INL = inner nuclear layer.

An antibody raised against mouse rhodopsin (Lab Vision) labeled the entire rod cell (outer segments, inner segments, perinuclear regions of rod cell bodies and rod termini at the outer regions of the OPL). Use of this antibody confirmed that there was an increase of rod segments as well as the number of ONL row with age in normal control retina (Figure 4.40A & 4.40C). Immunoreactivity of the perinuclear region of the *PDE6A* mutant rod photoreceptors was slightly reduced at 4 weeks of age but there appeared to be immunoreactivity at the level of photoreceptor termini (Figure 4.40B). By 8 weeks of age when rods had suffered a decrease in their outer segment length and a decrease in total numbers in the *PDE6A* mutant retina, there was a reduction in immunoreactivity in the rod soma as well as in the rod termini. Neurite outgrowth was observed extending from rod termini horizontally within the OPL and also vertically to the inner retina. A small number of immunoreactive cells still remained in particular at the mid periphery, in the *PDE6A* mutant retina at 60 weeks of age, with some immunoreactive cell processes within the photoreceptor cell layer (Figure 4.40E). By 210 weeks of age (Figure 4.40F), there was only 1 or 2 immunoreactive cell bodies per section remained in the *PDE6A* mutant retina that expressed rhodopsin.

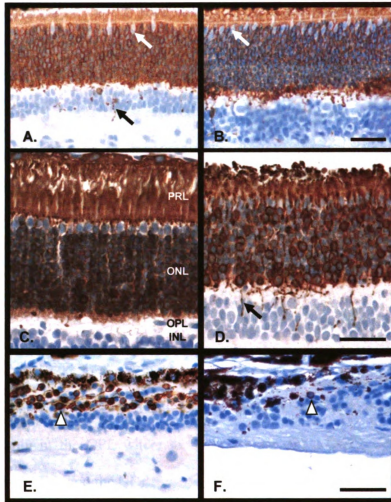


Figure 4.40. Immunohistochemical expression of anti-rhodopsin (Lab Vision) in retinal sections of normal control (A & C) and the *PDE6A* mutant dogs (B, D, E and F) at 4 (A & B), 8 (C & D), 60 (E) and 210 (F) weeks of age. Bar = 25 μ m. Note that this antibody stains the entire rods cell (outer segments, inner segments, perinuclear region of rod cell bodies and synaptic termini) in the retina of normal control (A & C) while cone nuclei (white arrows) are not rhodopsin-labeled. Compared to normal control at 8 weeks of age, not only rod outer segments of the *PDE6A* mutant are short (D), but there is a reduction of rhodopsin staining at the perinuclear region of rod cell bodies. Profound rod neurite sprouting (black arrow) extending into the inner retina is present in the OPL the mutant dog at 8 weeks of age (D). At 60 and 210 weeks of age in the mutant dog there are some remaining rhodopsin-immunoreactive cell bodies (arrowheads) even though they are very much reduced in number. Neurite sprouting in the residual ONL is still present at this age but is primarily in a horizontal direction (E). Note that RPE cells are present in the neurosensory retina (F). Key: PRL = photoreceptor layer, ONL = outer nuclear layer, OPL = outer plexiform layer, INL = inner nuclear layer.

4.3.2.b. Immunohistochemistry using cone arrestin

Immunohistochemical staining of sections using an antibody against rabbit cone arrestin in the normal canine retina resulted in labeling of the cone outer segments, cell bodies, axons and synapses at the inner regions of the OPL (Figure 4.41A). Compared to normal control retinal section, cone arrestin-immunopositive outer segments of the *PDE6A* mutant retina at 9 weeks of age were shorter and appeared swollen. The fainter staining of inner segments showed that they were considerably shorter than normal (Figure 4.41B). Additionally the expression of the antibody in the cone termini was reduced. Retinal sections from the *PDE6A* mutant dog showed that even though the retina had thinned at 210 weeks of age, a number of cones were still present in different retinal regions (Figure 4.41C & 4.41D). In addition, the sprouting of cone axonal processes was observed not only in the OPL where the cone termini are normally located, but also ectopically into the IPL and the GCL.

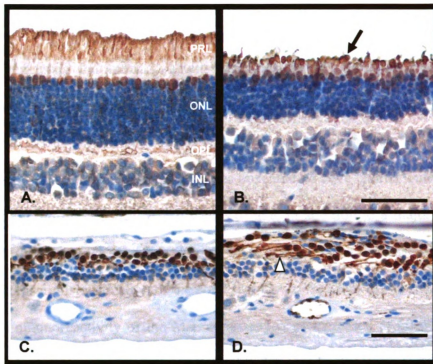


Figure 4.41. Immunohistochemical expression of anti-cone arrestin (a gift from Dr. S. Craft, University of Southern California) in retinal sections of normal control (A & C) and the *PDE6A* mutant dogs (B & D) at 9 (A & B) and 210 (C & D) weeks of age. Bar = 50 μ m. Note that cone arrestin labels outer segments, cytoplasm of the cell bodies and synapses of all cones and some cells of the INL in the normal control retina (A). Compared to retinal section of a normal control, the retina of the *PDE6A* mutant has stunted cone outer segments (black arrow) connected to short inner segments. There appear to be reduced immunoreactivity of cone arrestin at the cone synapses in the OPL compared to the normal control. A cluster of remaining cone nuclei are seen in tapetal and nontapetal retinal regions of the *PDE6A* mutant at 210 weeks of age (C & D). Sprouting of cones processes within the residual ONL is apparent at this age (arrowhead). Key: RPE = retinal pigment epithelium, PRL = photoreceptor layer, ONL = outer nuclear layer, INL = inner nuclear layer.

4.3.2.c. Immunohistochemistry using red/green opsin

Staining using the antibody against red/green rabbit opsin was predominantly restricted to the outer segments of the canine green cones (M/L cones) (Figure 4.42A) although weak labeling was present in the cell bodies, axons and synaptic termini (Figure 4.42E). In the *PDE6A* mutant retina, M/L cones appeared to have shorter outer segments compared to the normal control. At 16 weeks of age, in addition to a major loss of the number of M/L cone outer segments (Figure 4.42C), there was a decrease of the axonal length as well as a mislocalization of the cone segment in the ONL of the *PDE6A* mutant retina. The immunoreactivity of the M/L cones appeared increased at 60 weeks of age when at which age the cone axons were stunted and showed ectopic processes extending in to the IPL (Figure 4.42D).

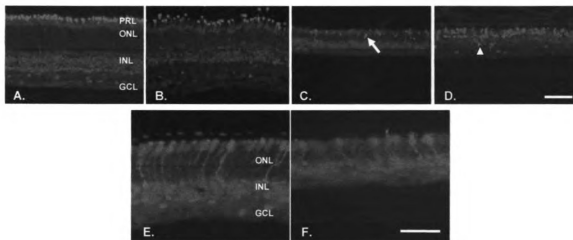


Figure 4.42. Immunohistochemical expression of anti-red/green opsin fluorescence in retinal sections of normal control (A & E) and the *PDE6A* mutant dogs (B, C, D & F) at 5 (A & E), 7 (B), 16 (C & F), and 60 (D) weeks of age. Bar = 50 μ m (A to D) and 25 (E & F) μ m. Note in normal control, red/green opsin strongly labels red/green cone outer segments (A), and weakly labels their cell bodies and axons (E). Localization of red/green opsin immunoreactivity in the *PDE6A* mutant retina at 7 weeks of age shows a decrease in length and number of cone outer segments (B). Displaced short outer segment (white arrow) is noticed in the ONL (C), an age at which cone axon has a reduced length (F). At 60 weeks of age, cone cell bodies with some residual brighter staining (arrowhead) are present (D). Key: PRL = photoreceptor layer, ONL = outer nuclear layer, INL = inner nuclear layer, GCL = ganglion cell layer.

4.3.2.d. Immunohistochemistry using PKC α

Immunoreactivity to mouse anti-PKC α antibody in normal canine retina was present in the dendrites, perinuclear region of the cell bodies, axons and synaptic termini (in the outer region of the IPL) of rod bipolar cells (Figure 4.43A, 4.43C & 4.43E). PKC α -labeled rod bipolar cells in the *PDE6A* mutant retina showed a progressive decrease in number and length with age. Some retraction of the dendritic arborization of rod bipolar cells could be seen in the *PDE6A* mutant retina at 7 weeks of age (Figure 4.43B). By 9 weeks of age, at which approximately one row of rod bipolar cell soma remained at the outer region of the ONL compared to the usual two layers. Rod bipolar cell axonal processes were significantly shorter and dendritic arborization was considerably retracted and disorganized compared to those of the bipolar cells in the retina of normal control dogs (Figure 4.43C & 4.43D). A mislocalization of rod bipolar cell to the ONL of the *PDE6A* mutant retina could be seen sporadically at 60 weeks of age (Figure 4.43F). Although the overall expression of PKC α -positive rod bipolar cell soma was less compared to an age-matched control, additional number of small axonal branches of rod bipolar cells were located throughout the IPL.

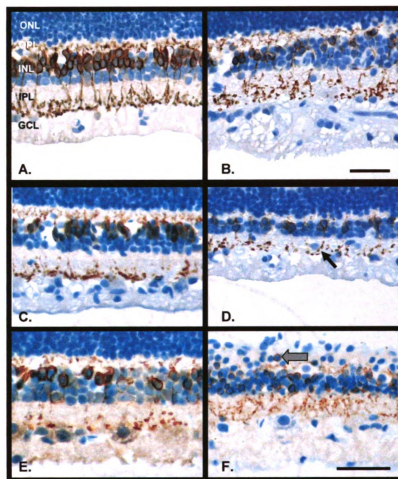


Figure 4.43. Immunohistochemical expression of anti-protein kinase C alpha (PKC α) in retinal sections of normal control (A, C & E) and the *PDE6A* mutant dogs (B, D & F) at 7 (A & B), 9 (C & D) and 60 (E & F) weeks of age. Bar = 25 μ m. Note in normal control, PKC α immunoreactivity is localized in rod bipolar cell dendrites in the OPL, perinuclear region of cell bodies in the outer region of the INL, axonal processes, and terminal branches located at the inner region of the IPL (A, C & E). Compared to the retina of a normal control, there appears to be a decrease in number of PKC α positive soma in the *PDE6A* mutant retina at 7 weeks of age (B). By 9 weeks of age there is a marked loss of PKC α immunoreactive cell dendrites, as well as cell bodies in the INL (D). The thickness of the IPL is reduced and the number of axonal processes (black arrow) is also reduced. By 60 weeks of age, a reduction of immunoreactive labeling of rod bipolar cell nuclei is noticed in the *PDE6A* mutant retina (F), and a displaced rod bipolar cell is found in the ONL (solid arrow) (F). At this age, there is a ramification of cell processes in the OPL and the IPL. Key: ONL = outer nuclear layer, OPL = outer plexiform layer, INL = inner nuclear layer, IPL = inner plexiform layer, GCL = ganglion cell layer.

4.3.2.e. Immunohistochemistry using calbindin

The mouse anti-calbindin antibody stained canine horizontal cell soma and axons positioned at the outer border of the INL. The retina of the *PDE6A* mutant dog had a similar pattern of calbindin immunoreactivity to the normal control at 10 weeks of age (Figure 4.44A & 4.44B). However, a hypertrophy of horizontal cell soma could be seen in the *PDE6A* mutant retina by 60 weeks of age (Figure 4.44D).

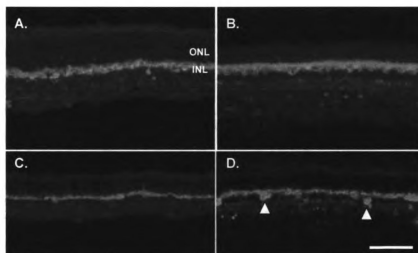


Figure 4.44. Immunohistochemical expression of anti-calbindin fluorescence in retinal sections of normal control (A & C) and the *PDE6A* mutant dogs (B & D) at 10 (A & B) and 60 (B & D) weeks of age. Bar = 50 μ m. Note that at 10 weeks of age the retina of mutant dog exhibits normal morphology of horizontal cells (A & B). Anti-calbindin immunoreactive horizontal cells from the *PDE6A* mutant retina at 60 weeks of age (D) are well preserved and appear to be hypertrophic (arrowheads) compared to the control. Key: ONL = outer nuclear layer, INL = inner nuclear layer.

4.3.2.f. Immunohistochemistry using Hu C/D

Hu C/D immunoreactivity was present in cell bodies located in the outer region of the INL (amacrine cells) and in the GCL (ganglion cells). No difference was observed between the normal control and the *PDE6A* mutant retina at 7 weeks of age in the number of Hu-immunoreactive cells per unit length of the retina and the degree of immunoreactivity (Figure 4.45A & 4.45B). A decrease in the number of Hu-immunoreactive cells and the size of their soma was apparent in the *PDE6A* mutant retina at 60 weeks of age (Figure 4.45C) by which age there was retinal thinning.

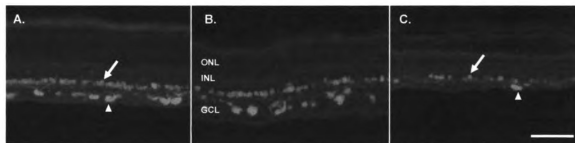


Figure 4.45. Immunohistochemical expression of anti-Hu C/D fluorescence in retinal sections of normal control (A) and the *PDE6A* mutant dogs (B & C) at 5 (A), 7 (B) and 60 (C) weeks of age. Bar = 50 μ m. Note the presence of Hu staining of the cell bodies of ganglion cells (arrowheads) and amacrine cells (white arrows). No difference is detected between the normal control and the *PDE6A* mutant retina at 7 weeks of age. However, in the *PDE6A* mutant retina the number of cell bodies immunopositive for Hu per unit length of retina has declined by 60 weeks of age (C). Key: ONL = outer nuclear layer, INL = inner nuclear layer, GCL = ganglion cell layer.

4.3.2.g. Immunohistochemistry using calretinin

Immunohistochemistry of retinal sections using an antibody against calretinin showed calretinin immunoreactivity in horizontal cell soma and axons, amacrine and ganglion cell soma and processes in the IPL and GCL. No difference in calretinin immunoreactivity between normal control and the *PDE6A* mutant retina could be detected at 5 weeks of age (Figure 4.46A & 4.46B). In the *PDE6A* mutant retina at 10 weeks of age, calretinin immunoreactivity was reduced in the outer border of the INL where horizontal cells were located. By 60 weeks of age there appeared to be increased immunoreactivity in horizontal cells. A decrease of calretinin labeling was noticed in the IPL (Figure 4.46F) of the *PDE6A* mutant retina compared to normal control at this age.

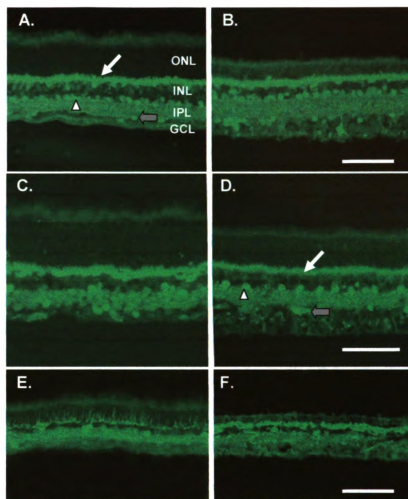


Figure 4.46. Immunohistochemical expression of anti-calretinin fluorescence in retinal sections of normal control (A, C & E) and the *PDE6A* mutant dogs (B, D & F) at 5 (A & B), 10 (C & D) and 60 (E & F) weeks of age. Bar = 50 μ m. Note that immunoreactivity of calretinin is present in cell bodies of amacrine cells (arrowheads) and ganglion cells (solid arrows), as well as in horizontal cell processes (white arrows) and other processes located in the IPL, the GCL and the NFL (A & D). The retina of the 5 and 10 week old *PDE6A* mutants shows a similar calretinin staining pattern to that of normal controls (A, B, C & D). At 60 weeks of age there appear to be slightly increased calretinin staining in horizontal cell processes in the *PDE6A* mutant dog (F) however, the overall staining pattern appears similar between mutant and control. Key: ONL = outer nuclear layer, INL = inner nuclear layer, IPL = inner plexiform layer, GCL = ganglion cell layer.

4.3.2.h. Immunohistochemistry using GFAP

Immunoreactivity to GFAP was present in the inner region of the OPL, the IPL and the NFL of normal canine retina. There was a weak GFAP labeling in the NFL at 3 weeks of age, but more intense labeling in sections from older normal dog (Figure 4.47C & 4.47E). The GFAP labeling was similar between normal control and the *PDE6A* mutant retina at 3 weeks of age. However, GFAP staining of the *PDE6A* mutant retina at 5 weeks of age was increased. The entire Müller cell was labeled extending vertically from the OLM to the ILM of the retina (Figure 4.47D). Increased GFAP immunoreactivity was present in the *PDE6A* mutant retina at 60 weeks of age, at which GFAP-positive glial tissue occupied almost the entire remaining retina (Figure 4.47F).

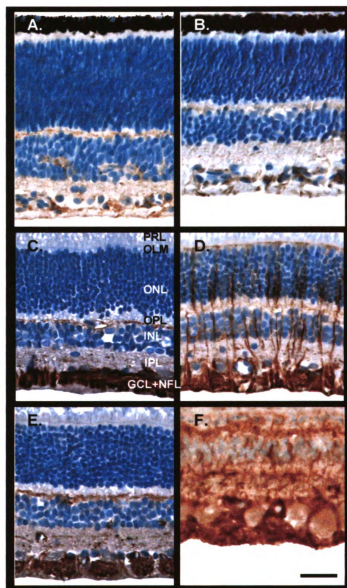


Figure 4.47. Immunohistochemical expression of anti-GFAP in retinal sections of normal control (A, C & E) and the *PDE6A* mutant dogs (B, D, & F) at 3 (A & B), 5 (C & D) and 60 (E & F) weeks of age. Bar = 25 μ m. Note that GFAP labeling is present in the normal control retina in the inner region of the OPL, the IPL and the NFL (astrocyte processes) (A, C & E). The entire Müller cells stretching from the OLM to the NFL is stained for GFAP in the *PDE6A* mutant retina by 5 weeks of age (D) indicating increased GFAP levels in Müller cells. GFAP-positive glial tissue occupies almost the entire of the remaining retina of the *PDE6A* mutant at 60 weeks of age (F). Key: PRL = photoreceptor layer, OLM = outer limiting membrane, ONL = outer nuclear layer, OPL = outer plexiform layer, INL = inner nuclear layer, IPL = inner plexiform layer, GCL = ganglion cell layer, NFL = nerve fiber layer.

4.4. Discussion

The normal canine retina is immature at birth. Retinal differentiation, morphogenesis and maturation occur over the first 7 to 8 weeks of life. The results of this study including detailed morphological examination, ultrastructural and immunohistochemical analysis revealed early postnatal abnormalities and failure of maturation of photoreceptors, in particular rods, of the *PDE6A* mutant dogs. In the mutant dogs there was a failure of normal development of rod outer segments. Soon after the outer segments of the mutant dogs started to form their development was halted and they failed to elongate. The outer segment discs that did form were disorganized. This was followed by a rapid decrease in the number of rod cells. Plotting the number of rod nuclei per unit length against age gives an indication of the kinetics of rod cell loss. There appears to be an initial stage where few cells are lost. This period is during the time when there is initial development of rod outer segments. There is then a rapid loss of cells between 4 to 6 weeks of age after which the rate of cell loss plateaus and there is a proportionally slower rate of loss of the residual cells. It is interesting to note that there is a lag between the loss of rod nuclei and the narrowing of the outer nuclear layer. This can be explained by the fact that during the period of rapid cell loss the normally tight packing of photoreceptor nuclei in the ONL is lost and spaces appear between the nuclei. In the later stages of the disease the remaining nuclei in the outer nuclear layer are more closely packed again so that the nuclei density more closely resembles that of the normal control sections. The kinetics of cell loss characterized by an initial period of rapid loss cell death followed by a period of more gradual cell loss has been described for several retinal degeneration and neuronal cell loss situations (Clarke et al., 2000). A so called

'one-hit model' has been developed to explain this kinetics. The model proposes that there is a constant risk of death of each neuron, that death occurs randomly and that it is independent of other neurons. The proponent of this theory went on to suggest that the one-hit model is modified by local microenvironment effects (Clarke & Lumsden, 2005) thus accounting for regional variations in the rate of cell loss.

Light and electron morphological examinations of retinas of 3 to 4 week old puppies revealed the presence of many apoptotic nuclei in the ONL of *PDE6A* mutant retinas, compared to normal controls. Apoptosis occurs as part of the normal development of the nervous system (Cellerino et al., 2000) including the maturing retina (Biehlmaier et al., 2001). Apoptosis has also been shown to be the process by which cells die in inherited retina dystrophies (Lolley, 1994). For example, a dramatic increase in cell death in the outer nuclear layer occurs in *rd1* mice occurs during the third week of postnatal life (Porteracailliau et al., 1994). Apoptotic cell death has also been described in the *RCS* rat model (Tso et al., 1994). Apoptosis is also responsible for retinal cell death in environmentally induced diseases such as light-damage (Hao et al., 2002).

The TUNEL staining technique was used to verify that cell death was occurring by apoptosis in the *PDE6A* mutant. The TUNEL technique detects internucleosomal DNA fragmentation in apoptotic cells. Significant TUNEL staining was present in the early stages of retinal degeneration at 3 to 4 weeks of age but at later stages (5 and 9 weeks of age) there were not significant numbers of TUNEL-positive cells in the ONL. This shows that death of a large number of photoreceptors occurs early in the disease

process and after the initial period there is a much more gradual cell loss and indeed at these later ages less nuclei with morphological changes suggestive of apoptosis were apparent in the ONL.

Caspase 3 immunohistochemistry was performed to further characterize cell death in the *PDE6A* mutant retina. There was an apparent lack of immunoreactivity to the anti-caspase 3 antibody. This finding is similar to studies of the *rcd1* mouse where apoptosis was shown to occur by a caspase-independent pathway (Doonan et al., 2003; Zeiss et al., 2004). In another inherited retinal degeneration model the *RCS* rat immunohistochemistry showed that caspases 1 and 2 were activated suggesting that apoptosis in this model was via a caspase-dependent pathway, although immunohistochemistry for caspase 3 was not (Katai et al., 1999b). Additional investigation of the mechanism of apoptosis in the *PDE6A* mutant dogs would facilitate an understanding of disease mechanism and perhaps suggested possible therapeutic intervention.

Cone photoreceptors are also affected in the *PDE6A* mutant dog retina. Ultrastructural examination suggests that cone outer segments are also stunted and lost rapidly and cone inner segments become enlarged and club-shaped early in the disease process. Immunohistochemistry using cone arrestin and red/green cone opsin antibodies suggested that by 7 weeks of age there were abnormalities in cone photoreceptors. The mean number of cone nuclei per unit length of the retina however seemed maintained until 16 weeks of age despite the fact that the mean number of rod nuclei had dramatically decreased. Retinal degeneration in the *PDE6A* mutant dogs is expressed

across the retina and progressed with increasing age. Loss of photoreceptors was more severe in the central retina with a slower loss at the periphery, and it proceeded more rapidly in the superior quadrants than the inferior quadrants. As the retina matures centrally first it is perhaps not surprising that the central retina would be affected earlier than the peripheral retina. The difference between superior and inferior retina could be accounted for by the presence of the tapetum in the superior fundus. This structure reflects light back through the photoreceptors and thus may result in a greater risk of light induced damage and also the formation of greater number of free radicals within the tapetal retina meaning that apoptosis is more readily triggered in this region. Immunohistochemistry using cone arrestin antibody to label cones showed that clusters of cone nuclei remained in the inferior hemisphere of the *PDE6A* mutant retina at 210 weeks of age. The quadrant-specific disease progression in the *PDE6A* mutant dogs is similar to that reported in the *prcd* dogs (Aguirre & Acland, 1988) but dissimilar to that of the *rd1* mouse, in which the longest cone survival was in the mid-peripheral superior region (Ogilvie et al., 1997) and the inferior quadrants where s-cones are exclusively located was more severely affected (Jimenez et al., 1996). Further investigations in the *PDE6A* dogs to see if there is a differential rate of loss of blue cones compared to green cones could be considered. The loss of cone photoreceptors that themselves are genetically normal, the *PDE6A* gene being rod specific, is in keeping with the findings in other retinal degeneration models. Recent work has shown the presence of a rod derived cone trophic factor (Sahel et al., 2001). This is released from rods and is a survival factor for cones that is necessary to maintain cones in species like dog and human that has a rod dominated retina. The loss of rods results in a reduction of this rod derived factor and

leads to a secondary loss of cones. It is tempting to also speculate that the rapid loss of large numbers of rod cells would alter the environment around the cones meaning that it was not conducive to their survival.

Increased Müller cell immunoreactivity to GFAP developed at an early stage of retinal degeneration in the *PDE6A* mutant dog retina. This indicates glial cell activity and has been described as a feature of several other forms of retinal dystrophy including the *rd* chicken (Semplerowland, 1991), *rge* chicken (Inglehearn et al., 2003), *rd1* mouse (Frasson et al., 1999), *RCS* rat (Kimura et al., 2000) and RP patients (Rodrigues et al., 1986). The role of Müller cells in neuroprotection and regeneration after retinal damage has been studied. Not only do they express neurotropic factors, but they also express antioxidant agents that could have an important role in preventing excitotoxic damage to retinal neurons (Garcia & Vecino, 2003).

The initial stages of retinal degeneration in the *PDE6A* mutant dog involved thinning of outer retinal layers with relative preservation of the thickness of the inner retinal layers. It was not until the outer retina was very thinned that significant decreases in the inner retinal layers started to become apparent. Despite this apparent initial lack of effect on the inner retina the immunohistochemical studies using antibodies to various retinal neurons revealed that quite profound effects on some inner retinal cells occurred relatively early in the disease process. Perhaps not surprising, given their synaptic connections with rod photoreceptors, the PKC α immunoreactive rod bipolar cells were affected early in the process of retinal degeneration. The EM study showed that there was

a decrease in the number of synaptic ribbons in the rod photoreceptor termini in the outer plexiform layer of the *PDE6A* mutant retina suggesting the presence of abnormalities in the synaptic connections between rods and rod bipolar cells and horizontal cells. In the *rd1* mouse there is a failure of normal synaptogenesis between rods and rod bipolar cells (Strettoi & Pignatelli, 2000). There was an early loss of the normal bi-layer arrangement of rod bipolar cell nuclei and a reduction in the branching of the bipolar cell axonal processes. However later in the disease process, the surviving PKC α immunoreactive cells appeared to develop larger numbers of axonal processes. Horizontal cells also synapse with rod photoreceptor termini and yet there was no apparent alteration in calbindin immunoreactivity until later in the disease process indicating that the horizontal cells were better preserved than rod bipolar cells. Alterations in the rod bipolar cells were also observed in the *rd1* mouse. Following degeneration of rods, the metabotropic glutamate receptors were displaced from rod bipolar cell dendrites toward their soma and axons (Strettoi & Pignatelli, 2000) and in vitro studies showed that the abnormal rod bipolar cells from the *rd1* mouse retina do not respond to glutamate (the neurotransmitter at the rod synaptic space) while they increase their sensitivity to GABA (the horizontal cell neurotransmitter) (Varela et al., 2003).

Later in the disease process sprouting of dendrites from several types of surviving retinal neurons was apparent. The surviving rod cells had developed axons that extended beyond their normal site of termination in the outer plexiform layer, into the inner retina. Surviving cone photoreceptors reacted in a similar manner. Interestingly the initial



direction of axonal growth was from outer to inner retina but in the very degenerate retina axons tended to ramify in a horizontal direction.

Overgrowth (sprouting) of rhodopsin immunoreactive rod axonal processes seen in the *PDE6A* mutant dogs was similar to that described in other retinal dystrophies such as the *rdy* cat (Chong et al., 1999) and the *rd1* mouse (Zeiss & Johnson, 2004). Rod sprouting was noted in the retina of RP patients with significant photoreceptor loss, where rod neurite overgrowth was found to project into the inner retina to contact the somata of GABA-positive amacrine cells (Fariss et al., 2000) and also found to associate with the surfaces of the hypertrophic Müller cell processes (Li et al., 1995). Zeiss and Johnson (2004) suggested that rod neurite overgrowth may be influenced by changes in the neighboring reactive Müller cells. There is also a possibility that the small number of rhodopsin staining neurons that can be detected in the very degenerate retinas of older *PDE6A* mutant dogs may be transformed Müller cells. Studies have shown that in response to neurotoxin-induced damage in rat retina Müller glia can differentiate to express markers for rod photoreceptors and bipolar cells (Ooto et al., 2004). A similar response was described in the *rd1* mouse where Müller cells were found to be able to differentiate into progenitor cells that then give rise to different neuronal cell types (Zeiss & Johnson, 2004).

Horizontal cells stained by calbindin appeared relatively unchanged in the early stages of the degeneration, but in the later stages they appear hypertrophic. Hypertrophy of horizontal cells following photoreceptor degeneration has been described in *rd1* mice

(Strettoi & Pignatelli, 2000). It is suggested that it may relate to an increase of GABA sensitivity found in the remaining rod bipolar cells (Varela et al., 2003) or GABAergic amacrine cells (Lee et al., 2004).

Changes in amacrine and ganglion cells were not marked in the disease process in the *PDE6A* mutant dog retina. There was possibly a reduction in ganglion cell number later in the disease process that could be detected on regular stained sections and calretinin stained sections. Counting of ganglion cells on retinal flat mounts would be preferable to quantify changes in ganglion cell numbers.

Chapter 5

Investigation of the tissue expression of the PDE6A gene

5.1. Introduction

Photoreceptor proteins function together in modulating the phototransduction cascade in the retina. Not only are they functional in the retina, but some are expressed in other tissues such as pineal gland. The pineal gland in lower vertebrates is directly responsive to light stimulation. It expresses some genes that are involved in phototransduction (Zatz et al., 1988). For example, guanylate cyclase activating protein (GCAP) and guanylate cyclase (GC) genes are expressed in normal and *rd* chicken pineal (Semple-Rowland et al., 1999), Chicken pineal transducin alpha-subunit, which is identical to the one in retina, was found to mediate the phototransduction pathway in chicken pinealocytes (Kasahara et al., 2000). Other genes reported to be expressed in pineal gland include both rod and cone forms of the beta cGMP PDE (Morin et al., 2001), the cyclic nucleotide-gated channel (Bonigk et al., 1996) and rhodopsin kinase (Zhao et al., 1999).

In addition to pineal gland, some photoreceptor genes are expressed in other tissues in higher vertebrates as well, for example PDE6B is expressed in human brain (Collins et al., 1992) and in pigeon brain (Wada et al., 2000), recoverin in pinealocytes of

rat, sheep, and human (Korf et al., 1992; Ruiz-Avila et al., 1995b), the transducin alpha-subunit in vertebrate taste receptor cells (Ruiz-Avila et al., 1995a) and scanning of EST databases showed PDE6A in other human tissues such as colon (www.genome.ucsc.edu). Sequencing online database EST shows PDE6A expression in colon.

In view of the fact that rod phototransduction genes are expressed in other tissues in other species, we investigated the tissue expression of the dog PDE6A gene.

5.2. Materials and Methods

5.2.1. Tissue collection

Prior to euthanasia, animals were examined for any evidence of ophthalmic disease. Euthanasia was performed using an overdose of pentobarbital sodium (Fatal-Plus; Vortech pharmaceuticals, Dearborn, MI) intravenously. Immediately following sacrifice, the tissues listed below were collected, snap frozen in liquid nitrogen, and stored at -80°C until processed.

From *PDE6A* normal control dogs:-

Ocular tissues: cornea, iris, lens, retina, RPE/choroid.

Abdominal organs: spleen, liver, pancreas, kidney, small intestine, stomach wall, urinary bladder, uterus, and ovary.

Thoracic organs: heart, lung, and diaphragm.

Central nervous system tissues: pituitary gland, pineal gland, cerebrum, cerebellum, spinal cord, optic chiasm, and visual cortex.

Miscellaneous tissues: striated muscle, buccal membrane, tongue epithelium, and blood.

In view of the preliminary results in normal dogs, the following tissues were collected from *PDE6A* mutant dogs:-

Ocular tissues: retina

Abdominal organs: kidney, small intestine

Note: Blood was collected into a tube containing sodium citate and placed on ice only when separation of white blood cells from red blood cell was to be performed immediately. Lysis of red blood cells was performed by incubating with red blood cell lysis buffer, pH 8.0 (see Appendix) for 30 minutes on ice before centrifugation at maximum speed (14,000 rpm) for 15 minutes at 4°C to pellet white blood cell nuclei. Supernatant was discarded and the lysis incubation was repeated for 10 minutes, followed by 10 minutes of centrifugation. Supernatant was discarded and the pellet was stored at -80°C until processed.

5.2.2. Isolation of total RNA

5.2.2.a. Preparation of instruments and RNA handling

Mortar, pestle, metallic instruments and glassware were cleaned with a detergent, thoroughly rinsed, soaked with RNaseZapTM (Sigma-Aldrich Co., St Louis, MO) mixed with diethyl pyrocarbonate-treated water (DEPC-treated water; see Appendix), air-dried, wrapped with aluminum foil and then baked at 180°C overnight prior to use.

Proper microbiological, aseptic techniques were always used. RNA was prepared using sterile RNase-free instruments and DEPC-treated water. Sterile barrier pipette tips were used to avoid aerosol contamination.

5.2.2.b. Isolation of total RNA using RNeasy Mini Kit (Qiagen Inc., Valencia, CA)

A tissue sample (20-30mg) was ground in liquid nitrogen (with a mortar and pestle) to a fine powder.

RNA isolation with DNaseI digestion was performed in all tissues (see section 1. in Appendix) by using RNeasy Mini protocol for isolation of total RNA from animal tissues (3rd Edition RNeasy Mini handbook, 2001, Qiagen Inc., Valencia, CA). Proteinase K (20mg/ml) was added in the isolation process when total RNA was isolated from heart, striated muscle, urinary bladder, buccal membrane, lens, and white blood cells to improve the extraction rate.

5.2.2.c. Visualization of total RNA for integrity using a formaldehyde gel

5.2.2.c.(i). Preparation of materials

Details of stock solutions are given in Appendix.

5.2.2.c.(ii). Formaldehyde (FA) gel electrophoresis

Details of formaldehyde gel preparation are given in Appendix.

RNA samples were mixed 4:1 with 5X RNA loading buffer, incubated for 3-5 minutes at 65°C, chilled on ice, and loaded onto the equilibrated FA gel. An aliquot of RNA size marker (0.2-10 kb, Sigma-Aldrich Co., St Louis, MO) was incubated at 65°C for 5 minutes then chilled on ice. FA gel was run at 7volt/cm in 1x FA gel running buffer for 1.5 hours.

5.2.2.c.(iii). Analysis of total RNA by FA gel electrophoresis

Following electrophoresis, the FA gel was soaked in ethidium bromide solution (5µg/ml) for no longer than 15 minutes, and then washed in DEPC-treated water to destain ethidium bromide for up to 2 hours. The FA gel was viewed by UV light and the integrity of RNA was assessed by examination of the two bands corresponding to 28S and 18S ribosomal RNAs (sharp bands of ~1.5kb and ~700bp size, respectively), looking

for evidence of RNA degradation (a smear of smaller sized RNA) and genomic DNA contamination (a band larger than 1.5kb). The upper band of 28S ribosomal RNA was expected to be twice as bright as the lower band of 18S ribosomal RNA.

5.2.3. Spectrophotometry of RNA

Two aliquots of each total RNA mixed with DEPC-treated water at a concentration of 1:100 were prepared on ice, and then transferred to a 96-well microplate. Spectrophotometry was performed using a microplate scanning spectrophotometer (PowerWave_xTM; Bio-Tek Instruments Inc, Winooski, VT). Mean of the optical density (OD) of the RNA solution compared with balanced well containing DEPC-treated water as a blank at wavelengths 260 and 280nm was calculated. The ratio OD_{260}/OD_{280} gives an estimate of the RNA purity. Pure RNA solution should have a ratio of 1.9 to 2.1. Contamination with protein results in lower ratios. The concentration of RNA was calculated by multiplying the absorbance at 260 nm (A_{260}) by 40 to give the RNA concentration in $\mu\text{g/ml}$.

5.2.4. Reverse Transcription-Polymerase Chain Reaction (RT-PCR)

5.2.4.a. Synthesis of cDNA

Full-length first strand cDNA was made from total RNA using a first strand cDNA synthesis kit (Fermentas Inc., Hanover, MD) following the manufacturer's

instructions. Approximately 2µg of total RNA was used as a template and mixed with 0.5µg oligo(dT)₁₈ primer, 1X reaction buffer, 20U RiboLock™ Ribonuclease inhibitor, 0.4 mM dNTP mix, and 40U M-MuLV reverse transcriptase. The mixture was incubated at 37°C for 60 minutes, followed by 70°C for 10 minutes to denature the enzyme.

5.2.4.b. Polymerase Chain Reaction (PCR) for PDE6A gene expression

CDNAs of all tissue types were used as templates for PCR with gene-specific primers for PDE6A (listed below). PDE6A-specific primers were designed (Integrated DNA Technologies Inc., Coralville, IA) to amplify portions of the PDE6A gene spanning a known intron to distinguish amplicons that were from cDNA rather than genomic DNA.

Figure 5.2 shows the primer pairs used on a map of the PDE6A cDNA. All primers were designed and ordered from Integrated DNA Technologies Inc (Coralville, IA).

Forward primers:

SPJ220 = GGG GCG GCC GCC AGG CCA GCT TTA GGC TCT

7048 = AAT GGC ATC GCA GAG CTA GC

7050 = CCT CAC TGA GTA CCA GAC CA

7057 = ATG TGT GGC CAG TCC TGA TG

7064 = TGG ATG AGT CTG GAT GGA TGA

7070 = AGA GCT GCC AGA AGC AGA GA

PDEA1 = AGA CAC CAC TTG GAG TTC GG

6836 = TCC CAT GCT GGA TGG GAT CA

Reverse primers:

7049 = TGT CCA CAA GGA TGC TGT CC

7056 = TAT TCT GGT CCC AGG ACT CC

7065 = GAT GAA ATG GAT GAG ACC CT

7071 = CCG AAC TGG AGC TGG TGA AA

PDEA2 = AAC CTC AAT CGC AGG CAG CA

6835 = GCT CGC CGA TGA GTA CGA CA

SPJ442 = GGG GCG GCC GCG GTG GTA CCA TTC GGT GCA G

The 50 μ l reaction PCR mixture consisted of: 1X PCR buffer, 1X bovine serum albumin (BSA), 0.2mM dNTPs, 1.5mM MgCl₂, 0.4 μ M of each forward and reverse primer, and 1.25U of *Taq* DNA polymerase (Invitrogen Corporation, Carlsbad, CA). The standard PCR protocol consisted of an initial denaturing step at 94°C for 3 minutes, followed by 29 rounds of denaturing at 94°C for 30 seconds, annealing at 52°C for 30 seconds and extension at 72°C for 1 minute, and then a final extension at 72°C for 3 minutes. A PCR reaction containing retinal cDNA was included as a positive control, because PDE6A is known to be expressed in the retina, whereas a PCR reaction without cDNA template served as a negative control. A PCR reaction with primers for β -actin gene (a forward primer: 5'- ATG GAT GAC GAT ATC GCT GCG CTT- 3' and a reverse primer: 5'- AGA GGC ATA CAG GGA CAG CAC A -3') was also performed as

a positive control. The PCR reaction mixture and protocol using with β -actin primers were the same as previously described except the annealing temperature was 55°C. A negative control for the entire RT-PCR was included, in which reverse transcriptase was not added. The PCR products were visualized by agarose gel electrophoresis (see Appendix).

5.2.5. Sequencing of PCR products

5.2.5.a. DNA preparation. When a single strong band was visualized on the agarose check gel, the PCR product was purified as followed: to the product 1/10 volume of 3M sodium acetate and 7/10 volume of 100% isopropanol were added, mixed well and the mixture incubated at room temperature. The DNA pellet was precipitated by centrifugation at 20,800 g for 10 minutes and the supernatant was removed. The pellet was air-dried for 10 minutes and re-suspended in molecular-grade water. When two or more products were present, they were separated by appropriate agarose gel electrophoresis and the separated bands were cut out of the gel. A QIAquick Gel Extraction kit, (Qiagen Inc., Valencia, CA) was used to extract DNA from the gel slice (see Appendix for detail of gel extraction).

5.2.5.b. DNA sequencing. The purified PCR product was submitted to the Genomics Technology Support Facility, MSU for sequencing using the gene-specific primers. Sequences were determined on an ABI PRISM® 3100 genetic analyzer (Applied Biosystems, Foster city, CA).

5.2.6. Rapid Amplification of cDNA Ends (RACE) to determine full-length sequence of kidney transcript

This is a method to obtain full-length 5' and 3' ends of cDNA sequence. The GeneRacer™ Kit (Invitrogen Corporation, Carlsbad, CA) was used. Kidney total RNA was used as a template. At least one gene-specific primer (GSP) was designed for 5' and for 3' RACE. Hela total RNA provided in the kit was used as a positive control for all reactions. This protocol is designed to only make cDNA from full-length processed mRNA, not other RNAs or partially spliced mRNAs.

5.2.6.a. Dephosphorylation of RNA

This step was to treat total RNA with Calf Intestinal Phosphatase (CIP) to dephosphorylate the 5' end of non-mRNA or truncated mRNA, which prevents ligation with the oligo dT primer. Mature full-length mRNA is not dephosphorylated due to the presence of the 5' cap. 1.2µg of total RNA (7µl), 1X CIP buffer, 40U RNaseOut™, and 10U CIP were added for a final volume of 10µl reaction. The mixture was incubated at 50°C for 1 hour, and the RNA was purified by a phenol/chloroform extraction (see Appendix).

5.2.6.b. Removal of the mRNA cap structure

This step removes the 5' cap structure from full-length mRNA using Tobacco Acid Pyrophosphatase (TAP). For a final volume of 10µl, 7µl of dephosphorylated RNA (see 5.2.6.a), 1X TAP buffer, 40U RNaseOut™, and 0.5U TAP were added and mixed. The mixture was incubated at 37°C for 1 hour, and then the RNA was purified by a phenol/chloroform extraction (see Appendix).

5.2.6.c. Ligation of the RNA oligo to de-capped mRNA

This step ligates an oligo dT primer to the 5' end of the mRNA using RNA ligase. Dephosphorylated, de-capped RNA (see 5.2.6.b) was added to a microcentrifuge tube containing lyophilized GeneRacer™ RNA oligo primer (0.25µg). The mixed reaction was incubated at 65°C for 5 minutes to relax the RNA secondary structure. 1X ligase buffer, 1.0 mM ATP, 40U RNaseOut™, and 5U T4 RNA ligase were added for a final volume of 10µl and mixed. The reaction mixture was incubated at 37°C for 1 hour, and the RNA was purified by a phenol/chloroform extraction (see Appendix).

5.2.6.d. Reverse transcription of mRNA

Full-length mRNA with a 5' poly T-linker was reverse-transcribed into cDNA using SuperScript™ III RT Reaction (Invitrogen Corporation, Carlsbad, CA). To the 10µl of ligated RNA (see 5.2.6.c), 0.15µg of GeneRacer™ RNA oligo primer, 1µl of dNTP mix, and 1µl of sterile, distilled water were added, the mixture was then incubated at 65°C for 5 minutes, chilled on ice for 1 minute. 1X First Strand buffer, 5mM DTT,

40U RNaseOut™, and 200U SuperScript™ III RT (reverse transcriptase) were added to the mixture for a final volume of 20µl. The mixture was incubated at 50°C for 1 hour, followed by 70°C for 15 minutes and then chilled on ice for 2 minutes. 2U RNaseH was then added to the mixture, which was incubated at 37°C for 20 minutes.

5.2.6.e. Amplification of cDNA ends

PCR was used to amplify the cDNA ends.

For 5' end amplification, cDNA made from 5.2.6.d. was used for the first PCR reaction. The PCR mixtures contained: 1X high fidelity PCR buffer, 0.2mM dNTP solution, 2mM MgSO₄, 0.12µM of 5'RACE forward primer, 2.5µM of a PDE6A-specific primer #7071 (CCG AAC TGG AGC TGG TGA AA), 2.5U Platinum® *Taq* DNA polymerase (Invitrogen Corporation, Carlsbad, CA) and sterile water were added to make a 50µl final volume reaction. The PCR protocol consisted of an initial denaturing step at 94°C for 2 minutes, followed by 25 cycles of denaturing at 94°C for 30 seconds, annealing at 55°C for 30 seconds and extension at 68°C for 2 minutes, and then a final extension at 68°C for 10 minutes. Nested PCR was performed afterward using 2 µl of the previous RT-PCR product as a template. The PCR reaction mixture contained the same ingredients as previously used except for primers; 0.12µM of the 5' nested forward primer and 2.5µM of a PDE6A-specific reverse primer #7065 (CCG AAC TGG AGC TGG TGA AA). The PCR protocol was the same as previously described except for the

annealing temperature, which was 65°C. The PCR products were visualized by agarose gel electrophoresis (see Appendix).

For 3' end amplification, a modified touchdown PCR was used, PCR reaction mixtures contained: 1X high fidelity PCR buffer, 0.2mM dNTP solution, 2mM MgSO₄, 2.5μM of a PDE6A-specific forward primer #6836 (TCC CAT GCT GGA TGG GAT CA), 0.12μM of the 3'RACE reverse primer (GCT GTC AAC GAT ACG CTA CGT AAC G), 2.5U Platinum® *Taq* DNA polymerase (Invitrogen Corporation, Carlsbad, CA), and sterile water were added to make a 50μl final volume reaction. Modified touchdown PCR conditions consisted of an initial denaturing step at 94°C for 2 minutes, 5 cycles of denaturing at 94°C for 30 seconds, annealing and extension at 72°C for 2 minutes, 5 cycles of denaturing at 94°C for 30 seconds, annealing and extension at 70°C for 2 minutes, 20 cycles of denaturing at 94°C for 30 seconds, annealing at 65°C for 2 minutes and extension at 68°C for 2 minute, and then a final extension at 68°C for 10 minutes. The PCR products were visualized by agarose gel electrophoresis (see Appendix).

PCR products for cloning were extracted from the gel using QIAquick Gel Extraction Kit Protocol (Qiagen Inc., Valencia, CA) as previously described.

5.2.7. Cloning of PCR products

PCR products were cloned using the TOPO TA Cloning® Kit (Invitrogen Corporation, Carlsbad, CA). This kit allows for a direct insertion of *Taq* polymerase-amplified PCR products into a plasmid vector for manipulations such as sequencing.

5.2.7.a. Cloning reaction

4µl of purified DNA fragment, 1µl of salt solution (1.2M NaCl, 0.06M MgCl₂), and 1µl of TOPO® vector (10ng plasmid DNA) were added and mixed. The mixture was incubated at room temperature for 5 minutes and then placed on ice.

5.2.7.b. Transformation of competent cells

This step was to transform competent *E. coli* (One Shot® TOP10 competent *E. coli*) provided in the kit with DNA-vector construct. 2µl of the cloning reaction mixture (see 5.2.7.a.) was added to a vial of competent *E. coli*, the mixture incubated on ice for 15 minutes then heated for 30 seconds at 42°C. S.O.C. medium (2% Tryptone, 0.5% yeast extract, 10mM NaCl, 2.5mM KCl, 10mM MgCl₂, 10mM MgSO₄, and 20mM glucose) was added to the mixture. The tube was shaken (200 rpm) at 37°C for 1 hour. 50µl of the mixture was spread on each of two pre-warmed LB plates containing 50µg/ml ampicillin and the plates incubated overnight at 37°C.

5.2.7.c. Analysis of transformed clones

Ten individual colonies from each plate were selected and cultured overnight in LB broth containing 50µg/ml ampicillin. Plasmid DNA was isolated using the QIAprep® Miniprep kit (Qiagen Inc., Valencia, CA) (see Appendix for detail of plasmid DNA isolation). The plasmid was analyzed for presence and size of insert by *EcoRI* digestion followed by agarose gel electrophoresis. To 5µl of plasmid, 1X React-3 buffer and 10U *EcoRI* (Invitrogen Corporation, Carlsbad, CA) were mixed and water added to make final volume of 20µl. The mixture was mixed and incubated at 37°C for 1 hour. Gel electrophoresis was used to show that the plasmid had been digested and to estimate the size of the cloned fragment.

5.2.8. Northern hybridization

Northern hybridization was used to detect the presence and measure the size of PDE6A mRNA transcripts in a range of tissues.

5.2.8.a. Preparation of FA gel for electrophoresis

A 1.5% FA gel 20.5*20.5*0.8cm was prepared (see Appendix for preparation solutions) and equilibrated at 120volt/cm in 1X formaldehyde gel running buffer for 1 hour.

5.2.8.b. FA gel electrophoresis

5.2.8.b.(i). Preparation of RNA samples and RNA size marker

30µg of total RNA isolated from pituitary gland, pineal gland, lens, small intestine, *PDE6A* mutant kidney, normal control kidney and retina were used for northern hybridization. The RNA samples were mixed with 5X RNA loading buffer (see Appendix for preparation solution) at a ratio of 4:1, incubated for 3-5 minutes at 65°C, quickly chilled on ice, and then loaded onto the equilibrated FA gel. 3µl of RNA size marker (0.2-10 kb, Sigma-Aldrich Co., St Louis, MO) was added to 3µl of 5X RNA loading buffer, 1µl of 200mM sodium acetate and 2µl of DEPC-treated water, incubated at 65°C for 10 minutes, immediately cooled on ice and loaded onto the equilibrated FA gel.

5.2.8.b.(ii). FA gel electrophoresis

Electrophoresis was carried out at 3volt/cm in 1X formaldehyde gel running buffer overnight, until the bromophenol blue had migrated approximately 8 cm from the loading wells. RNA was visualized with the UV transilluminator. A transparent ruler was aligned to the gel to indicate the distance from the loading well to each of the band of RNA and a photograph was taken. The 28S and 18S species of rRNA were clearly visible under UV illumination.

5.2.8.c. Preparation for an upward capillary transfer

5.2.8.c.(i). Preparation of FA gel

The unused areas of the gel were trimmed and a small triangular piece was cut off the bottom left-hand corner of the gel to aid in orientation. To partially hydrolyze RNA samples, the gel was rinsed with DEPC-treated water, soaked in 5 gel volumes of 0.05M NaOH for 20 minutes and then in 20X SSC (see Appendix) for 40 minutes.

5.2.8.c.(ii). Preparation of nylon membrane, wicked papers and blotting papers

Positively charged nylon membrane (Boehringer Mannheim GmbH, Mannheim, Germany) was used. The corner of the membrane was cut to match the corner cut from the gel. The membrane was cut into a size of 10*15 cm, floated on DEPC-treated water until it was completely wet from beneath and then immersed in 10X SSC for 5 minutes. Filter paper (Whatman 3MM paper, MidWest Scientific Company, Valley Park, MO) was used as wicked and blotting papers. To make wicked papers, two pieces of filter paper at size of 27*14 cm and 24*17 cm were cut and prewet in 20X SSC. Four pieces of filter paper of the same size as that of nylon membrane were cut and soaked in 20X SSC to use as blotting papers.

5.2.8.c.(iii). Assembly of the capillary transfer system

The gel support (small baking dish with Plexiglas on top) was placed in large glass baking dish filled with transfer buffer (20X SSC). Two prewet wicked papers were placed on Plexiglas in the opposite direction, so that the edges of the papers were immersed in the transfer buffer (Figure 5.1). The gel was carefully placed on wicked papers in an inverted position. Parafilm was placed on the wicked papers to surround the edges of the gel. The wet nylon membrane was transferred with care and placed on top of the gel, the cut corners of the gel and nylon membrane aligned, air bubbles removed to maximize contact between the gel and nylon membrane. Four pieces of prewet blotting paper were placed on the top of nylon membrane. Blotting papers were smoothed with a glass rod. A stack of paper towels (same size as that of the nylon membrane) was placed on blotting papers, and a sheet of Plexiglas on top of it. Two 100-gram weights were put on top of the paper towels.

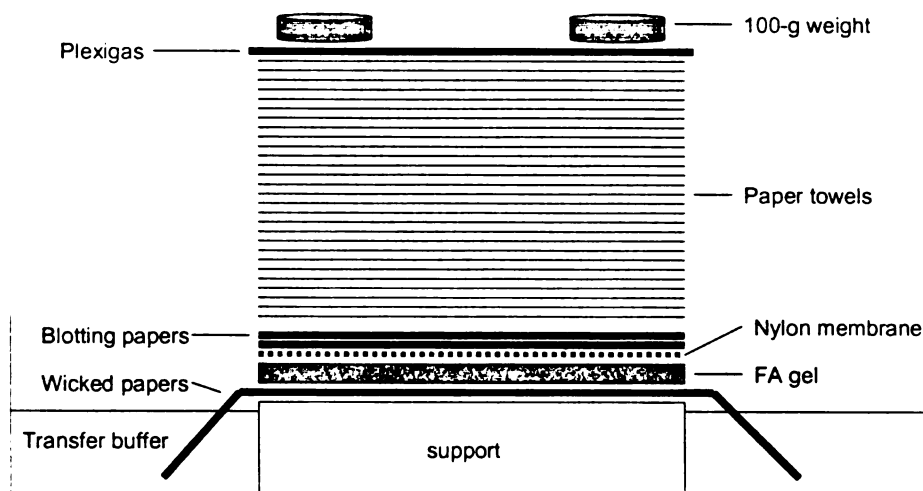


Figure 5.1. Upward capillary transfer apparatus. RNA was transferred from FA gel to a nylon membrane by capillary reaction drawing transfer buffer from the reservoir upward through the gel into a stack of dry paper towels. Weights applied on top of a stack of paper towels helped to ensure a tight connection between layers of materials. The apparatus was leveled using a spirit level.

The capillary transfer was allowed to occur over night, and then the apparatus was dismantled. The positions of the loading wells were marked on the nylon membrane with a pencil; the nylon membrane was then transferred to 6X SSC at room temperature, slowly agitated for 5 minutes. The nylon membrane, RNA side upward, was air-dried on a dry sheet of filter paper for a few minutes.

5.2.8.c.(iv). Fixation of the transferred RNA to the membrane

The dry nylon membrane was placed between 2 pieces of filter papers and baked in a vacuum oven at 80°C for 2 hours.

5.2.8.d. Northern hybridization

5.2.8.d.(i). Preparation of the DNA probe

A plasmid containing full-length canine PDE6A cDNA was available from another project. Restriction enzyme digestion was performed with *Not*I enzyme to cut the full-length canine PDE6A cDNA from the plasmid. Agarose gel electrophoresis was performed to confirm the cut PDE6A cDNA. The PDE6A cDNA was purified with QIAquick Gel Extraction kit (Qiagen Inc., Valencia, CA). PCR (see 5.2.4.b for PCR protocol) was performed using the PDE6A-specific primers to confirm the PDE6A fragment generated from the cut PDE6A cDNA, which was afterward visualized by gel electrophoresis. Gel electrophoresis of an aliquot of the PDE6A cDNA was performed and DNA size markers (100bp DNA ladder; New England BioLabs Inc, Beverly, MA) of known concentration included. The concentration of DNA in the PDE6A cDNA solution was estimated by comparison with the intensity and size ladder bands.

6 μ l of distilled water was added to 3 μ l of PDE6A cDNA (~25ng), and heated in boiling water for 10 minutes, immediately cooled on ice, and then briefly centrifuged. The probe was radioactively labeled using the Random Primed DNA labeling Kit (Roche Diagnostics GmbH, Penzberg, Germany) as follows: 9 μ l of PDE6A cDNA solution, 0.025mM of each of dCTP, dGTP, and dTTP, 1X hexanucleotide mixture, 12.5 μ Ci [α -

^{32}P]dATP, and 2U/ Klenow enzyme. The mixture was mixed, incubated at 36°C for 1 hour and then chilled on ice.

Chromatography (Chromaspin + TE-30, BD Sciences ClonTech, Mountain View, CA) was used to remove unincorporated nucleotides. Integrity of the DNA- $[\alpha\text{-}^{32}\text{P}]$ -labeled probe was verified using a hand-held monitor (Sambrook et al., 1989).

5.2.8.d.(ii). Prehybridization

The nylon membrane was carefully transferred to a hybridization bottle, incubated in a hybridized oven (4rpm) for 2 hours at 68°C in 100 ml of prehybridization solution (see Appendix).

5.2.8.d.(iii). Hybridization

The ^{32}P -labeled double-stranded DNA was denatured by heating for 10 minutes at 100°C, then rapidly chilled on ice water. Prehybridization solution was partially removed from the bottle, and 7ml was reserved. To make the hybridization solution, the denatured ^{32}P -labeled probe was added directly to the 7 ml prehybridization solution and mixed gently. The nylon membrane was incubated in hybridization solution (4rpm) for 16 hours at 50°C.

5.2.8.d.(iv). Washing of the membrane

After hybridization, hybridization solution was removed from the bottle, the membrane was washed gently 2 times; twice with 100 ml of Wash A solution (see Appendix) at 50°C, followed by 100 ml of Wash B solution (see Appendix) at 50°C for 25 minutes for each wash. The membrane was then washed in 100 ml of 0.1X SSC, 0.5% SDS solution at 65°C for 30 minutes and then in 70ml of 0.1x SSC, 0.1% SDS solution at room temperature 5 times, each time for 5 minutes.

5.2.8.e. Exposure of the nylon membrane to phosphor-imager

The membrane was slightly air-dried on a filter paper and then placed in a phosphor-imager cassette for 72 hours at room temperature. An image of the membrane was obtained by scanning the phosphor-imager (Storm 860; Molecular Dynamics, Sunnyvale, CA).

5.3. Results

5.3.1. Expression of PDE6A mRNA in canine tissues

5.3.1.a. Investigation of PDE6A expression by RT-PCR

Tissue expression of PDE6A was investigated using RT-PCR with primers described as in 5.2.4.b and the primer pairs shown graphically in Figure 5.2. Positive controls for the RT-PCR using beta actin primers were used to confirm the presence of mRNAs in all samples (Figure 5.3). Agarose gel electrophoresis revealed size of RT-PCR products in normal control retina tested with all primer sets.

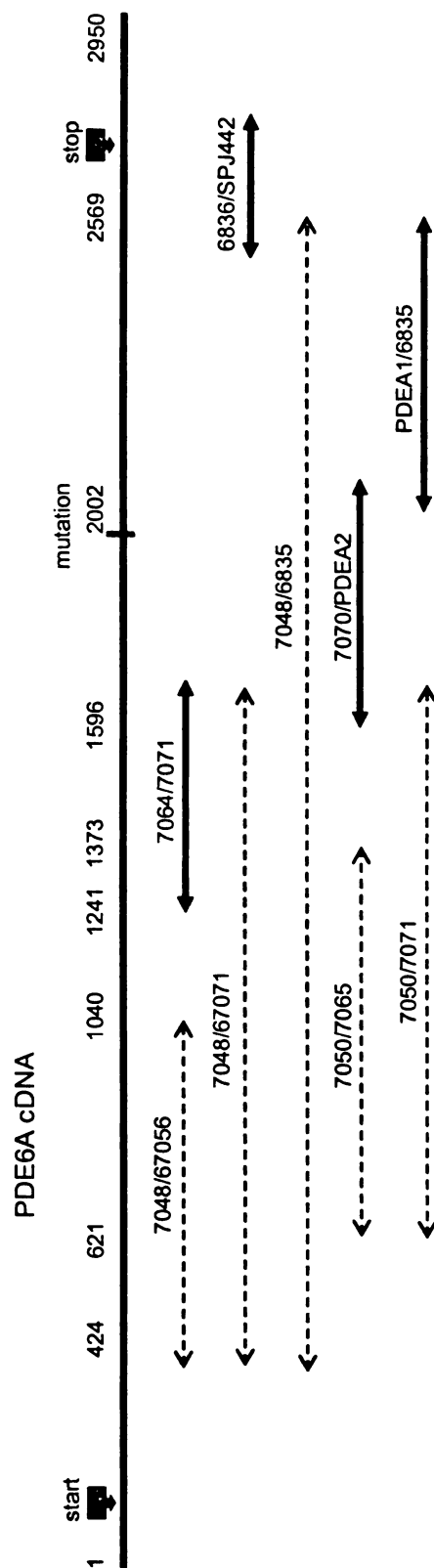


Figure 5.2. Diagram illustrating PDE6A fragments amplified from RT-PCR with various designed primer sets. Canine PDE6A cDNA is shown in a thick black line with start, stop, and mutation sites. Numbers on PDE6A cDNA indicate number of base pairs (numbering according to canine sequence by Veske and others (1997)). All primers used in this study successfully amplify PDE6A products from normal retina. Bold arrows represents PDE6A fragment that could be amplified in other tissues while dot arrows represent PDE6A fragment that could not be amplified in other tissues.

RT-PCR amplifications using 4 of the 9 PDE6A primer sets (Figure 5.2); 7064/7071, 7070/PDEA2, PDEA1/6835 and 6836/SPJ442 yielded amplicons from a variety of tissues. With 7064/7071 and 6836/SPJ442 primers, a single fragment of 398 bp and 426 bp in size, respectively were detected in normal retina, iris, choroid, normal kidney, mutant kidney and mutant small intestine (data not shown). With 7070/PDEA2 primers (Figure 5.2), a single fragment with 446 bp in size was amplified from normal retina, mutant retina at 5 weeks of age, iris, choroid, lens, normal kidney, the mutant kidney at 1 yr of age while multiple fragments were detected in normal small intestine (Figure 5.3). Larger amounts of PDE6A product was obtained from the mutant retina, iris, and choroid while less product was obtained in the reactions utilizing normal kidney, mutant kidney and normal small intestine. Similar amounts of template were added to each PCR reaction. The additional RT-PCR products from the normal small intestine were approximately 600 bp and 300 bp in size. Sequences of fragments from the normal small intestine have not been investigated at this point.

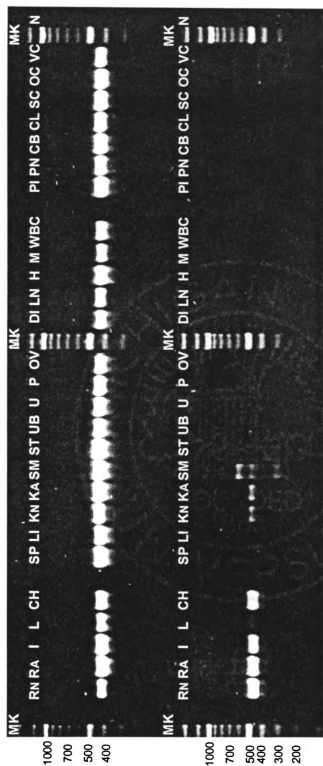


Figure 5.3. RT-PCR analysis of the PDE6A gene expression in various tissues. The PDE6A specific primers 7070/PDEA2 (Figure 5.2) were used for amplification of PDE6A (lower panel). Upper panel shows results of RT-PCR for beta actin. Note that PDE6A products are amplified from normal control retina (RN), the mutant retina from dog at 5 weeks of age (RA), iris (I), lens (L), choroid (CH), normal control kidney (KN), the mutant kidney (KA) and small intestine (SM). Key: RN = normal control retina, RA = the mutant retina, I = iris, L = lens, CH = choroid, SP = spleen, LI = liver, KN = normal control kidney, KA = the mutant kidney, SM = the small intestine, ST = stomach, UB = urinary bladder, U = uterus, P = pancreas, OV = ovary, DI = diaphragm, LN = lung, H = heart, M = muscle, WBC = white blood cells, PI = pituitary gland, PN = pineal gland, CB = cerebellum, CL = cerebellum, SC = spinal cord, OC = optic chiasm, VC = visual cortex, N = negative control, MK = DNA size marker (100bp; NewEngland Biolabs; Beverly, MA). Numbers indicate sizes of 100bp ladder marker.

With PDEA1/6835 primers (Figure 5.2), RT-PCR product 527 bp in size was amplified from normal retina, iris, choroid, lens, normal kidney, normal small intestine, mutant small intestine, pituitary gland, and pineal gland cDNA (Figure 5.4). Smaller products were also amplified from mutant retina and mutant kidney (Figure 5.4). The two amplicons from mutant kidney were cloned and sequenced and the size was shown to be due to alternative splicing. Sequencing showed that 2 out of 3 fragments amplified from the mutant retina had the same size as the two fragments amplified from the mutant kidney. A faint additional product amplified from the mutant retina is approximately 500 bp in size and has not been further investigated.

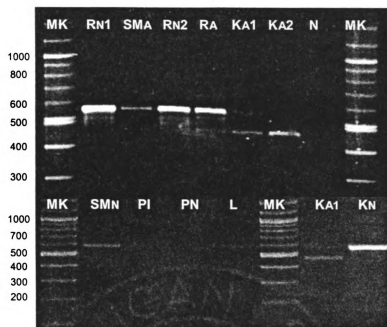


Figure 5.4. RT-PCR analysis of the *PDE6A* gene expression in various tissues using gene specific primers (PDEA1/6835; Figure 5.1). Very faint products from pituitary and pineal gland are confirmed by sequencing. Note that small intestine from the *PDE6A* mutant dog shows the same size of product as is amplified from the normal control retina (RN1 & RN2) but at a lower yield. PCR amplification of the retina from the *PDE6A* mutant dog shows 3 products, one of which with the strongest expression has the same size as the product from the normal control retina. Two products are amplified from the kidney of the *PDE6A* mutant dog. Note the amount of the upper product from the kidney of the *PDE6A* mutant dog is lower than the amount of the shorter product. Key: RN1 = normal control retina sample 1, SMN = normal small intestine, SMA = mutant small intestine, RN2 = normal control retina sample 2, RA = mutant retina, KA1 = normal control kidney sample 1, KA2 = normal control kidney sample 1, PI = pituitary gland, PN = pineal gland, L = lens, N = negative control, MK = DNA size marker (100bp; NewEngland Biolabs; Beverly, MA). Numbers indicate sizes of 100bp ladder marker.

Sequence of the 527-bp amplicon from mutant kidney cDNA matches that amplified from normal control retina (Figure 5.6). The sequence of the 426-bp mutant kidney product reveals alternative splicing with the skipping of exon 16 (Figure 5.5 & 5.6). Based on the normal and mutant retina PDE6A sequence, analysis of the PDE6A amino acid predicted to be encoded by the shorter transcript from the mutant kidney revealed that the premature termination codon is no longer present (it is positioned in the skipped exon 16). There are predicted to be 27 altered amino acids after the mutation site, followed by a deletion of the 33 amino acids coded by exon 16 (Figure 5.6), preceding the resumption of normal amino acid sequence (the deletion of exon 16 puts the predicted codon usage back in phase) (Figure 5.6).

5.3.1.b. Investigation of kidney transcript of the normal control

The 5' and 3' RACE and sequencing of amplicons amplified from normal kidney suggested that the kidney had a shorter transcript than retina (Figure 5.5 & 5.7). There was a start of transcription in intron 7 (numbering corresponds to retinal PDE6A gene) and inclusion of the following 15 exons. Two 3' RACE products were amplified and cloned. Sequencing these products showed that they corresponded to the 3' end of two of the published retinal cDNA sequences, which had different lengths of 3' UTR (Figure 5.5). Analyses of intron 7 sequence by promoter prediction software (www.fruitfly.org) (Reese, 2001) detected the 5' most nucleotide obtained by the 5' RACE technique as a potential transcription start site.

1 AGTTAATCAT TGAAAACCAT CTCGAGCATG TCTACCTGAT GAAAGAATGT
51 GAACGCCTTG GGCAAGGACG TAGCATTCTT GAAGATAGCA CGCAGGGCTT
101 ACTGGGTATG CTATAGAATC TAATCATGGC TCCATTATTC CTCTTCACGG
151 CTTTCAGATT TGCAACATCA TGAATGCACC TGCAGAGGAC TTTTTTGCAT
M N A P A E D F F A
201 TCCAGAAAGA GCCTCTGGAT GAGTCTGGAT GGATGATTAA GAATGTCCTT
F Q K E P L D E S G W M I K N V L
251 TCTATGCCAA TTGTGAACAA GAAGGAGGAA ATTGTTGGGG TGGCCACGTT
S M P I V N K K E E I V G V A T F
301 TTACAATCGC AAAGATGGAA AACCCCTTGA TGAAATGGAT GAGACCCTCA
Y N R K D G K P F D E M D E T L
351 TGGAGTCTTT GGCTCAATTC CTGGGCTGGT CCGTCTTAAA TCCTGATACT
M E S L A Q F L G W S V L N P D T
401 TACGAGTCAA TGAACAGACT TGAAAACAGG AAGGATATTT TCCAGGACAT
Y E S M N R L E N R K D I F Q D M
451 GGTAAAATAC CACGTGAAGT GTGACAATGA AGAGATCCAG AAAATCCTGA
V K Y H V K C D N E E I Q K I L
501 AAACCAGAGA GGTGTATGGG AAGGAGCCGT GGGAGTCCGA GGAAGAGGAA
K T R E V Y G K E P W E C E E E E
551 CTCGCTGAGA TCCTGCAAGG AGAGCTGCCA GATGCAGAGA AATATGAAAT
L A E I L Q G E L P D A E K Y E I
601 CAATAAATTC CACTTCAGCG ACTTGCCCCT GACCGAACTG GAGCTGGTGA
N K F H F S D L P L T E L E L V
651 AATGTGGGAT ACAGATGTAC TATGAGCTCA AAGTGGTGGG TAAATTTTAC
K C G I Q M Y Y E L K V V D K F H
701 ATTCCCTCAGG AGGCCCTGGT GCGCTTCATG TACTCGCTGA GCAAGGGCTA
I P Q E A L V R F M Y S L S K G Y
751 CCGCAGGATC ACCTACCACA ACTGGCGGCA CGGCTTCAAC GTGGGGCAGA
R R I T Y H N W R H G F N V G Q
801 CCATGTTCTC CTTGCTGGTG ACCGGAAAGC TGAAGCGATA CTTACAGAC
T M F S L L V T G K L K R Y F T D
851 CTAGAGGCCT TGGCCATGGT CACCGCTGCC TTCTGCCATG ACATTGACCA
L E A L A M V T A A F C H D I D H
901 CAGAGGCACC AACAATCTCT ACCAGATGAA GTCCCAGAAC CCACTGGCCA
R G T N N L Y Q M K S Q N P L A
951 AGCTCCATGG GTCCTCCATC TTGGAAAGAC ACCACTTGGG GTTCGGCAAA
K L H G S S I L E R H H L E F G K
1001 ACGTTGCTGC GAGATGAGAG CCTGAATATC TTTCAAAACC TCAATCGCAG
T L L R D E S L N I F Q N L N R R
1051 GCAGCACGAG CACGCCATCC ACATGATGGA CATAGCAATC ATTGCCACAG
Q H E H A I H M M D I A I I A T
1101 ACCTCGCCCT GTATTTCAAG AAGAGGACAA TGTTCAAAA GATCGTGGAT
D L A L Y F K K R T M F Q K I V D

```

1151 CAGTCTAAAA CATATGAAAC TCAGCAGGAG TGGACACAGT ACATGATGCT
      Q S K T Y E T Q Q E W T Q Y M M Y
1201 GGAGCAGACA CGGAAGGAAA TTGTTATGGC CATGATGATG ACCGCCTGTG
      E Q T R K E I V M A M M M T A C
1251 ATCTCTCAGC CATCACCAAG CCCTGGGAGG TGCAGAGTAA GGTAGCTCTA
      D L S A I T K P W E V Q S K V A L
1301 CTGGTTGCTG CCGAATTCTG GGAACAAGGT GACCTGGAGC GCACAGTGCT
      L V A A E F W E Q G D L E R T V L
1351 GCAGCAGAAT CCCATTCCCA TGATGGACAG GAACAAGGCA GATGAACTCC
      Q Q N P I P M M D R N K A D E L
1401 CCAAGCTTCA AGTCGGCTTC ATTGACTTTG TTTGCACCTT TGTCTACAAG
      P K L Q V G F I D F V C T F V Y K
1451 GAATTCTCCC GTTTCACGA GGAGATCACT CCCATGCTGG ATGGGATCAC
      E F S R F H E E I T P M L D G I T
1501 CAACAACCGC AAGGAGTGGG AGGCGCTCGC CGATGAGTAC GACACCAAGA
      N N R K E W K A L A D E Y D T K
1551 TGAAGGCCCT GGAGGAGGAG AAGCAGAAGC AGCAGACAGC CAAGCAAGGG
      M K A L E E E K Q K Q Q T A K Q G
1601 GCGGCAGGAG ATCAGCCGGG GGGCAACCCC AGCCCGGCCG GGGGCGCACC
      A A G D Q P G G N P S P A G G A P
1651 TGCATCCAAG TCCTGCTGCA TCCAGTAACG CTGCCTGGCA TCAGCTGCAC
      A S K S C C I Q .
1701 CGAATGGTAC CACCCTTCCT GGAAAGAGAC CACCCAAGCC AGCAGAAAAC

1751 CAAAACCCTG CTTGTGAAGT AAAATAGTAA TCGGATTGGA AAGCTGGGAG

1801 AGAATTTAGC TTACTTTCAT CTAGTGGTTT TTGAACATT TTTTCACTTTT

1851 GAATACTTTT TACTGAGCTA AAACCAACAT TCTAGCTTTA ATAGACATCA

1901 ATTAAACATT TAATTAAGGC CAAGTTCATC TGCTTGCTTA GAATCATTTTT

1951 CACTCTTATA CTTCCATTTT ATGTTTTCTT ATAACAATTG TCTAGCATCC

2001 TCAAAAGTAG AGAATTGTTC AGTGAATCCC TCCTCCTCAT CACCCAGATT

2051 CCAATATCAG GGTTTTGCCC CATTTGCTTC ATCCATTCTT TTACATTTCT

2101 TTCGCATTTT TTTCTTAGCT GAAGTGAAGT ATTTTCTTTA TTAAATTGAT

2151 GGTCTTTTTT CTTTAAAAAA AAAAAAAAAA AAAAAA

```

Figure 5.5. Nucleotide sequence of the assembled kidney PDE6A full-length transcript, the shorter product missing exon 16 from the *PDE6A* mutant kidney and predicted translated amino acid sequence. The 2164-base pair sequence of the kidney PDE6A full-length transcript is assembled from the RT-PCR contigs combined with the products obtained by 3' and 5' RACE. Sequence derived from the 5' RACE is indicated in green and sequence derived from the alternative 3' RACE is indicated in blue. The potential translation start (ATG), and stop codon (TAA) are shown in pink and brown,

respectively. The sequence of exon 16 (retinal PDE6A exon numbering), which is skipped in a subset of transcripts from kidney from *PDE6A* mutant dogs is underlined. Below the nucleotide sequence is amino acid sequence predicted if the transcript was translated. The two A nucleotides, one of which is deleted in the *PDE6A* mutant dog are shown in red and the site of the premature termination codon induced by this deletion (following the resulting frame shift) is shown in purple.

Mutant kidney 1

```

                                Exon 14      Exon 15
901  CAGAGGCACC AACAATCTCT ACCAGATGAA GTCCCAGACC CACTGGCCAA
      R G T N N L Y Q M K S Q T H W P

951  GCTCCATGGG TCCTCCATCT TGGAAAGACA CCACTTGGAG TTCGGCAAAA
      S S M G P P S W K D T T W S S A K

                                Exon 16
1001 CGTTGCTGCG AGATGAGAGC CTGAATATCT TTCAAACCT CAATCGCAGG
      R C C E M R A .

1051 CAGCAGGAGC ACGCCATCCA CATGATGGAC ATAGCAATCA TTGCCACAGA

                                Exon 17
1101 CCTCGCCCTG TATTCAAGA AGAGGACAAT GTCCAAAAG ATCGTGGATC

```

Mutant kidney 2

```

                                Exon 14      Exon 15
901  CAGAGGCACC AACAATCTCT ACCAGATGAA GTCCCAGACC CACTGGCCAA
      R G T N N L Y Q M K S Q T H W P

951  GCTCCATGGG TCCTCCATCT TGGAAAGACA CCACTTGGAG TTCGGCAAAA
      S S M G P P S W K D T T W S S A K

                                Exon 17
1001 CGTTGCTGCG AGATGAGGAA GAGGACAATG TTCCAAAAGA TCGTGGATCA
      R C C E M R K R T M F Q K I V D Q

```

Figure 5.6. Comparison of a portion of the two fragments of mutant canine kidney PDE6A transcript and amino acid sequence in the region of the mutation responsible for PRA in the *PDE6A* mutant dog. Note that complete sizes of mutant kidney 1 and mutant kidney 2 fragments are 527 and 426 bp, respectively. The 527-bp fragment contains 28 altered amino acids after the mutation site leading to a frame shift and a premature termination codon (labeled in green). The 426-bp fragment has skipped exon 16 and it contains 27 altered amino acid sequences (labeled in pink).

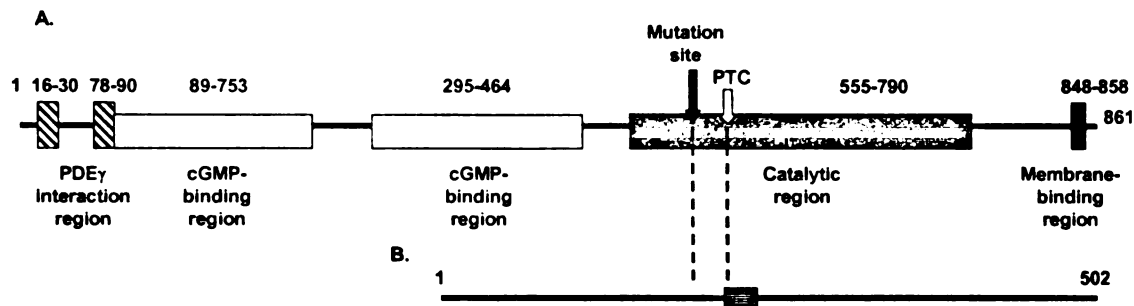


Figure 5.7. Diagram demonstrating different PDE6A domains from the retina (A) (Oppert et al., 1991) and PDE6A fragment from kidney (B). The sites of interaction with the inhibitory gamma subunits of PDE, the cGMP binding sites, the catalytic region and membrane binding region are indicated. Note that the mutation site responsible for PRA in the *PDE6A* mutant dog is indicated by a black arrow and the resulting premature termination codon (PTC) is indicated by a white arrow. The region of the kidney transcript deleted by exon skipping is shown by the filled box. Numbers indicate number of amino acids.

5.3.1.c. Investigation of PDE6A expression by northern blot (Figures 5.8 & 5.9)

A northern blot hybridization of canine total RNA using the PDE6A clone cDNA as a probe revealed a prominent signal of approximate 3.0-kb transcript in the retina (Figure 5.9). No signals could be detected in the lanes from normal kidney, mutant kidney, small intestine, pituitary gland, pineal gland, and lens.

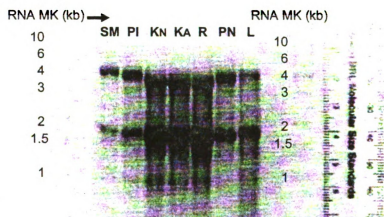


Figure 5.8. Total RNAs separated by gel electrophoresis using 1.5% formaldehyde prior to blotting on a nylon membrane. The 28S (the upper band; ~ 4kb in size) and 18S (the lower band; ~ 2kb in size) species of rRNA are clearly visible in all tissues. Arrow indicates the location of wells. Key: SM = small intestine, PI = pituitary gland, KN = normal control kidney, KA = the *PDE6A* mutant kidney, R = retina, PN = pineal gland, L = lens, MK = RNA size marker (0.2-10KB; Sigma, St. Louis, MO); kb = kilobase. Numbers indicate sizes of 0.2-10KB ladder marker.

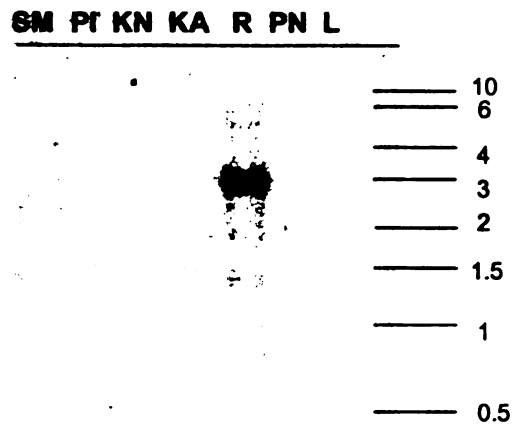


Figure 5.9. Northern blot probed with full-length canine retinal PDE6A cDNA probe. Total RNA is isolated from various canine tissues, fractionated on a formaldehyde gel, blotted on to a nylon membrane and then analyzed with the PDE6A cDNA probe. The signals observed are obtained following a 3-day exposure. Note that strong expression of PDE6A mRNA of ~ 3.0 kb is present in the retina but not in other tissues. Line indicates wells. Key: SM = small intestine, PI = pituitary gland, KN = normal control kidney, KA = the *PDE6A* mutant kidney, R = retina, PN = pineal gland, L = lens. Numbers indicate sizes of 0.2-10KB ladder marker in kilobase (RNA size marker 0.2-10KB; Sigma, St. Louis, MO).

5.4. Discussion

PDE6A is expressed as an abundant transcript in the retina as revealed by the northern blot. Previously the presence of two canine retinal PDE6A transcripts of 3.0 and 3.3 kb in size had been reported (Farber et al., 1992). However, in the current study only a single band at ~3.0kb was seen on the retinal northern blot. The two products described in the previous study probably are accounted for by a difference in length of the 3' untranslated region. Comparisons of different canine PDE6A cDNAs in Genbank suggest the presence of two different polyadenylation sites. The 3' RACE performed in this study on normal kidney PDE6A cDNA yielded two products that matched the presumed different polyadenylation sites represented by the different Genbank submissions. The difference in our northern blot results from those previously published may be because the proximal polyadenylation site is more frequently used than the distal site and the abundance of the 3.3kb transcript was below the detection limit of our northern blot. Examination of the RNA size markers suggests that the percentage gel used should have allowed differentiation between bands at ~3.0 and ~3.3 kb. A repeat of the retinal northern blot could be considered using a heavier loading of mRNA to see if the second transcript could be detected.

PDE6A transcript could be detected in the mutant retina at 5 weeks of age by RT-PCR suggesting that the mutated PDE6A transcript is not completely degraded by the mechanism of nonsense-mediated decay. In the *rcd1* dogs, level of the PDE6B mRNA began to decrease after postnatal day 25, and it continued to decrease over a year (Farber

et al., 1992). In order to determine level of retinal PDE6A gene expression in the *PDE6A* mutant dog, a comparison should be performed using age-matched animals. To quantify the amount of transcript, quantitative real time RT-PCR, northern or slot blot would be required. RT-PCR across the region of the mutation site revealed the presence of different sized transcripts for mutant but not normal retina. There was a similar finding in kidney from mutant dog. This was further investigated as discussed below.

The northern blot did not detect PDE6A transcript in any of the other tissues tested, although several tissues (iris, choroid, lens, kidney, small intestine, pituitary gland and pineal gland) were positive on RT-PCR. This reflects the greater sensitivity of RT-PCR over northern blot hybridization. It would still be useful to be able to judge the size of PDE6A transcripts in other tissues, so an additional northern blot using a heavier loading of mRNA from the various tissues could be performed in an attempt to detect PDE6A transcripts in other tissues.

The amount of product on RT-PCR from iris and choroid was comparable to that of the retina, although this amplification is not quantitative, it may give some indication of the amount of starting template. Further studies utilizing northern analysis and quantitative real time RT-PCR would be needed to quantify the transcript in the other tissues. Phototransduction genes have been previously identified in iris and ciliary body epithelium (Ghosh et al., 2004; Diehn et al., 2005), perhaps not surprising as the inner epithelium of both are derived from the inner layer of the optic cup that also gives rise to the neurosensory retina. Another possibility to explain the presence of PDE6A transcripts

in other ocular tissues is that there have may have been some retinal contamination of these adjacent tissues during collection.

PDE6A expression in kidney was further investigated. Only primer pairs amplifying the more 3' portion of the retinal PDE6A transcript resulted in an amplicon. The combination of sequencing overlapping amplicons and of 3' and 5' RACE enabled us to construct a predicted full-length normal kidney PDE6A transcript. A computer program designed to detect transcript start sites detected the apparent start site of the kidney transcript in the equivalent of intron 7 (retinal exon/intron numbering). Sequence of a full-length kidney transcript fully matches to that of the published PDE6A mRNA from exon 8 to exon 22 with the additional 157 nucleotides located in the PDE6A intron 7. According to this matching sequence, we found that the full-length kidney transcript consists of 15 exons. The fact that a start site prediction program selected the start of the product obtained by 5' RACE as a potential start site suggests that the deduced product may represent a full-length transcript. Additionally the kit used to make cDNA is specifically designed to only allow cDNA synthesis from mature full-length mRNA, again suggesting that the kidney transcript we have detected does not represent an intermediate splicing product. Demonstration of product size by a northern blot would be desirable to confirm this and further techniques such as *in situ* hybridization to show the histological location of kidney transcripts and western blots to show protein production would be needed to further define the expression of the short PDE6A product in kidney.

Alternative splicing of the shorter PDE6A transcript was found in the *PDE6A* mutant kidney. Detailed investigation of the mutant kidney PDE6A transcripts revealed that the shorter transcript lacks exon 9, which corresponds to exon 16 in the published retinal dog PDE6A sequence. Note that the skipped exon contains the premature termination codon in the mutant dog, and a splicing-generated exon-exon junction (exon 15 and exon 17) is 79 base pairs downstream from the mutation site. Thus, skipping exon 9 (exon 16 in retina) leads to removal of the premature termination codon and may reflect a cellular response known as nonsense-associated altered splicing (NAS). NAS is a response that increases the level of alternatively spliced transcripts that skip a premature termination codon to restore the reading frame (Wang et al., 2002a). Because the skipping of exon 16 not only removes the premature termination codon but also restores the correct reading frame, if the shorter kidney PDE6A transcript was translated in the mutant dogs, we predict that the protein would have a run of 27 altered amino acids, skip 33 amino acids and then go back into the normal protein sequence. The disrupted part of the protein corresponds to a known catalytic site in retinal PDE6A. As it is not known whether or not the PDE6A transcript is expressed and plays a functional role in normal kidney it is difficult to predict what effect on function this would have.

It is interesting to note that on amplification of the transcript from mutant kidney across the region of the skipped exon that there was much less of the full-length product with the premature stop codon than of the product with the skipped exon. Nonsense-mediated decay (NMD), a mechanism that degrades aberrant mRNA transcript harboring a premature termination codon (Wang et al., 2002b) may be involved and act to increase

the relative amount of the alternatively spliced transcript. However in RT-PCR of the same region from mutant retina, the transcript of a size that matches that without the skipped exon predominates suggesting tissue differences affecting the ratio of full-length transcript (with the PTC) to shorter product with the alternative splicing (skipped exon 16) in the mutant dog.

The results of these studies suggest many additional studies aiming to improve our understanding of the PDE6A gene and its role in normal and mutant dogs; for example, experiments to establish the ratio of the various transcripts in different tissues; an investigation of the alteration of level of PDE6A expression in the mutant dog during the time course of the disease; an investigation of expression of the PDE6A gene and its role in other tissues.

Chapter 6

Final discussion & conclusions

This study showed that the *PDE6A* mutant dogs never develop normal rod function. Abnormalities in developing rods can be detected as early as 2 weeks of age, which is around the time the rod photoreceptor outer segments are starting to form. Rod-driven ERG responses, if present are very reduced and if present at all are rapidly lost over the first few weeks of retinal maturation. There are significantly reduced scotopic a-wave responses. Plots of dark-adapted a- and b-wave amplitude against stimulus intensity show the reduced sensitivity of the photoreceptors responsible for those responses and the plots are similar to the plots of cone-only responses recorded from the light-adapted dogs. Furthermore the shape of the scotopic ERG waveforms from mutant dogs more closely resembles light-adapted (cone) responses. Attempts to isolate a rod response by subtracting cone only responses from dark-adapted (rod and cone responses combined) only yielded a very small negative waveform that was delayed and was of such a low amplitude to be difficult to be certain it was a true rod response. Although this technique has been suggested for the analyses of human a-wave the amplitude of the rod response is usually greater than that isolated from the *PDE6A* mutant dogs. When the response is so low the difference in response between dark-adapted and light-adapted cones may be more significant and have significance on the resulting substantial waveform. It has been known that the amplitude of cone responses increases with light adaptation, so this would tend to artificially reduce the amplitude of the subtracted (rod-only) waveform.

Additional studies using a system that allows the rod saturating background light to be switched off and then in a very short period of time delivers a flash of light that stimulates cones can be used to record the dark adapted cone only response (Robson et al., 2003). This works because cones dark adapt very rapidly while rods dark adapt relatively slowly. The dark-adapted cone only responses could then be used to subtract from the combined rod-cone responses. Unfortunately this technique is not possible with our ERG equipment. Additional attempts to isolate rod responses from the mutant dogs using blue flashes of light and rod flicker responses likewise failed to yield convincing rod responses. The lack of rod responses would be predicted because the PDE6A gene mutation is most likely a functional *null* mutation, and it is known that cGMP phosphodiesterase beta subunits alone can combine and have been shown *in vitro* to have only about one tenth of the phosphodiesterase activity of combined alpha:beta subunits (Piriev et al., 1993).

The histological study showed that in the mutant dog rods start to develop from 2 to 3 weeks of age, and then degenerate with increasing age. The thickness of the outer segment layer between mutant and control is similar on light microscopy at three weeks of age and the mutant dog outer segments contain rhodopsin. However ultrastructural examination at this age shows a difference in the morphology of the developing outer segments. The outer segments of the mutant dog become halted during development and show disorganization of the stacks of membrane discs within them. This is very obvious by 4 weeks of age. The halting of rod development is very similar to that described in animal models with *null* mutations of PDE6B (Bowes et al., 1990). At a similar age there

is morphological evidence of death of photoreceptors. Apoptotic rod nuclei are visible in the outer nuclear layer. TUNEL staining shows significant numbers of TUNEL positive nuclei in the outer nuclear layer at 28 days of age. By 5 weeks of age there are very few TUNEL positive nuclei. A similar short-lived burst of apoptosis has been described in the *rdl* mouse (Porteracailliau et al., 1994). This burst of cell death followed by a slower continued phase of more gradual cell death is shown by the plots of rod photoreceptor cell number per unit length against age and is in keeping with the kinetics of cell loss described in other retinal and neurodegenerative diseases (Clarke & Lumsden, 2005). These kinetics gave rise to the One-Hit theory of neurodegeneration (Clarke et al., 2000). The lack of caspase 3 immunoreactivity of the apparently apoptotic photoreceptor cells suggest that apoptosis in the *PDE6A* mutant dogs may be able to occur by a caspase-3 independent mechanism. This has been shown to be the case for the *rdl* mice (Doonan et al., 2003). Apoptosis in this animal model may be triggered by other caspase enzymes within the caspase family, alternative proteases or other mechanisms independent of caspase.

In addition to the loss of rods, cones are also affected. Cone function initially appears to develop normally but at an early age cone a-wave amplitudes are reduced. Morphological changes are also seen in cone outer and inner segments at an early age, before there is complete maturation of the normal retina and this is confirmed using immunohistochemistry to stain cone photoreceptors. The loss of cone function as recorded by ERG is gradual but progressive. Loss of cone function appears to develop secondary to the loss of rod function and cone functional abnormalities are present before

there is a significant loss of rod cells. It is known that rods secrete a cone survival factor and that loss of rods will lead to a secondary loss of cones (Mohand-Said et al., 1998; Mohand-Said et al., 2000). However it would appear that cones in the *PDE6A* mutant dog are adversely affected by other mechanisms because of the development of altered function before there is a significant loss of rods. It seems likely that the failure in rod phototransduction will lead to elevated cyclic GMP levels, as found in the *rd1* dog (Lolley et al., 1987) and *rd1* mouse (Fletcher et al., 1986; Farber et al., 1988). This is likely to occur as soon as the outer segments start to develop and phototransduction would normally start to occur. It is known that abnormally elevated cyclic GMP is detrimental to the retina and this may have an early adverse effect on the cone photoreceptors as well as the rods. Rods outnumber cones by approximately 19 to 1 so cones are existing amongst large numbers of rods so alterations of cyclic GMP levels in rods could also adversely effect neighboring cones.

Immunohistochemistry revealed the early development of abnormalities in the rod bipolar cells. It was shown in the *rd1* mouse that the synaptogenesis between rods and second order neurons was abnormal and rod bipolar cells had a lack of dendrites (Strettoi et al., 2002). Ultrastructural examination of the outer plexiform layer of the mutant dog showed abnormalities of synaptic terminals. A more detailed immunohistochemical study utilizing confocal microscopy and double labeling techniques would be needed to see if a similar lack of synaptogenesis occurs in the *PDE6A* mutant dog.

Following outer retinal degeneration alterations in the axonal processes of some retinal neurons became apparent. So called retinal “rewiring” has been the subject of recent detailed studies in mouse models (Strettoi & Pignatelli, 2000; Varela et al., 2003). At a relatively early age surviving rod cells show axonal sprouting with extensions into the inner retina, later on the axonal growth occurs horizontally within the outer nuclear layer. Cones also showed a similar abnormal extension of axonal processes. Müller cells undergo hypertrophy early during the disease process and have increased expression of GFAP. Similar reactivity of glial cells has been reported in other models of retinal degeneration (Ekstrom et al., 1988; Hartig et al., 1995; Kimura et al., 2000). Inner retinal cells such as rod bipolar cells showed changes in axonal processes as the outer retinal cells died. The extensive changes that developed in the inner retina of mutant dogs have implications for attempted therapies utilizing retinal prostheses. Such therapies often rely on the presence of normal inner retinal cells and circuitry to conduct impulses generated in the implant to the central visual pathways.

RT-PCR showed that PDE6A is expressed in other tissues in addition to retina. The transcript in kidney was investigated and appeared to be a shorter product consisting of the 3' portion of the retinal transcript. Interestingly in the mutant dog this shorter transcript had alternative splicing. The predominant product in the mutant dog kidney was the alternative splicing product with skipping of the exon immediately downstream to the exon containing the mutation. This skipped exon contained the premature termination codon. Exon skipping in this case may represent nonsense-mediated altered

splicing. Further studies are required to investigate any possible function of the shorter PDE6A product in kidney.

In conclusion, the *PDE6A* mutant dog is valuable not only to provide an understanding of retinal function and to improve the knowledge of the disease mechanism but also for the investigation of possible therapies eventually aimed for use in arRP patients with an early onset of retinal degeneration. The large eye of dog models offer the opportunity to perform surgical manipulations for gene therapy or drug therapy, using techniques comparable to those that would be used in the human eye.

Chapter 7

Future studies

7.1. Investigation of retinal PDE activity and cGMP levels

7.1.1. Background and Hypothesis

Morphologic studies of *PDE6A* mutant dogs revealed a rapid loss of rods starting at young age, followed by a slower degeneration of cones. This is similar to the pattern of photoreceptor cell degeneration observed in the retinas of *rd1* mice and *rcd1* dogs, both models having mutations in the beta subunit of PDE. Both alpha and beta subunits of cGMP PDE are required for full enzymatic activity (Piriev et al., 1993). Retinas of *rcd1* dogs, when examined at 34 days of age, did not have measurable beta PDE levels suggesting the mRNA for the mutant beta PDE was degraded (Suber et al., 1993). The lack of PDE activity results in the accumulation of cGMP. This can be detected in the retinas of *rd1* mice by about 20 days after birth at which time photoreceptor degeneration is occurring rapidly. In the retina of *rcd1* dogs raised cGMP is detectable at about 10 days after birth, prior to the appearance of morphological degenerative changes. The concentration of cGMP in the retina of *rcd1* dogs rises to a level approximately 10 times greater than that in control retina (Aguirre et al., 1978).

We predict that CWC with a mutation in the gene encoding PDE6A will have a lack of the alpha subunit of PDE resulting in a severely reduced rod PDE activity, leading to an accumulation of the cGMP level during the course of photoreceptor degeneration.

7.1.2. Methods

7.1.2.a. Investigation of PDE activity of the retina

7.1.2.a.(i) HPLC analysis

Retinas of *PDE6A* mutant and age-matched normal control CWCs at 2, 4, 6 and 8 weeks of age will be dissected on ice and homogenized in a buffer containing Tris, dithiothreitol and phenylmethylsulfonyl fluoride. The homogenate will be centrifuged and the supernatant will be applied to a Mono-Q (Pharmacia) anion exchange HPLC column, which allows for a separation of rod and cone PDE (Hurwitz et al., 1985). The resulting fractions will be collected every 30 seconds, and aliquots of each fraction will be assayed for cGMP hydrolysis in the presence and absence of histone H3. PDE activity is indicated by the degree of hydrolysis of cGMP.

7.1.2.a.(ii) Western blot analysis

SDS/PAGE of retinal homogenates from *PDE6A* mutant and age-matched normal control CWCs as described in 7.1.2.a.(i) will be performed, and the separated proteins

will be transferred to nitrocellulose. The blot will be incubated with polyclonal anti-bovine antibody to retinal cGMP PDE (Cytosignal Research Products, Irvine, CA) and processed with ECL western blot detection system (Amersham). Horseradish peroxidase-conjugated goat anti-rabbit antibody (Promega) will be used as secondary antibody. Alpha and beta subunits of rod PDE will be shown as two close bands in western blots from normal control retina probed with anti-PDE antibody.

7.1.2.b. Investigation of cGMP level of the retina

Cyclic nucleotides will be extracted from retinal tissue from *PDE6A* mutant and age-matched normal control CWC at 2, 4, 6 and 8 weeks of age using hydrochloric acid, followed by heating (Barbehenn et al., 1988). Following addition of sodium acetate, cGMP will be assayed by radioimmunoassay (Steiner et al., 1972); cGMP containing extract will be added to a buffer solution of rabbit anti-cGMP antibody and ^{125}I -labeled cGMP. After goat anti-rabbit antibody is added and the reaction mixture incubated, bound and free ^{125}I -labeled cGMP are separated, and the radioactivity in the precipitate will be counted using a gamma spectrometer.

7.2. Assessment of canine cone-specific electroretinography

7.2.1. Background and Hypothesis

Dogs are diurnal animals and similar to humans approximately 95% of the photoreceptors are rods. Daylight vision is provided by cones, which make up approximately 5% of total photoreceptors. Dogs have blue or short-wavelength (S) cones (430-475 nm) and green or middle-wavelength (M) cones (500-620 nm) (Neitz et al., 1989). Several ERG methods have been reported to study different cone function (Tsuruoka et al., 2004; Marmor et al., 2004a) in human and mice.

We anticipate that canine cone type-specific ERGs can be separated, not only to characterize normal cone function but also to be able to be used as a diagnostic tool to detect functional abnormalities of different cone types in the future.

7.2.2. Methods

Various ERG techniques will be performed in *PDE6A* mutant and age-matched normal control CWCs at 7, 16, 24 and 60 weeks of age. For all ERG recordings, dogs will be anesthetized with intravenous thiopental sodium (Pentothal®; 6-12 mg/kg), and anesthesia maintained with halothane delivered in oxygen. The left pupil will be maximally dilated using 1% tropicamide (Mydracyl®, Alcon Laboratories, Honolulu, HI) and 10% phenylephrine hydrochloride (AK-Dilate®, Akorn Inc, Buffalo Grove, IL). Burian-Allen bipolar contact lenses (Hansen Ophthalmic Development Laboratory, Coralville, IA) will be used. The ground electrode will be placed subcutaneously at the back of cervical region. Dogs will be light-adapted with the background light of 30 cd/m²

for 10 minutes prior to a recording. Full-field short flash ERGs will be recorded using the UTAS-E 3000 electrophysiology unit (LKC Technologies Inc; Gaithersburg, MD).

7.2.2.a. ERG assessment of S cone function

A deep blue flash of 440 nm will be presented on a bright orange background of 590 nm from 0.01 to 0.05 cds/m^2 (Marmor et al., 2004b)

7.2.2.b. ERG assessment of M cone function

A red flash of 640 nm will be presented on a bright orange background of 590 nm from 0.2 to 2.0 cds/m^2 to study red/green cone function (Marmor et al., 2004c). A green flash of 525 nm will be presented on a white background light of 30 cd/m^2 (Maehara et al., 2005).

7.3. Investigation of the distribution of canine cone photoreceptors and the pattern of cell loss

7.3.1. Background and Hypothesis

The numbers of the different photoreceptors and their pattern of distribution varies between species. The average human retina contains 92 million rods and 4.6 million cones (Curcio et al., 1990). The highest rod densities are located along an

elliptical ring at the eccentricity of the optic disc, and then slowly decline to the far periphery. Cone density peaks at the fovea and falls steeply with increasing eccentricity. Cone density is higher in the nasal compared to temporal retina and in the mid periphery of inferior, compared to superior retina. Two cone types, short-wavelength (S) cones and middle-wavelength (M) cones, can be identified in mouse and rabbit using cell-specific markers (Szel et al., 1996). The pattern of cone topography in these species is more uniform in the dorsal compared to the ventral retina. The M cones are present exclusively in the dorsal retina while the majority of S cones occupy the ventral retina (Szel et al., 1992).

We anticipate that canine retina will have a non-uniform distribution of cone photoreceptors as reported in other species with the majority of M cones being present in the dorsal retina and S cones exclusively located in the ventral retina. We will investigate whether the pattern of cone loss varies across the retina in *PDE6A* mutant dogs.

7.3.2. Methods

Globes from *PDE6A* mutant and age-matched normal control CWCs at 7, 28 and 60 weeks of age will be collected immediately after euthanasia. The globes will be initially fixed in a mixture of 4% paraformaldehyde in 0.1M phosphate buffered saline (PBS) for two hours at 4°C. After the anterior segment of the globe, lens, and vitreous body are removed, the posterior eyecup will be further fixed in the same fixative for 48 hours at 4°C. The entire retina will be dissected free from other tissue layers of the eyes,

the orientation marked, the retina gently washed in PBS buffer, and then placed on a gelatin-coated slide with the photoreceptor layer oriented up. The retina will be fumed in a formalin chamber for up to 72 hours, and then cover slipped in glycerin. Differential interference contrast (DIC) in combination with NeuroLucida software; version 3 (MicroBrightField Inc, VT) will be used to count the number of rods and cones across the surface of the retina (cell population).

For immunohistochemistry, the posterior eyecup will be fixed in the same fixative for no longer than 20 hours. After the retina is dissected free from other tissue layers of the eyes, the orientation marked, the retina gently washed in PBS buffer, it will be overnight incubated in the following primary antibodies:-

Mouse anti-rhodopsin (Lab Vision): specific for rod photoreceptors

Rabbit anti-blue opsin (Chemicon): specific for blue cone

Rabbit anti-red/green opsin (Chemicon): specific for red/green cone

After that, the retina will be rinsed in PBS buffer and incubated in an avidin-biotin-peroxidase complex (DakoCytomation, Carpinteria, CA). The retina will be reacted with 3,3'-diaminobenzidine substrate (Liquid DAB substrate chromogen system, DakoCytomation, Carpinteria, CA). The retina will be whole-mounted on gelatin-coated slides with the photoreceptor layer oriented up, cover slipped in glycerin. Differential interference contrast (DIC) in combination with NeuroLucida software; version 3

(MicroBrightField Inc, VT) will be used to count the number of different types of cones across the surface of the retina (cell population).

Appendix

RBC lysis buffer (pH 8.0)

0.32M Sucrose

10mM Tris-HCl; pH 7.8

5mM MgCl₂

- Bring up the volume to 990ml with double-distilled water, filter sterilize
10ml Triton X-100 added after sterilization
- Keep at 4°C

DEPC-treated water

1ml diethyl pyrocarbonate (Sigma-Aldrich Co., St Louis, MO)

1000ml distilled water

- Solution was shaken vigorously to bring the DEPC into solution, then incubated at 37°C for 12 hours and autoclaved for 15 minutes before use.

10X formaldehyde gel buffer (RNeasy® Mini Handbook, 3rd edition, 2001, Qiagen Inc)

200mM 3-[N-morpholino] propanesulfonic acid (MOPS) (free acid)

50mM Na acetate

10mM EDTA

Adjust pH to 7.0 with NaOH

1X formaldehyde gel running buffer (RNeasy® Mini Handbook, 3rd edition, 2001, Qiagen Inc)

100ml 10x formaldehyde gel buffer

20ml 37% formaldehyde

880ml DEPC-treated water

5X RNA loading buffer (RNeasy® Mini Handbook, 3rd edition, 2001, Qiagen Inc)

16µl saturated aqueous bromophenol blue solution

500mM EDTA, pH 8.0

720µl 37% formaldehyde

2ml 100% glycerol

3084µl formamide

4ml 10x formaldehyde gel buffer

DEPC-treated water to a final volume of 10ml

FA gel

5.1gm agarose

34ml 10X FA gel buffer

DEPC-treated water to bring to a final volume of 340ml.

- A gel mixture was heated, cooled down to approximately 65°C and then 1.8ml of 37% formaldehyde and 7µl of 10mg/ml ethidium bromide were added.

Agarose gel electrophoresis

To make 1% agarose gel

1gm agarose

100ml 1X TAE buffer

- A gel mixture was heated, cooled down to approximately 65°C and then 10mg/ml ethidium bromide solution was added.
- Electrophoresis was carried out at 3volt/cm in 1X TAE buffer. A DNA size marker (100bp DNA ladder; New England BioLabs Inc, Beverly, MA) was used to estimate the size of the PCR products.

RNA size marker (0.2-10 kb, Sigma-Aldrich Co., St Louis, MO)

2-4µl RNA size marker, bring to 5µl with DEPC-treated water

3µl RNA loading buffer

1µl 200mM Potassium Acetate

- The RNA marker solution was incubated at 65°C for 10 minutes and immediately cooled on ice prior to loading.

Bacterial medium

LB (Luria-Botani) agar (Sambrook et al., 1989)

15g/L of Bacto-agar (Difco Laboratories, Detroit, MI)

25g/L of LB base (Invitrogen Corporation, Carlsbad, CA)

Adjust volume to 1 liter with distilled water

Adjust pH to 7.0 with NaOH

LB broth

25g of LB base (Invitrogen Corporation, Carlsbad, CA)

Adjust volume to 1 liter with distilled water

Adjust pH to 7.0 with NaOH

- Mixtures were autoclaved for 20 minutes and cooled to 50°C. 50mg/ml of ampicillin was added and gently mixed. 90-mm plates were poured allowing ~35ml of medium per plate. When the medium had hardened the plates were stored at 4°C.

20X SSC (pH 7.0)

175.3 g of NaCl

88.2 g of sodium citrate

Adjust volume to 1 liter with distilled water, adjust pH to 7.0 with HCl

Prehybridization solution (pH 7.2), filtered

0.5M NaPO₄ (pH 7.2)

7% (w/v) SDS

1mM EDTA (pH 7.0)

Wash A solution, filtered

5% SDS

1mM EDTA

40mM NaPO₄

Wash B solution, filtered

1% SDS

1mM EDTA

40mM NaPO₄

RNeasy protocol for animal tissue (with Dnase digestion) (Qiagen Inc., Valencia, CA)

Homogenization step

- Disrupt the sample with a mortar and pestle, and homogenize with a needle and syringe or a cut-off pipette tip
- Place no more than 30 mg tissue in liquid nitrogen and grind tissue to a fine powder with mortar and pestle under liquid nitrogen
- Transfer tissue powder and any remaining to liquid nitrogen to a cooled 2ml micro centrifuge tube, and allow liquid nitrogen to evaporate. Do not allow tissue to thaw.
- Add RLT buffer and homogenize by passing the lysate 5-10 times through a 20G needle fitted to a syringe

Up to 0.02 g tissue ~ 350 µl

0.02 g to 0.03 g tissue ~ 600 µl

(Ensure β-ME is added to RLT buffer before use: freshly prepared)

(10 μ l β -ME per 1 ml RLT buffer)

- Centrifuge lysate for 3 minutes at maximum speed in a micro centrifuge machine and then remove supernatant for use in subsequent steps.

Precipitation step

- Add 1 volume (same as RLT buffer) of 70% ethanol to the cleared lysate (supernatant). Mix well by pipetting. Do not centrifuge. Continue without delay to the next step.
- Apply 700 μ l of sample, including any precipitate that may have formed, to an RNeasy mini spin column, which is sitting in a 2-ml collection tube. Spin for 15 seconds at $>10,000$ rpm. Discard flow-through. (For tissue with a low yield of RNA, repeat this step with adjusted amount of sample, and discard the flow-through after each centrifugation step) Use the same collection tube for the next step.
- Pipet 350 μ l RW1 buffer onto RNeasy column and centrifuge for 15 seconds at $> 8000 \times g$ ($>10,000$ rpm) to wash. Discard the flow-through.

DNase treatment

- Add 10 μ l DnaseI stock solution to 70 μ l buffer RDD. Mix by gently inverting the tube (do not vortex).
- Pipet the Dnase I incubation mix (80 μ l) directly onto the RNeasy column (a membrane), and place on the bench top (20-30°C) for 15 minutes.

Washing step

- Pipet 350 µl buffer RW1 into the RNeasy column, and centrifuge for 15 seconds at $>8000 \times g$. Discard the flow-through.
- Transfer RNeasy column to a new 2-ml collection tube (supplied). Pipet 500 µl RPE buffer onto RNeasy column, and centrifuge for 15 seconds at $>10,000$ rpm to wash. Discard flow-through.
- Pipet 500 µl RPE buffer onto RNeasy column and centrifuge for 2 minutes at maximum speed to dry the RNeasy column.

Eluting step

- Transfer the RNeasy column into a new 1.5-ml collection tube (supplied) and pipet 30-50 µl of RNase-free water directly onto RNeasy membrane. Centrifuge for 1 minute at $>10,000$ rpm to elute.
- If the expected RNA yield is above 30 µg, repeat the step 12 by adding a second volume (30-50µl) of RNase-free water to the same tube, and elute.

RNA precipitation (Invitrogen Corporation, Carlsbad, CA)

100µl of phenol:chloroform (1:1) and 90µl of DEPC-treated water were added to the mixture, the mixture was centrifuged and supernatant was collected. 2µl of 10mg/ml mussel glycogen, 10µl of 3M sodium acetate and 220µl of 95% ethanol were added, and

then RNA was placed on ice for 10 minutes. The RNA pellet was collected by centrifugation for 20 minutes at 4°C. The supernatant was discarded and the pellet washed in 500µl of 70% ethanol and collected by centrifugation for 2 minutes at 4°C 14,000rpm. The pellet was then air-dried for 2 minutes at room temperature, and then re-suspended in 7µl DEPC-treated water.

QIAquick Gel Extraction kit, (Qiagen Inc., Valencia, CA)

- Excise the DNA fragment from the agarose gel with a clean, sharp scalpel
- Weigh the gel slice in a colorless tube. Add 3 volumes of Buffer QG to 1 volume of gel
- Incubate at 50°C for 10 minutes (or until the gel slice has completely dissolved).
- After the gel slice has dissolved completely, check that the color of the mixture is yellow.
- Add 1 volume of isopropanol to the sample and mix
- Place a spin column in a 2-ml collection tube
- To bind DNA, apply the sample to the column and centrifuge at maximum speed for 1 minute
- Discard the flow-through and place the spin column back in the same collection tube
- Add 0.5ml of Buffer QG to the spin column and centrifuge for 1 minute

- To wash, add 0.75ml of Buffer PE to the spin column, let the column stand for 2-5 minutes and then centrifuge for 1 minute
- Discard the flow-through and centrifuge the spin column for an additional 1 minute at 13,000rpm
- Place a spin column into a clean 1.5ml microcentrifuge tube
- To elute DNA, add 50µl of Buffer EB (10mM Tris-Cl, pH 8.5) or molecular water to the center of the spin column membrane and centrifuge the column for 1 minute.

QIAprep Miniprep kit (Qiagen Inc., Valencia, CA)

- Resuspend pelleted bacterial cells in 250µl Buffer P1 and transfer to a microcentrifuge tube
- Add 250µl Buffer P2 and gently invert the tube 4 to 6 times to mix
- Add 350µl Buffer N3 and invert the tube immediately but gently 4 to 6 times
- Centrifuge for 10 minutes at maximum speed in a tabletop microcentrifuge
- Apply the supernatants from the previous step to the QIAprep column by decanting pipetting
- Centrifuge for 30 to 60 seconds. Discard the flowthrough
- Wash the column by adding 0.75 ml Buffer PE and centrifuge for 30 to 60 seconds

- Discard the flowthrough, and centrifuge for an additional 1 minute to remove residual wash buffer
- Place the column in a clean 1.5ml microcentrifuge tube. To elute DNA, add 50 μ l Buffer EB to the column, let stand for 1 minute and then centrifuge for 1 minute.

BIBLIOGRAPHY

- Acland,G.M. (1988). Diagnosis and differentiation of retinal diseases in small animals by electroretinography. Semin Vet Med Surg (Small Anim), 3, 15-27.
- Acland,G.M. & Aguirre,G.D. (1987). Retinal degenerations in the dog: IV. Early retinal degeneration (erd) in Norwegian elkhounds. Exp Eye Res, 44, 491-521.
- Acland,G.M., Blanton,S.H., Hershfield,B. & Aguirre,G.D. (1994). XLPRA: a canine retinal degeneration inherited as an X-linked trait. Am.J.Med.Genet., 52, 27-33.
- Acland,G.M., Ray,K., Mellersh,C.S., Gu,W.K., Langston,A.A., Rine,J., Ostrander,E.A. & Aguirre,G.D. (1998). Linkage analysis and comparative mapping of canine progressive rod-cone degeneration (prcd) establishes potential locus homology with retinitis pigmentosa (RP17) in humans. Proc Natl Acad Sci U S A, 95, 3048-3053.
- Aguirre,G., Farber,D., Lolley,R., Fletcher,R.T. & Chader,G.J. (1978). Rod-Cone Dysplasia in Irish Setters - Defect in Cyclic-Gmp Metabolism in Visual Cells. Science, 201, 1133-1134.
- Aguirre,G.D. & Acland,G.M. (1988). Variation in Retinal Degeneration Phenotype Inherited at the Prcd Locus. Exp Eye Res, 46, 663-687.
- Aguirre,G.D. & Rubin,L.F. (1975). Rod-Cone Dysplasia (Progressive Retinal Atrophy) in Irish Setters. J Am Vet Med Assoc, 166, 157-164.
- Aguirre,G.D. & Rubin,L.F. (1971). Progressive retinal atrophy (rod dysplasia in the Norwegian Elkhound. J Am Vet Med Assoc, 158, 208-218.
- Aguirre,G.D., Rubin,L.F. & Bistner,S.I. (1972). Development of the canine eye. Am.J.Vet.Res., 33, 2399-2414.
- Ali,R.R., Sarra,G.M., Stephens,C., Alwis,M.D., Bainbridge,J.W., Munro,P.M., Fauser,S., Reichel,M.B., Kinnon,C., Hunt,D.M., Bhattacharya,S.S. & Thrasher,A.J. (2000). Restoration of photoreceptor ultrastructure and function in retinal degeneration slow mice by gene therapy. Nat.Genet., 25, 306-310.
- Allikmets,R. (2004). Leber congenital amaurosis: a genetic paradigm. Ophthalmic Genet., 25, 67-79.
- Alloway,P.G. & Dolph,P.J. (1999). A role for the light-dependent phosphorylation of visual arrestin. Proc Natl Acad Sci U S A, 96, 6072-6077.
- Arning,S., ApfelstedtSylla,E., Seeliger,M., Gendo,K., Wissinger,B. & Zrenner,E. (1996). Rhodopsin mutations in patients with autosomal dominant retinitis pigmentosa. Vision Res., 36, 439.

Baehr,W., Champagne,M.S., Lee,A.K. & Pittler,S.J. (1991). Complete cDNA sequences of mouse rod photoreceptor cGMP phosphodiesterase alpha- and beta-subunits, and identification of beta'-, a putative beta-subunit isozyme produced by alternative splicing of the beta-subunit gene. FEBS Lett., 278, 107-114.

Baldrige,W.H. & Ball,A.K. (1993). A New-Type of Interplexiform Cell in the Goldfish Retina Is Pnmt-Immunoreactive. Neuroreport, 4, 1015-1018.

Baldrige,W.H., Kurenniy,D.E. & Barnes,S. (1998). Calcium-sensitive calcium influx in photoreceptor inner segments. J Neurophysiol, 79, 3012-3018.

Barbehenn,E., Gagnon,C., Noelker,D., Aguirre,G. & Chader,G. (1988). Inherited Rod-Cone Dysplasia - Abnormal Distribution of Cyclic-Gmp in Visual Cells of Affected Irish Setters. Exp Eye Res, 46, 149-159.

Barnett,K.C. & Curtis,R. (1978). Lens luxation and progressive retinal atrophy in the Tibetan terrier. Vet Rec, 103, 160.

Beech,P.L., Pagh-Roehl,K., Noda,Y., Hirokawa,N., Burnside,B. & Rosenbaum,J.L. (1996). Localization of kinesin superfamily proteins to the connecting cilium of fish photoreceptors. J Cell Sci, 109 (Pt 4), 889-897.

Berntson,A., Smith,R.G. & Taylor,W.R. (2004). Transmission of single photon signals through a binary synapse in the mammalian retina. Vis Neurosci, 21, 693-702.

Besharse,J.C. & Dunis,D.A. (1983). Methoxyindoles and Photoreceptor Metabolism - Activation of Rod Shedding. Science, 219, 1341-1343.

Besharse,J.C., Hollyfield,J.G. & Rayborn,M.E. (1977). Photoreceptor Outer Segments - Accelerated Membrane Renewal in Rods After Exposure to Light. Science, 196, 536-538.

Biehlmaier,O., Neuhauss,S.C.F. & Kohler,K. (2001). Onset and time course of apoptosis in the developing zebrafish retina. Cell Tissue Res, 306, 199-207.

Birch,D.G. & Anderson,J.L. (1992). Standardized full-field electroretinography. Normal values and their variation with age. Arch.Ophthalmol., 110, 1571-1576.

Birch,D.G. & Fish,G.E. (1987). Rod Ergs in Retinitis-Pigmentosa and Cone Rod Degeneration. Invest Ophthalmol Vis Sci, 28, 140-150.

Bjerkas,E. (1990). Generalised progressive retinal atrophy in the English setter in Norway. Vet Rec, 126, 217.

Bjerkas,E. & Narfstrom,K. (1994). Progressive retinal atrophy in the Tibetan spaniel in Norway and Sweden. Vet Rec, 134, 377-379.

- Bloomfield,S.A. (1996). Effect of spike blockade on the receptive-field size of amacrine and ganglion cells in the rabbit retina. J Neurophysiol, 75, 1878-1893.
- Bonigk,W., Muller,F., Middendorff,R., Weyand,I. & Kaupp,U.B. (1996). Two alternatively spliced forms of the cGMP-gated channel alpha-subunit from cone photoreceptor are expressed in the chick pineal organ. J Neurosci, 16, 7458-7468.
- Boughman,J.A., Conneally,P.M. & Nance,W.E. (1980). Population Genetic-Studies of Retinitis Pigmentosa. Acta Ophthalmol Scand, 32, 223-235.
- Bowes,C., Li,T., Danciger,M., Baxter,L.C., Applebury,M.L. & Farber,D.B. (1990). Retinal degeneration in the rd mouse is caused by a defect in the beta subunit of rod cGMP-phosphodiesterase. Nature, 347, 677-680.
- Bowmaker,J.K. & Dartnall,H.J. (1980). Visual pigments of rods and cones in a human retina. J Physiol, 298, 501-511.
- Boycott,B.B. & Hopkins,J.M. (1991). Cone Bipolar Cells and Cone Synapses in the Primate Retina. Vis Neurosci, 7, 49-60.
- Brown,K.T. (1979). Citation Classic - Electroretinogram - Its Components and Their Origins. Current Contents/Life Sciences, 10.
- Bui,B.V. & Fortune,B. (2004b). Ganglion cell contributions to the rat full-field electroretinogram. J Physiol, 555, 153-173.
- Bui,B.V. & Fortune,B. (2004a). Ganglion cell contributions to the rat full-field electroretinogram. J Physiol, 555, 153-173.
- Buntmilam,A.H., Saari,J.C., Klock,I.B. & Garwin,G.G. (1985). Zonulae-Aderentes Pore-Size in the External Limiting Membrane of the Rabbit Retina. Invest Ophthalmol Vis Sci, 26, 1377-1380.
- Burstedt,M.S., Forsman-Semb,K., Janunger,T., Wachtmeister,L. & Sandgren,O. (2000). Bothnia dystrophy, a variant of autosomal recessive retinitis pigmentosa with punctata albescens and macular degeneration associates with an R234W point mutation in the RLBP1 gene. Invest Ophthalmol.Vis.Sci., 41, S616.
- Bush,R.A. & Sieving,P.A. (1994). A Proximal Retinal Component in the Primate Photopic Erg A-Wave. Invest Ophthalmol Vis Sci, 35, 635-645.
- Bush,R.A. & Sieving,P.A. (1996). Inner retinal contributions to the primate photopic fast flicker electroretinogram. J Opt Soc Am A Opt Image Sci Vis, 13, 557-565.
- Buyukmihci,N., Aguirre,G. & Marshall,J. (1980). Retinal Degenerations in the Dog .2. Development of the Retina in Rod-Cone Dysplasia. Exp Eye Res, 30, 575-591.

Cellerino,A., Bahr,M. & Isenmann,S. (2000). Apoptosis in the developing visual system. Cell Tissue Res, 301, 53-69.

Chen,L., Yang,P.Z. & Kijlstra,A. (2002). Distribution, markers, and functions of retinal microglia. Ocul Immunol Inflamm, 10, 27-39.

Chong,N.H., Alexander,R.A., Barnett,K.C., Bird,A.C. & Luthert,P.J. (1999). An immunohistochemical study of an autosomal dominant feline rod/cone dysplasia (Rdy cats). Exp Eye Res, 68, 51-57.

Chun,M.H. & Wassle,H. (1993). Some Horizontal Cells of the Bovine Retina Receive Input Synapses in the Inner Plexiform Layer. Cell Tissue Res, 272, 447-457.

Citron,M.C., Erinoff,L., Rickman,D.W. & Brecha,N.C. (1985). Modification of electroretinograms in dopamine-depleted retinas. Brain Res., 345, 186-191.

Clarke,G., Collins,R.A., Leavitt,B.R., Andrews,D.F., Hayden,M.R., Lumsden,C.J. & McInnes,R.R. (2000). A one-hit model of cell death in inherited neuronal degenerations. Nature, 406, 195-199.

Clarke,G. & Lumsden,C.J. (2005). Heterogeneous cellular environments modulate one-hit neuronal death kinetics. Brain Res Bull, 65, 59-67.

Collins,C., Hutchinson,G., Kowbel,D., Riess,O., Weber,B. & Hayden,M.R. (1992). The human beta-subunit of rod photoreceptor cGMP phosphodiesterase: complete retinal cDNA sequence and evidence for expression in brain. Genomics, 13, 698-704.

Colotto,A., Falsini,B., Salgarello,T., Iarossi,G., Galan,M.E. & Scullica,L. (2000). Photopic negative response of the human ERG: losses associated with glaucomatous damage. Invest Ophthalmol Vis Sci, 41, 2205-2211.

Cruz,R.D. & chi-Usami,E. (1989). Quantitative evaluation of electroretinogram before cataract surgery. Jpn J Ophthalmol, 33, 451-457.

Curcio,C.A. (1986). Aging and Topography of Human Photoreceptors. J Opt Soc Am A Opt Image Sci Vis, 3, 59.

Curcio,C.A., Sloan,K.R., Kalina,R.E. & Hendrickson,A.E. (1990). Human Photoreceptor Topography. J Comp Neurol, 292, 497-523.

Curtis,R. & Barnett,K.C. (1993). Progressive Retinal Atrophy in Miniature Longhaired Dachshund Dogs. Br Vet J, 149, 71-85.

Curtis,R., Barnett,K.C. & Leon,A. (1987). An early-onset retinal dystrophy with dominant inheritance in the Abyssinian cat. Clinical and pathological findings. Invest Ophthalmol Vis Sci, 28, 131-139.

- D'Cruz,P.M., Yasumura,D., Weir,J., Matthes,M.T., Abderrahim,H., Lavail,M.M. & Vollrath,D. (2000). Mutation of the receptor tyrosine kinase gene MerTK in the retinal dystrophic RCS rat. Hum Mol Genet, 9, 645-651.
- Danciger,M., Blaney,J., Gao,Y.Q., Zhao,D.Y., Heckenlively,J.R., Jacobson,S.G. & Farber,D.B. (1995). Mutations in the Pde6B Gene in Autosomal Recessive Retinitis-Pigmentosa. Genomics, 30, 1-7.
- Dean,A.F. & Tolhurst,D.J. (1983). On the distinctness of simple and complex cells in the visual cortex of the cat. J Physiol, 344, 305-325.
- Dekomien,G., Runte,M., Godde,R. & Epplen,J.T. (2000). Generalized progressive retinal atrophy of Sloughi dogs is due to an 8-bp insertion in exon 21 of the PDE6B gene. Cytogenet Cell Genet, 90, 261-267.
- Derouiche,A. (1996). Possible role of the Muller cell in uptake and metabolism of glutamate in the mammalian outer retina. Vision Res, 36, 3875-3878.
- Dice,P.F. (1980). Progressive retinal atrophy in the Samoyed. Mod.Vet.Pract., 61, 59-60.
- Dick,E. & Miller,R.F. (1985a). Extracellular K⁺ activity changes related to electroretinogram components. I. Amphibian (I-type) retinas. J Gen Physiol, 85, 885-909.
- Dick,E. & Miller,R.F. (1985b). Extracellular K⁺ activity changes related to electroretinogram components. I. Amphibian (I-type) retinas. J Gen Physiol, 85, 885-909.
- Dick,E. & Miller,R.F. (1985c). Extracellular K⁺ activity changes related to electroretinogram components. I. Amphibian (I-type) retinas. J Gen Physiol, 85, 885-909.
- Dick,E., Miller,R.F. & Bloomfield,S. (1985). Extracellular K⁺ activity changes related to electroretinogram components. II. Rabbit (E-type) retinas. J Gen Physiol, 85, 911-931.
- Dick,E., Miller,R.F. & Dacheux,R.F. (1979). Neuronal Origin of B-Wave and D-Wave in the I-Type Erg. Invest Ophthalmol Vis Sci, 34-35.
- Diehn,J.J., Diehn,M., Marmor,M.F. & Brown,P.O. (2005). Differential gene expression in anatomical compartments of the human eye. Genome Biol, 6, R74.
- Dilley,K.J., Bron,A.J. & Habgood,J.O. (1976). Anterior Polar and Posterior Subcapsular Cataract in A Patient with Retinitis Pigmentosa - Light-Microscopic and Ultrastructural Study. Exp Eye Res, 22, 155-167.
- Dong,C.J. & Hare,W.A. (2000). Contribution to the kinetics and amplitude of the electroretinogram b-wave by third-order retinal neurons in the rabbit retina. Vis Res, 40, 579-589.

- Doonan,F., Donovan,M. & Cotter,T.G. (2003). Caspase-independent photoreceptor apoptosis in mouse models of retinal degeneration. J Neurosci, 23, 5723-5731.
- Dryja,T.P., Rucinski,D.E., Chen,S.H. & Berson,E.L. (1999). Frequency of mutations in the gene encoding the alpha subunit of rod cGMP-phosphodiesterase in autosomal recessive retinitis pigmentosa. Invest Ophthalmol Vis Sci, 40, 1859-1865.
- Duarte,C.B., Ferreira,I.L., Santos,P.F., Carvalho,A.L., Agostinho,P.M. & Carvalho,A.P. (1998). Glutamate in life and death of retinal amacrine cells. Gen Pharmacol, 30, 289-295.
- Eckmiller,M.S. & Toman,A. (1998). Association of kinesin with microtubules in diverse cytoskeletal systems in the outer segments of rods and cones. Acta Anat.(Basel), 162, 133-141.
- Ekstrom,P., Sanyal,S., Narfstrom,K., Chader,G.J. & van,V.T. (1988). Accumulation of glial fibrillary acidic protein in Muller radial glia during retinal degeneration. Invest Ophthalmol Vis Sci, 29, 1363-1371.
- Elliott,J.H. & Futterman,S. (1963). Fluorescence in the Tapetum of the Cats Eye. Invest Ophthalmol, 2, 287.
- Engerman,R.L., Molitor,D.L. & Bloodwor,J.M. (1966). Vascular System of Dog Retina - Light and Electron Microscopic Studies. Exp Eye Res, 5, 296-&.
- Evers,H.U. & Gouras,P. (1986). 3 Cone Mechanisms in the Primate Electroretinogram - 2 With, One Without Off-Center Bipolar Responses. Vis Res, 26, 245-254.
- Fain,G.L., Matthews,H.R., Cornwall,M.C. & Koutalos,Y. (2001). Adaptation in vertebrate photoreceptors. Physiol Rev, 81, 117-151.
- Farber,D.B., Danciger,J.S. & Aguirre,G. (1992). The Beta-Subunit of Cyclic-Gmp Phosphodiesterase Messenger-Rna Is Deficient in Canine Rod Cone Dysplasia-1. Neuron, 9, 349-356.
- Farber,D.B., Park,S. & Yamashita,C. (1988). Cyclic GMP-phosphodiesterase of rd retina: biosynthesis and content. Exp.Eye Res., 46, 363-374.
- Fariss,R.N., Li,Z.Y. & Milam,A.H. (2000). Abnormalities in rod photoreceptors, amacrine cells, and horizontal cells in human retinas with retinitis pigmentosa. Am.J.Ophthalmol., 129, 215-223.
- Feng,W., Yasumura,D., Matthes,M.T., Lavail,M.M. & Vollrath,D. (2002). MERTK triggers uptake of photoreceptor outer segments during phagocytosis by cultured retinal pigment epithelial cells. J Biol Chem, 277, 17016-17022.
- Fletcher,R.T., Sanyal,S., Krishna,G., Aguirre,G. & Chader,G.J. (1986). Genetic expression of cyclic GMP phosphodiesterase activity defines abnormal photoreceptor

differentiation in neurological mutants of inherited retinal degeneration. J.Neurochem., 46, 1240-1245.

Flower,R.W., McLeod,D.S., Luty,G.A., Goldberg,B. & Wajner,S.D. (1985). Postnatal retinal vascular development of the puppy. Invest Ophthalmol Vis Sci, 26, 957-968.

Frasson,M., Picaud,S., Leveillard,T., Simonutti,M., Mohand-Said,S., Dreyfus,H., Hicks,D. & Sabel,J. (1999). Glial cell line-derived neurotrophic factor induces histologic and functional protection of rod photoreceptors in the rd/rd mouse. Invest Ophthalmol Vis Sci, 40, 2724-2734.

Frishman,L.J. & Steinberg,R.H. (1990). Origin of negative potentials in the light-adapted ERG of cat retina. J Neurophysiol, 63, 1333-1346.

Frishman,L.J. & Steinberg,R.H. (1989). Intraretinal analysis of the threshold dark-adapted ERG of cat retina. J Neurophysiol, 61, 1221-1232.

Gabriel,R. & Witkovsky,P. (1998). Cholinergic, but not the rod pathway-related glycinergic (AII), amacrine cells contain calretinin in the rat retina. Neurosci Lett, 247, 179-182.

Garcia,M. & Vecino,E. (2003). Role of Muller glia in neuroprotection and regeneration in the retina. Histol Histopathol, 18, 1205-1218.

Gegenfurtner,K.R., Mayser,H.M. & Sharpe,L.T. (2000). Motion perception at scotopic light levels. J Opt Soc Am A Opt Image Sci Vis, 17, 1505-1515.

Ghosh,S., Salvador-Silva,M. & Coca-Prados,M. (2004). The bovine iris-ciliary epithelium expresses components of rod phototransduction. Neurosci.Lett., 370, 7-12.

Gleason,E., Borges,S. & Wilson,M. (1994). Control of Transmitter Release from Retinal Amacrine Cells by Ca²⁺ Influx and Efflux. Neuron, 13, 1109-1117.

Goldberg,A.F.X. & Molday,R.S. (2000). Expression and characterization of peripherin/rds-rom-1 complexes and mutants implicated in retinal degenerative diseases. Vertebrate Phototransduction and the Visual Cycle, Pt B, 316, 671-687.

Gorfinkel,J., Lachapelle,P. & Molotchnikoff,S. (1988). Maturation of the Electroretinogram of the Neonatal Rabbit. Documenta Ophthalmologica, 69, 237-245.

Gorin,M.B., To,A.C. & Narfstrom,K. (1995). Sequence analysis and exclusion of phosducin as the gene for the recessive retinal degeneration of the Abyssinian cat. Biochim.Biophys.Acta, 1260, 323-327.

Gould,D.J., Petersen-Jones,S.M., Lin,C.T. & Sargan,D.R. (1997). Cloning of canine rom-1 and its investigation as a candidate gene for generalized progressive retinal atrophies in dogs. Anim Genet, 28, 391-396.

- Gould,D.J. & Sargan,D.R. (2002). Autosomal dominant retinal dystrophy (Rdy) in Abyssinian cats: exclusion of PDE6G and ROM1 and likely exclusion of Rhodopsin as candidate genes. Anim Genet, 33, 436-440.
- Granit,R. (1933). The components of the retinal action potential and their relation to the discharge in the optic nerve. J Physiol, 77, 207-240.
- Grover,S., Fishman,G.A., Anderson,R.J., Tozatti,M.S.V., Heckenlively,J.R., Weleber,R.G., Edwards,A.O. & Brown,J. (1999). Visual acuity impairment in patients with retinitis pigmentosa at age 45 years or older. Ophthalmology, 106, 1780-1785.
- Grunert,U. & Martin,P.R. (1991). Rod Bipolar Cells in the Macaque Monkey Retina - Immunoreactivity and Connectivity. J Neurosci, 11, 2742-2758.
- Haase,W., Friese,W., Gordon,R.D., Muller,H. & Cook,N.J. (1990). Immunological characterization and localization of the Na⁺/Ca²⁺(+)-exchanger in bovine retina. J Neurosci, 10, 1486-1494.
- Hack,I., Peichl,L. & Brandstatter,J.H. (1999). An alternative pathway for rod signals in the rodent retina: rod photoreceptors, cone bipolar cells, and the localization of glutamate receptors. Proc Natl Acad Sci U S A, 96, 14130-14135.
- Hanitzsch,R. & Lichtenberger,T. (1997). Two neuronal retinal components of the electroretinogram c-wave. Documenta Ophthalmologica, 94, 275-285.
- Hao,W.S., Wenzel,A., Obin,M.S., Chen,C.K., Brill,E., Krasnoperova,N.V., Eversole-Cire,P., Kleyner,Y., Taylor,A., Simon,M.I., Grimm,C., Reme,C., Reme,C.E. & Lem,J. (2002). Evidence for two apoptotic pathways in light-induced retinal degeneration. Nat Genet, 32, 254-260.
- Hare,W.A. & Ton,H. (2000). Effects of APB, PDA, and TTX on first and second order response components of the multifocal ERG response in monkey. Invest Ophthalmol Vis Sci, 41, S497.
- Hart,A.W., McKie,L., Morgan,J.E., Gautier,P., West,K., Jackson,I.J. & Cross,S.H. (2005). Genotype-phenotype correlation of mouse pde6b mutations. Invest Ophthalmol.Vis.Sci., 46, 3443-3450.
- Hartig,W., Grosche,J., Distler,C., Grimm,D., el-Hifnawi,E. & Reichenbach,A. (1995). Alterations of Muller (glial) cells in dystrophic retinæ of RCS rats. J Neurocytol, 24, 507-517.
- Hartveit,E. (1999). Reciprocal synaptic interactions between rod bipolar cells and amacrine cells in the rat retina. J Neurophysiol, 81, 2923-2936.
- Heckenlively,J.R., Yoser,S.L., Friedman,L.H. & Oversier,J.J. (1988). Clinical Findings and Common Symptoms in Retinitis Pigmentosa - Reply. Am.J.Ophthalmol., 106, 508.

- Henkind,P. (1966). Retinal Vascular System of Domestic Cat. Exp Eye Res, 5, 10-&.
- Heynen,H., Wachtmeister,L. & Vannorren,D. (1985). Origin of the Oscillatory Potentials in the Primate Retina. Vis Res, 25, 1365-1373.
- Hoang,Q.V., Linsenmeier,R.A., Chung,C.K. & Curcio,C.A. (2002). Photoreceptor inner segments in monkey and human retina: Mitochondrial density, optics, and regional variation. Vis Neurosci, 19, 395-407.
- Holopigian,K., Seiple,W., Greenstein,V.C., Hood,D.C. & Carr,R.E. (2001). Local cone and rod system function in patients with retinitis pigmentosa. Invest Ophthalmol Vis Sci, 42, 779-788.
- Hood,D.C. & Birch,D.G. (1996). Assessing abnormal rod photoreceptor activity with the a-wave of the electroretinogram: applications and methods. Doc.Ophthalmol., 92, 253-267.
- Hood,D.C. & Birch,D.G. (1994). Rod Phototransduction in Retinitis-Pigmentosa - Estimation and Interpretation of Parameters Derived from the Rod A-Wave. Invest Ophthalmol Vis Sci, 35, 2948-2961.
- Hood,D.C. & Birch,D.G. (1990). A quantitative measure of the electrical activity of human rod photoreceptors using electroretinography. Vis Neurosci, 5, 379-387.
- Hopkins,J.M. & Boycott,B.B. (1995). Synapses Between Cones and Diffuse Bipolar Cells of A Primate Retina. J Neurocytol, 24, 680-694.
- Hsu,Y.T. & Molday,R.S. (1993). Modulation of the cGMP-gated channel of rod photoreceptor cells by calmodulin. Nature, 361, 76-79.
- Hultborn,H., Mori,K. & Tsukahara,N. (1978). The neuronal pathway subserving the pupillary light reflex. Brain Res, 159, 255-267.
- Humphries,P., Farrar,G.J., Kenna,P. & Mcwilliam,P. (1990). Retinitis-Pigmentosa - Genetic-Mapping in X-Linked and Autosomal Forms of the Disease. Clin Genet, 38, 1-13.
- Hurwitz,R.L., Bunt-Milam,A.H., Chang,M.L. & Beavo,J.A. (1985). cGMP phosphodiesterase in rod and cone outer segments of the retina. J.Biol.Chem., 260, 568-573.
- Inglehearn,C.F., Morrice,D.R., Lester,D.H., Robertson,G.W., Mohamed,M.D., Simmons,I., Downey,L.M., Thaung,C., Bridges,L.R., Paton,I.R., Smith,J., Petersen-Jones,S., Hocking,P.M. & Burt,D.W. (2003). Genetic, ophthalmic, morphometric and histopathological analysis of the Retinopathy Globe Enlarged (rge) chicken. Mol Vis, 9, 295-300.

- Jacobs,G.H., Deegan,J.F., Crognale,M.A. & Fenwick,J.A. (1993). Photopigments of Dogs and Foxes and Their Implications for Canid Vision. Vis Neurosci, 10, 173-180.
- Jamison,J.A., Bush,R.A., Lei,B. & Sieving,P.A. (2001). Characterization of the rod photoresponse isolated from the dark-adapted primate ERG. Vis Neurosci, 18, 445-455.
- Jeon,C.J., Strettoi,E. & Masland,R.H. (1998). The major cell populations of the mouse retina. J Neurosci, 18, 8936-8946.
- Jimenez,A.J., Garcia-Fernandez,J.M., Gonzalez,B. & Foster,R.G. (1996). The spatio-temporal pattern of photoreceptor degeneration in the aged rd/rd mouse retina. Cell Tissue Res, 284, 193-202.
- Jomary,C., Vincent,K.A., Grist,J., Neal,M.J. & Jones,S.E. (1997). Rescue of photoreceptor function by AAV-mediated gene transfer in a mouse model of inherited retinal degeneration. Gene Ther., 4, 683-690.
- Jonas,J.B., Schneider,U. & Naumann,G.O.H. (1992). Count and Density of Human Retinal Photoreceptors. Graefes Arch Clin Exp Ophthalmol, 230, 505-510.
- Karschin,A., Wassle,H. & Schnitzer,J. (1986). Immunocytochemical Studies on Astroglia of the Cat Retina Under Normal and Pathological Conditions. J Comp Neurol, 249, 564-576.
- Kasahara,T., Okano,T., Yoshikawa,T., Yamazaki,K. & Fukada,Y. (2000). Rod-type transducin alpha-subunit mediates a phototransduction pathway in the chicken pineal gland. J.Neurochem., 75, 217-224.
- Katai,N., Kikuchi,T., Shibuki,H., Kuroiwa,S., Arai,J., Kurokawa,T. & Yoshimura,N. (1999b). Caspase-like proteases activated in apoptotic photoreceptors of Royal College of Surgeons rats. Invest Ophthalmol Vis Sci, 40, 1802-1807.
- Katai,N., Kikuchi,T., Shibuki,H., Kuroiwa,S., Arai,J., Kurokawa,T. & Yoshimura,N. (1999a). Caspase-like proteases activated in apoptotic photoreceptors of Royal College of Surgeons rats. Invest Ophthalmol Vis Sci, 40, 1802-1807.
- Kawamura,S. & Murakami,M. (1991). Calcium-dependent regulation of cyclic GMP phosphodiesterase by a protein from frog retinal rods. Nature, 349, 420-423.
- Keep,J.M. (1972). Clinical Aspects of Progressive Retinal Atrophy in Cardigan Welsh Corgi. Aust Vet J, 48, 197-&.
- Kijas,J.W., Cideciyan,A.V., Aleman,T.S., Pianta,M.J., Pearce-Kelling,S.E., Miller,B.J., Jacobson,S.G., Aguirre,G.D. & Acland,G.M. (2002). Naturally occurring rhodopsin mutation in the dog causes retinal dysfunction and degeneration mimicking human dominant retinitis pigmentosa. Proc Natl Acad Sci U S A, 99, 6328-6333.

- Kijas,J.W., Miller,B.J., Pearce-Kelling,S.E., Aguirre,G.D. & Acland,G.M. (2003). Canine models of ocular disease: outcross breedings define a dominant disorder present in the English mastiff and bull mastiff dog breeds. J Hered, 94, 27-30.
- Kimura,N., Nishikawa,S. & Tamai,M. (2000). Muller cells in developing rats with inherited retinal dystrophy. Tohoku J Exp Med, 191, 157-166.
- Kirk,G.R. & Boyer,S.F. (1973b). Maturation of the electroretinogram in the dog. Exp Neurol, 38, 252-264.
- Kirk,G.R. & Boyer,S.F. (1973a). Maturation of the electroretinogram in the dog. Exp Neurol, 38, 252-264.
- Knapp,A.G. & Schiller,P.H. (1984b). The Contribution of On-Bipolar Cells to the Electroretinogram of Rabbits and Monkeys - A Study Using 2-Amino-4-Phosphonobutyrate (Apb). Vis Res, 24, 1841-1846.
- Knapp,A.G. & Schiller,P.H. (1984a). The contribution of on-bipolar cells to the electroretinogram of rabbits and monkeys. A study using 2-amino-4-phosphonobutyrate (APB). Vis Res, 24, 1841-1846.
- Koch,S.A. & Rubin,L.F. (1972). Distribution of Cones in Retina of Normal Dog. Am.J.Vet.Res., 33, 361-&.
- Kolb,H. (1979). Inner Plexiform Layer in the Retina of the Cat - Electron-Microscopic Observations. J Neurocytol, 8, 295-329.
- Komaromy,A.M., Brooks,D.E., Dawson,W.W., Kallberg,M.E., Ollivier,F.J. & Ofri,R. (2002). Technical issues in electrodiagnostic recording. Vet Ophthalmol, 5, 85-91.
- Kommonen,B. & Karhunen,U. (1990). A late receptor dystrophy in the Labrador retriever. Vision Res, 30, 207-213.
- Koontz,M.A. & Hendrickson,A.E. (1987). Stratified Distribution of Synapses in the Inner Plexiform Layer of Primate Retina. J Comp Neurol, 263, 581-592.
- Koontz,M.A., Hendrickson,L.E., Brace,S.T. & Hendrickson,A.E. (1993). Immunocytochemical Localization of Gaba and Glycine in Amacrine and Displaced Amacrine Cells of Macaque Monkey Retina. Vision Res, 33, 2617-2628.
- Korf,H.W., White,B.H., Schaad,N.C. & Klein,D.C. (1992). Recoverin in pineal organs and retinae of various vertebrate species including man. Brain Res, 595, 57-66.
- Koskinen,L., Raitta,C. & Kommonen,B. (1985). Fluorescein angiography in homozygote and carrier state of progressive retinal atrophy of the poodle: comparative aspects with human retinitis pigmentosa. Acta Ophthalmol (Copenh), 63, 297-304.

- Kylma,T., Paulin,L., Hurwitz,M.Y., Hurwitz,R.L. & Kommonen,B. (1997). Cloning of the cDNA encoding rod photoreceptor cGMP-phosphodiesterase alpha and gamma subunits from the retinal degenerate Labrador retriever dog. Res.Vet.Sci., 62, 293-296.
- Lamb,T.D. & Pugh,E.N., Jr. (1992b). A quantitative account of the activation steps involved in phototransduction in amphibian photoreceptors. J Physiol, 449, 719-758.
- Lamb,T.D. & Pugh,E.N., Jr. (1992a). A quantitative account of the activation steps involved in phototransduction in amphibian photoreceptors. J Physiol, 449, 719-758.
- Lee,E.J., Kim,H.J., Lim,E.J., Kim,I.B., Kang,W.S., Oh,S.J., Rickman,D.W., Chung,J.W. & Chun,M.H. (2004). All amacrine cells in the mammalian retina show disabled-1 immunoreactivity. J Comp Neurol, 470, 372-381.
- Lee,I., Kim,J. & Lee,C. (1999). Anatomical characteristics and three-dimensional model of the dog dorsal lateral geniculate body. Anat Rec, 256, 29-39.
- Lei,B. (2003). The ERG of guinea pig (*Cavia porcellus*): comparison with I-type monkey and I-type rat. Documenta Ophthalmologica, 106, 243-249.
- Lewis,D.G. (1977). Reappearance of PRA in the Irish setter. Vet Rec, 101, 122-123.
- Li,Z.Y., Kljavin,I.J. & Milam,A.H. (1995). Rod photoreceptor neurite sprouting in retinitis pigmentosa. J Neurosci, 15, 5429-5438.
- Lin,C.T., Gould,D.J., Petersen-Jonest,S.M. & Sargan,D.R. (2002). Canine inherited retinal degenerations: update on molecular genetic research and its clinical application. J.Small Anim Pract., 43, 426-432.
- Lin,C.T., Petersen-Jones,S.M. & Sargan,D.R. (1998). Isolation and investigation of canine phosphodiesterase as a candidate for canine generalized progressive retinal atrophies. Exp.Eye Res., 67, 473-480.
- Linden,R. & Esberard,C.E.L. (1987). Displaced Amacrine Cells in the Ganglion-Cell Layer of the Hamster Retina. Vision Res, 27, 1071-&.
- Linn,D.M., Blazynski,C., Redburn,D.A. & Massey,S.C. (1991). Acetylcholine-Release from the Rabbit Retina Mediated by Kainate Receptors. J Neurosci, 11, 111-122.
- Loewen,C.J.R., Moritz,O.L. & Molday,R.S. (2001). Molecular characterization of peripherin-2 and Rom-1 mutants responsible for digenic retinitis pigmentosa. J Biol Chem, 276, 22388-22396.
- Lolley,R.N. (1994). The Rd Gene Defect Triggers Programmed Rod Cell-Death - the Proctor-Lecture. Invest Ophthalmol Vis Sci, 35, 4182-4191.

- Lolley,R.N., Navon,S.E., Fung,B.K. & Lee,R.H. (1987). Inherited disorders of rd mice and affected Irish setter dogs: evaluation of transducin and cGMP-phosphodiesterase. Prog.Clin.Biol.Res., 247, 269-287.
- Lyser,K.M., Li,A.I. & Nunez,M. (1994). Horizontal Cells in the Rabbit Retina - Differentiation of Subtypes at Neonatal and Postnatal Stages. Int J Dev Neurosci, 12, 673-682.
- Lyubarsky,A.L., Falsini,B., Pennesi,M.E., Valentini,P. & Pugh,E.N., Jr. (1999). UV- and midwave-sensitive cone-driven retinal responses of the mouse: a possible phenotype for coexpression of cone photopigments. J Neurosci, 19, 442-455.
- Mack,A.F., Sussmann,C., Hirt,B. & Wagner,H.J. (2004). Displaced amacrine cells disappear from the ganglion cell layer in the central retina of adult fish during growth. Invest Ophthalmol Vis Sci, 45, 3749-3755.
- MacMillan,A.D. & Lipton,D.E. (1978). Heritability of multifocal retinal dysplasia in American Cocker Spaniels. J Am Vet Med Assoc, 172, 568-572.
- Maehara,S., Itoh,N., Itoh,Y., Wakaiki,S., Tsuzuki,K., Seno,T., Kushiro,T., Yamashita,K., Izumisawa,Y. & Kotani,T. (2005). Electroretinography using contact lens electrode with built-in light source in dogs. J Vet Med Sci, 67, 509-514.
- Marmor,M.F., Cabel,L., Shukla,S., Hwang,J.C. & Marcus,M. (2004). Clinical S-cone ERG recording with a commercial hand-held full-field stimulator. Doc.Ophthalmol., 109, 101-107.
- Marmor,M.F., Holder,G.E., Seeliger,M.W. & Yamamoto,S. (2004d). Standard for clinical electroretinography (2004 update). Doc.Ophthalmol., 108, 107-114.
- Marroni,P., Giannessi,E. & Coli,A. (1995). A Morphological and Morphometrical Study of Displaced Amacrine Cells in Dog Retina. Arch Ital Biol, 133, 89-97.
- Matsumoto,B., Blanks,J.C. & Ryan,S.J. (1984). Topographic Variations in the Rabbit and Primate Internal Limiting Membrane. Invest Ophthalmol Vis Sci, 25, 71-82.
- Merin,S. (1982). Cataract Formation in Retinitis Pigmentosa. Birth Defects Orig Artic Ser, 18, 187-191.
- Migdale,K., Herr,S., Klug,K., Ahmad,K., Linberg,K., Sterling,P. & Schein,S. (2003). Two ribbon synaptic units in rod photoreceptors of macaque, human, and cat. J Comp Neurol, 455, 100-112.
- Mohand-Said,S., Hicks,D., Dreyfus,H. & Sahel,J.A. (2000). Selective transplantation of rods delays cone loss in a retinitis pigmentosa model. Arch Ophthalmol, 118, 807-811.
- Mohand-Said,S., udon-Combe,A., Hicks,D., Simonutti,M., Forster,V., Fintz,A.C., Leveillard,T., Dreyfus,H. & Sahel,J.A. (1998). Normal retina releases a diffusible factor

stimulating cone survival in the retinal degeneration mouse. Proc Natl Acad Sci U S A, 95, 8357-8362.

Molday,R.S. (1998). Photoreceptor membrane proteins, phototransduction, and retinal degenerative diseases. The Friedenwald Lecture. Invest Ophthalmol Vis Sci, 39, 2491-2513.

Moore,K.L. & Persaud,T.V.N. (1998). Before we are born. Essential for embryology and birth defects. Saunders.

Morgans,C.W. (2000). Neurotransmitter release at ribbon synapses in the retina. Immunol Cell Biol, 78, 442-446.

Morimura,H., Fishman,G.A., Grover,S.A., Fulton,A.B., Berson,E.L. & Dryja,T.P. (1998). Mutations in the RPE65 gene in patients with autosomal recessive retinitis pigmentosa or Leber congenital amaurosis. Proc.Natl.Acad.Sci.U.S A, 95, 3088-3093.

Morin,F., Lugnier,C., Kameni,J. & Voisin,P. (2001). Expression and role of phosphodiesterase 6 in the chicken pineal gland. J.Neurochem., 78, 88-99.

Muresan,V., dala-Tufanisco,E., Hollander,B.A. & Besharse,J.C. (1997). Evidence for kinesin-related proteins associated with the axoneme of retinal photoreceptors. Exp Eye Res, 64, 895-903.

Musarella,M.A. (1990). Mapping of the X-Linked Recessive Retinitis-Pigmentosa Gene - A Review. Ophthalmic Paediatr Genet, 11, 77-88.

Narfstrom,K. (1983). Hereditary progressive retinal atrophy in the Abyssinian cat. J Hered, 74, 273-276.

Narfstrom,K., Ekestén,B., Rosolen,S.G., Spiess,B.M., Percicot,C.L. & Ofri,R. (2002). Guidelines for clinical electroretinography in the dog. Doc.Ophthalmol., 105, 83-92.

Narfstrom,K., Katz,M.L., Ford,M., Redmond,T.M., Rakoczy,E. & Bragadottir,R. (2003). In vivo gene therapy in young and adult RPE65^{-/-} dogs produces long-term visual improvement. J Hered, 94, 31-37.

Narfstrom,K. & Wrigstad,A. (1999). Clinical, electrophysiological and morphological changes in a case of hereditary retinal degeneration in the Papillon dog. Vet Ophthalmol, 2, 67-74.

Neitz,J., Geist,T. & Jacobs,G.H. (1989). Color vision in the dog. Vis Neurosci, 3, 119-125.

Newman,E. & Reichenbach,A. (1996). The Muller cell: A functional element of the retina. Trends Neurosci, 19, 307-312.

- Nguyenlegros,J. (1991). Interplexiform Cells of the Mammalian Retina. Annales des Sciences Naturelles-Zoologie et Biologie Animale, 12, 71-88.
- Obata,S. & Usukura,J. (1992). Morphogenesis of the Photoreceptor Outer Segment During Postnatal-Development in the Mouse (Balb/C) Retina. Cell Tissue Res, 269, 39-48.
- Ogilvie,J.M., Tenkova,T., Lett,J.M., Speck,J., Landgraf,M. & Silverman,M.S. (1997). Age-related distribution of cones and ON-bipolar cells in the rd mouse retina. Curr Eye Res, 16, 244-251.
- Olsson,J.E., Gordon,J.W., Pawlyk,B.S., Roof,D., Hayes,A., Molday,R.S., Mukai,S., Cowley,G.S., Berson,E.L. & Dryja,T.P. (1992). Transgenic mice with a rhodopsin mutation (Pro23His): a mouse model of autosomal dominant retinitis pigmentosa. Neuron, 9, 815-830.
- Ong,O.C., Ota,I.M., Clarke,S. & Fung,B.K. (1989). The membrane binding domain of rod cGMP phosphodiesterase is posttranslationally modified by methyl esterification at a C-terminal cysteine. Proc.Natl.Acad.Sci.U.S A, 86, 9238-9242.
- Ooto,S., Akagi,T., Kageyama,R., Akita,J., Mandai,M., Honda,Y. & Takahashi,M. (2004). Potential for neural regeneration after neurotoxic injury in the adult mammalian retina. Proc Natl Acad Sci U S A, 101, 13654-13659.
- Oppert,B., Cunnick,J.M., Hurt,D. & Takemoto,D.J. (1991). Identification of the retinal cyclic GMP phosphodiesterase inhibitory gamma-subunit interaction sites on the catalytic alpha-subunit. J Biol Chem, 266, 16607-16613.
- Palczewski,K., Subbaraya,I., Gorczyca,W.A., Helekar,B.S., Ruiz,C.C., Ohguro,H., Huang,J., Zhao,X., Crabb,J.W., Johnson,R.S. & . (1994). Molecular cloning and characterization of retinal photoreceptor guanylyl cyclase-activating protein. Neuron, 13, 395-404.
- Parshall,C.J., Wyman,M., Nitroy,S., Acland,G.M. & Aguirre,G.D. (1991). Photoreceptor dysplasia: an inherited progressive retinal atrophy of Minature Schnauzer dogs. Progress in Veterinary & Comparative Ophthalmology, 1, 187-203.
- Petersen-Jones,S.M. & Entz,D.D. (2002). An improved DNA-based test for detection of the codon 616 mutation in the alpha cyclic GMP phosphodiesterase gene that causes progressive retinal atrophy in the Cardigan Welsh Corgi. Vet Ophthalmol, 5, 103-106.
- Petersen-Jones,S.M., Entz,D.D. & Sargan,D.R. (1999). CGMP phosphodiesterase-alpha mutation causes progressive retinal atrophy in the Cardigan Welsh corgi dog. Inves Ophthalmol Vis Sci, 40, 1637-1644.
- Piriev,N.I., Yamashita,C., Samuel,G. & Farber,D.B. (1993). Rod photoreceptor cGMP-phosphodiesterase: analysis of alpha and beta subunits expressed in human kidney cells. Proc Natl Acad Sci U S A, 90, 9340-9344.

- Pittler,S.J. & Baehr,W. (1991). Identification of A Nonsense Mutation in the Rod Photoreceptor Cgmp Phosphodiesterase Beta-Subunit Gene of the Rd Mouse. Proc Natl Acad Sci U S A, 88, 8322-8326.
- Porteracailliau,C., Sung,C.H., Nathans,J. & Adler,R. (1994). Apoptotic Photoreceptor Cell-Death in Mouse Models of Retinitis-Pigmentosa. Proc Natl Acad Sci U S A, 91, 974-978.
- Priester,W.A. Canine progressive retinal atrophy: Occurence by age, breed, and sex. Am.J.Vet.Res. 35[4], 571-574. 1974.
Ref Type: Generic
- Rabin,J. (1996). Cone-specific measures of human color vision. Invest Ophthalmol Vis Sci, 37, 2771-2774.
- Rah,H., Maggs,D.J., Blankenship,T.N., Narfstrom,K. & Lyons,L.A. (2005). Early-onset, autosomal recessive, progressive retinal atrophy in Persian cats. Invest Ophthalmol Vis Sci, 46, 1742-1747.
- Rangaswamy,N.V., Frishman,L.J., Dorotheo,E.U., Schiffman,J.S., Bahrani,H.M. & Tang,R.A. (2004b). Photopic ERGs in patients with optic neuropathies: comparison with primate ERGs after pharmacologic blockade of inner retina. Invest Ophthalmol Vis Sci, 45, 3827-3837.
- Rangaswamy,N.V., Frishman,L.J., Dorotheo,E.U., Schiffman,J.S., Bahrani,H.M. & Tang,R.A. (2004a). Photopic ERGs in patients with optic neuropathies: comparison with primate ERGs after pharmacologic blockade of inner retina. Invest Ophthalmol Vis Sci, 45, 3827-3837.
- Ray,K., Acland,G.M. & Aguirre,G.D. (1996). Nonallelism of erd and prcd and exclusion of the canine RDS/peripherin gene as a candidate for both retinal degeneration loci. Invest Ophthalmol.Vis.Sci., 37, 783-794.
- Ray,K., Wang,W., Czarnecki,J., Zhang,Q., Acland,G.M. & Aguirre,G.D. (1999). Strategies for identification of mutations causing hereditary retinal diseases in dogs: Evaluation of opsin as a candidate gene. J Hered, 90, 133-137.
- Redmond,T.M., Yu,S., Lee,E., Bok,D., Hamasaki,D., Chen,N., Goletz,P., Ma,J.X., Crouch,R.K. & Pfeifer,K. (1998). Rpe65 is necessary for production of 11-cis-vitamin A in the retinal visual cycle. Nat Genet, 20, 344-351.
- Reese,M.G. (2001). Application of a time-delay neural network to promoter annotation in the Drosophila melanogaster genome. Comput Chem, 26, 51-56.
- Robson,J.G., Saszik,S.M., Ahmed,J. & Frishman,L.J. (2003). Rod and cone contributions to the a-wave of the electroretinogram of the macaque. J Physiol, 547, 509-530.

- Rodrigues,M.M., Wiggert,B., T'so,M.O. & Chader,G.J. (1986). Retinitis pigmentosa: immunohistochemical and biochemical studies of the retina. Can J Ophthalmol, 21, 79-83.
- Roe,A.W., Pallas,S.L., Hahm,J.O. & Sur,M. (1990). A map of visual space induced in primary auditory cortex. Science, 250, 818-820.
- Ruiz-Avila,L., McLaughlin,S.K., Wildman,D., McKinnon,P.J., Robichon,A., Spickofsky,N. & Margolskee,R.F. (1995a). Coupling of bitter receptor to phosphodiesterase through transducin in taste receptor cells. Nature, 376, 80-85.
- Ruiz-Avila,L., McLaughlin,S.K., Wildman,D., McKinnon,P.J., Robichon,A., Spickofsky,N. & Margolskee,R.F. (1995b). Coupling of bitter receptor to phosphodiesterase through transducin in taste receptor cells. Nature, 376, 80-85.
- Runggerbrandle,E., Messerli,J.M., Niemeyer,G. & Eppenberger,H.M. (1993). Confocal Microscopy and Computer-Assisted Image-Reconstruction of Astrocytes in the Mammalian Retina. Eur J Neurosci, 5, 1093-1106.
- Sahel,J.A., Mohand-Said,S., Leveillard,T., Hicks,D., Picaud,S. & Dreyfus,H. (2001). Rod-cone interdependence: implications for therapy of photoreceptor cell diseases. Prog Brain Res, 131, 649-661.
- Saito,H.A. (1983). Morphology of Physiologically Identified X-Type, Y-Type, and W-Type Retinal Ganglion-Cells of the Cat. J Comp Neurol, 221, 279-288.
- Sambrook,J., Maniatis,T. & Fritsch,E.F. (1989). Molecular Cloning: a Laboratory Manual. Woodbury: Cold Spring Harbor Laboratory Pr.
- Savy,C., Moussafi,F., Durand,J., Yelnik,J., Simon,A. & Nguyenlegros,J. (1995). Distribution and Spatial Geometry of Dopamine Interplexiform Cells in the Retina .2. External Arborizations in the Adult-Rat and Monkey. J Comp Neurol, 355, 392-404.
- Scott,K., Sieving,P.A., Bingham,E., Bhagat,V.J., Sullivan,J., Alpern,M. & Richards,J.E. (1993). Rhodopsin Mutations Associated with Autosomal-Dominant Retinitis-Pigmentosa. Acta Ophthalmol Scand, 53, 147.
- Semple-Rowland,S.L., Larkin,P., Bronson,J.D., Nykamp,K., Streit,W.J. & Baehr,W. (1999). Characterization of the chicken GCAP gene array and analyses of GCAP1, GCAP2, and GC1 gene expression in normal and rd chicken pineal. Mol.Vis., 5, 14.
- Semplerowland,S.L. (1991). Expression of Glial Fibrillary Acidic Protein by Muller Cells in Rd Chick Retina. J Comp Neurol, 305, 582-590.
- Shady,S., Hood,D.C. & Birch,D.G. (1995). Rod Phototransduction in Retinitis-Pigmentosa - Distinguishing Alternative Mechanisms of Degeneration. Invest Ophthalmol Vis Sci, 36, 1027-1037.

- Shirao, Y., Wajima, R., Kaneko, T. & Nishimura, A. (1997). Neural retinal contribution to the slow negative potential of the canine electroretinogram. Doc. Ophthalmol., 94, 293-306.
- Sieving, P.A. (1993). Photopic on- and off-pathway abnormalities in retinal dystrophies. Trans Am Ophthalmol Soc, LXXXI, 701-773.
- Sieving, P.A., Murayama, K. & Naarendorp, F. (1994). Push-Pull Model of the Primate Photopic Electroretinogram - A Role for Hyperpolarizing Neurons in Shaping the B-Wave. Vis Neurosci, 11, 519-532.
- Sikora, M.A., Gottesman, J. & Miller, R.F. (2005). A computational model of the ribbon synapse. J Neurosci Methods, 145, 47-61.
- Simoens, P., Demoor, A. & Lauwers, H. (1988). Blood-Vessel Patterns of the Retina in Domestic-Animals. Vlaams Diergeneeskundig Tijdschrift, 57, 174-191.
- Smith, R.G. (1995). Simulation of An Anatomically Defined Local Circuit - the Cone-Horizontal Cell Network in Cat Retina. Vis Neurosci, 12, 545-561.
- Soetedjo, R., Kaneko, C.R. & Fuchs, A.F. (2002). Evidence that the superior colliculus participates in the feedback control of saccadic eye movements. J Neurophysiol, 87, 679-695.
- Soucy, E., Wang, Y.S., Nirenberg, S., Nathans, J. & Meister, M. (1998). A novel signaling pathway from rod photoreceptors to ganglion cells in mammalian retina. Neuron, 21, 481-493.
- Spafford, M.M., Nurani, A. & Flanagan, J.G. (1993). Suitable Color Flash Filters for Erg Testing - A Comparative-Study. Clinical Vision Sciences, 8, 13-20.
- Steinberg, R.H., Fisher, S.K. & Anderson, D.H. (1980). Disk Morphogenesis in Vertebrate Photoreceptors. J Comp Neurol, 190, 501-518.
- Steiner, A.L., Parker, C.W. & Kipnis, D.M. (1972). Radioimmunoassay for cyclic nucleotides. I. Preparation of antibodies and iodinated cyclic nucleotides. J. Biol. Chem., 247, 1106-1113.
- Steuer, H., Jaworski, A., Stoll, D. & Schlosshauer, B. (2004). In vitro model of the outer blood-retina barrier. Brain Res Brain Res Protoc, 13, 26-36.
- Stockton, R.A. & Slaughter, M.M. (1989). B-Wave of the Electroretinogram - A Reflection of on Bipolar Cell-Activity. J Gen Physiol, 93, 101-122.
- Strettoi, E., Dacheux, R.F. & Raviola, E. (1994). Cone Bipolar Cells As Interneurons in the Rod Pathway of the Rabbit Retina. J Comp Neurol, 347, 139-149.

Strettoi,E. & Masland,R.H. (1995). The Organization of the Inner Nuclear Layer of the Rabbit Retina. J Neurosci, 15, 875-888.

Strettoi,E. & Pignatelli,V. (2000). Modifications of retinal neurons in a mouse model of retinitis pigmentosa. Proc Natl Acad Sci U S A, 97, 11020-11025.

Strettoi,E., Porciatti,V., Falsini,B., Pignatelli,V. & Rossi,C. (2002). Morphological and functional abnormalities in the inner retina of the rd/rd mouse. J Neurosci, 22, 5492-5504.

Stryer,L. (1991). Molecular mechanism of visual excitation. Harvey Lect., 87, 129-143.

Suber,M.L., Pittler,S.J., Qin,N., Wright,G.C., Holcombe,V., Lee,R.H., Craft,C.M., Lolley,R.N., Baehr,W. & Hurwitz,R.L. (1993). Irish-Setter Dogs Affected with Rod Cone Dysplasia Contain A Nonsense Mutation in the Rod Cgmp Phosphodiesterase Beta-Subunit Gene. Proc Natl Acad Sci U S A, 90, 3968-3972.

Sung,C.H., Davenport,C.M., Hennessey,J.C., Maumenee,I.H., Jacobson,S.G., Heckenlively,J.R., Nowakowski,R., Fishman,G., Gouras,P. & Nathans,J. (1991). Rhodopsin Mutations in Autosomal Dominant Retinitis-Pigmentosa. Proc.Natl.Acad.Sci.U.S A, 88, 6481-6485.

Szel,A., Rohlich,P., Caffè,A.R., Juliusson,B., Aguirre,G. & vanVeen,T. (1992). Unique Topographic Separation of 2 Spectral Classes of Cones in the Mouse Retina. J Comp Neurol, 325, 327-342.

Szel,A., Rohlich,P., Caffè,A.R. & vanVeen,T. (1996). Distribution of cone photoreceptors in the mammalian retina. Microsc Res Tech, 35, 445-462.

Toole,O. & Roberts,S. (1984). Generalized progressive retinal atrophy in two Akita dogs. Vet Pathol, 21, 457-462.

Tso,M.O.M., Zhang,C., Abler,A.S., Chang,C.J., Wong,F., Chang,G.Q. & Lam,T.T. (1994). Apoptosis Leads to Photoreceptor Degeneration in Inherited Retinal Dystrophy of Rcs Rats. Invest Ophthalmol Vis Sci, 35, 2693-2699.

Tsuruoka,M., Yamamoto,S., Ogata,K. & Hayashi,M. (2004). Built-in LED contact lens electrode for S-cone electroretinographic recordings. Doc.Ophthalmol., 108, 61-66.

Tzekov,R.T., Locke,K.G., Hood,D.C. & Birch,D.G. (2001). Cone and rod phototransduction parameters in retinitis pigmentosa patients. Invest Ophthalmol Vis Sci, 42, S76.

Ueno,S., Kondo,M., Niwa,Y., Terasaki,H. & Miyake,Y. (2004). Luminance dependence of neural components that underlies the primate photopic electroretinogram. Invest Ophthalmol Vis Sci, 45, 1033-1040.

Ullrich,B. & Sudhof,T.C. (1994). Distribution of Synaptic Markers in the Retina - Implications for Synaptic Vesicle Traffic in Ribbon Synapses. J Physiol (Paris), 88, 249-257.

VAEGAN & Millar,T.J. (1994). Effect of Kainic Acid and Nmda on the Pattern Electroretinogram, the Scotopic Threshold Response, the Oscillatory Potentials and the Electroretinogram in the Urethane-Anesthetized Cat. Vis Res, 34, 1111-1125.

Vanduffel,W., Tootell,R.B., Schoups,A.A. & Orban,G.A. (2002). The organization of orientation selectivity throughout macaque visual cortex. Cereb.Cortex, 12, 647-662.

Vardi,N. & Smith,R.G. (1996). The AII amacrine network: Coupling can increase correlated activity. Vision Res, 36, 3743-3757.

Varela,C., Igartua,I., De la Rosa,E.J. & De,l., V (2003). Functional modifications in rod bipolar cells in a mouse model of retinitis pigmentosa. Vision Res, 43, 879-885.

Venkataraman,V., Duda,T., Vardi,N., Koch,K.W. & Sharma,R.K. (2003). Calcium-modulated guanylate cyclase transduction machinery in the photoreceptor-bipolar synaptic region. Biochemistry, 42, 5640-5648.

Vervoort,R., Lennon,A., Bird,A.C., Tulloch,B., Axton,R., Miano,M.G., Meindl,A., Meitinger,T., Ciccodicola,A. & Wright,A.F. (2000). Mutational hot spot within a new RPGR exon in X-linked retinitis pigmentosa. Nat Genet, 25, 462-466.

Viswanathan,S., Frishman,L.J., Robson,J.G., Harwerth,R.S. & Smith,E.L., III (1999). The photopic negative response of the macaque electroretinogram: reduction by experimental glaucoma. Invest Ophthalmol Vis Sci, 40, 1124-1136.

Vuong,T.M. & Chabre,M. (1991). Deactivation kinetics of the transduction cascade of vision. Proc Natl Acad Sci U S A, 88, 9813-9817.

Wachtmeister,L. (1998). Oscillatory potentials in the retina: what do they reveal. Prog Retin Eye Res, 17, 485-521.

Wada,Y., Okano,T. & Fukada,Y. (2000). Phototransduction molecules in the pigeon deep brain. J.Comp Neurol., 428, 138-144.

Wakabayashi,K., Gieser,J. & Sieving,P.A. (1988). Aspartate Separation of the Scotopic Threshold Response (Str) from the Photoreceptor A-Wave of the Cat and Monkey Erg. Invest Ophthalmol Vis Sci, 29, 1615-1622.

Wang,J., Chang,Y.F., Hamilton,J.I. & Wilkinson,M.F. (2002a). Nonsense-associated altered splicing: a frame-dependent response distinct from nonsense-mediated decay. Mol.Cell, 10, 951-957.

- Wang,J., Chang,Y.F., Hamilton,J.I. & Wilkinson,M.F. (2002b). Nonsense-associated altered splicing: a frame-dependent response distinct from nonsense-mediated decay. Mol.Cell, 10, 951-957.
- Wassle,H., Boycott,B.B. & Illing,R.B. (1981a). Morphology and Mosaic of On-Beta and Off-Beta Cells in the Cat Retina and Some Functional Considerations. Proc R Soc Lond B Biol Sci, 212, 177-&.
- Wassle,H., Peichl,L. & Boycott,B.B. (1981b). Morphology and Topography of On-Alpha and Off-Alpha Cells in the Cat Retina. Proc R Soc Lond B Biol Sci, 212, 157-&.
- Whiteley,H.E. & Young,S. (1986). The External Limiting Membrane in Developing Normal and Dysplastic Canine Retina. Tissue Cell, 18, 231-239.
- Williams,D.S., Hallett,M.A. & Arikawa,K. (1992). Association of Myosin with the Connecting Cilium of Rod Photoreceptors. J Cell Sci, 103, 183-190.
- Wojciechowski,A.B., Englund,U., Lundberg,C., Victorin,K. & Warfvinge,K. (2002). Subretinal transplantation of brain-derived precursor cells to young RCS rats promotes photoreceptor cell survival. Exp Eye Res, 75, 23-37.
- Wolf,E.D., Vainisi,S.J. & Santos-Anderson,R. (1978). Rod-cone dysplasia in the collie. J Am Vet Med Assoc, 173, 1331-1333.
- Wong,R.O.L. & Hughes,A. (1987). The Morphology, Number, and Distribution of A Large Population of Confirmed Displaced Amacrine Cells in the Adult Cat Retina. J Comp Neurol, 255, 159-177.
- Wurziger,K., Lichtenberger,T. & Hanitzsch,R. (2001). On-bipolar cells and depolarising third-order neurons as the origin of the ERG-b-wave in the RCS rat. Vis Res, 41, 1091-1101.
- Yanase,J. & Ogawa,H. (1997). Effects of halothane and sevoflurane an the electroretinogram of dogs. Am.J.Vet.Res., 58, 904-909.
- Yanase,J., Ogawa,H. & Ohtsuka,H. (1996). Scotopic threshold response of the electroretinogram of dogs. Am.J.Vet.Res., 57, 361-366.
- Zatz,M., Mullen,D.A. & Moskal,J.R. (1988). Photoendocrine transduction in cultured chick pineal cells: effects of light, dark, and potassium on the melatonin rhythm. Brain Res, 438, 199-215.
- Zeiss,C.J. & Johnson,E.A. (2004). Proliferation of microglia, but not photoreceptors, in the outer nuclear layer of the rd-1 mouse. Invest Ophthalmol Vis Sci, 45, 971-976.
- Zeiss,C.J., Neal,J. & Johnson,E.A. (2004). Caspase-3 in postnatal retinal development and degeneration. Invest Ophthalmol Vis Sci, 45, 964-970.

- Zeiss,G.J., Acland,G.M. & Aguirre,G.D. (1999). Retinal pathology of canine X-linked progressive retinal atrophy, the locus homologue of RP3. Invest Ophthalmol Vis Sci, 40, 3292-3304.
- Zeumer,C., Hanitzsch,R. & Mattig,W.U. (1994). The c-wave of the electroretinogram possesses a third component from the proximal retina. Vis Res, 34, 2673-2678.
- Zhang,Q., Acland,G.M., Parshall,C.J., Haskell,J., Ray,K. & Aguirre,G.D. (1998). Characterization of canine photoreceptor phosducin cDNA and identification of a sequence variant in dogs with photoreceptor dysplasia. Gene, 215, 231-239.
- Zhang,Q., Acland,G.M., Wu,W.X., Johnson,J.L., Pearce-Kelling,S., Tulloch,B., Vervoort,R., Wright,A.F. & Aguirre,G.D. (2002). Different RPGR exon ORF15 mutations in Canids provide insights into photoreceptor cell degeneration. Hum Mol Genet, 11, 993-1003.
- Zhang,Q., Baldwin,V.J., Acland,G.M., Parshall,C.J., Haskel,J., Aguirre,G.D. & Ray,K. (1999). Photoreceptor dysplasia (pd) in miniature schnauzer dogs: evaluation of candidate genes by molecular genetic analysis. J.Hered., 90, 57-61.
- Zhang,Z., Melia,T.J., He,F., Yuan,C., McGough,A., Schmid,M.F. & Wensel,T.G. (2004). How a G protein binds a membrane. J Biol Chem, 279, 33937-33945.
- Zhao,X., Yokoyama,K., Whitten,M.E., Huang,J., Gelb,M.H. & Palczewski,K. (1999). A novel form of rhodopsin kinase from chicken retina and pineal gland. FEBS Lett., 454, 115-121.

MICHIGAN STATE UNIVERSITY LIBRARIES



3 1293 02845 3631